

## THESIS / THÈSE

### DOCTOR OF SCIENCES

#### Synthesis and applications of novel fullerenes and silsesquioxanes based structures

Cinà, Valerio

*Award date:*  
2020

*Awarding institution:*  
University of Namur

[Link to publication](#)

#### General rights

Copyright and moral rights for the publications made accessible in the public portal are retained by the authors and/or other copyright owners and it is a condition of accessing publications that users recognise and abide by the legal requirements associated with these rights.

- Users may download and print one copy of any publication from the public portal for the purpose of private study or research.
- You may not further distribute the material or use it for any profit-making activity or commercial gain
- You may freely distribute the URL identifying the publication in the public portal ?

#### Take down policy

If you believe that this document breaches copyright please contact us providing details, and we will remove access to the work immediately and investigate your claim.



UNIVERSITÀ  
DEGLI STUDI  
DI PALERMO

Università degli Studi di Palermo  
Dottorato di Ricerca in  
Scienze Molecolari e Biomolecolari  
Dipartimento STEBICEF  
S. S. D. – CHIM/06



Université de Namur  
Doctorat en Sciences  
Faculté de Sciences  
Département de Chimie

## SYNTHESIS AND APPLICATIONS OF NOVEL FULLERENES AND SILSESQUOXANES BASED STRUCTURES

PhD STUDENT  
**VALERIO CINÀ**

COORDINATOR  
**PROF. PATRIZIA DIANA**

TUTOR  
**PROF. FRANCESCO GIACALONE**

TUTOR  
**PROF. CARMELA APRILE**

CICLO XXXII  
2019



# *Table of contents*

Acknowledgment	<i>iv</i>
Chapter 1 General introduction	1
1. Introduction	2
1.1. Carbon Allotropes and its Nanoforms	3
1.2. Applications of main Carbon Nanoforms	6
1.2.1. Graphene	7
1.2.2. Carbon Nanotubes	7
1.2.3. Fullerene	9
1.2.3.1. Synthesis	9
1.2.3.2. Properties	10
1.2.3.3. Common application	11
1.3. Silicon and its evolution	15
1.3.1. Silicon Dioxide	16
1.3.2. Mesostructured Silica	18
1.3.3. Polyhedral Oligomeric Silsesquioxanes	20
1.3.3.1. POSS Common applications	22
1.4. Aim of the Thesis	30
1.5. References	34
Chapter 2 Bisoxazoline-C <sub>60</sub> Hybrid Systems for Asymmetric Catalysis	50
2. Introduction	51
2.1. C <sub>60</sub> -Fullerene in Catalysis	51
2.1.1. C <sub>2</sub> -Symmetry catalysts	54
2.1.1.1. Bisoxazoline (BOX)	55
2.2. Aim of Chapter	58
2.3. Results and discussion	59
2.3.1. Synthesis and characterization of catalysts	59
2.3.1.1. BOX Synthesis	59

2.3.1.2.	Synthesis of C <sub>60</sub> -BOX (monoadducts)	62
2.3.1.3.	Synthesis of C <sub>60</sub> -BOX <sub>6</sub> (hexakisadducts)	65
2.3.1.4.	Synthesis of IL Hybrids (C <sub>60</sub> -IL <sub>10</sub> -BOX)	68
2.3.2.	Catalytic applications	72
2.3.2.1.	Asymmetric Henry	72
2.3.2.2.	Asymmetric Diels-Alder	78
2.4.	Conclusions	81
2.5.	Experimental section	81
2.6.	References	91
Chapter 3 Novel nanobuilding blocks for 3D emitting materials		97
3.	Introduction	98
3.1.	Photochemistry of Lanthanides	100
3.2.	C <sub>60</sub> -BOX <sub>6</sub> : complexation study of novel Carbon building-blocks	101
3.3.	Conclusions	106
3.4.	References	108
Chapter 4		110
Tuneable Emission of Polyhedral Oligomeric Silsesquioxane- Based Nanostructures Self-Assembled in the Presence of Europium(III) Ions: Reversible trans-to-cis Isomerization		
4.	Introduction	111
4.1.	Results and Discussion	113
4.2.	Conclusions	129
4.3.	References	131
Chapter 5 Photoluminescence Lanthanide@POSS-based materials		135
5.	Photoluminescence Lanthanide@POSS-based materials	136
5.1.	<sup>139</sup> La-NMR characterisation	140
5.2.	Replacing water molecules	143
5.3.	“Rainbow” full emission spectrum	149

5.4. Conclusions	152
5.5. Experimental Section	154
5.6. References	156
Chapter 6 General conclusions	157
6. General conclusions	158
Chapter 7 Outlooks	160
7. Outlooks	161
7.1. C <sub>60</sub> -PyBOX asymmetric catalysts	161
7.2. POSS terpyridine evolution	163
7.3. References	165
List of abbreviation	167
Curriculum vitae	170

## *Acknowledgements*

Thanks go, first of all, to the University of Palermo and the University of Namur for the co-funded PhD fellowship.

In particular part of this research used the resources of the “Plateforme Technologique Physico-Chemical Characterization” (PC<sup>2</sup>) and the resources of the “Plateforme Technologique Morphologie – Imagerie” (MORPH-IM). Many thanks therefore go to the staff of the platforms: Valérie Charles and Nicolay Tumanov for the PC<sup>2</sup> and Corry Charlier of the electron microscopy service. Thanks also to Giuseppe Barbera of the “Unité de chimie organique et biorganique supramoléculaire” for solving many technical and instrumental problems.

Special thanks go to my two tutors, Professor Carmela Aprile and Professor Francesco Giacalone, for welcoming me into their laboratories and giving me this opportunity for professional growth. Thanks go also to Professor Michelangelo Gruttadauria for welcoming in his research group.

Thanks go also to Professor H. Garcia that welcomed me at the “Instituto de Tecnología Química (ITQ) at the Polytechnic University of Valencia (UPV) were I spent two month learning that not always all results are positive, but it is possible, in any case, to learn something.

I want to thanks Dr Esther Carbonell Llopis for following me during the first part of my PhD, for helping me prepare for my mid-doctoral exam, for supporting me during my journey to the ITQ and for being available always to talk about the results obtained even when she was no formally part of the University staff.

Special tanks go to Dr Luca Fusaro, who taught me how to work with nmr and trusted me by letting me work alone with the instrument under his responsibility, for the wise advice and above all for motivating me to work hard in times of low productivity.

A special thanks also go to Dr. Vincenzo Campisciano who, with his experience in the laboratory suggested to me many small tricks to improve operationally and manually my laboratory skills, and with his computing experience, has taught me how to process data in the best way.

I want to thank also Alvis Vivian and Andrea Carletta with whom I shared special moments during my periods in Belgium and with whom I have forged a special friendship.

Last but not least special thanks go to my family that supported me during these three years and to Elena that, with her love, has sustained and encouraged me also and above all at a distance.



*Chapter 1*  
*General Introduction*

# 1 Introduction

When we talk about matter in its Nanoform we are led to think that it is a prerogative of modern science, whereas nanoparticles have a surprisingly long history. The term “nano” comes from the ancient greek word *νᾶνος* (nanos) through the Latin *nanus* meaning literally dwarf and, by extension, very small. Within the convention of International System of Units (SI) it is used to indicate the reduction factor of  $10^{-9}$  times, and “nanoscale” generally refers to objects with a dimension between 1-100 nm. But what defines nanomaterials are not only their dimensions. Obviously, what attracts are their peculiar properties. In fact, isolated molecules exhibit properties that follow quantum mechanical rules, while the chemical and physical properties of bulk materials obey the laws of classical physics. In the middle, nanosystems display electronic, photochemical, electrochemical, optical, magnetic, mechanical or catalytic properties that differ significantly not only from those of molecular units, but also from those of macroscopic systems.<sup>1</sup>

Their preparation is neither an exclusive result of modern research nor restricted to man-made materials. Naturally occurring nanoparticles include organic (proteins, polysaccharides, viruses) as well as inorganic compounds (iron oxyhydroxides, aluminosilicates, metals) and are produced by weathering, volcano eruptions, wildfires or microbial processes.<sup>2</sup>

Most current nanoparticles and nanomaterials can be organized into four categories: Carbon-based nanomaterials that include carbon allotrope forms, Organic-based nanomaterials that include nanomaterials from organic matter (excluding the carbon-based ones), Inorganic-based nanomaterials and Composite nanomaterials. All of these are further classified depending their crystalline forms and chemical composition,<sup>3</sup> their dimension, their spatial arrangement (0D, 1D, 2D, 3D),<sup>4</sup> and their production. In the latter case, nanomaterials can formed in nature either by biological species or through anthropogenic activities,<sup>5</sup> or are synthesized by physical, chemical, biological or hybrid methods.<sup>6</sup>

Among all the existing elements studied and by ever used, Carbon and Silicon-based solids are two of the most important materials involved in the history of science and technology development.<sup>7</sup> In fact, carbon-based chemical industry has produced the various synthetic materials for daily life and silicon-based

semiconductor industry has moved people to digital age. In recent decades, the discovery and synthesis of carbon (e.g., fullerenes, carbon nanotubes, graphene) and silicon nanostructures (e.g. Si quantum dots, Si nanowires) have pushed the rapid advancement of nanoscience and nanotechnology. Nowadays, carbon and silicon nanostructures are finding application in various fields, such as electronics,<sup>8</sup> photonics,<sup>9</sup> sensors,<sup>10</sup> biotechnology,<sup>11</sup> and recently, in energy related applications such as catalysis,<sup>12</sup> batteries,<sup>13</sup> solar cells.<sup>14</sup>

## 1.1 Carbon Allotropes and its Nanoforms

By the very first human activities, carbon-based materials played immediately an important role. In China there is evidence of the existence of a coal mine dating back more or less to 1000 BC.<sup>15</sup> It is known that also the Greeks used coal in their everyday life for example after reducing it to powder they mixed it with wine to treat toothache. In Roman times, in England, coal was used not only to heat up, but also to create jewellery and ornaments of various kinds given its shiny black colour.<sup>16</sup> In the late Middle Ages, it was used by blacksmiths to produce lime, salt and to provide the minimum energy necessary for domestic life. It was then around 1750, with the Industrial Revolution, that coal acquired its true importance becoming the main source of energy for man.<sup>17</sup>

Carbon is a chemical element with the symbol C and atomic number 6. The fourth most abundant element in the universe, it is the sixth element of the periodic table. It is non-metallic and tetravalent, and it naturally occurs in three isotopes, <sup>12</sup>C and <sup>13</sup>C being stable, while <sup>14</sup>C is a radionuclide, decaying with a half-life of about 5,730 years.<sup>18</sup>

Carbon is an ancient fossil mineral originating from the carbonification of material and plant residues that have accumulated in an anaerobic environment.<sup>19</sup> Carbon, due to its valency, can form many allotropes. Well-known allotropes of carbon include diamond and graphite (**Figure 1.1**).



**Figure 1.1** The two most know carbon allotropes graphite and diamond. In figure, representative atoms arrangement in the space.

Both are known by ever; graphite owes its name to Abraham Gottlob Werner that named it in this way, from the greek γράφειν (graphein), "to draw/write",<sup>20</sup> for its use in pencils. Graphite is a crystalline form of carbon with its atoms arranged in a hexagonal structure. In graphite the bonds are hybridized  $sp^2$  and the atoms form in planes with each bound to three nearest neighbours 120 degrees apart. It occurs naturally in this form, and it is the most stable form of carbon under standard conditions. Graphite is structurally composed of planes of polycyclic carbon atoms in an hexagonal structure.<sup>21</sup>

Graphite possess delocalized electrons that are free to move throughout the plane (above and below the planes of the carbon atoms), and for this reason it conducts electricity along the planes, but does not through the planes. These conductivity properties allow to use the graphite in electronic products such as electrodes,<sup>22</sup> batteries,<sup>23</sup> and solar panels.<sup>24</sup>

In diamond the bonds are hybridized  $sp^3$  and the carbon atoms are arranged in space in a tetrahedral arrangement. These tetrahedrons together form a 3D network of six-membered carbon rings (similar to cyclohexane), in the chair conformation, allowing for zero bond angle strain.<sup>25</sup> This stable network of covalent bonds and hexagonal rings is the reason that diamond is so strong.

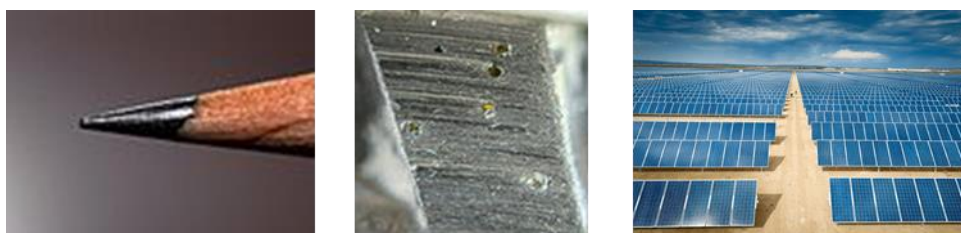


**Figure 1.2.** Some graphite and diamond applications: lead pencil (left), diamond blade (middle), graphite solar panel (right)

Diamond is the hardest known natural mineral in which carbon atoms are arranged in a crystal structure called diamond cubic. Diamond has the highest hardness and thermal conductivity of any natural material, properties that are utilized in major industrial applications such as cutting and polishing tools.<sup>26</sup> Furthermore its hardness, the high dispersion of light of diamond make it useful in jewellery.

But the carbon allotropes family has not only two members. In fact, although these two were the only ones known for years, in the middle of 1980's the discovery of a new allotrope starts to open the doors towards the exploration of this big family that is the family of the Carbon Nanoforms (CNFs).

In particular the date that changed the way the scientists look at the Carbon was the 1985 with the discovery of the Buckminsterfullerene by Kroto, Smalley and Curl that won for this the Nobel prize.<sup>27</sup>

Although already theoretically hypothesized in 1966 by D.E.H. Jones that considered the possibility of making large hollow carbon cages, structures now called giant fullerenes,<sup>28</sup> (without finding positive reactions from the scientific community). Later, in 1970 Osawa proposed a spherical  $I_h$ -symmetric football structure for the  $C_{60}$  molecule, simulated by the synthesis of the bowl shaped corannulene (**Figure 1.3**),<sup>29</sup> by.<sup>30</sup>

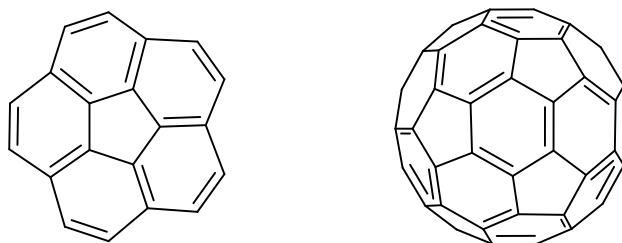


**Figure 1.3.** Corannulene structure and fullerene hollow cage.

In 1984 it was observed that, by laser vaporization of graphite, large carbon clusters  $C_n$  with  $n = 30-190$  can be produced. Unfortunately, despite being present in the produced soot, fullerene was not detected.<sup>31</sup> The year of the breakthrough was 1985, when Kroto met Smalley at Rice university in Huston. There they started together to simulate the conditions under which carbon nucleates in the atmospheres of red giant stars with a mass spectroscopy method developed by Smalley. To this purpose, they began bombarding a graphite rod with a pulsed laser. These studies found that, under specific clustering conditions, the 720 mass peak attributed to  $C_{60}$ ,

and to a lesser extent the peak attributed to  $C_{70}$ , exhibits a pronounced intensity in the spectra.<sup>32</sup>

As already said, this discovery was a turning point in the development of the CNFs. In fact, just few years later, in the 1991, Iijima wrote in an abstract of a Nature article: “*Here I report the preparation of a new type of finite carbon structure consisting of needle-like tubes*”. Announcing the discovery of a new nanocarbon allotrope, the Carbon Nanotube (CNT).<sup>33</sup>

Fascinatingly, Carbon Nanotubes and Fullerene are only the tip of the iceberg. In the years that followed their discovery, a wide variety of new carbon Nanoforms such as nanohorns, nano-onions, cup-stacked nanotubes, nanotori, nanobuds, and graphene, have emerged (**Figure 1.4**).

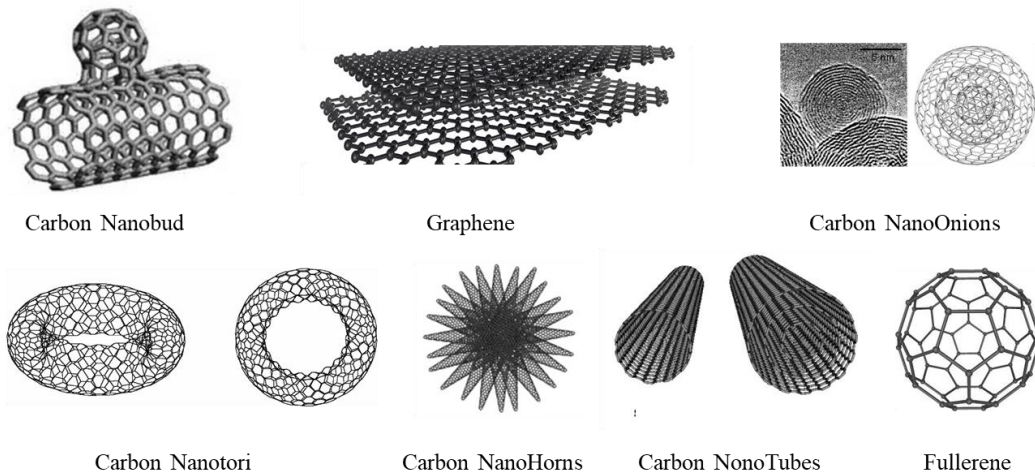


**Figure 1.4.** Representative Carbon Nanoforms (CNFs)

## 1.2 Applications of main Carbon Nanoforms

Since the discovery of Kroto, carbon-based nanostructures have become one of the most investigated class of nanomaterials in the world. During the past years research efforts have mainly been devoted to the investigation on fullerene, carbon nanotubes and graphene although the ability of carbon to exist in many allotropic forms has provided a variety of nanoscale sized structures with fascinating properties.

### 1.2.1 Graphene

Graphene is defined as the “oldest and the newest of the carbon nanoform”.<sup>34</sup> It is a two-dimensional near planar structure that consist of hexagonal rings constructed from  $sp^2$ -hybridized carbon atoms.<sup>35</sup> The discovery of this carbon allotrope was awarded with the Nobel Prize for Physics in 2010.<sup>36</sup> About its production, the techniques to produce it are developing rapidly, just for mentioning a few: exfoliation, hydrothermal self-assembly, chemical vapor deposition, spin coating, supersonic spray, laser, microwave-assisted oxidation etc.<sup>34</sup> In general, different production methods can be divided into three classes: the first consists in removing layers from graphite, via mechanical exfoliation (scotch tape method),<sup>37</sup> using surfactants to disperse graphite layers.<sup>38</sup> The second lie on exfoliation of graphene from SiC films via heating bulk SiC (graphene is then formed by Si removing).<sup>39</sup> The third one uses epitaxial growth (the most promising for large-scale production).<sup>40</sup>

Regarding its application, it is still under investigation or at proposal stage. Due to its electrical and structural properties, graphene is considered transparent and flexible conductor that shows great promise for numerous material/device applications, such as solar cells,<sup>41</sup> light-emitting diodes (LED),<sup>42</sup> touch panels and smart windows or phones.<sup>43</sup> It was successfully employed to improve mechanical properties of solid material like in coating epoxy plastic increasing significantly Young’s Modulus of the final material.<sup>44</sup> Graphene based transistors have been successfully produced and tested establishing the state of the art for graphene transistors.<sup>45</sup>

### 1.2.2 Carbon nanotubes

A carbon nanotube can be imaged as a rolled graphene single layer<sup>33</sup> (**Figure 1.5**). Carbon nanotubes display intriguing electronic<sup>46</sup> and mechanical<sup>47</sup> properties that have attracted the attention of many scientists all around the world. About CNTs a first splitting can be done focusing on their morphology. There exist in single-walled nanotubes (SWNT) and multiwalled nanotubes (MWNT) of different lengths and diameters.

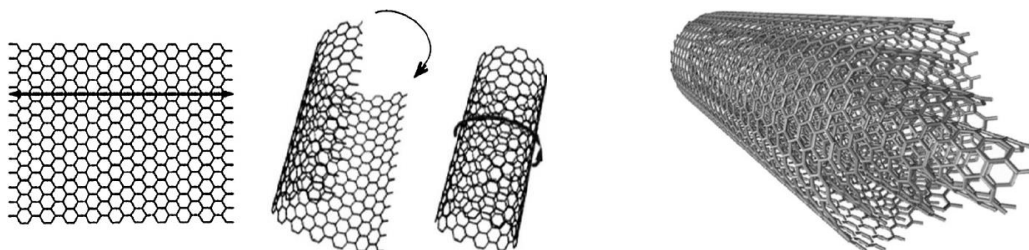


**Figure 1.5.** Fictitious way to represent CNT formation (left). Multiwalled Carbon Nanotube (right).

In the case of the single walled nanotubes, beside dimensions, the way the graphite layer is rolled influences the final properties of the tube.

According to IUPAC, a whole new system has been established to classify carbon nanotubes in order to distinguish between different tubes, but also to understand certain properties: zig-zag, armchair, and chiral carbon nanotubes (**Figure 1.6**).

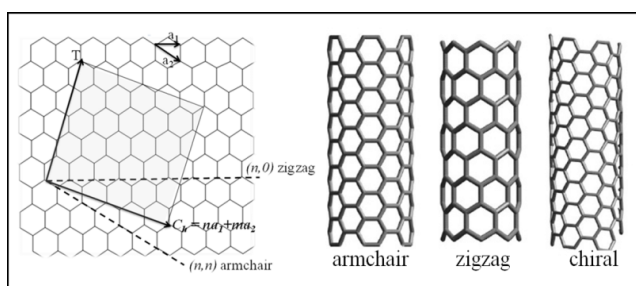


**Figure 1.6.** CNTs classification accordingly with the way they are rolled.

All the different CNTs possess various interesting properties and they found applications in several fields. A great variety of CNT derivatives can be realized by different synthetic approaches. CNTs can be chemically modified by the following strategies: (a) functionalization of defects on the sidewall and on the rims; (b) noncovalent interactions; (c) sidewall covalent functionalization and (d) endohedral inclusion (**Figure 1.7**).

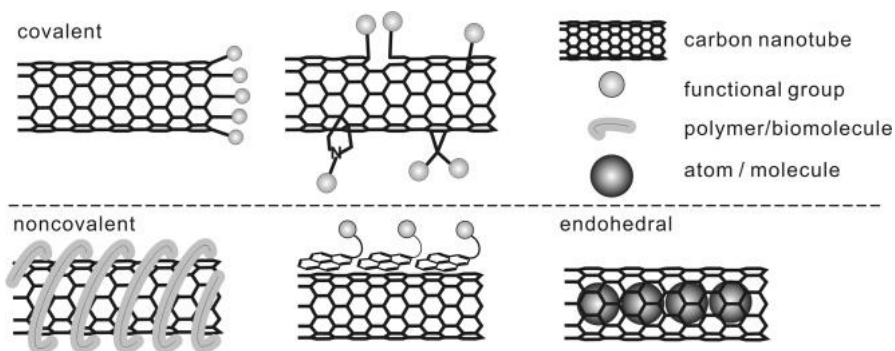


**Figure 1.7.** Different ways of CNTs functionalization



Among the others, CNTs can be employed in electronic as tips in atomic force microscopy,<sup>48</sup> in field emission (with an electric field applied, carbon nanotubes are able to emit electrons from their tips),<sup>49</sup> field effect transistors,<sup>50</sup> as sensor (physical or chemical),<sup>51</sup> as support for catalyst,<sup>52</sup> hydrogen storage,<sup>53</sup> carrier for systems in targeted drug delivery to living cells.<sup>54</sup>

### **1.2.3 Fullerene**

#### *1.2.3.1 Synthesis*

The discovery of fullerene has represented the real turn off in the development of nanocarbon materials. An innovative method that allowed to obtain fullerene in a larger scale, making it available to the scientific community, was firstly reported by Krätschmer and Huffman.<sup>55</sup> They found that during the vaporization of graphite in helium atmosphere it was possible produce fullerene in a 10% yield.

Macroscopic amounts of fullerenes can be nowadays produced in different ways grouped in three categories: a) fullerene production by vaporization of graphite, b) fullerene synthesis in combustion, c) fullerenes production by pyrolysis of hydrocarbons.

The first group consists of three methods. One, resistive heating of graphite, consists of applying a voltage to two graphite rods (one with a conical shape end, and the other one with a flat shape end) kept in contact by a spring under a Helium pressure of 140 mbar. This method produces a carbon soot with a 10% yield in fullerene.<sup>55</sup>

Alternatively, there is the arc heating of graphite.<sup>56</sup> The difference to the first one is that graphite rods are not strictly in contact and when a voltage is applied power is dissipated in an arc and not in Ohmic heating. The method reaches the highest performance when the electrodes are barely in contact and it allows to produce fullerene in 15% of yield.<sup>56a</sup> About the other two members of this group must be underlined that they are only proof of concept in fact they produce fullerene in very low yield. One consists in focusing sunlight, with a parabolic mirror, onto a tip of a graphite rod. Producing so a carbon soot leveraging solar light.<sup>57</sup> Fullerene can also be produced by direct inductive heating of a carbon sample. Evaporation at

high temperature (2700 °C) in a He atmosphere affords a soot containing less than 1% of yield.<sup>58</sup>

But if we want to talk in term of industrial production, the methods above are not suitable. The ideal method is the fullerene synthesis in combustion. In this way a pilot plant of the Mitsubishi's Frontier Carbon Corporation is operating. The method consists in producing a soot burning a mix of benzene, oxygen and argon, under a range of conditions that include different pressures, temperatures and carbon-to-oxygen ratios. The yield of fullerenes, as well as the C<sub>70</sub>:C<sub>60</sub> ratio, strongly depends on the operation mode. Just to have an idea, the yields varies from  $2 \cdot 10^{-4}$  to 0.3% for a non-sooting flame, at a pressure of 20 Torr, a carbon: oxygen ratio of 0.995 with 10% argon and a flame temperature of about 1800 K. The C<sub>70</sub>:C<sub>60</sub> ratio varies from 0.26 to 5.7, which is much larger than that observed for graphite vaporization methods (0.02–0.18).<sup>59</sup>

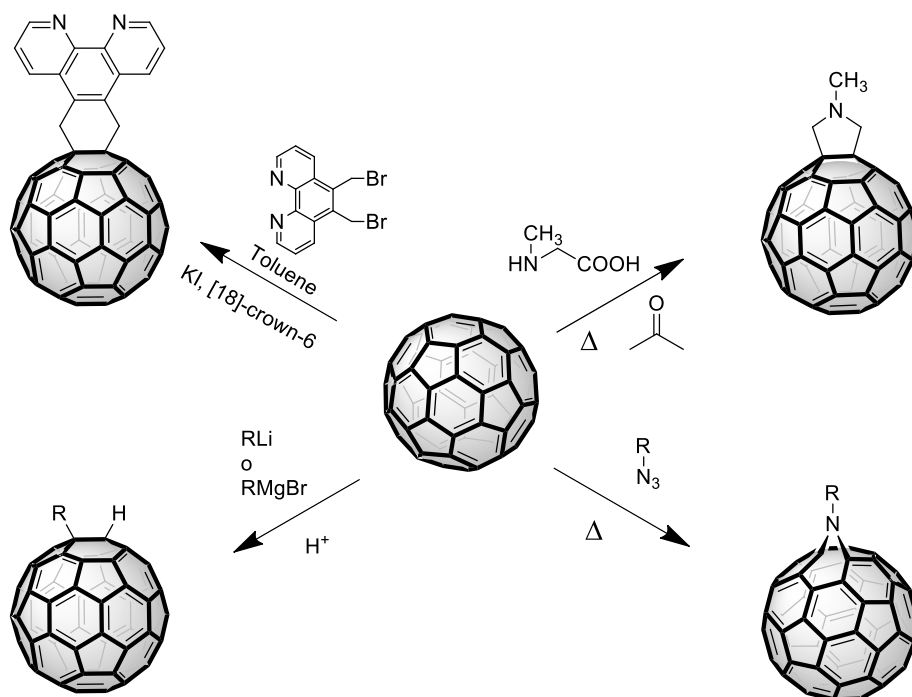
#### *1.2.3.2 Properties*

Fullerene family consists of several members that differ each other by the number of carbon atoms. In principle the building method follows the Euler's principle: Fullerene contain  $2(10+M)$  carbon atoms divided in 12 pentagons and M hexagons. Following this principle, the smallest member of the family should be the C<sub>20</sub>, but it is unstable. On the contrary, the C<sub>60</sub> [60-*I<sub>h</sub>*] fullerene is the smallest stable fullerene built up of fused pentagons and hexagons in which the pentagons provide curvature, and its structure was theoretically and experimentally demonstrated.<sup>60</sup> Two features of the C<sub>60</sub> structure are of special significance: a) all twelve pentagons are isolated by hexagons; b) the bonds at the junctions of two hexagons ([6,6] bonds) are shorter than the bonds at the junctions of a hexagon and a pentagon ([5,6] bonds). The bond length alternation in [60-*I<sub>h</sub>*]fullerene shows that, in the lowest energy Kekulé structure, the double bonds are located at the junctions of the hexagons ([6,6] double bonds) and there are no double bonds in the pentagonal rings. Each hexagon in [60-*I<sub>h</sub>*]fullerene exhibits cyclohexatriene character and each pentagon a radialene character. Regarding its reactivity, theoretical calculations of the molecular orbital levels of C<sub>60</sub> show that the lowest unoccupied molecular orbitals (LUMO) is triply degenerated Therefore, C<sub>60</sub> was predicted to be a fairly

electronegative molecule, being reducible up to the hexa-anion.<sup>61</sup> This was supported by cyclic voltammetry studies carried out with C<sub>60</sub> in solution which showed that it can accept up to six electrons. This electronic and geometric properties imply that C<sub>60</sub> behaves like an electron-poor conjugated polyolefin, rather than a “super-arene”. Consequently, C<sub>60</sub> undergoes various nucleophilic additions with carbon, nitrogen, phosphorous and oxygen nucleophiles. Functionalization has been done through various methods such as, cycloaddition, electrophilic reaction like, halogenation, alkylation, arylation, oxidation, reduction, free radical addition, metalation, hydrogenation, and polymerization by using various reagents (**Figure 1.8**).<sup>62</sup>

[4+2] Cycloaddition

Prato Reaction



Hydroalkylation

[3+2] Cycloaddition

**Figure 1.8.** C<sub>60</sub> possible functionalization strategies.

### 1.2.3.3 Common applications

Fullerene, with its symmetrical hollow carbon structure, since its discovery has been the object of intensive research. The wide number of books, and articles (**Figure 1.9**) published on fullerene reactivity, properties and applications in

different areas evidences the progress made in the knowledge of these unique three-dimensional structures.<sup>63</sup>

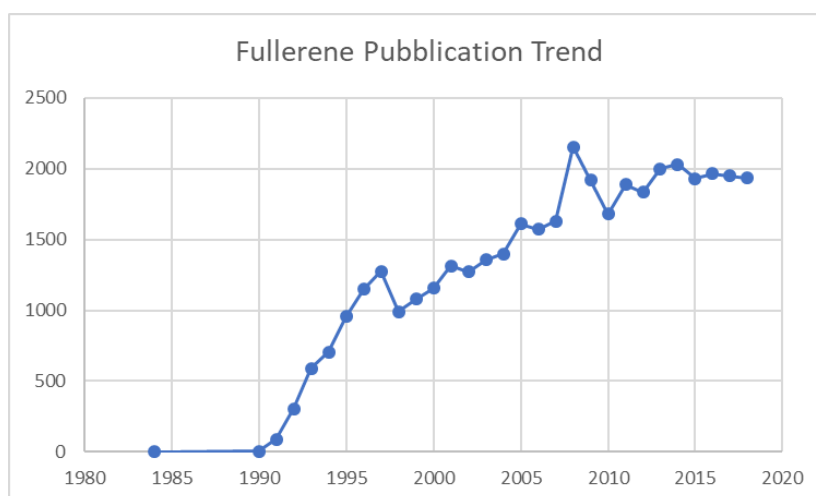


**Figure 1.9.** Trend of the topic fullerene searching in scopus database since its discovery by now.

[60] Fullerene has been investigated in several fields of chemistry, biomedicine, in the development of solar based cells, photovoltaic instruments, cosmetics, etc (**Figure 1.10**). C<sub>60</sub> has a broad range of charming properties, such as high electronic conductivity, large specific surface area, good biocompatibility, inert behaviour, stable structure and good adsorption capacity towards organic molecules.

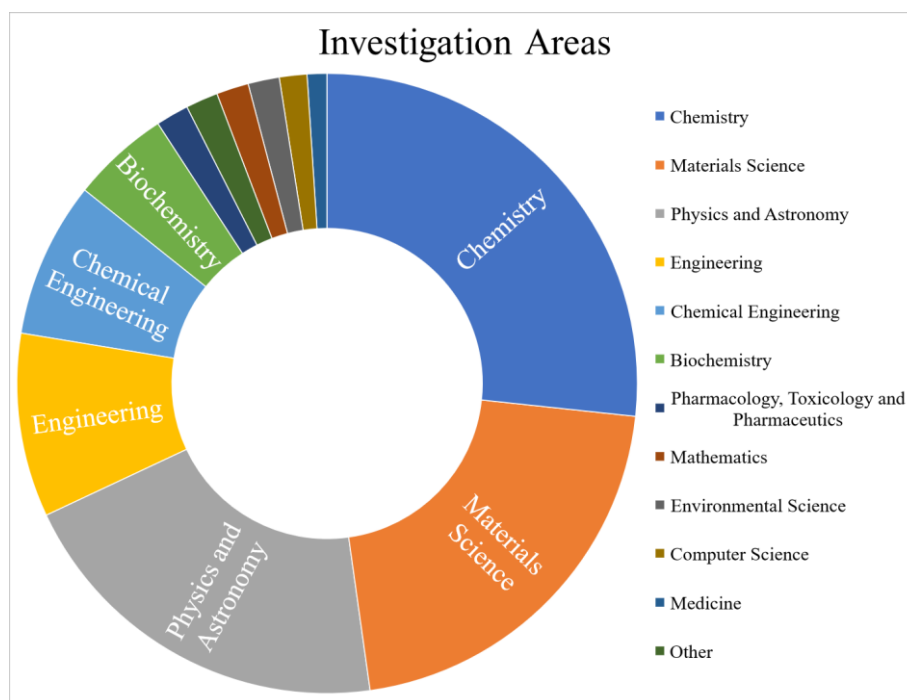


**Figure 1.10.** Graph of different field of investigations.

Since it was discovered that films based on the fullerides compounds (alkali elements doped C<sub>60</sub> obtained by Diels-Alder cycloaddition reaction)<sup>64</sup> showed excellent conductivity at room temperature, a road in the direction of understanding these properties of fullerene was opened.<sup>65</sup>

Photoinduced charge transfer from the polymer to the fullerene cage, was first identified by Sariciftci *et al.*, who showed the potential of C<sub>60</sub> in the solar cell field.<sup>66</sup> Recently, Chengbo *et al.* reported two novel fullerene derivatives with different specific functional groups, namely benzylthiophene-C<sub>60</sub> bisadducts (BTCBA) and 2-(4-methoxybenzyl)thiophene-C<sub>60</sub> bis-adducts (MBTCBA), which have been utilized as acceptors for polymer solar cells (PSCs).<sup>67</sup> The MBTCBA PSCs showed a power conversion efficiency superior to that of [6,6]-phenyl-C<sub>61</sub>-butyric acid methyl ester (PCBM) based control devices (utilized as a role model and reference acceptor for all kinds of fullerene acceptors, because of easy preparation, good solubility, electron mobility, low lying LUMO energy levels, and stability than comparing with their pristine fullerenes).

In 2019, Kielar *et al.* reported the preparation of organic optoelectronic rubrene-fullerene diodes as tactile sensors for soft-touch applications.<sup>68</sup> This organic optoelectronic diode can act as light emitters or detectors as well as solar cells solving the need of having separate light sources and detectors. In fact, the use of fullerene in the preparation of electrochemical sensor and biosensor led to the development of a variety of new nanomaterials. Due to its excellent electron accepting capacity and its ability to accelerate charge separation in any electrochemical process, fullerene can be used in various types of sensors, e.g., potentiometric, ampero-metric, piezoelectric, etc.

Planning biosensors for versatile biomedical applications is a challenge and the use of modified C<sub>60</sub> fullerene can open the doors for today and tomorrow's nanoscience and nanotechnology. Fullerene-based material revealed to be suitable nanosensors for the detection of glucose and as urea biosensor.<sup>69</sup> Remaining in biological application of fullerene, gadolinofullerenol was successfully tested to modulate tumour microenvironment (TME) rather than kill cancerous cells directly.<sup>70</sup> Although C<sub>60</sub> fullerene and its derivatives are daily investigated as possible drug carrier as well as in the treatment against of some diseases, their potential side

effects still need to be deeply investigated. A recent study was conducted to verify the effect of buckminsterfullerene on *Drosophila melanogaster* at DNA, tissue and organism levels.<sup>71</sup> A first result indicates that pristine C<sub>60</sub> at the concentration of 20 µg/mL and 40 µg/mL induced high level damage in DNA, but astonishingly there are not effects at the organismal level, and this could be explained by the activation of repair systems or by active elimination of damaged cells. The study demonstrated also that at the concentration of 40 µg/ml does not exert any genotoxic effect on adult organism, pristine C<sub>60</sub> also does not affect the reproductive system and embryogenesis.

Very recently, Elessawy *et al.*, proposed an innovative synthesis of functionalized magnetic fullerene nanocomposite (FMFN) via catalytic thermal decomposition of PET bottle wastes as feedstock and ferrocene as a catalyst and precursor of magnetite.<sup>72</sup> This kind of material was then used for removing pollutants from the environment, thanks to its porous and high surface area in addition to superparamagnetic property, to adsorption of Ciprofloxacin antibiotic from aqueous solution.<sup>73</sup>

Fullerene is finding application also in catalysis, although in this field in the past decades it has been less exploited, it is now experiencing a novel renaissance.<sup>74</sup> C<sub>60</sub> has been, for instance, directly functionalized with metals such as Palladium and used as catalyst for the catalytic hydrogenation of acetylenic alcohols,<sup>75</sup> or it has employed as support for catalysts such as proline for asymmetric reactions.<sup>76</sup> The use of fullerene as catalyst is one of the topics of this Thesis because was widely demonstrated its ability as molecular scaffold allowing easy handling of the resulting catalysts. Thus, several aspects of fullerene in catalysis will be discussed later in the present Thesis.

### 1.3 Silicon and its evolution

If today we can put a calculator in our pocket or wear a clock that also measures our heartbeats and air temperature, if we talk about telematic networks, computers and information highways, we owe much to the extraordinary capabilities of the silicon. Silicon is the 7<sup>th</sup> most abundant element in the universe and the second most abundant element in the earth's crust (27.7%) second only to the oxygen. The name Silicon (assigned by Berzelius) comes from the Latin "*silex*", meaning flint. Silicon was first identified by Antoine Lavoisier in 1787<sup>77</sup> and was later mistaken for a compound by Humphry Davy in 1800. In 1811 Gay Lussac and Thenard probably prepared impure amorphous silicon by heating potassium with SiF<sub>4</sub>. In 1824 Berzelius prepared amorphous silicon using the same method as Lussac, isolating it and describing it as an element.<sup>78</sup>

It is found in clay, feldspar, granite and quartz, mainly in the form of silicon dioxide (SiO<sub>2</sub>), silicates and metasilicates (compounds containing silicon, oxygen and metals). Silicon is the main component of glass, cement, ceramic, etc. Crystalline silicon was obtained only after 1854, when it was obtained as a product of electrolysis.<sup>79</sup> The manufacture of glass containing SiO<sub>2</sub> was carried out both by the Egyptians at least as early as 1500 BC and by the Phoenicians. Certainly, many of the naturally occurring compounds called silicates were used in various kinds of mortar for construction of habitat by the earliest people.<sup>78</sup>

Two allotropes of silicon exist at room temperature: amorphous and crystalline.<sup>80</sup> Amorphous appears as a brown powder while crystalline silicon has a shine metallic and greyish colour. Single crystals of crystalline silicon can be grown with a process known as the Czochralski process. These crystals, doped with boron or gallium or germanium or phosphorus or arsenic, are used in the manufacture of solid-state electronic devices, such as transistors, solar cells, rectifiers and microchips.<sup>81</sup>

But talking about silicon it is mandatory to spend some word on the most common Si compound that is the Silicon dioxide (SiO<sub>2</sub>). It usually takes the form of ordinary sand, but also exists as flint, quartz, etc. SiO<sub>2</sub> is largely used in the manufacture of glass and bricks. Silica gel, a colloidal form of SiO<sub>2</sub>, is able to absorb moisture and is then used as a desiccant. Silicon forms compounds that is possible to found in daily use as: Silicon carbide (SiC), hard as diamond and used as abrasive,<sup>82</sup> Sodium

silicate ( $\text{Na}_2\text{SiO}_3$ ), used in the production of soaps<sup>83</sup> and adhesives<sup>84</sup> and Silicon tetrachloride ( $\text{SiCl}_4$ ), used to create smoke screens. Silicon is also an important ingredient in silicones, a class of material used for such things as electrical insulators, lubricants, medical implants and polishing agents.

### 1.3.1 Silicon dioxide

As already mentioned, silicon dioxide ( $\text{SiO}_2$ ), generally named Silica (**Figure 11**), is the most common form of Silicon. Pure silica looks like a white crystalline powder, but can be found in different forms: hydrate (diatomaceous earth or kieselguhr); anhydrous (pumice stone, molten silica, quartz glass); crystalline (quartz, tridimite and cristobalite)

In these solids, the internal arrangement of the silicon and oxygen atoms can take on a regular or disorderly course. In the first case we talk about free crystalline silica. In its crystalline state each silicon atom is tetrahedron bound to 4 oxygen atoms, and each oxygen atom is tetrahedron bound to two silicon atoms (**Figure 1.11**). While in the second case we talk about free amorphous silica (hydrated and anhydrous).<sup>85</sup>

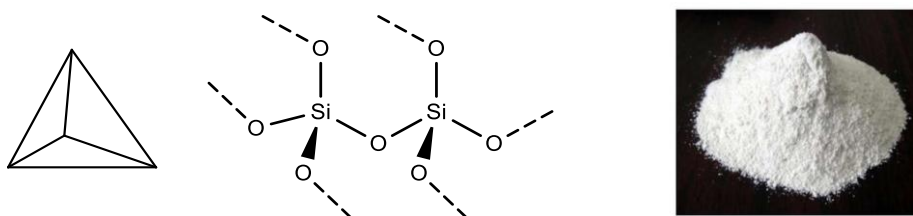


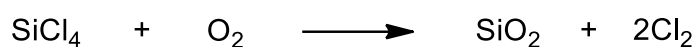
**Figure 1.11.** Schematic silica representation (left) Solid crystalline silica.

Silica is present in many minerals that, together with oxygen, make up about 75% of the earth's crust: It is present in granite and sedimentary rocks (e.g. sand, radiolites and quartzites), in marble and in various minerals in their raw state (such as plaster and quartz). The latter is the primary constituent of many volcanic, sedimentary and metamorphic rocks and represents the most common form of free crystalline silica present in nature. Cristobalite and tridimite are rarer but are present in products used by industries.



The high bonding energy leads the silica having a rather high melting temperature (1710°C) and is chemically inert (it only reacts with F<sub>2</sub>, HF and strong alkali at high temperature).

Pure silica is obtained by reaction between silicon tetrachloride and oxygen (**Scheme 1.1**) and depending on the final content of OH-groups, silica is commonly divided into dry and wet silica (respectively, low or high content of OH-groups). Pure silica gives to the water a slight acidity (a suspension of 40 g in a litre of water has a pH between 3,7 and 4,7).



**Scheme 1.1.** Preparation scheme of SiO<sub>2</sub> by burning SiCl<sub>4</sub> in an oxygen-rich hydrogen flame to produce a "smoke" of SiO<sub>2</sub>

Silica found applications in our daily life: It is used in ceramic materials<sup>86</sup> as an insulator and one example is the heat shield of space probes or space shuttles or as refractory material in ovens.<sup>87</sup> To realize the isolation oxide inside the integrated circuits, and the gate oxide of the MOSFET transistors.<sup>88</sup> Together with its derivatives it is one of the materials of choice in analytical chemistry for separating compounds by chromatography: most stationary phases for chromatography contain silica derivatives or pure silica.<sup>89</sup> SiO<sub>2</sub> is used as modern tyre component to reduce rolling resistance and improve wet grip.<sup>90</sup> Having hardness 7 in the Mohs scale is a relatively hard material, therefore it is used as an abrasive.<sup>82</sup>

Unfortunately, all that glitters are not gold. The crystalline forms of silica, in addition to be the most common in nature, are also most analysed because they are more dangerous to health and responsible for diseases of a disabling nature.<sup>91</sup> The minerals and rocks mentioned above, in fact, do not represent any kind of problem if they remain intact, but you cannot say the same when they are subject to processing. In this case, cutting, grinding, crushing and similar operations produce dust which, if inhaled, damages the lung tissue, causing serious damage to health.<sup>92</sup> Among the diseases caused by inhalation of these powders, the most common is silicosis:<sup>93</sup> lung disease responsible for lung granulomatosis (presence of granulomas in the lungs) and pulmonary fibrosis (cicatrisation of lung tissue that

interposes between the alveoli). The people most at risk of contracting this disease are people working in mines and quarries who come into contact with minerals, rocks, granite and sand; workers in steel mills, foundries and cement works; potters and glassmakers.<sup>94</sup> Depending on the duration of exposure to silica dust and the quantities inhaled, silicosis can occur in more or less severe forms ranging from chronic (the most common form that occurs after exposure of 15-20 years to low levels of silica) to acute (occurs after inhalation of high levels of silica dust, even if only for a few years).<sup>95</sup>

### 1.3.2 Mesostructured Silica

Mesoporous materials are, according to IUPAC definition, materials having pore size in the range of 2–50 nm. Mesoporous silica is synthesized by reacting tetraethyl orthosilicate with a template agent, a surfactant. By removing this one, by calcination or extraction, porosity is generated

The first article in which the words silica and mesoporous appear together is a report on the measurement of the porosity of mesoporous materials, and dates back to 1971.<sup>96</sup> The first mesoporous silica material as meant it today was reported in 1992 by Mobil Research and Development Corporation, who synthesize mesoporous solids using liquid crystal template mechanism (**Figure 1.12**). They designated it as (Mobil Crystalline Materials or Mobil Composition of Matter) MCM-41.<sup>97</sup> Six years later, silica nanoparticles with much larger pores (4.6 to 30 nm) were produced at the University of California, Santa Barbara.<sup>98</sup> The material was named Santa Barbara Amorphous type material, or SBA-15.

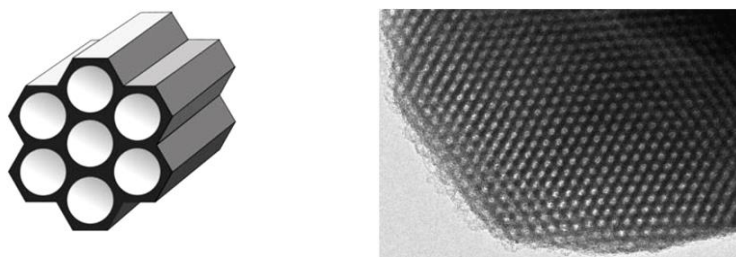


**Figure 1.12.** Schematic representation of mesoporous silica (left) and a TEM image of an SBA-15.

The pore size of the final material can be tuned by varying the surfactant used, the starting precursors and the synthesis conditions such as: source of silica, ionic strength, pH, composition of the reaction mixture, temperature and duration of synthesis. For example, MCM-41 is hexagonal with a pore diameter of 2.5 to 6 nm wherein cationic surfactants were used as templates.<sup>99</sup> Changes in the ratio between silica and surfactant are reflected to strong changes in the geometry of the pores. In fact, when the surfactant/silica ratio is less than 1, the hexagonal structure of the MCM-41 is obtained, while when this ratio is higher than 1, the result is the MCM-48, that shows a cubic arrangement.<sup>100</sup> Same concept can be applied to the synthesis of the SBA type mesoporous silica; it is possible to change geometry of the pores passing from SBA-11 (cubic) to SBA-12 (3-d hexagonal) to SBA-15 (hexagonal) and SBA-16 (cubic cage-structured) by only changing the copolymer used as templating agent and the ratio between the copolymer and the silica.<sup>98</sup>

Due to its porous and morphological characteristics, mesoporous silica found application as supports for immobilizing biomolecules, catalysts, agents for polymers reinforcement and templates for the synthesis of other materials.

Mesoporous silica (MS) are suitable materials, due to their high surface area and their organized porous structure, as stationary phases for high performance liquid or gas chromatography.<sup>101</sup> The chemical nature of the surface and the morphologic and porous properties determine the efficiency of the separation. Recently was reported a separation of a mixture of alkane (C<sub>5</sub>-C<sub>10</sub>), using a new type of pillar with mesoporous silica. A good separation performance was realized (the peak area of nonane is increased by 349.8%) by using a MS with large specific surface area as stationary phase, which would have a greatly application prospect in the micro gas chromatography system.

Ordered mesoporous silica was fabricated as a nickel catalyst support for CO methanation. This exhibited very high activity for CO methanation from 240 to 600 °C, due to the highest dispersion of Ni. In addition, the catalyst shows superior anti-coking and anti-sintering properties than the SiC catalysts used as reference. The good performance of the catalyst can be attributed to a good thermal conductivity and stability, to the confinement effect of the mesoporous structure and the strong metal-support interaction.<sup>102</sup> Also in catalysis, to prove the importance of a pre-

ordered structure, a recent work demonstrate that SBA-15 is able to improve catalytic effect of the  $\text{Bu}_4\text{NI}$  salt in the conversion of epoxides into cyclic carbonates with  $\text{CO}_2$ .<sup>103</sup> The pre-organization of reactants and catalyst on the surface leads to a decrease of the activation energy of the reaction, leading to high yields and selectivity for a wide variety of substrates under mild conditions ( $80^\circ\text{C}$ ).

### 1.3.3 Polyhedral Oligomeric Silsesquioxanes

Commonly named with their acronym, POSS, Polyhedral Oligomeric Silsesquioxanes are hollow Nanoform of silica. They are almost cubic shaped organosilicon compounds with empirical formula  $\text{RSiO}_{1.5}$  (**Figure 1.13**) where R, can be hydrogen or any alkyl, alkylene, aryl, arylene, or organofunctional derivative of alkyl, alkylene, aryl, or arylene groups.

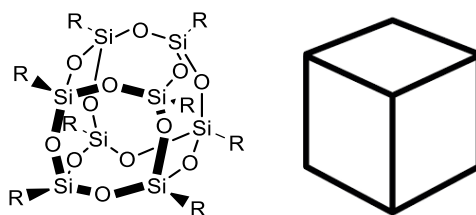


**Figure 1.13.** Schematic representation of POSS almost cubic structure.

Silsesquioxanes are known in molecular form with 6, 8, 10, or 12 Si vertices, as well as polymers and the cages are sometimes labelled  $\text{T}_6$ ,  $\text{T}_8$ ,  $\text{T}_{10}$ , and  $\text{T}_{12}$ , respectively (T = tetrahedral vertex). The term sil-sesqui-ox-ane indicates that each two silicon atoms are connected to three oxygen atoms.<sup>104</sup>

This nomenclature can be understood as follows:

- sil = silicon;
- sesqui = each Si atom is bound to an average of one and a half oxygens;
- ane = Si atom bound to one hydrocarbon group.

Polyhedral silsesquioxanes are compounds with structures based on several Si-O linkages forming a cage having a silicon atom at each vertex. Substituents on the cage are located on the eight silicon vertices. The R groups are important due to their strongly influence on the physical and chemical properties of the nanocage, while the silica core confers rigidity and thermal stability. The architecture of these

compounds varies. Although ideally the POSS have completed condensed structures (**Figure 1.14a**), however there exist also not completely condensed POSS in which in one corner a Si atom is missing (**Figure 1.14b**). In this case the oxygen atom of the hydroxy group can complex metals resulting in a so called metallasilsesquioxane. Metallasilsesquioxanes can also result in completely condensed cage structure as reported in **Figure 1.14c**.

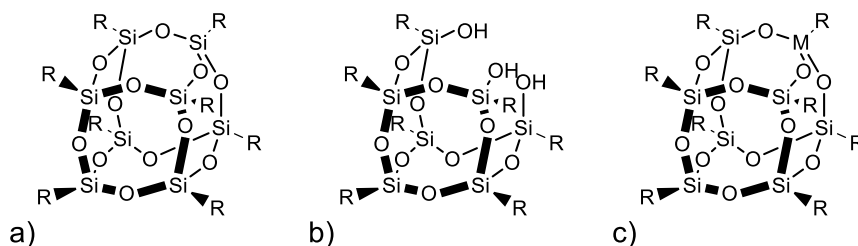
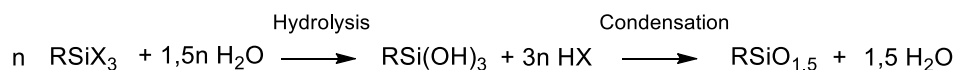


**Figure 1.14.** Different POSS structures: a) completely condensed cage, b) partially condensed and c) metallasilsesquioxane (M = metal).

Regarding their synthesis, a first preparation of a silsesquioxanes structure, obtained by hydrolysis of alkyltriethoxysilanes in water, was reported by Andrianov in 1937,<sup>105</sup> but unfortunately a misunderstanding in the publication language and a diffused distrust in eastern publications, has seen this early pioneering work not generally acknowledged. After this work, a series of silsesquioxanes were synthesized with hydrothermal treatment of organochlorosilane.<sup>106</sup> A first complete report on the preparation and characterization of a POSS dates back to 1946, when Scott described the synthesis of a  $(\text{CH}_3\text{SiO}_{1.5})_n$  obtained in a two-step synthetic process started with the hydrolysis of methyltrichlorosilane to form the trisilanol derivative, followed by condensation to form a silsesquioxane oligomer.<sup>107</sup>

The common method that is still used in the synthesis of polyhedral oligomeric silsesquioxanes, is the hydrolytic condensation of trifunctional monomers  $\text{RSiX}_3$ , where R is an organic substituent, and X is a highly reactive substituent such as Cl or alkoxy (**Scheme 1.2**).



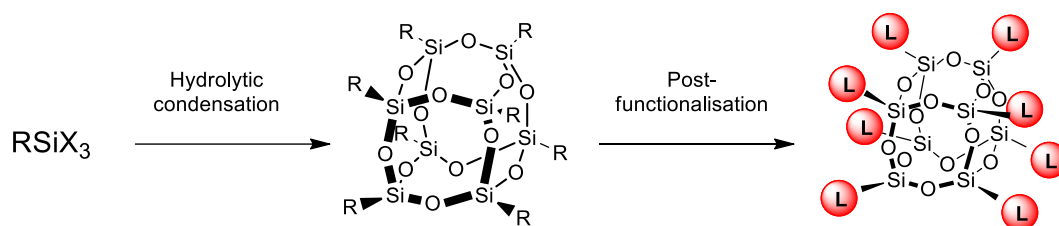
**Scheme 1.2.** Schematic sequence of reaction for the silsesquioxane condensation.

The first step of the hydrolytic condensation reaction is always the hydrolysis of the monosilane to give the corresponding trisilanol. It was then suggested, for the

second step, an intramolecular hydrogen bonding transition state<sup>108</sup> and finally an intramolecular condensation leading to the cage-like structure.<sup>109</sup>

In addition, it was found that factors that may influence the condensation reaction include the nature of the organic group R and the nature of the exit group X, but also the reaction time and temperature, the solvent used and the amount of water and, finally, the amount of silane used.<sup>110</sup>

The interesting aspect of this kind of material is that is possible to tune properly the synthetic pathway, by changing the organic moiety, in order to obtain unique organic-inorganic hybrid materials. It means inorganic oxygen-silicon scaffold with peculiar thermal and mechanical properties of the nanosilica compounds, in addition to enormous potential of the really big class of organic molecules suitable for different fields, e.g. catalysis, polymer chemistry, photochemistry, chemistry of material, biomedicine, etc.<sup>111</sup>



**Scheme 1.3.** Schematic representation of the synthetic way for the synthesis of functionalized POSS.

So basically, to obtain a given functionalised-POSS, it is possible to proceed in two different ways (**Scheme 1.3**):

- 1) to choose an organochlorosilane with the organic moiety of interest, proceeding with the hydrolytic condensation and obtaining hence a POSS that already has the organic group for the desired purposes;
- 2) to leverage the chemistry of an organic functional group in the POSS for a post-functionalization of the structure with molecule suitable for the particular needs.

#### 1.3.3.1 POSS Common applications

Looking toward its applications, one that has attracted particular attention was the use of the POSS as possible molecular heterogeneous catalyst. As soluble molecular

analogues of silica, POSS was used to mimic the structure and chemistry of bulk silica. The silsesquioxane family represents the best molecular equivalent of the silica surface. Silsesquioxane-based homogeneous models for heterogeneous catalysts offer a unique opportunity to understand heterogeneous catalysis on a molecular level. In some case these models exhibit catalytic activities comparable to, or even better than, those of commercially used heterogeneous silica-supported catalysts.<sup>112</sup>

There are two ways to use POSS as catalysts: a) metallasilsesquioxanes and b) as molecular scaffold for the catalyst.

About metallasilsesquioxanes, Duchateau reported the use of an incompletely condensed POSS, a silsesquioxane disilanol complexed with a Zn species.<sup>113</sup> The complex was tested as catalyst for the copolymerization of cyclohexene oxide and CO<sub>2</sub> (**Figure 1.15**).

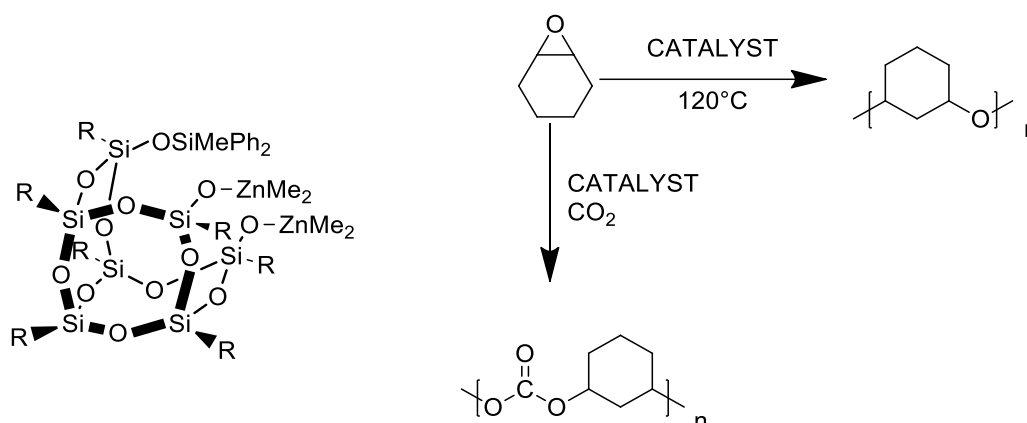


**Figure 1.15.** Example of uncondensed POSS-Zn based catalyst.

At 120°C, in the absence of CO<sub>2</sub>, the complex promotes the homo-polymerization of cyclohexene oxide to poly(cyclohexene oxide). Otherwise, in presence of carbon dioxide the promoted reaction is the formation of the poly(cyclohexene carbonate). Remaining within the area of CO<sub>2</sub> valorisation, our group of investigation recently reported a POSS functionalized with imidazolium chloride moieties used as catalyst for the conversion of CO<sub>2</sub> and epoxides into cyclic carbonates (**Figure 1.16**) with excellent results in terms of yields and selectivity.<sup>114</sup>

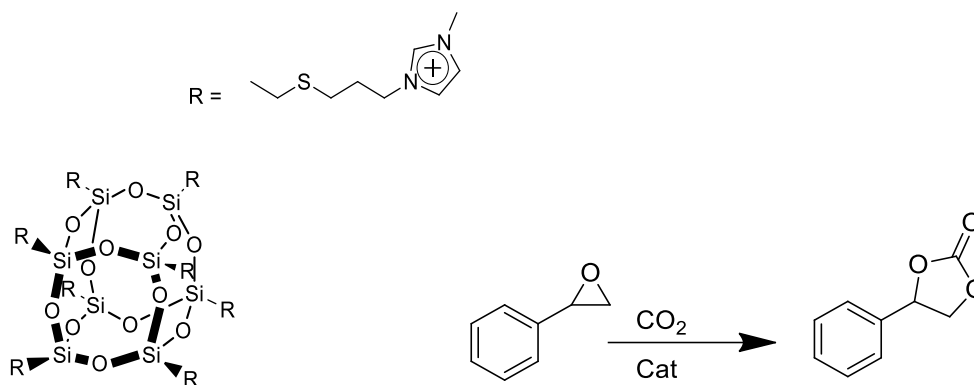


**Figure 1.16.** Example of POSS used as molecular scaffold for catalyst.

The catalyst displayed excellent catalytic performances in the synthesis of styrene carbonate and, under the best reaction conditions, an almost total conversion and complete selectivity was obtained. Moreover, the catalyst was recovered by simple extraction from the reaction mixture, demonstrating that the use of molecular nanoform of silica can act successfully as a bulk, easy recoverable, catalyst.

The use of POSS as a substituent in polymers and copolymers is an area of research that has gained great popularity in recent years.<sup>115</sup> The idea to have a high thermally and mechanically stable building block to insert in polymer matrixes to improve properties of the resulting polymeric materials, stimulated scientist all over the world. POSS copolymers have been synthesized by free radical polymerization,<sup>116</sup> anionic polymerization,<sup>117</sup> ring-opening metathesis polymerization,<sup>118</sup> step-growth polymerization,<sup>119</sup> grafting,<sup>120</sup> etc.

POSS -based polymers found application in different fields. Monovinyl-functional silsesquioxane cage was copolymerized with ethene and propene (**Figure 1.17**) to give high molar mass copolymers containing pendant octasiloxane cubes.<sup>121</sup>

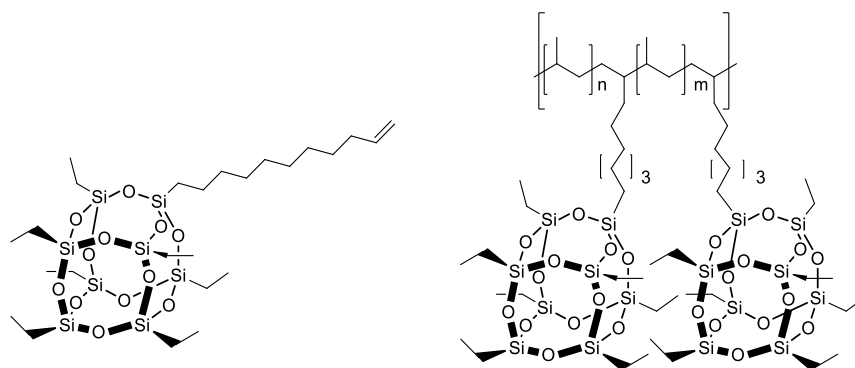


**Figure 1.17.** Schematic representation of POSS-based polymers.



Incorporation up to 25 wt % (1.2 mol %) of the POSS-based monomer accounted for:

- a decrease of the melting temperature with respect to polyethene;
- improvement of the thermostability under air in the polyethene copolymer in comparison to polyethene.

The novel copolymers poly(ethene-co-decanyl heptaethyl octasiloxane) and poly(propene-co-decanyl heptaethyl octasiloxane) are interesting materials with respect to the effect of T<sub>8</sub> cage as a structural irregularity on the crystallization and morphology of polypropene and polyethene.

As already mentioned, owing to their biocompatibility and ability to be easily incorporated into different polymers, POSS can be used in various biomedical applications. Thanks to their inert nature and low inflammatory response, POSS frameworks, consisting of Si-O and Si-C, are very similar to that of silicone which was used since the 1960s in breast implants.<sup>122</sup> An interesting application reported the use of nanocomposite material for cardiovascular implants obtained introducing POSS moieties into poly(carbonate-urea)urethane (POSS-PCU) as a pendent chain group.<sup>123</sup> The material was successfully employed for the construction of a prototype of a trileaflet heart valve.

POSS found application also in electronics<sup>124</sup> and energy applications. They are used as materials to enhance performance in various electronic, optical and energy-related applications such as their use in liquid crystal phase in LC devices, in light-emitting, in fabrication of electronic and optical devices in sensor systems, and in fuel cell membranes and battery electrolytes.<sup>125</sup>

Starting from the 90's, a series of vinyl-functionalized mesogens POSS, were synthesized with the idea of create a range of side-chain liquid crystalline polysiloxanes<sup>126</sup> exploiting the flexibility of the POSS backbone as an advantage in allowing mesogens to align (**Figure 1.18**). In 1999 Mehl *et al.* reported the use of an octa(hydridosilsesquioxane), Si<sub>8</sub>O<sub>12</sub>H<sub>8</sub> (T<sub>8</sub>H<sub>8</sub>) to prepare liquid crystal.<sup>127</sup>

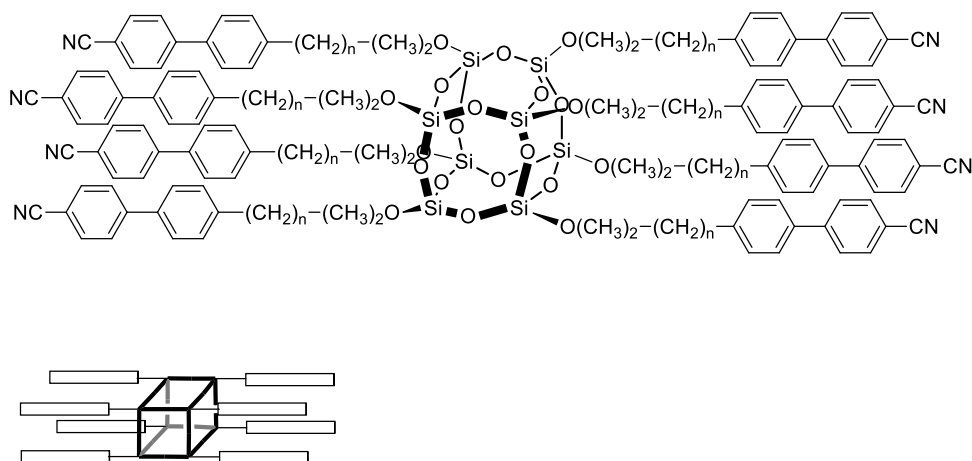


**Figure 1.18.** POSS-based LC. The POSS imparts right shape to the structure.

They used the  $T_8$  symmetry of the POSS with its almost cubic shape to provide the right shape to liquid crystals allowing the tailoring of glass transition temperatures, the type of liquid-crystalline phases and phase transition temperatures over a wide temperature range.

The use of POSS in electronics is not limited in LC applications. POSS structures Properly functionalized, with chromophores and fluorophores were extensively investigated as electroluminescent (EL) materials, or as sensors in order to improve performance, lifetime, stability and colour balance of the unsupported common materials (analogues?). The idea lies in the fact that all photoluminescent materials, which can be light emitting diode (LED), organic light emitting diode (OLED), electroluminescent displays, solar cells, photovoltaics, sensors, thin film organic transistors, lasers and light-emitting electrochemical cells, can undergo degradation due to the formation of aggregates, excimers and simply physical degradation of the material itself. The strategy is to introduce in the structure the POSS as support, improving the stability of the final product.

As often happens, the need to make improvements to a device derives from some problems inherent in the device itself. For example it just to think of the much-needed blue emission in OLED technology.<sup>104</sup> One of the most studied organic fluorophores for this kind of emission is the PFO (polydiocetylfluorene).<sup>128</sup> PFO and its derivatives are widely used as blue light emitters because they have high solid-state quantum yields, good solubility, and good chemical and thermal stability. Unfortunately, lateral chains of the PFO aggregate each other causing formation of

lower wavelength emitting excimers responsible of undesirable blue-green light emission, and in quenching. The functionalization of the PFO on a  $\text{Si}_8\text{O}_{12}$  led to the formation of a material in which the thermal stability was enhanced by  $50^\circ\text{C}$  and the solubility in organic solvent and the coating quality were improved. It is worth noting that the POSS reduced the excimer emission.<sup>129</sup>

In the field of sensors, Hartmann-Thompson reported a series of POSS nanosensors functionalized with fluorophores (**Figure 1.19**).<sup>130</sup>

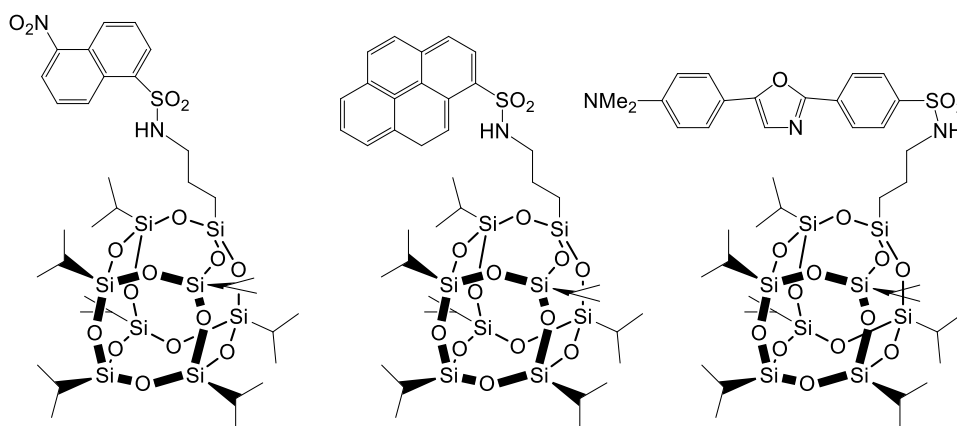


**Figure 1.19.** POSS used as support for fluorophores.

Each nanosensor is functionalized with a different wavelength shifting fluorophore and it was used to generate fingerprints for a diverse range of analytes, including common organic solvents, toxic industrial chemicals (TICs) and chemical warfare agent simulants. POSS was used first for its ability to form aerosols, making it suitable for threat cloud applications and as suitable nanoscaffold to generate a system with more sensor groups per unit of mass and greater sensitivity than a microscaffold system.

Remaining in the field of the photophysics, recently Liu *et al.* reported the synthesis of an octa functionalized POSS with eight azobenzene moieties (**Figure 1.20**).<sup>131</sup>

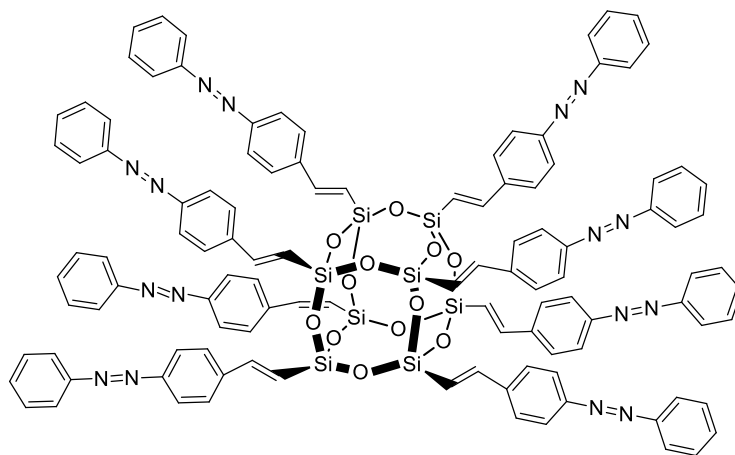


**Figure 1.20.** Octa-azabenzene-POSS

They demonstrated the good thermal stability of the inert support together with good emission of the fluorophores that exhibited fluorescence emission at 400 nm, making this material suitable for blue emitting devices.

Furthermore, Li *et al.* proved that octa functionalized POSS can be a good candidate for emitting not only alone but in a 3D polymer. They obtained a dendrimer with  $\beta$ -diketone-substituted POSS able to complex Eu and Tb ions to achieve novel photoluminescent materials (**Figure 1.21**).<sup>132</sup>

They finally incorporated the dendrimer in a poly(methyl methacrylate) matrix to obtain hybrid emitting nanocomposites with high thermal stability.

In the present Thesis, POSS will be presented as scaffold for novel organic-inorganic photoluminescent materials. In particular an eight branched silsesquioxane opportunely functionalized with a ligand displaying high ability to complex metals fluorophore, will be present as promising solid-state emitting material and as sensor for metals.

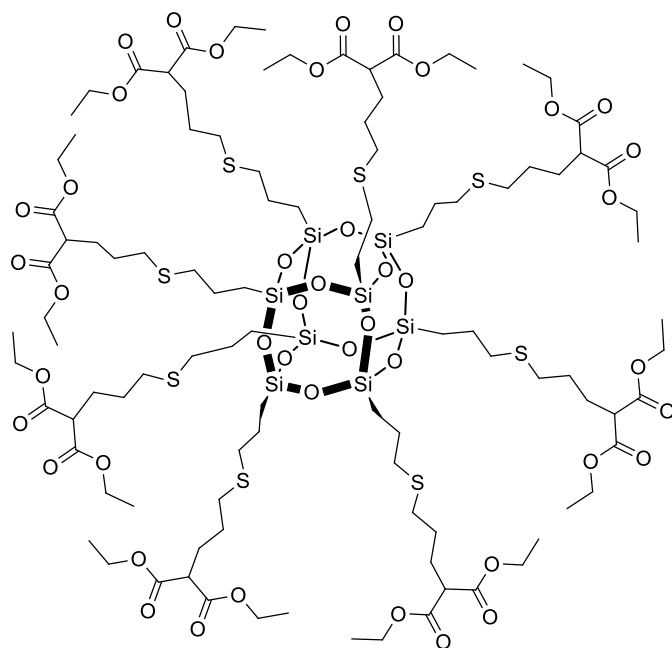


**Figure 1.21.** Octa- $\beta$ -diketone-substituted POSS

## 1.4 Aim of the Thesis

What was discussed in the introduction led to the idea that both carbon and silica Nanoforms, or rather silica in the case of POSS, can be extensively used for a wide variety of purposes. Here specifically, the  $C_{60}$  fullerene and the Polyhedral Oligomeric Silsesquioxanes (POSS) were chosen as representatives of the two respective groups of Nanoforms.

The idea is to use both cages to obtain nano building blocks with well-established geometry that will be used in catalysis or in the creation of photoluminescent (PL) materials. In fact, both nano-cages are suitable to be functionalized in order to achieve materials with a cubic or an octahedral or pseudo-octahedral geometry (**Figure 1.22**).

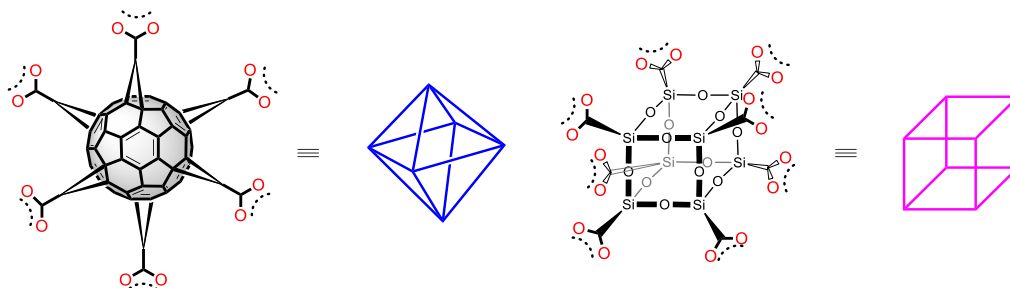


**Figure 1.22.** Schematic representation of the  $C_{60}$  octahedral (left) and POSS cubic (right) building blocks.

Regarding the fullerene, the idea was to functionalize  $C_{60}$  with molecules of catalytic interest and in particular, chiral molecules for enantioselective catalysis. Bisoxazoline (BOX) ligands that are (once complexed with a metal) widely used in asymmetric catalysis, were selected as suitable ligand to functionalise the fullerene cage<sup>133</sup> (**Figure 1.23**).



**Figure 1.23.**  $C_{60}$  fullerene support (left) and BOX-type ligand chosen to build novel catalytic systems.

The idea behind is trying to use the  $C_{60}$  fullerene as molecular scaffold instead of the common bulk supports for catalysts. In fact, usual bulk supports used to anchor

catalysts make these last heterogeneous with all the advantages and disadvantages. Although heterogeneous catalysts are useful because allow an easy separation of the catalysts from the reaction media making them reusable, they have a reduced activity in terms of interaction with the substrates.<sup>134</sup> On the other hand, a molecular scaffold can confer to the catalyst a double advantage. Firstly, it can thought as a homogeneous catalyst, since it gain the solubility profile that one want to confer to the catalytic system allowing him to work in solution closely to the substrates resulting in an more efficient catalysis and, once ended the reaction, it can be recovered by precipitation by changing the polarity of the reaction media. In addition, there is the possibility to functionalize the support in order to change the catalytic loading, allowing to drastically reduce the amount of support used. Here, for all these purposes, C<sub>60</sub> fullerene was selected as support because it can be easily functionalized with organic molecules forming multiple adduct and because of its easier separation from the reaction mixture which can allow a facile reuse in multiple cycles.<sup>74</sup>

Therefore, different BOX ligands, which differ in the type of substituent on the oxazoline moiety were synthesized in order to obtain different systems to test as catalytic systems.

In particular fullerene was functionalized to obtain three different series of catalytic systems (**Figure 1.24**) with three different solubility profiles and all the systems were tested in asymmetric Henry and Diels-Alder reactions.

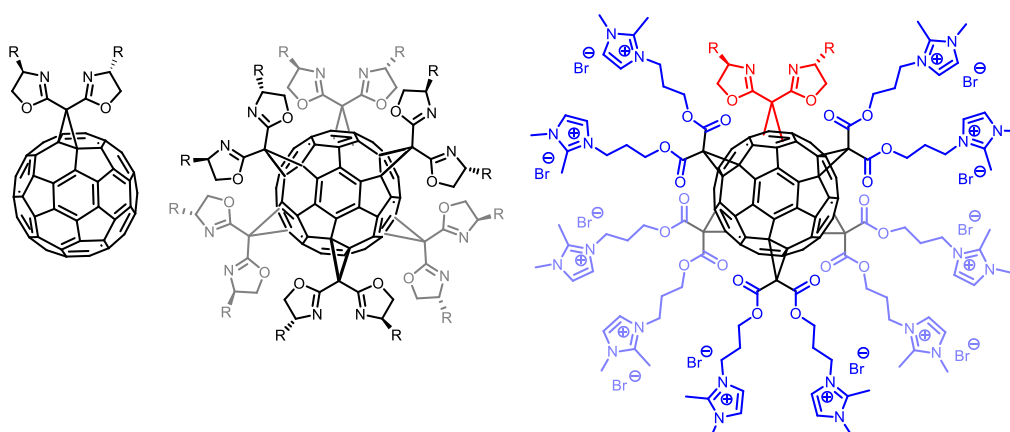


**Figure 1.24.** C<sub>60</sub>-BOX based catalyst synthesized: C<sub>60</sub>-Monoadduct (C<sub>60</sub>-BOX), C<sub>60</sub>-Hexakisadduct (C<sub>60</sub>-BOX<sub>6</sub>) and Ionic liquid hybrid (C<sub>60</sub>-IL<sub>10</sub>-BOX).

Moreover, due to excellent ability of the BOX in complexing metals, a second goal was to use the Hexa-adduct of the  $C_{60}$ , leveraging its octahedral geometry, to prepare a self-assembled 3D material with peculiar properties (**Figure 1.25**).

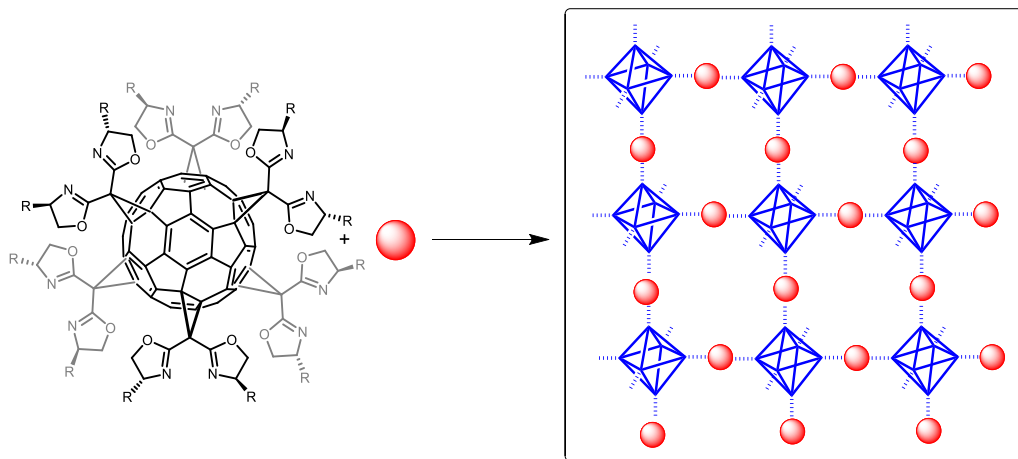


**Figure 1.25.** Schematic representation of the 3D self-assembled  $C_{60}$ -BOX<sub>6</sub>-M.

In particular the idea is to complex the  $C_{60}$  hexakis-adduct with a light emitting behaviour metal to have a novel three-dimensional material with photoluminescent properties. Due to the excellent light-emitting performance of the lanthanides,<sup>135</sup> the attention was focused to this series and in particular to, Eu trivalent ions which usually exhibit intense emission bands from  $f-f$  electronic transitions.<sup>136</sup> Since also the POSS has a rigid scaffold, with well-established geometry, the idea to use it as possible building block to prepare self-assembled 3D structure in presence of a metal was take into account (**Figure 1.26**).

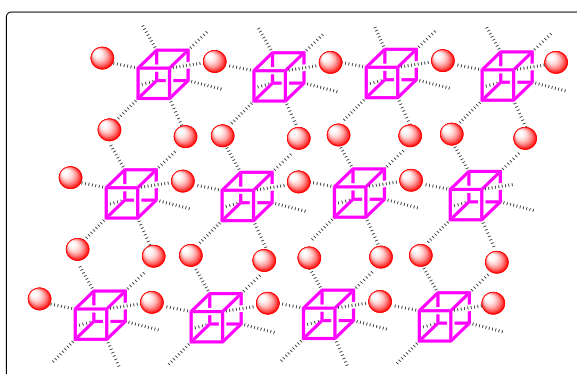


**Figure 1.26.** Hypothetical 3D POSS-M self-assembled structure.



Part of the work was then dedicated to the synthesis of materials based on polyhedral oligomeric silsesquioxanes functionalized with a derivative of terpyridine. Mono- and octa-vinyl-POSS (MV and OV, respectively, in **Figure 1.27**) were selected as building units. The presence of the double bond on both structures may allow obtaining complexes in which the final properties can be tuned via the *trans* to *cis* isomerization of this group. Both POSS nanocages were functionalized with 4'-phenyl-2,2':6',2''-terpyridine moieties chosen for their extraordinary binding affinity toward several metal ions.

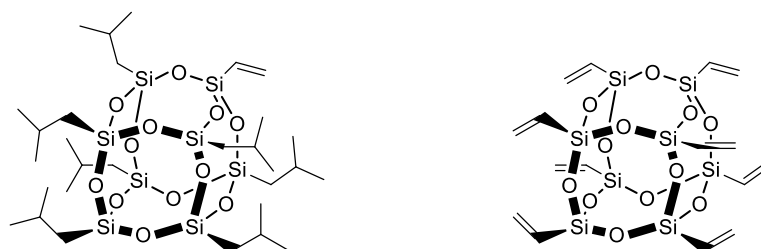


**Figure 1.27** Monovinyl-isobutyl substituted POSS (MV), Octavinyl POSS (OV).

The materials obtained by the complexation of the POSS-Terpyridine based systems were studied as possible sensor for metals and as photoluminescent materials. Herein, not only the Europium was used as light-emitting metal centre, but a complete screening of all the members of the lanthanides family was made with exciting result.

Just to summarize, the goal of the present work was to play with two different hallow nano caged scaffolds, opportunely functionalized, to synthesized innovative molecular materials useful in the field of catalysis and in the field of sensors and photoluminescent materials by complexing the resulting material with right metals (**Figure 1.28**).

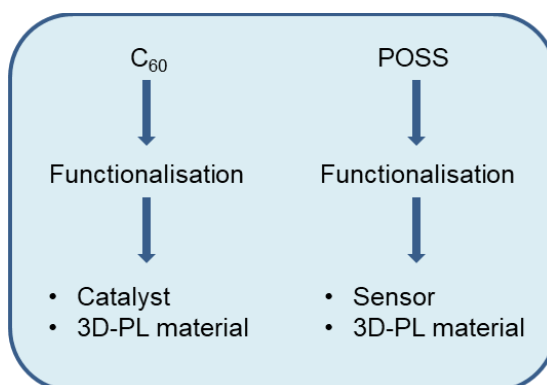


**Figure 1.28.** Working plan.

## 1.5 References

1. Irshad, A. W., Nanomaterials, Novel Preparation Routes, and Characterizations. In *Nanotechnology Applications for Improvements in Energy Efficiency and Environmental Management*, IGI Global: Hershey, PA, USA, 2015; pp 1-40.
2. (a) Lead, J. R.; Wilkinson, K. J., Aquatic Colloids and Nanoparticles: Current Knowledge and Future Trends. *Environ. Chem. Lett.* **2006**, *3* (3), 159-171; (b) Hough, R. M.; Noble, R. R. P.; Reich, M., Natural gold nanoparticles. *Ore Geol. Rev.* **2011**, *42* (1), 55-61.
3. Gleiter, H., Nanostructured materials: basic concepts and microstructure. *Acta Mater.* **2000**, *48* (1), 1-29.
4. Pokropivny, V. V.; Skorokhod, V. V., Classification of nanostructures by dimensionality and concept of surface forms engineering in nanomaterial science. *Mat. Sci. Eng. C* **2007**, *27* (5), 990-993.
5. (a) Hochella, M. F.; Spencer, M. G.; Jones, K. L., Nanotechnology: nature's gift or scientists' brainchild? *Environ. Sci. Nano* **2015**, *2* (2), 114-119; (b) Sharma, V. K.; Filip, J.; Zboril, R.; Varma, R. S., Natural inorganic nanoparticles – formation, fate, and toxicity in the environment. *Chem. Soc. Rev.* **2015**, *44* (23), 8410-8423.
6. Wagner, S.; Gondikas, A.; Neubauer, E.; Hofmann, T.; von der Kammer, F., Spot the Difference: Engineered and Natural Nanoparticles in the Environment—Release, Behavior, and Fate. *Angew. Chem. Int. Ed.* **2014**, *53* (46), 12398-12419.
7. Zhong, J.; Zhang, H.; Sun, X.; Lee, S. T., Synchrotron Soft X-ray Absorption Spectroscopy Study of Carbon and Silicon Nanostructures for Energy Applications. *Adv. Mater.* **2014**, *26* (46), 7786-7806.
8. Tans, S. J.; Verschueren, A. R. M.; Dekker, C., Room-temperature transistor based on a single carbon nanotube. *Nature* **1998**, *393* (6680), 49-52.
9. Gudixsen, M. S.; Lauhon, L. J.; Wang, J.; Smith, D. C.; Lieber, C. M., Growth of nanowire superlattice structures for nanoscale photonics and electronics. *Nature* **2002**, *415* (6872), 617-620.

10. Kong, J.; Franklin, N. R.; Zhou, C.; Chapline, M. G.; Peng, S.; Cho, K.; Dai, H., Nanotube Molecular Wires as Chemical Sensors. *Science* **2000**, *287* (5453), 622-625.
11. (a) Baughman, R. H.; Zakhidov, A. A.; de Heer, W. A., Carbon Nanotubes—the Route Toward Applications. *Science* **2002**, *297* (5582), 787-792; (b) He, Y.; Fan, C.; Lee, S.-T., Silicon nanostructures for bioapplications. *Nano Today* **2010**, *5* (4), 282-295.
12. (a) Kang, Z.; Liu, Y.; Tsang, C. H. A.; Ma, D. D. D.; Fan, X.; Wong, N.-B.; Lee, S.-T., Water-Soluble Silicon Quantum Dots with Wavelength-Tunable Photoluminescence. *Adv. Mater.* **2009**, *21* (6), 661-664; (b) Pan, X.; Bao, X., The Effects of Confinement inside Carbon Nanotubes on Catalysis. *Acc. Chem. Res.* **2011**, *44* (8), 553-562.
13. (a) Ji, L.; Rao, M.; Zheng, H.; Zhang, L.; Li, Y.; Duan, W.; Guo, J.; Cairns, E. J.; Zhang, Y., Graphene Oxide as a Sulfur Immobilizer in High Performance Lithium/Sulfur Cells. *J. Am. Chem. Soc.* **2011**, *133* (46), 18522-18525; (b) Sim, S.; Oh, P.; Park, S.; Cho, J., Critical Thickness of SiO<sub>2</sub> Coating Layer on Core@Shell Bulk@Nanowire Si Anode Materials for Li-Ion Batteries. *Adv. Mater.* **2013**, *25* (32), 4498-4503.
14. (a) Shen, X.; Sun, B.; Liu, D.; Lee, S.-T., Hybrid Heterojunction Solar Cell Based on Organic–Inorganic Silicon Nanowire Array Architecture. *J. Am. Chem. Soc.* **2011**, *133* (48), 19408-19415; (b) Song, X.; Hua, W.; Ma, Y.; Wang, C.; Luo, Y., Theoretical Study of Core Excitations of Fullerene-Based Polymer Solar Cell Acceptors. *J. Phys. Chem. C* **2012**, *116* (45), 23938-23944.
15. Lavinsky, D. R., *Crystalline treasure book*. The Arkenstone: **2013**.
16. Smith, A. H. V., Provenance of Coals from Roman Sites in England and Wales. *Britannia* **2011**, *28*, 297-324.
17. Fernihough, A., Coal and the european industrial revolution. *NBER* **2014**, *19802*.
18. Britannica, E., Carbon.
19. (a) Jones, D. T.; Wheeler, R. V., LIX.—The constitution of coal. *J. Chem. Soc., Trans.* **1916**, *109* (0), 707-714; (b) Major, T. J., *Genesis and the origin of coal and oil*. Apologetics Press, Inc. : **1996**.

20. Werner, A. G., Complete Dictionary of Scientific Biography. In *Encyclopedia.com*.
21. (a) Delhaes, P., *Graphite and Precursors*. Taylor & Francis: **2000**; (b) Pierson, H. O., *Handbook of Carbon, Graphite, Diamonds and Fullerenes: Processing, Properties and Applications*. Elsevier Science: **2012**.
22. Burns, R. M.; Hulett, G. A., Some properties of graphite. *J. Am. Chem. Soc.* **1923**, *45* (3), 572-578.
23. Armand, M.; Touzain, P., Graphite intercalation compounds as cathode materials. *Mat. Sci. Eng.* **1977**, *31* (C), 319-329.
24. Ralph, E. L.; Linder, E. B. In *Advanced solar panel designs*, Conference Record of the Twenty Fifth IEEE Photovoltaic Specialists Conference - 1996, 13-17 May 1996; **1996**; pp 297-300.
25. Bragg, W. H.; Bragg, W. L., The Structure of the Diamond. *Nature* **1913**, *91* (2283), 557-557.
26. Halliday, D.; Resnick, R.; Walker, J., *Fundamentals of Physics*. Wiley: **2002**.
27. Robert F. Curl, H. K., Richard E. Smalley The Nobel Prize in Chemistry 1996. <https://www.nobelprize.org/prizes/chemistry/1996/press-release/>.
28. David, E. H. J.; Wasserman, E.; Applewhite, E. J.; Kroto, H. W.; Iijima, S.; Haddon, R. C.; Pillinger, C. T., Dreams in a Charcoal Fire: Predictions about Giant Fullerenes and Graphite Nanotubes [and Discussion]. *Phil. Trans. Phys. Sci. Eng.* **1993**, *343* (1667), 9-18.
29. Barth, W. E.; Lawton, R. G., Dibenzo[ghi,mno]fluoranthene. *J. Am. Chem. Soc.* **1966**, *88* (2), 380-381.
30. (a) Osawa, E., Superaromaticity. *Kagaku (Kyoto, Japan)* **1970**, *25* (9), 854-863; (b) Z. Yoshida, Z. O., *Kagakudojin: Kyoto* **1971**, 174.
31. Rohlfing, E. A.; Cox, D. M.; Kaldor, A., Production and characterization of supersonic carbon cluster beams. *J. Chem. Phys.* **1984**, *81* (7), 3322-3330.
32. Kroto, H. W.; Heath, J. R.; O'Brien, S. C.; Curl, R. F.; Smalley, R. E., C<sub>60</sub>: Buckminsterfullerene. *Nature* **1985**, *318* (6042), 162-163.
33. Iijima, S., Helical microtubules of graphitic carbon. *Nature* **1991**, *354* (6348), 56-58.

34. Suarez-Martinez, I.; Grobert, N.; Ewels, C., *Encyclopedia of Carbon Nanoforms*. **2012**; pp 1-65.
35. Geim, A. K.; Novoselov, K. S., The rise of graphene. *Nat. Mater.* **2007**, *6* (3), 183-191.
36. Geim, A.; Novoselov, K. The Nobel Prize in Physics 2010. <https://www.nobelprize.org/prizes/physics/2010/summary/>.
37. Novoselov, K. S.; Geim, A. K.; Morozov, S. V.; Jiang, D.; Zhang, Y.; Dubonos, S. V.; Grigorieva, I. V.; Firsov, A. A., Electric Field Effect in Atomically Thin Carbon Films. *Science* **2004**, *306* (5696), 666-669.
38. Hernandez, Y.; Nicolosi, V.; Lotya, M.; Blighe, F. M.; Sun, Z.; De, S.; McGovern, I. T.; Holland, B.; Byrne, M.; Gun'Ko, Y. K.; Boland, J. J.; Niraj, P.; Duesberg, G.; Krishnamurthy, S.; Goodhue, R.; Hutchison, J.; Scardaci, V.; Ferrari, A. C.; Coleman, J. N., High-yield production of graphene by liquid-phase exfoliation of graphite. *Nat. Nanotechnol.* **2008**, *3* (9), 563-568.
39. Berger, C.; Song, Z.; Li, T.; Li, X.; Ogbazghi, A. Y.; Feng, R.; Dai, Z.; Marchenkov, A. N.; Conrad, E. H.; First, P. N.; de Heer, W. A., Ultrathin Epitaxial Graphite: 2D Electron Gas Properties and a Route toward Graphene-based Nanoelectronics. *J. Phys. Chem. B* **2004**, *108* (52), 19912-19916.
40. Berger, C.; Song, Z.; Li, X.; Wu, X.; Brown, N.; Naud, C.; Mayou, D.; Li, T.; Hass, J.; Marchenkov, A. N.; Conrad, E. H.; First, P. N.; de Heer, W. A., Electronic Confinement and Coherence in Patterned Epitaxial Graphene. *Science* **2006**, *312* (5777), 1191-1196.
41. Pang, S.; Hernandez, Y.; Feng, X.; Müllen, K., Graphene as Transparent Electrode Material for Organic Electronics. *Adv. Mater.* **2011**, *23* (25), 2779-2795.
42. (a) Diker, H.; Bozkurt, H.; Varlikli, C., Dispersion stability of amine modified graphene oxides and their utilization in solution processed blue OLED. *Chem. Eng. Trans.* **2020**, *381*, 122716; (b) Chen, D.; Chen, S.; Yue, S.; Lu, B.; Pan, X.; He, H.; Ye, Z., N-ZnO nanorod arrays/p-GaN light-emitting diodes with graphene transparent electrode. *J. Lumin.* **2019**, *216*, 116719.
43. Vlasov, A. I.; Terent'ev, D. S.; Shakhnov, V. A., Graphene flexible touchscreen with integrated analog-digital converter. *Russian Microelectronics* **2017**, *46* (3), 192-199.

44. Rafiee, M. A.; Rafiee, J.; Wang, Z.; Song, H.; Yu, Z.-Z.; Koratkar, N., Enhanced Mechanical Properties of Nanocomposites at Low Graphene Content. *ACS Nano* **2009**, *3* (12), 3884-3890.
45. Huard, B.; Sulpizio, J. A.; Stander, N.; Todd, K.; Yang, B.; Goldhaber-Gordon, D., Transport Measurements Across a Tunable Potential Barrier in Graphene. *Phys. Rev. Lett.* **2007**, *98* (23), 236803.
46. Gong, K.; Yan, Y.; Zhang, M.; Su, L.; Xiong, S.; Mao, L., Electrochemistry and Electroanalytical Applications of Carbon Nanotubes: A Review. *Anal. Sci.* **2005**, *21* (12), 1383-1393.
47. Xie, X.-L.; Mai, Y.-W.; Zhou, X.-P., Dispersion and alignment of carbon nanotubes in polymer matrix: A review. *Mat. Sci. Eng. R* **2005**, *49* (4), 89-112.
48. Romanishina, S. A.; Barchukov, D. A.; Slobodyan, S. M. In *The Stability of Single-Walled Carbon Nanotube: Lyapunov Function for Probe Needle*, 2019 IEEE 39th International Conference on Electronics and Nanotechnology (ELNANO), 16-18 April 2019; **2019**; pp 21-25.
49. Rinzler, A. G.; Hafner, J. H.; Nikolaev, P.; Nordlander, P.; Colbert, D. T.; Smalley, R. E.; Lou, L.; Kim, S. G.; Tománek, D., Unraveling Nanotubes: Field Emission from an Atomic Wire. *Science* **1995**, *269* (5230), 1550-1553.
50. (a) Tamersit, K.; Djeflal, F., Carbon Nanotube Field-Effect Transistor With Vacuum Gate Dielectric for Label-Free Detection of DNA Molecules: A Computational Investigation. *IEEE Sens. J.* **2019**, *19* (20), 9263-9270; (b) Freitag, M.; Johnson, A. T.; Kalinin, S. V.; Bonnell, D. A., Role of Single Defects in Electronic Transport through Carbon Nanotube Field-Effect Transistors. *Phys. Rev. Lett.* **2002**, *89* (21), 216801.
51. Rasheed, T.; Nabeel, F.; Adeel, M.; Rizwan, K.; Bilal, M.; Iqbal, H. M. N., Carbon nanotubes-based cues: A pathway to future sensing and detection of hazardous pollutants. *J. Mol. Liq.* **2019**, *292*, 111425.
52. (a) Tessonnier, J.-P.; Pesant, L.; Ehret, G.; Ledoux, M. J.; Pham-Huu, C., Pd nanoparticles introduced inside multi-walled carbon nanotubes for selective hydrogenation of cinnamaldehyde into hydrocinnamaldehyde. *Appl. Catal. A-GEN* **2005**, *288* (1), 203-210; (b) Nhut, J.-M.; Pesant, L.; Tessonnier, J.-P.; Winé, G.; Guille, J.; Pham-Huu, C.; Ledoux, M.-J., Mesoporous carbon nanotubes for use as

support in catalysis and as nanosized reactors for one-dimensional inorganic material synthesis. *Appl. Catal. A-GEN* **2003**, 254 (2), 345-363; (c) Serp, P.; Corrias, M.; Kalck, P., Carbon nanotubes and nanofibers in catalysis. *Appl. Catal. A-GEN* **2003**, 253 (2), 337-358.

53. Dillon, A. C.; Jones, K. M.; Bekkedahl, T. A.; Kiang, C. H.; Bethune, D. S.; Heben, M. J., Storage of hydrogen in single-walled carbon nanotubes. *Nature* **1997**, 386 (6623), 377-379.

54. Seyfoori, A.; Sarfarazijami, S.; Seyyed Ebrahimi, S. A., pH-responsive carbon nanotube-based hybrid nanogels as the smart anticancer drug carrier. *Artif. Cell. Nanomed. B* **2019**, 47 (1), 1437-1443.

55. Krätschmer, W.; Lamb, L. D.; Fostiropoulos, K.; Huffman, D. R., Solid C60: a new form of carbon. *Nature* **1990**, 347 (6291), 354-358.

56. (a) Haufler, R. E.; Conceicao, J.; Chibante, L. P. F.; Chai, Y.; Byrne, N. E.; Flanagan, S.; Haley, M. M.; O'Brien, S. C.; Pan, C.; et al., Efficient production of C60 (buckminsterfullerene), C60H36, and the solvated buckide ion. *J. Phys. Chem.* **1990**, 94 (24), 8634-8636; (b) Cyvin, S. J.; Brendsdal, E.; Cyvin, B. N.; Brunvoll, J., Molecular vibrations of footballene. *Chem. Phys. Lett.* **1988**, 143 (4), 377-380.

57. (a) Chibante, L. P. F.; Thess, A.; Alford, J. M.; Diener, M. D.; Smalley, R. E., Solar generation of the fullerenes. *J. Phys. Chem.* **1993**, 97 (34), 8696-8700; (b) Fields, C. L.; Pitts, J. R.; Hale, M. J.; Bingham, C.; Lewandowski, A.; King, D. E., Formation of fullerenes in highly concentrated solar flux. *J. Phys. Chem.* **1993**, 97 (34), 8701-8702.

58. (a) Peters, G.; Jansen, M., A New Fullerene Synthesis. *Angew. Chem. Int. Ed.* **1992**, 31 (2), 223-224; (b) Jenkins, G. M.; Holland, L. R.; Maleki, H.; Fisher, J., Continuous production of fullerenes by pyrolysis of acetylene at a glassy carbon surface. *Carbon* **1998**, 36 (12), 1725-1727; (c) Todorovic-Marković, B.; Marković, Z.; Mohai, I.; Károly, Z.; Gál, L.; Föglein, K.; Szabó, P. T.; Szépvölgyi, J., Efficient synthesis of fullerenes in RF thermal plasma reactor. *Chem. Phys. Lett.* **2003**, 378 (3), 434-439.

59. Howard, J. B.; McKinnon, J. T.; Makarovsky, Y.; Lafleur, A. L.; Johnson, M. E., Fullerenes C60 and C70 in flames. *Nature* **1991**, 352 (6331), 139-141.

60. (a) Schulman, J. M.; Disch, R. L.; Miller, M. A.; Peck, R. C., Symmetrical clusters of carbon atoms: The C<sub>24</sub> and C<sub>60</sub> molecules. *Chem. Phys. Lett.* **1987**, *141* (1), 45-48; (b) Lüthi, H. P.; Almlöf, J., AB initio studies on the thermodynamic stability of the icosahedral C<sub>60</sub> molecule “buckminsterfullerene”. *Chem. Phys. Lett.* **1987**, *135* (4), 357-360; (c) Scuseria, G. E., Ab initio theoretical predictions of the equilibrium geometries of C<sub>60</sub>, C<sub>60</sub>H<sub>60</sub> and C<sub>60</sub>F<sub>60</sub>. *Chem. Phys. Lett.* **1991**, *176* (5), 423-427; (d) Häser, M.; Almlöf, J.; Scuseria, G. E., The equilibrium geometry of C<sub>60</sub> as predicted by second-order (MP2) perturbation theory. *Chem. Phys. Lett.* **1991**, *181* (6), 497-500; (e) David, W. I. F.; Ibberson, R. M.; Matthewman, J. C.; Prassides, K.; Dennis, T. J. S.; Hare, J. P.; Kroto, H. W.; Taylor, R.; Walton, D. R. M., Crystal structure and bonding of ordered C<sub>60</sub>. *Nature* **1991**, *353* (6340), 147-149.
61. Echegoyen, L.; Echegoyen, L. E., Electrochemistry of Fullerenes and Their Derivatives. *Acc. Chem. Res.* **1998**, *31* (9), 593-601.
62. Hirsch, A.; Brettreich, M.; Wudl, F., *Fullerenes: Chemistry and Reactions*. Wiley: **2005**.
63. (a) Langa, F.; De La Puente, F. L.; Nierengarten, J. F.; Chemistry, R. S. o., *Fullerenes: Principles and Applications*. Royal Society of Chemistry: **2007**; (b) Hirsch, A., Principles of Fullerene Reactivity. In *Fullerenes and Related Structures*, Hirsch, A., Ed. Springer Berlin Heidelberg: Berlin, Heidelberg, **1999**; pp 1-65.
64. (a) Rosén, A.; Wästberg, B., Buckminsterfullerene C<sub>60</sub> — a surface with curvature and interesting properties. *Surf. Sci.* **1992**, *269-270*, 1121-1128; (b) Wudl, F., The chemical properties of buckminsterfullerene (C<sub>60</sub>) and the birth and infancy of fulleroids. *Acc. Chem. Res.* **1992**, *25* (3), 157-161.
65. Haddon, R. C., Electronic structure, conductivity and superconductivity of alkali metal doped (C<sub>60</sub>). *Acc. Chem. Res.* **1992**, *25* (3), 127-133.
66. Sariciftci, N. S.; Smilowitz, L.; Heeger, A. J.; Wudl, F., Photoinduced Electron Transfer from a Conducting Polymer to Buckminsterfullerene. *Science* **1992**, *258* (5087), 1474-1476.
67. Tian, C.; Chen, M.; Tian, H.-R.; Nan, Z.-A.; Liang, Y.; Wei, Z., Tuning the molecular packing and energy level of fullerene acceptors for polymer solar cells. *J. Mater. Chem. C* **2019**, *7*, 12688-12694.



68. Kielar, M.; Hamid, T.; Wu, L.; Windels, F.; Sah, P.; Pandey, A. K., Organic Optoelectronic Diodes as Tactile Sensors for Soft-Touch Applications. *ACS Appl. Mater. Interfaces*. **2019**, *11* (24), 21775-21783.
69. Afreen, S.; Muthoosamy, K.; Manickam, S.; Hashim, U., Functionalized fullerene (C60) as a potential nanomediator in the fabrication of highly sensitive biosensors. *Biosens. Bioelectron*. **2015**, *63*, 354-364.
70. Li, J.; Chen, L.; Su, H.; Yan, L.; Gu, Z.; Chen, Z.; Zhang, A.; Zhao, F.; Zhao, Y., The pharmaceutical multi-activity of metallofullerenol invigorates cancer therapy. *Nanoscale* **2019**, *11* (31), 14528-14539.
71. Yasinskyi, Y.; O, P.; O, M.; V, R.; Prylutsky, Y.; Tauscher, E.; Ritter, U.; Kozeretska, I., Reconciling the controversial data on the effects of C60 fullerene at the organismal and molecular levels using as a model *Drosophila melanogaster*. *Toxicol. Lett.* **2019**, *310*, 92-98.
72. Vendrame, L. F. O.; Zuchetto, T.; Fagan, S. B.; Zanella, I., Nanofilter based on functionalized carbon nanostructures for the adsorption of pentachlorophenol molecules. *Comput. Theor. Chem.* **2019**, *1165*, 112561.
73. Ellessawy, N. A.; Elnouby, M.; Gouda, M. H.; Hamad, H. A.; Taha, N. A.; Gouda, M.; Mohy Eldin, M. S., Ciprofloxacin removal using magnetic fullerene nanocomposite obtained from sustainable PET bottle wastes: Adsorption process optimization, kinetics, isotherm, regeneration and recycling studies. *Chemosphere* **2020**, *239*, 124728.
74. Campisciano, V.; Gruttadauria, M.; Giacalone, F., Modified Nanocarbons for Catalysis. *ChemCatChem* **2019**, *11* (1), 90-133.
75. Sulman, E.; Matveeva, V.; Semagina, N.; Yanov, I.; Bashilov, V.; Sokolov, V., Catalytic hydrogenation of acetylenic alcohols using palladium complex of fullerene C60. *J. Mol. Catal. Chem.* **1999**, *146* (1), 257-263.
76. (a) Chronopoulos, D. D.; Tsakos, M.; Karousis, N.; Kokotos, C. G.; Tagmatarchis, N., Fullerene–proline hybrids: Synthesis, characterization and organocatalytic properties in aldol reactions. *Mater. Lett.* **2014**, *137*, 343-346; (b) Andrés, J. M.; González, M.; Maestro, A.; Naharro, D.; Pedrosa, R., Recyclable Chiral Bifunctional Thioureas Derived from [60]Fullerene and Their Use as Highly

Efficient Organocatalysts for the Asymmetric Nitro-Michael Reaction. *Eur. J. Org. Chem.* **2017**, 2017 (19), 2683-2691.

77. Lavoisier, A., *Traité élémentaire de chimie, présenté dans un ordre nouveau et d'après les découvertes modernes*. Paris: Cuchet: **1793**.

78. Britannica, E., Silicon.

79. scientifique, A. d. s. C. n. d. l. r., *Comptes rendus hebdomadaires des séances de l'Académie des sciences*. publiés avec le concours du Centre national de la recherche scientifique par MM. les secrétaires perpétuels: **1854**.

80. Hart, P. R. In *Crystalline vs. Amorphous Silicon — a Comparison of their Respective Properties and their Significance in Photovoltaic Applications*, Dordrecht, Springer Netherlands: Dordrecht, **1987**; pp 521-527.

81. (a) Benster, B., The MPU revolution. *Ind. Commer. Train.* **1978**, 10 (10), 404-411; (b) Ghergia, V., New materials for optoelectronic devices. *Ceram. Int.* **1993**, 19 (3), 181-190; (c) Kanemitsu, Y., Light emission from porous silicon and related materials. *Phys. Rep.* **1995**, 263 (1), 1-91; (d) Prince, M. B., Silicon Solar Energy Converters. *J. Appl. Phys.* **1955**, 26 (5), 534-540.

82. Alpas, A. T.; Zhang, J., Effect of SiC particulate reinforcement on the dry sliding wear of aluminium-silicon alloys (A356). *Wear* **1992**, 155 (1), 83-104.

83. Foletto, E. L.; Gratieri, E.; Oliveira, L. H. d.; Jahn, S. L., Conversion of rice hull ash into soluble sodium silicate. *Mater. Res.* **2006**, 9, 335-338.

84. Rego, S. R.; Gomes, K. C.; Rosas, M.; Torres, S. M.; de Barros, S., Application of Geopolymeric Adhesives in Ceramic Systems Subjected to Cyclic Temperature Environments. *J. Adhes.* **2014**, 90 (1), 120-133.

85. (a) Lowry, T. M., The Properties of Silica. *Nature* **1929**, 123 (3091), 122-123; (b) Wiberg, E.; Holleman, A. F.; Wiberg, N.; Eagleson, M.; Brewer, W., *Inorganic Chemistry*. Academic Press: **2001**.

86. Pratsinis, S. E., Flame aerosol synthesis of ceramic powders. *Prog. Energy Combust. Sci.* **1998**, 24 (3), 197-219.

87. Houldsworth, H. S.; Cobb, J. W., The reversible thermal expansion of refractory materials. *J. Am. Ceram. Soc.* **1923**, 6 (5), 645-662.

88. (a) Madou, M. J.; Frese Jr., K. W.; Morrison, S. R., The silicon/silica electrode. *physica status solidi (a)* **1980**, 57 (2), 705-712; (b) Kobayashi, Y.;

- Fukami, A.; Suzuki, T., Zone-melting recrystallization of polycrystalline silicon films on fused silica substrates using RF-Heated carbon susceptor. *IEEE Electron Device Lett.* **1983**, *4* (5), 132-134; (c) Kobayashi, Y.; Fukami, A.; Suzuki, T., RF recrystallization of polycrystalline silicon on fused silica for MOSFET devices. *J. Electrochem. Soc.* **1984**, *131* (5), 1188-1194.
89. (a) Horváth, C., Reversed-phase chromatography. *Trends Anal. Chem.* **1981**, *1* (1), 6-12; (b) Stahl, E., A Quarter Century of Thin-Layer Chromatography—An Interim Report. *Angew. Chem. Int. Ed.* **1983**, *22* (7), 507-516; (c) Wulfson, A. N.; Yakimov, S. A., HPLC of nucleotides. II. General methods and their development for analysis and preparative separation. An approach to selectivity control. *J. High Resolut. Chromatogr.* **1984**, *7* (8), 442-460.
90. Limper, A.; Schramm, D., Better Process Description for the Extrusion of Silica and Carbon Black Compounds. *Rubber Chem. Technol.* **2001**, *74* (5), 899-914.
91. The silicosis scheme. *Lancet* **1919**, *193* (4995), 907.
92. Middleton, E. L., The ætiology of silicosis. *Tubercle* **1920**, *1* (6), 257-262.
93. (a) Silicosis. *Lancet* **1921**, *198* (5106), 83-84; (b) Pratt, R., Silicosis and tuberculosis of the lungs. *Lancet* **1922**, *199* (5146), 761-762.
94. (a) Ndlovu, N.; Richards, G.; Vorajee, N.; Murray, J., Silicosis and pulmonary tuberculosis in deceased female South African miners. *Occup. Med.* **2019**, *69* (4), 272-278; (b) Burki, T. K., The true scale of artisanal mining. *Lancet Respir. Med.* **2019**, *7* (5), 384-385.
95. Bukovitz, B.; Meiman, J.; Anderson, H.; Brooks, E. G., Silicosis: Diagnosis and Medicolegal Implications. *J. Forensic Sci.* **2019**, *64* (5), 1389-1398.
96. Mieville, R. L., Measurement of microporosity in the presence of mesopores. *J. Colloid Interface Sci.* **1972**, *41* (2), 371-373.
97. Kresge, C. T.; Leonowicz, M. E.; Roth, W. J.; Vartuli, J. C.; Beck, J. S., Ordered mesoporous molecular sieves synthesized by a liquid-crystal template mechanism. *Nature* **1992**, *359* (6397), 710-712.
98. Zhao, D.; Feng, J.; Huo, Q.; Melosh, N.; Fredrickson, G. H.; Chmelka, B. F.; Stucky, G. D., Triblock Copolymer Syntheses of Mesoporous Silica with Periodic 50 to 300 Angstrom Pores. *Science* **1998**, *279* (5350), 548-552.

99. Narayan, R.; Nayak, U. Y.; Raichur, A. M.; Garg, S., Mesoporous Silica Nanoparticles: A Comprehensive Review on Synthesis and Recent Advances. *Pharmaceutics* **2018**, *10* (3), 118.
100. Øye, G.; Sjöblom, J.; Stöcker, M., Synthesis, characterization and potential applications of new materials in the mesoporous range. *Adv. Colloid Interface Sci.* **2001**, *89-90*, 439-466.
101. Yang, X.-L.; Zhao, B.; Feng, F.; Zhou, H.-M.; Yang, H.; Li, X.-X., High Performance Micro Gas Chromatography Column Using Mesoporous Silica as Stationary Phase. *Chinese J. Anal. Chem.* **2019**, *47* (6), 832-837.
102. Han, Y.; Quan, Y.; Hao, P.; Zhao, J.; Ren, J., Highly anti-sintering and anti-coking ordered mesoporous silica carbide supported nickel catalyst for high temperature CO methanation. *Fuel* **2019**, *257*, 116006.
103. Lagarde, F.; Srour, H.; Berthet, N.; Oueslati, N.; Bousquet, B.; Nunes, A.; Martinez, A.; Dufaud, V., Investigating the role of SBA-15 silica on the activity of quaternary ammonium halides in the coupling of epoxides and CO<sub>2</sub>. *J. CO<sub>2</sub> Util.* **2019**, *34*, 34-39.
104. Hartmann-Thompson, C., *Applications of polyhedral oligomeric silsesquioxanes*. Springer Science & Business Media: **2011**; Vol. 3.
105. KA, A., *J Gen Chem (USSR)* **1938**, *8*, 1255.
106. (a) Andrianov KA, B. B., *J Gen Chem (USSR)* **1947**, *17*, 1522; (b) Barry AJ, G. G. 1949.
107. Scott, D. W., Thermal Rearrangement of Branched-Chain Methylpolysiloxanes. *J. Am. Chem. Soc.* **1946**, *68* (3), 356-358.
108. (a) Kudo, T.; Gordon, M. S., Theoretical Studies of the Mechanism for the Synthesis of Silsesquioxanes. 1. Hydrolysis and Initial Condensation. *J. Am. Chem. Soc.* **1998**, *120* (44), 11432-11438; (b) Kudo, T.; Gordon, M. S., Theoretical Studies of the Mechanism for the Synthesis of Silsesquioxanes. 2. Cyclosiloxanes (D 3 and D 4). *J. Phys. Chem. A* **2000**, *104* (17), 4058-4063.
109. (a) Voronkov, M. G.; Lavrent'yev, V. I. In *Polyhedral oligosilsesquioxanes and their homo derivatives*, Berlin, Heidelberg, Springer Berlin Heidelberg: Berlin, Heidelberg, **1982**; pp 199-236; (b) Kudo, T.; Gordon, M. S., Exploring the

Mechanism for the Synthesis of Silsesquioxanes. 3. The Effect of Substituents and Water. *J. Phys. Chem. A* **2002**, *106* (46), 11347-11353.

110. Pescarmona, P. P.; Aprile, C.; Swaminathan, S., *New and Future Developments in Catalysis: Chapter 16. Silsesquioxanes and Their Use as Precursors for Catalysts and as Model Compounds*. Elsevier Science: **2013**.

111. (a) Chen, Y.; Xia, L.; Liang, R.; Lu, Z.; Li, L.; Huo, B.; Li, G.; Hu, Y., Advanced materials for sample preparation in recent decade. *Trends Anal. Chem.* **2019**, *120*, 115652; (b) Chen, F.; Lin, F.; Zhang, Q.; Cai, R.; Wu, Y.; Ma, X., Polyhedral Oligomeric Silsesquioxane Hybrid Polymers: Well-Defined Architectural Design and Potential Functional Applications. *Macromol. Rapid Commun.* **2019**, *40* (17), 1900101; (c) Žak, P.; Pietraszuk, C., Application of olefin metathesis in the synthesis of functionalized polyhedral oligomeric silsesquioxanes (POSS) and POSS-containing polymeric materials. *Beilstein J. Org. Chem.* **2019**, *15*, 310-332.

112. Abbenhuis, H. C. L., Advances in Homogeneous and Heterogeneous Catalysis with Metal-Containing Silsesquioxanes. *Chem.: Eur. J.* **2000**, *6* (1), 25-32.

113. Duchateau, R.; van Meerendonk, W. J.; Huijser, S.; Staal, B. B.; van Schilt, M. A.; Gerritsen, G.; Meetsma, A.; Koning, C. E.; Kemmere, M. F.; Keurentjes, J. T., Silica-Grafted Diethylzinc and a Silsesquioxane-Based Zinc Alkyl Complex as Catalysts for the Alternating Oxirane– Carbon Dioxide Copolymerization. *Organometallics* **2007**, *26* (17), 4204-4211.

114. Bivona, L. A.; Fichera, O.; Fusaro, L.; Giacalone, F.; Buaki-Sogo, M.; Gruttadauria, M.; Aprile, C., A polyhedral oligomeric silsesquioxane-based catalyst for the efficient synthesis of cyclic carbonates. *Catal. Sci. Technol.* **2015**, *5* (11), 5000-5007.

115. Kausar, A., State-of-the-Art Overview on Polymer/POSS Nanocomposite. *Polym. Plast. Technol.* **2017**, *56* (13), 1401-1420.

116. (a) Haddad, T. S.; Lichtenhan, J. D., Hybrid Organic–Inorganic Thermoplastics: Styryl-Based Polyhedral Oligomeric Silsesquioxane Polymers. *Macromolecules* **1996**, *29* (22), 7302-7304; (b) Wu, J.; Haddad, T. S.; Kim, G.-M.; Mather, P. T., Rheological Behavior of Entangled Polystyrene–Polyhedral

- Oligosilsesquioxane (POSS) Copolymers. *Macromolecules* **2007**, *40* (3), 544-554;
- (c) Zhang, W.; Fu, B. X.; Seo, Y.; Schrag, E.; Hsiao, B.; Mather, P. T.; Yang, N.-L.; Xu, D.; Ade, H.; Rafailovich, M., Effect of methyl methacrylate/polyhedral oligomeric silsesquioxane random copolymers in compatibilization of polystyrene and poly (methyl methacrylate) blends. *Macromolecules* **2002**, *35* (21), 8029-8038.
117. (a) Hirai, T.; Leolukman, M.; Jin, S.; Goseki, R.; Ishida, Y.; Kakimoto, M.-a.; Hayakawa, T.; Ree, M.; Gopalan, P., Hierarchical self-assembled structures from POSS-containing block copolymers synthesized by living anionic polymerization. *Macromolecules* **2009**, *42* (22), 8835-8843; (b) Hirai, T.; Leolukman, M.; Hayakawa, T.; Kakimoto, M.-a.; Gopalan, P., Hierarchical nanostructures of organosilicate nanosheets within self-organized block copolymer films. *Macromolecules* **2008**, *41* (13), 4558-4560.
118. (a) Piotti, M. E., Ring opening metathesis polymerization. *Curr. Opin. Solid St. M.* **1999**, *4* (6), 539-547; (b) Xu, W.; Chung, C.; Kwon, Y., Synthesis of novel block copolymers containing polyhedral oligomeric silsesquioxane (POSS) pendent groups via ring-opening metathesis polymerization (ROMP). *Polymer* **2007**, *48* (21), 6286-6293.
119. (a) Fu, B. X.; Hsiao, B. S.; Pagola, S.; Stephens, P.; White, H.; Rafailovich, M.; Sokolov, J.; Mather, P. T.; Jeon, H. G.; Phillips, S.; Lichtenhan, J.; Schwab, J., Structural development during deformation of polyurethane containing polyhedral oligomeric silsesquioxanes (POSS) molecules. *Polymer* **2001**, *42* (2), 599-611; (b) Wang, W.; Guo, Y.-l.; Otaigbe, J. U., The synthesis, characterization and biocompatibility of poly (ester urethane)/polyhedral oligomeric silsesquioxane nanocomposites. *Polymer* **2009**, *50* (24), 5749-5757; (c) Brunsvold, A. L.; Minton, T. K.; Gouzman, I.; Grossman, E.; Gonzalez, R., An Investigation of the Resistance of Polyhedral Oligomeric Silsesquioxane Polyimide to Atomic-Oxygen Attack. *High Perform. Polym.* **2004**, *16* (2), 303-318; (d) Wright, M. E.; Schorzman, D. A.; Feher, F. J.; Jin, R.-Z., Synthesis and thermal curing of aryl-ethynyl-terminated co POSS imide oligomers: new inorganic/organic hybrid resins. *Chem. Mater.* **2003**, *15* (1), 264-268.
120. (a) Fang, Y.; Chen, L.; Chen, S., Facile and quick synthesis of poly(N-methylolacrylamide)/polyhedral oligomeric silsesquioxane graft copolymer

- hybrids via frontal polymerization. *J. Polym. Sci. Pol. Chem* **2009**, *47* (4), 1136-1147; (b) Kang, J.-M.; Cho, H.-J.; Lee, J.; Lee, J.-I.; Lee, S.-K.; Cho, N.-S.; Hwang, D.-H.; Shim, H.-K., Highly bright and efficient electroluminescence of new PPV derivatives containing polyhedral oligomeric silsesquioxanes (POSSs) and their blends. *Macromolecules* **2006**, *39* (15), 4999-5008; (c) Drazkowski, D. B.; Lee, A.; Haddad, T. S., Morphology and Phase Transitions in Styrene-Butadiene-Styrene Triblock Copolymer Grafted with Isobutyl-Substituted Polyhedral Oligomeric Silsesquioxanes. *Macromolecules* **2007**, *40* (8), 2798-2805.
121. Tsuchida, A.; Bolln, C.; Sernetz, F. G.; Frey, H.; Mülhaupt, R., Ethene and Propene Copolymers Containing Silsesquioxane Side Groups. *Macromolecules* **1997**, *30* (10), 2818-2824.
122. Silver, J. H.; Lin, J.-C.; Lim, F.; Tegoulia, V. A.; Chaudhury, M. K.; Cooper, S. L., Surface properties and hemocompatibility of alkyl-siloxane monolayers supported on silicone rubber: effect of alkyl chain length and ionic functionality. *Biomaterials* **1999**, *20* (17), 1533-1543.
123. (a) Kannan, R. Y.; Salacinski, H. J.; Ghanavi, J.-e.; Narula, A.; Odlyha, M.; Peirovi, H.; Butler, P. E.; Seifalian, A. M., Silsesquioxane Nanocomposites as Tissue Implants. *Plast. Reconstr. Surg.* **2007**, *119* (6), 1653-1662; (b) Kannan, R. Y.; Salacinski, H. J.; De Groot, J.; Clatworthy, I.; Bozec, L.; Horton, M.; Butler, P. E.; Seifalian, A. M., The Antithrombogenic Potential of a Polyhedral Oligomeric Silsesquioxane (POSS) Nanocomposite. *Biomacromolecules* **2006**, *7* (1), 215-223.
124. Kato, K.; Gon, M.; Tanaka, K.; Chujo, Y., Stretchable Conductive Hybrid Films Consisting of Cubic Silsesquioxane-capped Polyurethane and Poly(3-hexylthiophene). *Polymers* **2019**, *11* (7), 1195.
125. Zhang, Q.; Liu, Y.; Ma, J.; Zhang, M.; Ma, X.; Chen, F., Preparation and characterization of polypropylene supported electrospun POSS-(C<sub>3</sub>H<sub>6</sub>Cl)<sub>8</sub>/PVDF gel polymer electrolytes for lithium-ion batteries. *Colloids Surf.* **2019**, *580*, 123750.
126. Teyssié, D.; Boileau, S., Liquid Crystalline Silicon-Containing Polymers. In *Silicon-Containing Polymers: The Science and Technology of Their Synthesis and Applications*, Jones, R. G.; Ando, W.; Chojnowski, J., Eds. Springer Netherlands: Dordrecht, **2000**; pp 593-613.

127. Mehl, G. H.; Saez, I. M., Polyhedral liquid crystal silsesquioxanes. *Appl. Organomet. Chem.* **1999**, *13* (4), 261-272.
128. Palilis, L. C.; Lidzey, D. G.; Redecker, M.; Bradley, D. D.; Inbasekaran, M.; Woo, E. P.; Wu, W. W. In *Bright and efficient blue light-emitting diodes based on conjugated polymer blends*, Organic Light-Emitting Materials and Devices III, International Society for Optics and Photonics: **1999**; pp 383-397.
129. (a) Xiao, S.; Nguyen, M.; Gong, X.; Cao, Y.; Wu, H.; Moses, D.; Heeger, A. J., Stabilization of Semiconducting Polymers with Silsesquioxane. *Adv. Funct. Mater.* **2003**, *13* (1), 25-29; (b) Shin, S.-B.; Gong, S.-C.; Jang, J.-K.; Gong, M.-S.; Chang, Y.-C.; Sun, Y.-B.; Chang, H.-J., Properties of polymer light-emitting diodes coated on surface-treated ITO/glass substrates. *J. Appl. Polym. Sci.* **2008**, *110* (6), 3678-3682.
130. Hartmann-Thompson, C.; Keeley, D. L.; Pollock, K. M.; Dvornic, P. R.; Keinath, S. E.; Dantus, M.; Gunaratne, T. C.; LeCaptain, D. J., One-and two-photon fluorescent polyhedral oligosilsesquioxane (POSS) nanosensor arrays for the remote detection of analytes in clouds, in solution, and on surfaces. *Chem. Mater.* **2008**, *20* (8), 2829-2838.
131. Liu, Y.; Yang, W.; Liu, H., Azobenzene-Functionalized Cage Silsesquioxanes as Inorganic–Organic Hybrid, Photoresponsive, Nanoscale, Building Blocks. *Chem.: Eur. J.* **2015**, *21* (12), 4731-4738.
132. Li, L.; Feng, S.; Liu, H., Hybrid lanthanide complexes based on a novel  $\beta$ -diketone functionalized polyhedral oligomeric silsesquioxane (POSS) and their nanocomposites with PMMA via in situ polymerization. *RSC Adv.* **2014**, *4* (74), 39132-39139.
133. (a) Lowenthal, R. E.; Abiko, A.; Masamune, S., Asymmetric catalytic cyclopropanation of olefins: bis-oxazoline copper complexes. *Tetrahedron Lett.* **1990**, *31* (42), 6005-6008; (b) Evans, D. A.; Woerpel, K. A.; Hinman, M. M.; Faul, M. M., Bis(oxazolines) as chiral ligands in metal-catalyzed asymmetric reactions. Catalytic, asymmetric cyclopropanation of olefins. *J. Am. Chem. Soc.* **1991**, *113* (2), 726-728.
134. Rothenberg, G., *Catalysis: concepts and green applications*. John Wiley & Sons: **2017**.



135. Wang, X.-J.; Qu, Y.-R.; Zhao, Y.-L.; Chu, H.-B., Effect of the composition of lanthanide complexes on their luminescence enhancement by Ag@ SiO<sub>2</sub> core-shell nanoparticles. *Nanomaterials* **2018**, 8 (2), 98.
136. Takahashi, S.; Hashimoto, S.; Shimogori, Y.; Matsumoto, N.; Nakashima, T.; Tsuchimoto, M., Luminescent europium(III) complexes of tripodal heptadentate N7 ligands containing three imidazole groups. *Polyhedron* **2011**, 30 (12), 2026-2031.

*Chapter 2*

*Bisoxazoline-C<sub>60</sub> Hybrid Systems*

*for Asymmetric Catalysis*

## 2 Introduction

### 2.1 C<sub>60</sub>-Fullerene in Catalysis

Since their discovery, carbon nanoforms (CNFs) have attracted the attention of researchers all over the world. This has meant that their use ranges from chemistry, to sensors, to electronics and optoelectronics, and even to medicine.<sup>1</sup> In the chemical field, one of the most recent applications is certainly catalysis.<sup>2</sup> Fullerenes, nanotubes, graphene and other nanostructures are finding application as support for catalysts.<sup>3</sup> In this regard, fullerene can be considered as a molecular model for catalysts as CNFs-based heterogeneous catalysts. It is known that, despite its graphic representation, the fullerene does not behave like an aromatic molecule, but rather like a polyolefin allowing different synthetic strategies for its functionalization.

Since C<sub>60</sub> became available in ponderable amounts, the synthesis, study and application of hybrid materials composed by metal complexes or metal nanoparticles and fullerenes started to grow.<sup>4</sup>

A first example of catalytic applications of a fullerene-based metal complex was reported by Nagashima and co-workers. They used a Pd<sub>2</sub>(dba)<sub>3</sub>-C<sub>60</sub> derivative heterogeneous catalyst in the hydrogenation of alkenes.<sup>5</sup>

Exploiting the interaction  $\pi$  - ion with atoms of transition metals, it was possible to obtain compounds catalytically active with platinum,<sup>6</sup> palladium<sup>7</sup> or rhodium.<sup>8</sup> Subsequently, the development of proper protocols for the chemical functionalization of fullerenes (e.g. Prato reaction<sup>9</sup> and Bingel reaction<sup>10</sup>) allowed the anchoring of organic molecules of catalytic interest on C<sub>60</sub>. The proposed strategy allows combining the already known catalytic activity of the organic moieties with the peculiar solubility profile of C<sub>60</sub> which opens up to the possibility of recovery and recycling. Fullerene has served thus as support or as an active part of organo- and organometallic catalysts for promoting both asymmetric and non-asymmetric processes. In some cases, the results obtained pointed out that further optimization is still needed, while in others the C<sub>60</sub>-based heterogeneous catalysts displayed outstanding performances. As support in organocatalysis, C<sub>60</sub> was employed for the immobilization of 2,2,6,6-tetramethylpiperidine-1-oxyl

(TEMPO) moieties and the final solid showed excellent performance in the oxidation of primary and secondary alcohols (**Figure 2.1**).

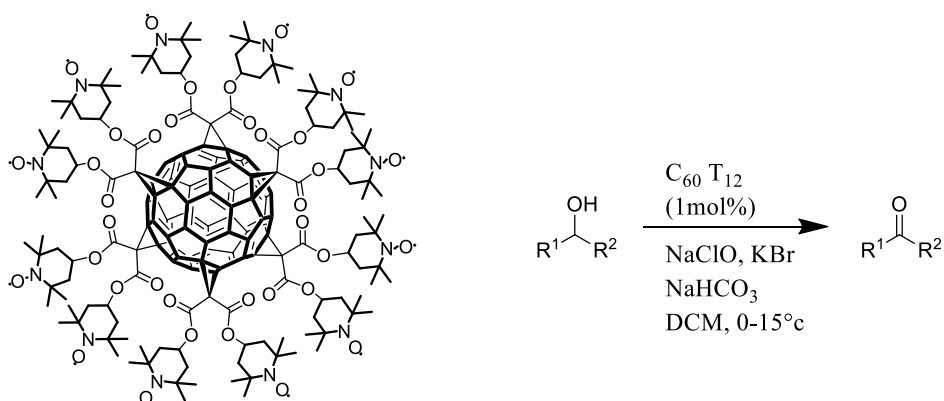


**Figure 2.1.** C<sub>60</sub>-TEMPO hybrid organocatalyst used in the oxidation of alcohols.

Different C<sub>60</sub>-TEMPO systems endowed with two (C<sub>60</sub>-T<sub>2</sub>), four (C<sub>60</sub>-T<sub>4</sub>) and twelve (C<sub>60</sub>-T<sub>12</sub>) TEMPO moieties, respectively, were tested in the oxidation of alcohols allowing, in the latter case, a really reduced use of material, due to the high loading of catalyst on the surface of the C<sub>60</sub>.<sup>11</sup> These systems have shown good applicability with a wide range of alcohols and were easily recovered and reused in multiple catalytic cycles.

An interesting evolution of the catalyst just described has been made functionalizing the C<sub>60</sub>-TEMPO (C<sub>60</sub>-T<sub>2</sub>) with ten “ionic liquid-like” arms of 1-propyl-3-methylimidazolium bromide (**Figure 2.2**).

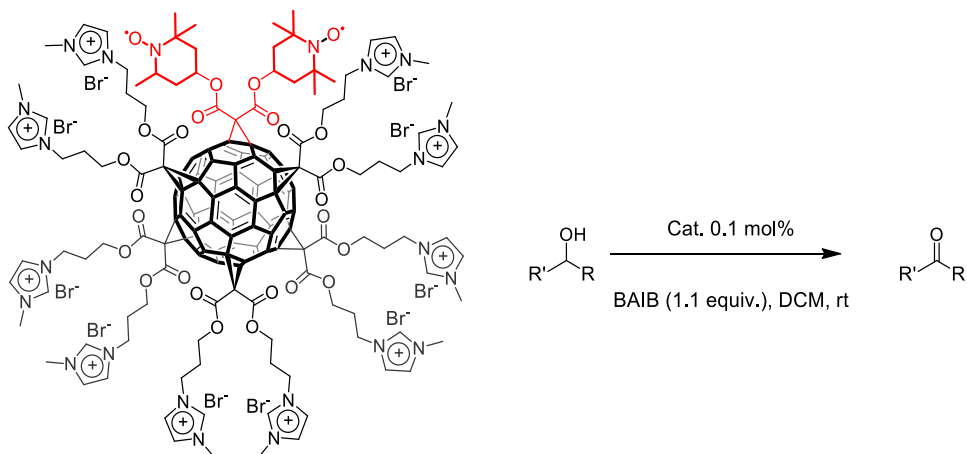


**Figure 2.2.** IL-TEMPO-C<sub>60</sub> hybrid for the oxidation of alcohols

Many approaches have been developed for the immobilization of catalysts in supported ionic liquid phases. Heterogenization of ILs offers many advantages in a

great number of reactions, one of these being easy separation from the reaction products for further reusability. Until now, several types of immobilized ILs materials have been proposed and the corresponding acronyms are widely used in the literature, being SILP (Supported Ionic Liquid Phase based on functionalized silica) one of them.<sup>12</sup> The research group where this PhD work has been carried out has already reported the synthesis of several types of this kind of materials.

The introduction of imidazolium functionalities, in addition to reducing the necessary catalytic load (only 0,1% in moles), greatly improved its recyclability: in fact, the catalyst can be recovered at the end of the reaction thanks to the interaction between the IL-TEMPO-C<sub>60</sub> hybrid and a IL-cross-linked polymeric network and released in further cycles through a mechanism named “*release and catch*”.<sup>13</sup>

More recently, a C<sub>60</sub>/IL dodecakis-adduct has been used to stabilize palladium nanoparticles and employed to catalyse coupling reactions (Suzuki, Heck) at 0.2% in moles. At the end of the reaction, the catalyst was recovered by simple centrifugation and reused up to 7 times without loss of activity.<sup>14</sup>

In 2017 Pedrosa and co-workers reported an interesting example of fullerothiureas, prepared according to Prato's methodology, able to act as organocatalysts in the enantioselective nitro-Michael addition reaction between 1,3-dicarbonyl compounds and  $\beta$ -nitrostyrene (**Figure 2.3**).<sup>15</sup>

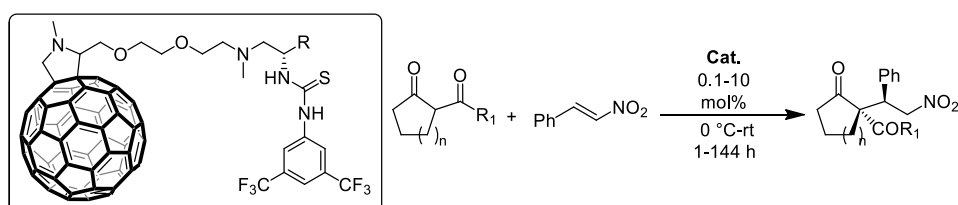


**Figure 2.3.** Structure of fullerothiureas-based organocatalysts employed for the asymmetric nitro-Michael reaction.

After exploring different conditions, they found that it is possible to obtain high yields and excellent diastereo- and enantioselectivities by carrying out the reactions in 1–10 h at room temperature. Noteworthy, the catalysts were able to promote the reaction even when very low loadings (0.5–2.0 mol%) were employed and were successfully recovered by filtration and re-used 5 times.

### 2.1.1 C<sub>2</sub>-Symmetry catalysts

In the field of asymmetric catalysis,<sup>16</sup> some of the most common chiral binders are those with C<sub>2</sub> symmetry that are generally bidentate binders but have been also employed as organocatalysts (**Figure 2.4**).<sup>17</sup>

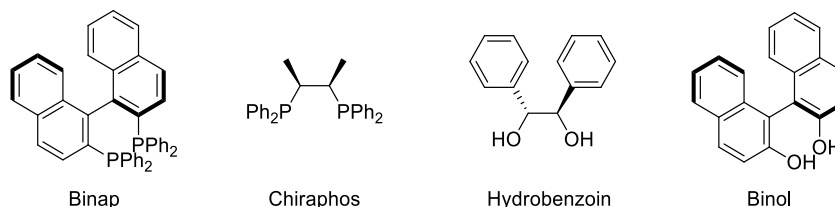


**Figure 2.4.** Common chiral C<sub>2</sub>-symmetry catalysts.

This class includes phosphorus-based catalysts as Chiraphos, DIPAMP, Binap as well as O-ligands such as chiral diols or binaphthyl-derivatives (**Figure 2.4**). Palladium complexed with Chiraphos were used to catalyze asymmetric conjugate addition of arylboronic acids to 2-nitroacrylates.<sup>18</sup> DIPAMP was used to complex rhodium in order to promote C–C bond formation.<sup>19</sup> On the other hand, Binap/copper-based catalysts were used in the photo-reductive pinacol-type couplings.<sup>20</sup> Chiral diols were employed with L-proline to catalyze aldol reaction<sup>21</sup> and binaphthyl-derivatives were used in electrophilic alkylation of cyclic keto esters and amides with benziodoxolone.<sup>22</sup> In catalysis, nitrogen-based chiral C<sub>2</sub>-symmetry ligands are commonly used and represent an important class. Bisoxazolines (BOX) are part of this family of ligands. They are systems made up of two variously substituted oxazoline rings connected through a bridge that, in the simplest case, is a methylene (**Figure 2.5**).<sup>23</sup>

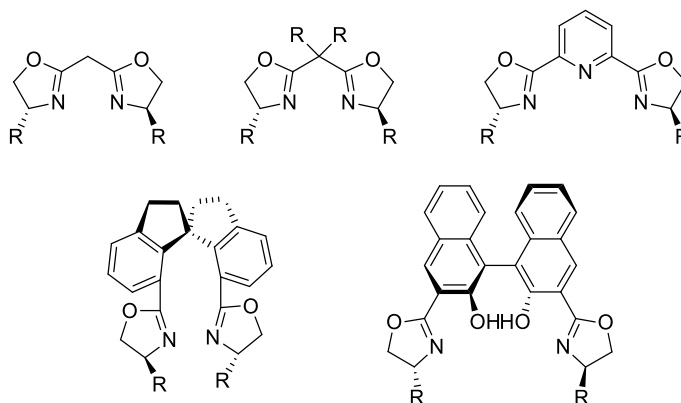


**Figure 2.5.** Different types of substituted bisoxazoline ligands with different bridge junction.

#### 2.1.1.1. Bisoxazoline (BOX)

Even though BOXs are commercially available, the literature is plenty of examples in which they are freshly synthesized, because of the simplicity and economicity of their direct preparation and purification. Talking about BOX's synthesis, three different processes are involved:

- the formation of the oxazoline ring;
- the functionalization of the methylene bridge;
- the modification of chiral functional groups.

The main structure of a bisoxazoline is commonly prepared from a malonic derivative (ester, amide, chloride) and two equivalents of an  $\alpha$ -aminoalcohol (**Figure 2.6**).<sup>24</sup>

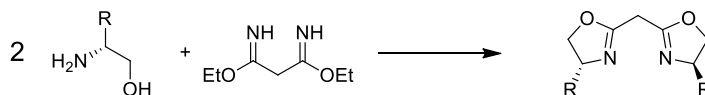


**Figure 2.6.** Example of BOX's synthesis. In the reaction an optically pure amino alcohol reacts with diethyl malonimidate (dihydrochloride) to give the chiral bisoxazoline.

Starting from an optically pure alcohol, it is possible to obtain a chiral BOX enantiomerically pure, in which the substituents of the amino alcohol will become the substituents of the oxazoline ring. The protons of the methylene bridge are acidic and, using a proper base, it is possible to generate an anionic and nucleophilic species that can take part in different reactions, and this allows inserting other functions on the bridge. Thanks to the easy synthesis and modification of these systems, more than 140 different types of BOX have been developed so far.<sup>25</sup>

The first example of catalytic applications of BOXs dates back to 1989, when PyBOX (pyridine bridged bisoxazoline) complexes were used by Nishiyama<sup>26</sup> in the asymmetric hydro-silylation of ketones.

The first work of catalysis with BOX with methylene bridge, was reported few years later by Masamune and co-workers, who used chiral copper complexes in the asymmetric cyclopropanation of alkenes, obtaining enantiomeric excesses (ee) higher than 99% with only 1 mol% of catalyst.<sup>27</sup> Although the literature contains examples of BOX complexes with various transition metals, the most widely used

are copper and iron salts. In the 1990s the works of Evans<sup>24</sup> and Corey<sup>28</sup> pioneered the way for the use of these catalysts and were the basis for all subsequent researches in this field. Evans employed a 1 mol% Cu(I) complex in the reaction of an alkene with diazoacetate, while Corey used a Fe(III) complex as catalyst for the Diels-Alder reaction. Both obtained high enantioselectivities (greater than 90%), although high catalytic loads (up to 10 mol%) were needed in the Diels-Alder reaction.

Heterogeneous BOX-copper complexes were also synthesized. One example, regards the anchoring of a bisoxazoline onto a polystyrenic support applied in the enantioselective Henry reaction,<sup>29</sup> a second example regards the covalent grafting of bisoxazoline ligands on amorphous silica and mesoporous MCM-41 to be applied in enantioselective Friedel–Crafts hydroxyalkylations.<sup>30</sup>

In addition to the above mentioned catalytic application, bisoxazoline-based catalysts were used in the asymmetric aziridination reactions,<sup>28</sup> aldol reactions,<sup>31</sup> Michael reactions,<sup>32</sup> Mannich reactions<sup>33</sup> and 1,3-dipolar cycloadditions.<sup>34</sup>

Among the various catalytic applications in which BOX-ligands are used, Henry and Diels-Alder reactions are still attracting interest in the scientific community

The Henry reaction, consists of an aldol reaction in which the nucleophilic species is a nitronate, generated by the action of a base to a nitroalkane.<sup>35</sup> The product obtained, a  $\beta$ -nitroalcohol, contains a new chiral centre and represents an important precursor for other molecules of interest. In fact, through simple reductions and oxidations it is possible to obtain a) amino-alcohol, b) amino acids, c) nitroalkenes, etc. (**Figure 2.7**).

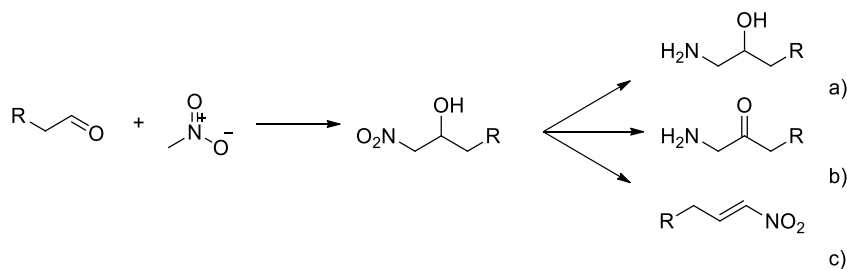


**Figure 2.7.** Possible fates of the products of Henry's reaction.

Henry's reaction was found to be a key step in the total synthesis of Bestatin, a protease inhibitor, currently under investigation as anticancer drug<sup>36</sup> and, among



other, in the synthesis of the carbohydrate subunit of the anthracycline class of antibiotics, L-Acosamine.<sup>37</sup>

The Diels-Alder reaction,<sup>38</sup> on the other hand, is of more general application; in this [4+2] cycloaddition a conjugated diene and an alkene (acting as a dienophile) react to give a six membered ring (**Figure 2.8**).

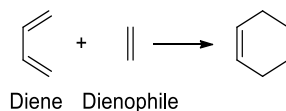


**Figure 2.8.** Schematic representation of a general Diels-Alder reaction.

There are many examples in which this reaction is used in the preparation of molecules of interest: the first historical application dates back to the famous Woodward synthesis of cortisone,<sup>39</sup> and to Corey's prostaglandin preparation.<sup>40</sup>

The Diels-Alder reaction occurs with a concerted mechanism, and, in the case in which diene and dienophile are not symmetrical (e.g. due to the presence of substituents) two transition states called *endo* and *exo* are possible. We talk about the *endo* transition state (or adduct) when the substituent on the dienophile is oriented towards the  $\pi$  system, and the *exo* transition state when the substituent is on the opposite side (**Figure 2.9**).

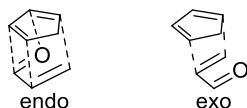


**Figure 2.9.** Diels-Alder reaction's transitional states.

Without a proper stereochemical control, a mixture of four products will form during the reaction and even in this case, asymmetric catalysis can provide an effective solution to the problem.

Furthermore, in the asymmetric Diels-Alder reactions conducted with BOX, published in literature, it is reported that big amount of catalyst is required (1-10 mol%). It is therefore clear that it becomes desirable to take into account the recovery and recycling of the catalysts. Among various strategies that it is possible to adopt, one is certainly the heterogenization of the catalyst.

## 2.2 Aim of the Chapter

Herein, a series of BOX (**Figure 2.10a**) was anchored on  $C_{60}$  fullerene in order to form different adducts: mono-adducts ( $C_{60}$ -BOX) and hexakis-adducts ( $C_{60}$ -BOX<sub>6</sub>) (**Figure 2.10b**).

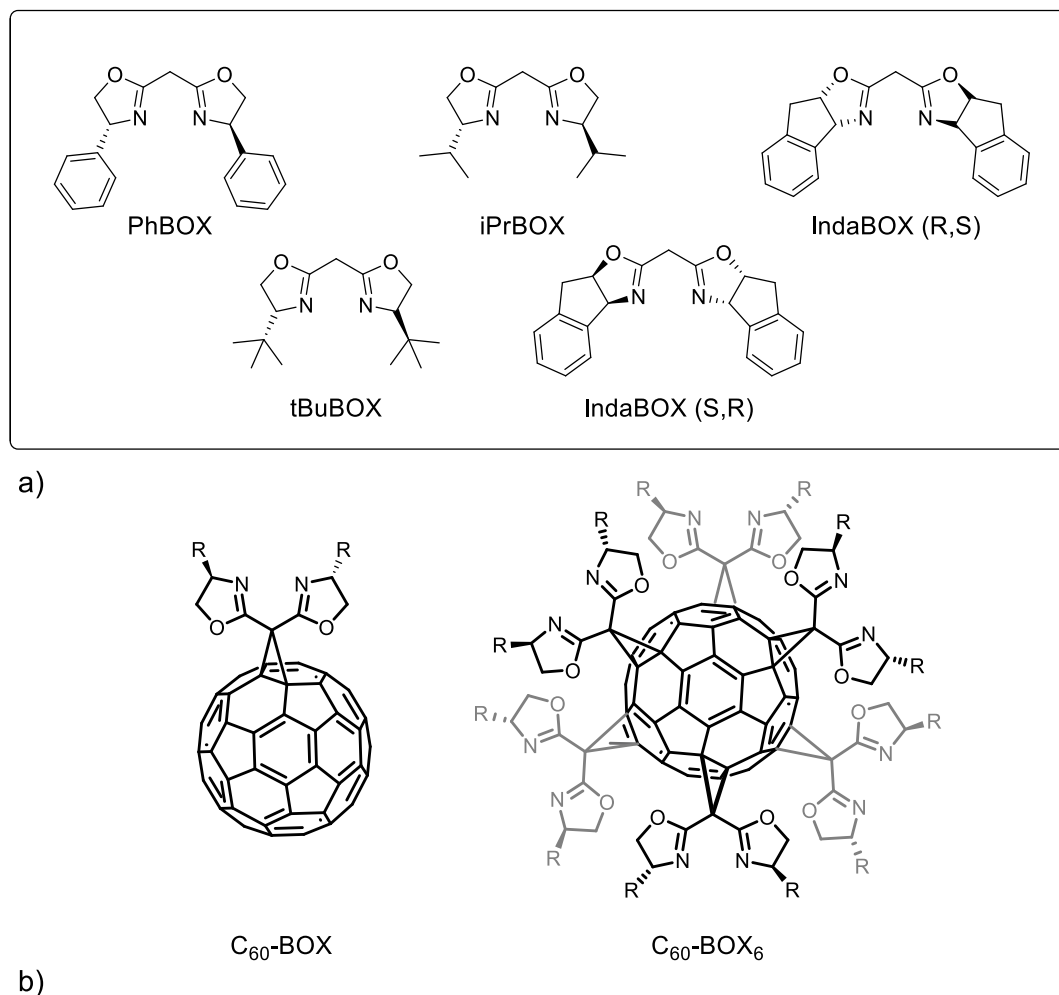
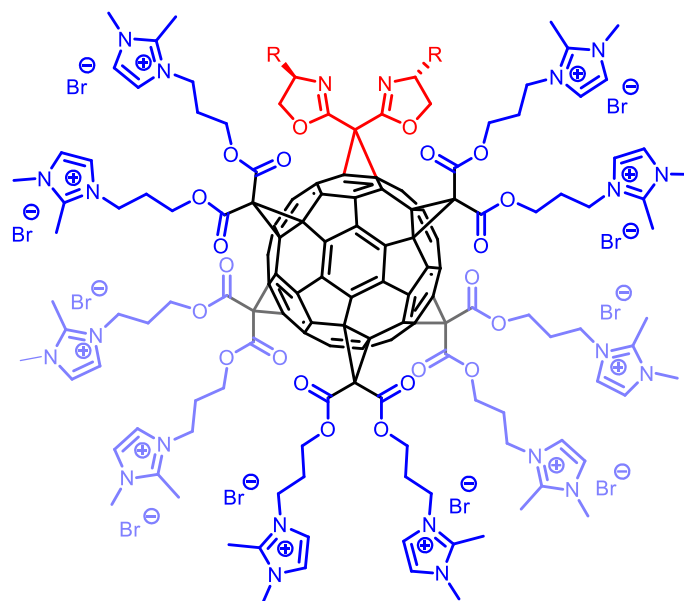


**Figure 2.10.** Series of synthesized chiral BOX (a). Different types of  $C_{60}$ -adducts obtained

Mono-adducts were also post-functionalized with ten 1,2-dimethylimidazolium moieties in order to get hybrid fullerene-ionic liquid-BOX with different solubility profile ( $C_{60}$ -IL<sub>10</sub>-BOX) (**Figure 2.11**). All the systems were employed, along with copper(II) salts, as catalysts in asymmetric Henry and Diels-Alder reactions.



C<sub>60</sub>-IL-BOX

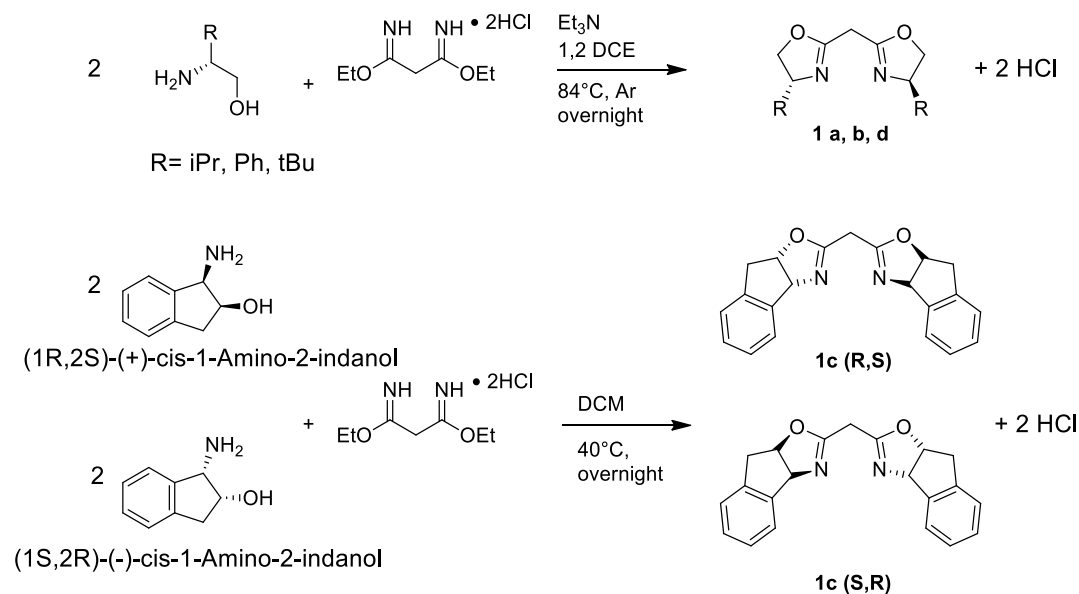
Figure 2.11. Fullerene-Ionic liquid-BOX hybrid

## 2.3 Results and discussion

### 2.3.1 Synthesis and characterization of catalysts

#### 2.3.1.1 BOX Synthesis

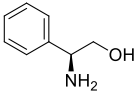
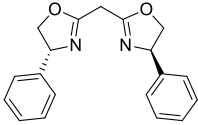
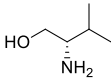
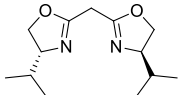
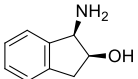
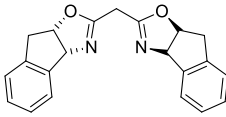
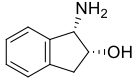
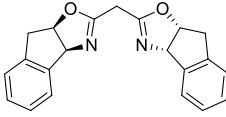
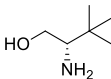
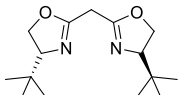
BOXs derivatives (**Table 2.1**) were obtained by reacting the diethyl malonimidate dihydrochloride with 2 equivalents of the respective aminoalcohol (**Scheme 2.1**).



Scheme 2.1. BOX syntheses

In the case of PhBOX, iPrBOX and tBuBOX derivatives, the reaction took place in dichloroethane in presence of triethylamine as a base and the products obtained were purified using silica gel columns. Particular attention must be paid to the purification step: since bisoxazolines are sensitive to acids, the silica must be deactivated by adding to the eluent mixture 0.2 v/v% of a base, in this case triethylamine.

**Table 2.1.** Series of aminoalcohols used for the synthesis of the corresponding BOXs with the respective yields.

Aminoalcohol	BOX	Yield (%)
 (S)-(+)-2-Phenylglycinol	 PhBOX <b>1a</b>	67%
 (S)-Valinol	 iPrBOX <b>1b</b>	63%
 (1R,2S)-(+)-cis-1-amino-2-indanol	 IndaBOX (R,S) <b>1c(R,S)</b>	65%
 (1S,2R)-(-)-cis-1-Amino-2-indanol	 IndaBOX (S,R) <b>1c(S,R)</b>	62%
 L-tert-Leucinol	 tBuBOX <b>1d</b>	57%

The synthesis of IndaBOX (**1c**(*R,S*) and (*S,R*)) was much simpler: this was obtained by reacting the malonic derivative with 1-amino-2-indanol in dichloromethane, without base addition and the purification consists of recrystallization by isopropanol. Two different IndaBOX have been obtained using two different amino indanols: (*1R,2S*)-(+)-*cis*-1-amino-2-indanol and (*1S,2R*)-(-)-*cis*-1-amino-2-indanol (**Figure 2.12**).



**Figure 2.12.** Different aminoindanols used for the synthesis of the IndaBOX.

The products obtained were characterized by  $^1\text{H-NMR}$  spectroscopy. In **Figure 2.13** the spectrum of PhBOX **1a** is reported as an example.

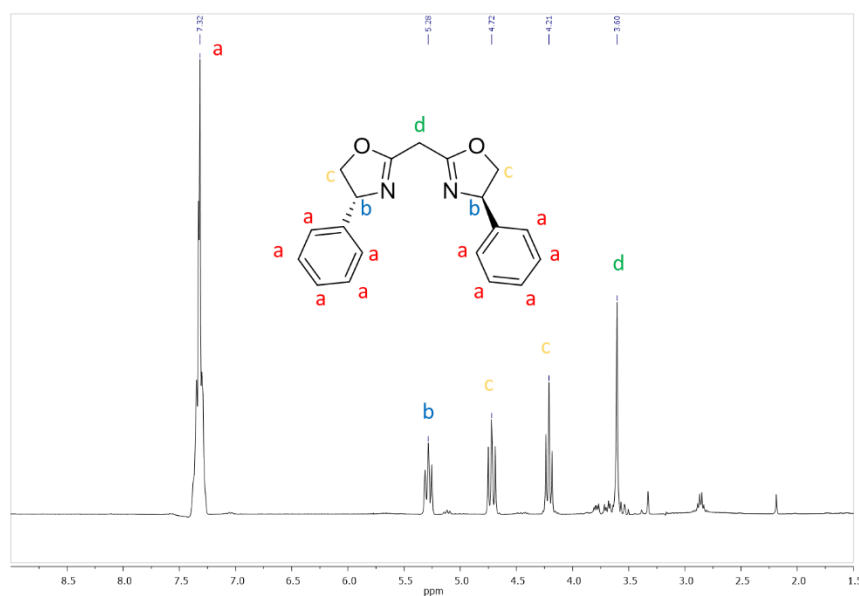


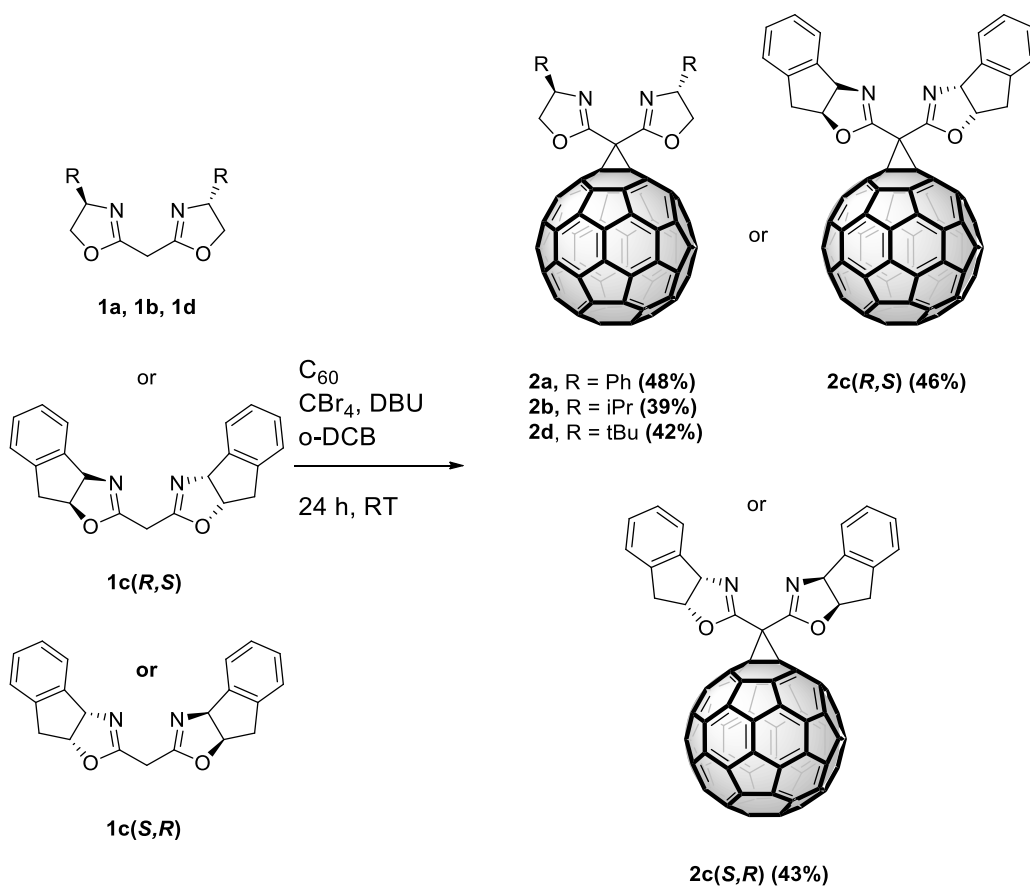
**Figure 2.13.**  $^1\text{H-NMR}$  spectrum of the PhBOX (300 MHz,  $\text{CDCl}_3$ ).

The  $^1\text{H-NMR}$  spectrum in **Figure 2.13** displays the signals for all the protons of the PhBOX with the right pattern. It is interesting to note that the protons labelled as “d”, corresponding to the methylene bridge, will disappear in the  $\text{C}_{60}$  conjugates, since, as we will see later, the functionalization will take place precisely by exploiting the reactivity of these acidic protons which.

### 2.3.1.2 Synthesis of C<sub>60</sub>-BOX (monoadducts).

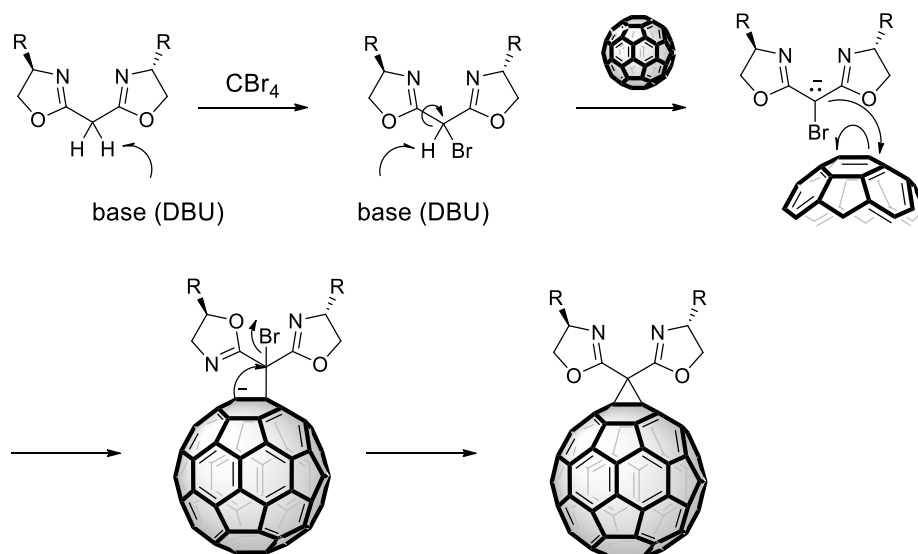
The mono addition of the BOX on the C<sub>60</sub>, was achieved by the Bingel-Hirsch reaction<sup>10, 41</sup>

Bisoxazoline was reacted for 24 hours with 1.3 equivalents of fullerene in 1,2-dichlorobenzene (*o*-DCB) in the presence of tetrabromomethane (CBr<sub>4</sub>) and 1,5-diazabicyclo(5.4.0)undec-7-ene (DBU) as base (**Scheme 2.2**).



**Scheme 2.2.** Mono-adduct synthesis.

The first part of the reaction is the *in situ* generation of the bromine derivative of the BOX using CBr<sub>4</sub>. Then the base removes the proton from the methylene bridge with consequential generation of a carbanion that reacts hence with a double bond on the fullerene. The nucleophilic addition on the double bond of the fullerene generate again a carbanion that reacts in an intramolecular nucleophilic aliphatic substitution with the bromine resulting in a ring closure obtaining finally the cyclopropanation (**Scheme 2.3**).



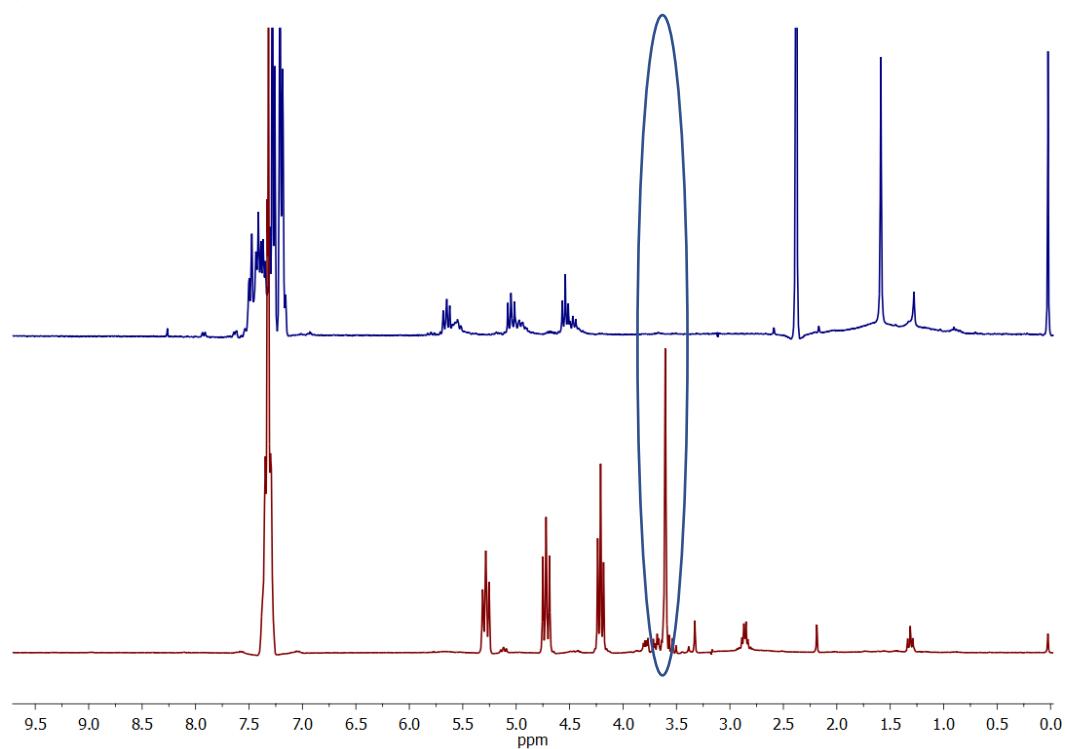
**Scheme 2.3.** Bingel's reaction mechanism for the  $\text{C}_{60}$  functionalization.

The mixture of products obtained was purified by flash chromatography in  $\text{SiO}_2$ , eluting with 5:1 toluene/ethyl acetate (+0.2 v/v% of triethylamine). An excess of fullerene was used to minimize the formation of multi-products and to maximize the formation of monoadducts.

The obtained monoadducts were successfully characterised by means of  $^1\text{H}$ - and  $^{13}\text{C}$ -NMR, and by FT-IR spectroscopy. In the  $^1\text{H}$ -NMR (**Figure 2.14**) it is possible to observe the disappearance of the signal for the methylene bridge, together with the integrity of the bisoxazoline, confirmed by the unchanged pattern of signals.

In the FT-IR spectra covalent functionalization is confirmed by the presence of the  $1661\text{ cm}^{-1}$  band related to the  $\text{C}=\text{N}$  bond of the oxazoline ring along with the bands at  $523$  and  $697\text{ cm}^{-1}$ , characteristic of the fullerene cage.

a)



b)

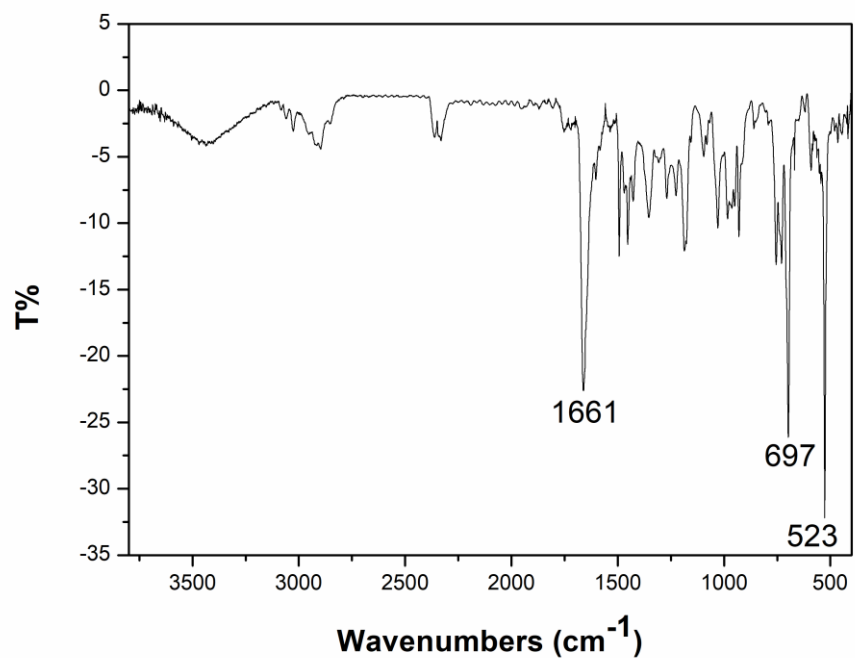
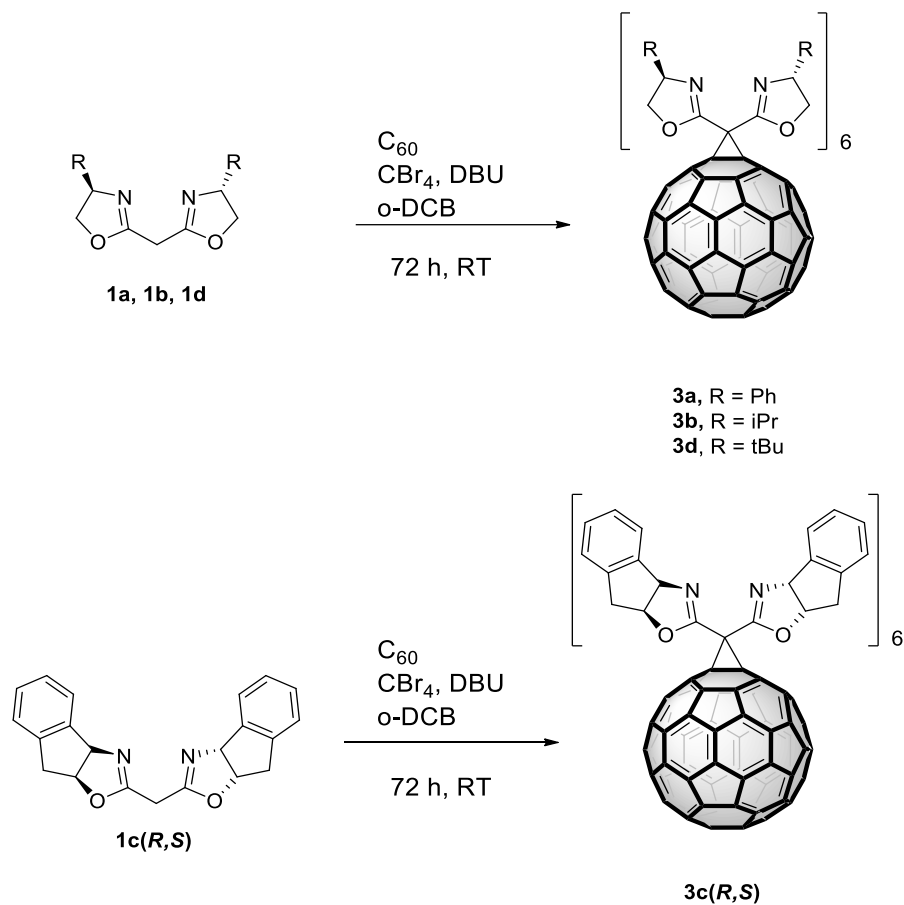


**Figure 2.14.** a) <sup>1</sup>H-NMR spectra of the PhBOX (red line) and the C<sub>60</sub>-PhBOX **2a** (blue line) in which is possible to note the disappearance of the protons of the methylene bridge. b) FT-IR spectrum of the C<sub>60</sub>-PhBOX.



### 2.3.1.3 Synthesis of C<sub>60</sub>-BOX<sub>6</sub> (hexakisadducts)

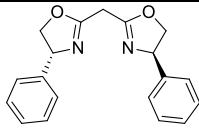
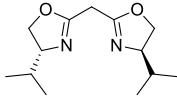
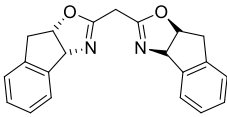
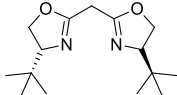
The C<sub>60</sub>-BOX<sub>6</sub> syntheses were performed by following the procedure reported by Seifermann *et al.*,<sup>42</sup> reacting C<sub>60</sub> with 10 equivalents of the proper BOX with a large excess of CBr<sub>4</sub> (100 eq.), DBU as base in *o*-DCB as solvent (**Scheme 2.4**).



**Scheme 2.4.** Synthesis of the hexakis-adducts.

The synthesized hexakisadducts are listed in **Table 2.2** with their yields. The mixture of products has been purified by silica gel column (toluene/ethyl acetate 9:1+ 0.1% v/v MeOH + 0,2% v/v triethylamine) and characterized.

**Table 2.2.** Series of hexakisadduct synthesized with respective yields.

BOX	Hexakisadduct	Yield (%)
 PhBOX <b>1a</b>	C <sub>60</sub> -PhBOX <sub>6</sub> ( <b>3a</b> )	68%
 iPrBOX <b>1b</b>	C <sub>60</sub> -iPrBOX <sub>6</sub> ( <b>3b</b> )	67%
 IndaBOX (R,S) <b>1c (R,S)</b>	C <sub>60</sub> -IndaBOX <sub>6</sub> ( <b>3c(R,S)</b> )	65%
 tBuBOX <b>1d</b>	C <sub>60</sub> -tBuBOX <sub>6</sub> ( <b>3d</b> )	67%

The structure of the hexakis-adducts was confirmed by <sup>13</sup>C-NMR analysis. In **Figure 2.15**, all the signals related to the PhBOX carbons are present (black square). The octahedral substitution pattern, typical for hexakis functionalised fullerenes, can be clearly discerned.<sup>43</sup> In particular, the signal at  $\delta$  70.20 ppm (violet diamond), is related to sp<sup>3</sup> functionalised carbon of the nanocage, whereas at  $\delta$  141.45 ppm and  $\delta$  145.58 ppm (green pentagons), it is possible to observe the signals for the sp<sup>2</sup> carbons of the C<sub>60</sub>. All these signals, along with that at  $\delta$  34.92 ppm belonging to the methanofullerene bridgehead, confirm the achievement of the T<sub>h</sub> symmetry of the obtained product (**Figure 2.15**).

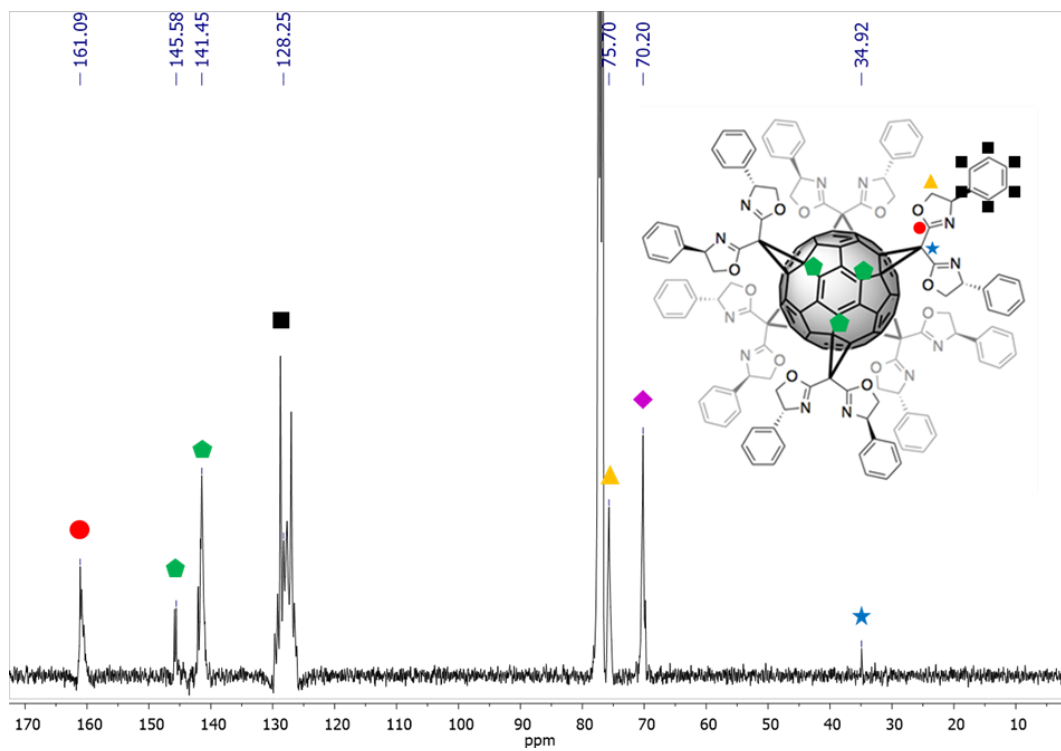
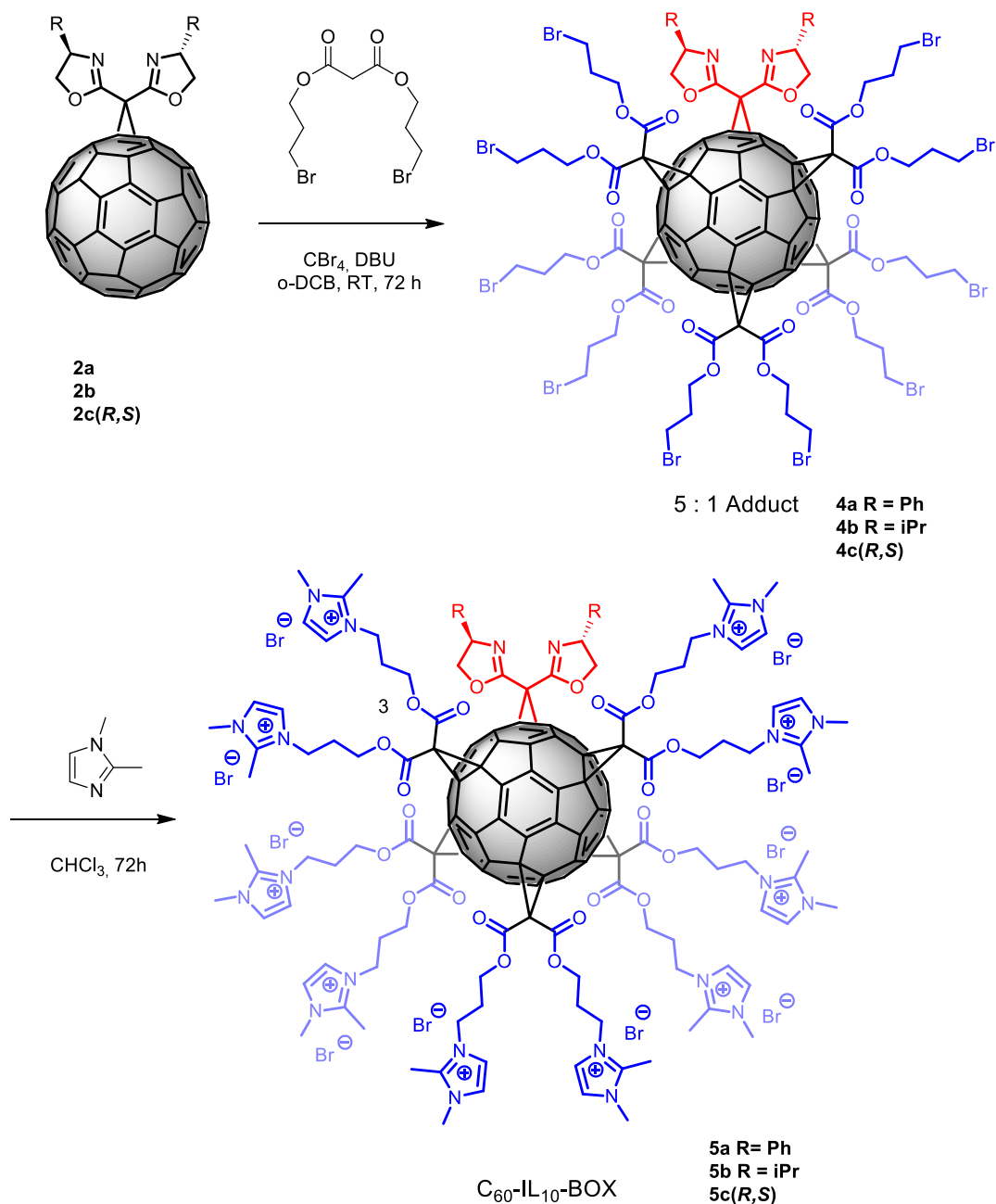


**Figure 2.15.**  $^{13}\text{C}$ -NMR of hexakis-adduct  $\text{C}_{60}$ -PhBOX<sub>6</sub>

### 2.3.1.4 Synthesis of IL Hybrids ( $C_{60}$ -IL<sub>10</sub>-BOX)

The synthesis of fullerene-ionic liquid-bisoxazoline hybrid ( $C_{60}$ -IL<sub>10</sub>-BOX) systems followed a previously reported modular approach described by our group of research<sup>13</sup> to get similar adducts (**Scheme 2.5**).



**Scheme 2.5.** Synthetic pathway for the synthesis of fullerene-ionic liquid-bisoxazoline hybrids.

The first step was the reaction between a  $C_{60}$ -BOX monoadduct with 10 equivalents of bis(3-bromopropyl) malonate, in the presence of  $CBr_4$  and DBU in *o*-DCB as

solvent. The so obtained [5:1] adducts were isolated after purification with flash chromatography, characterized (**Figure 2.16** and **2.17**) and subsequently reacted for 72 hours with 1,2-dimethylimidazole in chloroform to give the corresponding ionic liquid hybrids with quantitative yields (**Table 2.3**)

**Table 2.3.** [5:1] adducts and IL Hybrid obtained with the corresponding yields.

[5:1] Adduct	Yield	IL Hybrid	Yield
[5:1] PhBOX ( <b>4a</b> )	31%	C <sub>60</sub> - <b>IL</b> <sub>10</sub> -PhBOX ( <b>5a</b> )	87%
[5:1] iPrBOX ( <b>4b</b> )	36%	C <sub>60</sub> - <b>IL</b> <sub>10</sub> -iPrBOX ( <b>5b</b> )	97%
[5:1] IndaBOX ( <b>4c(R,S)</b> )	38%	C <sub>60</sub> - <b>IL</b> <sub>10</sub> -IndaBOX ( <b>5c(R,S)</b> )	93%

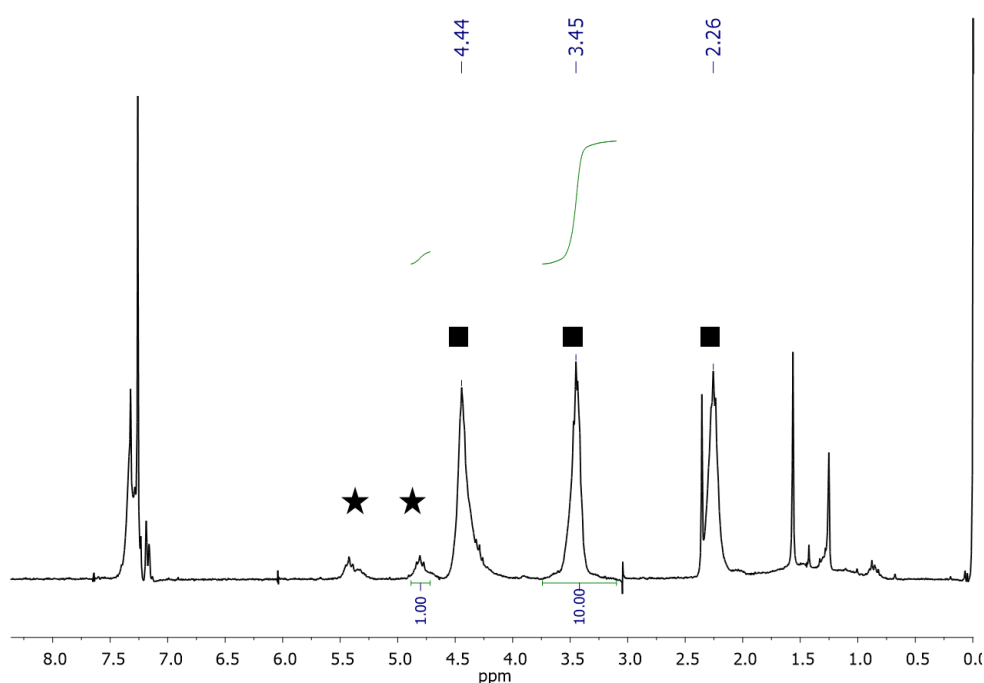


**Figure 2.16.** <sup>1</sup>H-NMR of [5:1] adduct of the PhBOX (**4a**). Black stars point out PhBOX while black squares -CH<sub>2</sub> related to bis(3-bromopropyl).

In **Figure 2.16** <sup>1</sup>H-NMR of the [5:1] adduct of the PhBOX. It is possible to see, labelled by black squares, the pattern of the protons of the aliphatic chain of the bis(3-bromopropyl) malonate and at the same time the signals related to the PhBOX (black stars). In the spectrum is also possible to see that the integrated area confirms the right functionalization of five bis(3-bromopropyl) malonate and one PhBOX.

FTIR spectrum also confirm the functionalization of the C<sub>60</sub>-BOX monoadduct with five malonate moieties (**Figure 2.17**).

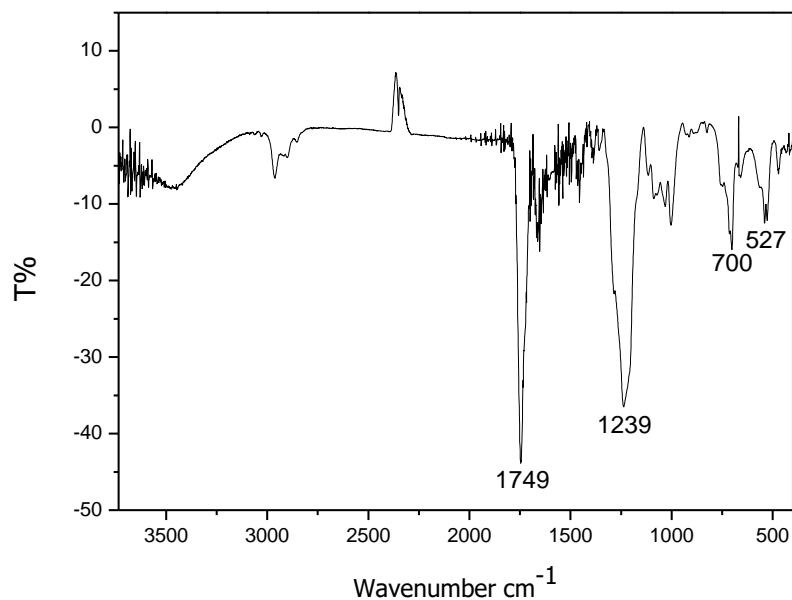


**Figure 2.17.** FT-IR spectrum of the [5:1] adduct of the PhBOX (**4a**).

In particular is possible to observe: 1) the bands at 1749 cm<sup>-1</sup> (C=O stretching) and 1239 cm<sup>-1</sup> (C-O stretching) that confirm the presence of the malonate bands and 2) the bands at 700 cm<sup>-1</sup> and 527 cm<sup>-1</sup> that confirm the presence of the fullerene.

About the IL-Hybrid in **Figure 2.18** is reported <sup>1</sup>H-NMR of the **5a**. Signals labelled with black squares are related to 1,2-dimethylimidazole. In particular at 2.65ppm and 3.83ppm are related to the protons of the methyl group. Otherwise, stars point out the signals of the proton of the bis(3-bromopropyl) malonate.

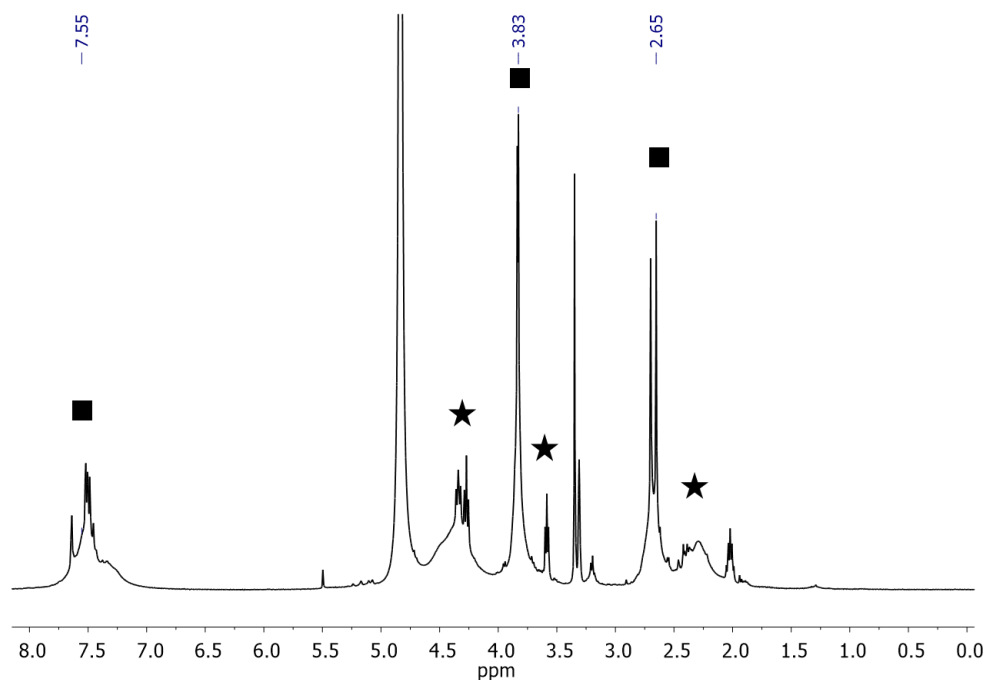


**Figure 2.18.**  $^1\text{H}$ NMR of IL-Hybrid of the PhBOX (**5a**). Black stars point out  $-\text{CH}_2$  related to bis(3-bromopropyl) while black squares Signals of 1,2-dimethylimidazole.

The three types of fullerene-BOX systems (monoadducts, hexakisadducts and  $\text{C}_{60}$ - $\text{IL}_{10}$ -BOX hybrids) show different solubility profiles:

- the monoadducts displays a solubility similar to the non-functionalised fullerene: they are very soluble in toluene and slightly soluble in chlorinated solvents.
- The hexakisadducts, on the other hand, having less  $\text{C}_{60}$  surface area exposed than the parent fullerene, are very soluble in dichloromethane and chloroform and, basically, they acquire the solubility of the BOXs.
- $\text{C}_{60}$ - $\text{IL}_{10}$ -BOX hybrids are soluble in polar solvents such as methanol, ethanol and water, thanks to the presence of numerous imidazolium bromide moieties.

The above systems with different solubility profiles could be useful for catalysis purposes, since explore a number of solvent media in order to obtain the best reaction conditions. The three classes of compounds, finally, are insoluble in non-polar solvents (hexane, petroleum ether, diethyl ether) and this feature could be exploited to separate and recover catalysts at the end of each catalytic cycle.

## 2.3.2 Catalytic applications

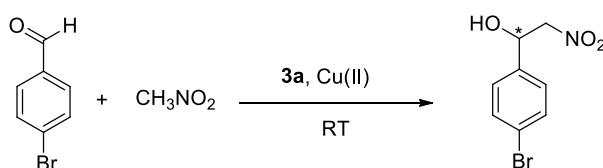
### 2.3.2.1 Asymmetric Henry

As already said, Henry reaction takes place between a nitroalkane and an aldehyde using a copper salt as catalyst (**Figure 2.7**). In order to make the reaction asymmetric, it is possible to complex the copper salt with a proper chiral ligand that can provide the desired configuration to the final product.

Based on previous studies in literature, 4-bromobenzaldehyde was chosen as benchmark substrate, given that it provides the best compromise between conversion and enantiomeric excess.<sup>29, 44</sup>

Preliminary tests were performed to find the best reaction conditions by varying solvent, amount of catalyst and metal salt (**Table 2.5**). In these tests the hexakisadduct **3a** was chosen as it represents the system with the highest catalytic loading per fullerene molecule.

**Table 2.5.** Screening of the reaction conditions for the asymmetric Henry reaction.<sup>a</sup>



Entry	Conditions	Time (h)	Conv. (%) <sup>b</sup>	ee (%) <sup>c</sup>
1	$\text{CH}_3\text{NO}_2$ , <b>3a</b> 2 mol % + $\text{Cu(OAc)}_2$	48	14	34
2	EtOH 4:1, <b>3a</b> 2 mol % + $\text{Cu(OAc)}_2$	48	44	26
3	EtOH 4:1, <b>3a</b> 2 mol % + $\text{Cu(OTf)}_2$	48	26	21
4	EtOH 2:1, <b>3a</b> 2 mol % + $\text{Cu(OAc)}_2$	48	48	33
5	EtOH 1:1, <b>3a</b> 5 mol % + $\text{Cu(OAc)}_2$	24	82	31

a) Reaction conditions: 0.4 mmol aldehyde, 4 mmol nitromethane,  $\text{CH}_3\text{CH}_2\text{OH}$  according to the reported ratio with nitromethane. b) Determined by  $^1\text{H}$  NMR spectroscopic analysis of the crude product. c) Determined by HPLC using a chiral column (OD-H hexane-*i*PrOH 90:10).

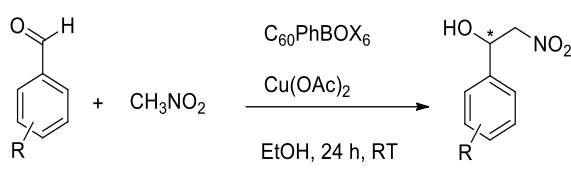
The chosen catalyst, the copper salt and the solvent were mixed for 30 minutes in a vial resulting in a homogeneous system for the hexakisadducts and for the  $\text{C}_{60}\text{-IL}_{10}$ -



BOX hybrids, while resulting in a heterogeneous system for the monoadducts. Then aldehyde and nitromethane were added, and the mixture was left under stirring for the appropriate time at room temperature.

The best reaction conditions resulted those reported in entry 5: 5 mol % of ligand, using copper acetate as salt and 200  $\mu$ L of EtOH as solvent. Using these conditions, other substrates were tested for analysing the effect of substituents on the aldehyde (**Table 2.6**).

**Table 2.6.** Asymmetric Henry reaction promoted by  $C_{60}$ PhBOX<sub>6</sub> on a set of aromatic aldehydes.<sup>a</sup>



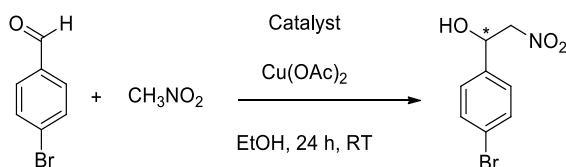
Entry	R	Conv. (%) <sup>b</sup>	ee (%) <sup>c</sup>
1	4-Br	82	31
2	2-NO <sub>2</sub>	91	11
3	4-NO <sub>2</sub>	92	6
4	4-CN	65	2
5	2,4-OMe	42	5
6	4-OMe	10	16
7	4-Cl	96	6

Reaction conditions: 0.4mmol aldehyde, 4mmol nitromethane, 200 $\mu$ L  $CH_3CH_2OH$ . b) Determined by <sup>1</sup>H NMR spectroscopic analysis of the crude product. c) Determined by HPLC using a chiral column OD-H (hexane-iPrOH 90:10).

As expected, since Henry's reaction is a nucleophilic addition to carbonyl compounds, the electron-withdrawing substituents had a positive effect on the yield (entries 1,2,3 and 7). However, although in several cases almost quantitative conversion was achieved (entries 3-7), the enantiomeric excesses resulted low. Nevertheless, in all subsequent tests, 4-bromobenzaldehyde remained the benchmark substrate in the asymmetric Henry reaction for the assessment of the

catalytic activity of all the prepared C<sub>60</sub>-BOX systems. The results are collected in **Table 2.7**.

**Table 2.7.** Results of catalytic tests for all the catalytic systems.



	Entry	Cat.	Conv. (%) <sup>b</sup>	ee (%) <sup>c</sup>
<b>BOX</b>	1	<b>PhBOX (1a)</b> 5% mol + Cu(OAc) <sub>2</sub>	27	-10
	2	<b>iPrBOX (1b)</b> 5% mol + Cu(OAc) <sub>2</sub>	43	-50
	3	<b>IndaBOX (1c(R,S))</b> 5% mol + Cu(OAc) <sub>2</sub>	27	33
	4	<b>IndaBOX (1c(S,R))</b> 5% mol + Cu(OAc) <sub>2</sub>	57	-39
	5	<b>tBuBOX (1d)</b> 5% mol + Cu(OAc) <sub>2</sub>	60	-53.4
<b>C<sub>60</sub>-BOX</b>	6	<b>C<sub>60</sub>-PhBOX (2a)</b> 5% mol + Cu(OAc) <sub>2</sub>	24	-4
	7	<b>C<sub>60</sub>-iPrBOX (2b)</b> 5% mol + Cu(OAc) <sub>2</sub>	20	racemic
	8	<b>C<sub>60</sub>-IndaBOX (2c(R,S))</b> 5% mol + Cu(OAc) <sub>2</sub>	22	13
	9	<b>C<sub>60</sub>-IndaBOX (2c(S,R))</b> 5% mol + Cu(OAc) <sub>2</sub>	27	-17
	10	<b>C<sub>60</sub>-tBuBOX (2d)</b> 5% mol + Cu(OAc) <sub>2</sub>	39	Racemic
<b>C<sub>60</sub>-BOX<sub>6</sub></b>	11	<b>C<sub>60</sub>-PhBOX<sub>6</sub> (3a)</b> 5% mol + Cu(OAc) <sub>2</sub>	46	-10
	12	<b>C<sub>60</sub>-iPrBOX<sub>6</sub> (3b)</b> 5% mol + Cu(OAc) <sub>2</sub>	19	-4
	13	<b>C<sub>60</sub>-IndaBOX<sub>6</sub> (3c(R,S))</b> 5% mol + Cu(OAc) <sub>2</sub>	67	46
	14	<b>C<sub>60</sub>-tBuBOX<sub>6</sub> (3d)</b> 5% mol + Cu(OAc) <sub>2</sub>	13	-4
<b>IL-Hybrid</b>	15	<b>C<sub>60</sub>-IL<sub>10</sub>-PhBOX (5a)</b> 2% mol + Cu(OAc) <sub>2</sub>	54	-10
	16	<b>C<sub>60</sub>-IL<sub>10</sub>-iPrBOX (5b)</b> 2% mol + Cu(OAc) <sub>2</sub>	65	-14
	17	<b>C<sub>60</sub>-IL<sub>10</sub>-IndaBOX (5c(R,S))</b> 2% mol + Cu(OAc) <sub>2</sub>	68	18

Reaction conditions: 0.4 mmol 4-bromobenzaldehyde, 4 mmol of nitromethane, 200  $\mu$ L of ethanol.

b) Determined by <sup>1</sup>H NMR spectroscopic analysis of the crude product. c) Determined by HPLC using a chiral column (OD-H hexane-iPrOH 90:10).

Firstly, the unsupported BOXs **1a-1d** were tested under the same conditions in order to have an insight on the performances of the catalytic systems without fullerene (entries 1-5).

Fullerene-BOX monoadducts showed, generally speaking, low conversions in comparison with the unsupported systems (entries 6-10), being derivative **2c(S,R)**

the most active of the series (entry 9). This finding could be probably due to the fact that C<sub>60</sub>-BOX hybrids were not soluble in ethanol and took part in the reaction as heterogeneous catalysts. Monoadducts remain suspended in the reaction mixture as solids and suffer from mass transport limitations.

On the other hand, hexakisadducts endowed with aromatic substituents (PhBOX, IndaBOX) showed better result than the corresponding mono-adducts but also than the unsupported BOXs (entries 11, 13). This fact can be ascribed to their improved solubility in the nitromethane, which allows them to take part to the reaction as homogeneous catalysts. Conversely, C<sub>60</sub>BOX<sub>6</sub> systems **3b** and **3d** with alkyl chains displayed similar performances than the parent monoadducts (entries 12, 14).

Regarding C<sub>60</sub>-IL<sub>10</sub>-BOX hybrids, these were used at 2 mol% to reduce the amount of substance employed in each reaction, given their high molecular weights. Even in this case, they took part in the reaction as homogeneous catalysts since they were soluble in ethanol, giving the highest levels of conversion among all the hybrids tested, included the unsupported (entries 15-17).

Unfortunately, enantiomeric excesses were low and worse than those obtained with the other systems.

For all the catalytic tests, the chirality of the major enantiomer was *S* and depended on the stereochemistry of the catalysts used (PhBOX, *i*PrBOX and *t*BuBOX derivatives).

Separate considerations should be made for the IndaBOXs derivatives. In fact, they were synthesized in two different stereoisomers: **1c(R,S)** from (*1R,2S*)-(+)-*cis*-1-amino-2-indanol and **1c(S,R)** from (*1S,2R*)-(+)-*cis*-1-amino-2-indanol (Figure 10). As expected, they gave back opposite results: in fact, the **1c(R,S)** catalysed the formation of the enantiomer (*R*) for the nitroaldol adducts, while the **1c(S,R)** the formation of the (*S*) enantiomer (**Figure 2.19**).

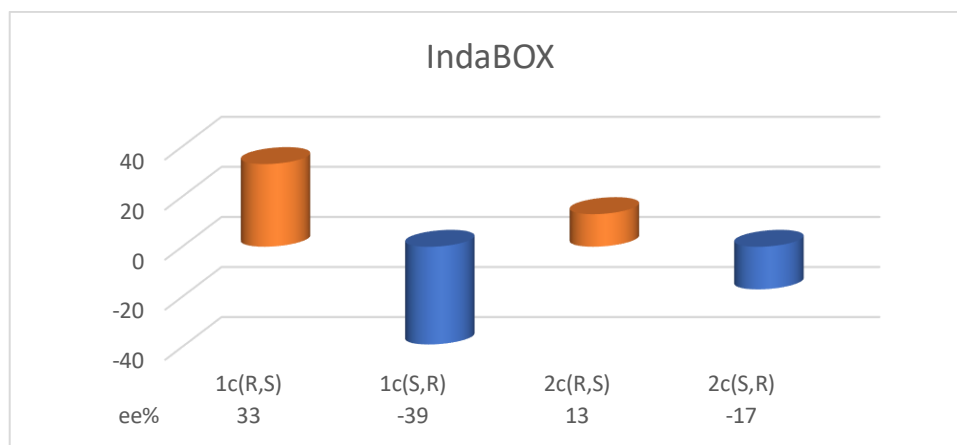
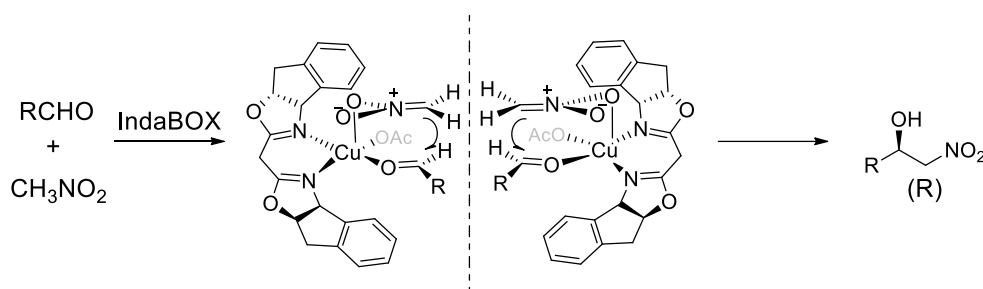


**Figure 2.19.** Comparison of different IndaBOX enantiomers.

The different asymmetric induction is rationalized by means of the specular transition states formed during the catalytic cycle with the two different enantiomers, as described in **Scheme 2.6**. These have a distorted square pyramidal configuration with the nucleophiles in an axial position in correspondence to the less bulky face of the electrophile, which is instead on the plane of the ligand.<sup>45</sup>



**Scheme 2.6.** Transition state in asymmetric Henry reaction with BOX ligands

Among all the prepared systems, IndaBOX derivatives showed the best results in terms of conversion and enantiomeric excess. In **Figure 2.20** IndaBOX-derivatives **1c(R,S)**, **2c(R,S)**, **3c(R,S)** and **5c(R,S)** are collected for comparison.

In this series, the mono-adduct **2c(R,S)** is the less active whereas the hexakis-adduct **3c(R,S)** and the IL-hybrid **4c(R,S)** gave good result in terms of conversion, even better than the unsupported **1c(R,S)**. In addition, the hexakisadduct gave also a higher enantioselectivity than the unsupported IndaBOX.

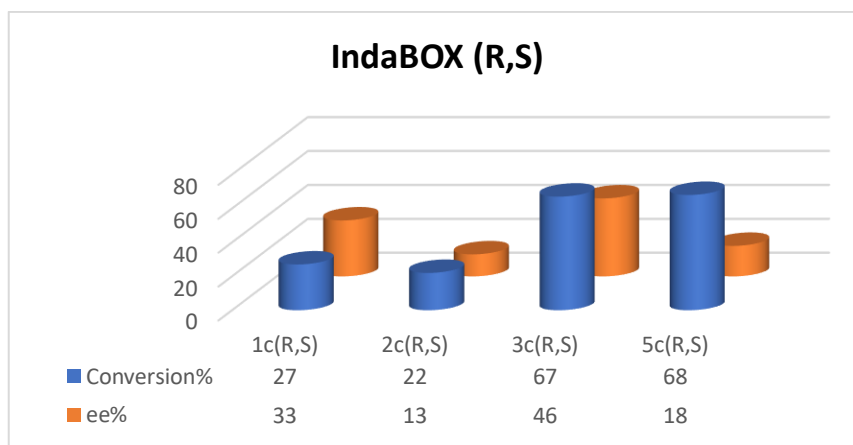


**Figure 2.20.** Comparison of all the IndaBOX-based catalysts.

Finally, the recyclability of the synthesized adducts that gave the best performance (IndaBOX derivative **3c(R,S)**) was tested. At the end of each reaction, the catalyst was precipitated by adding diethyl ether, recovered by centrifugation and used in a new cycle. In fact, the low solubility of the catalyst in diethyl ether represents an outstanding advantage over unsupported boxes, which cannot be separated from the reaction mixture and, moreover, quickly decompose at the end of the first cycle. The recovered catalyst was reacted with fresh copper salt to reform the catalytic complex and then aldehyde and nitromethane are added for a new cycle. The catalyst showed good recyclability, maintaining the same conversion level for up to five consecutive reactions (**Figure 2.21**).

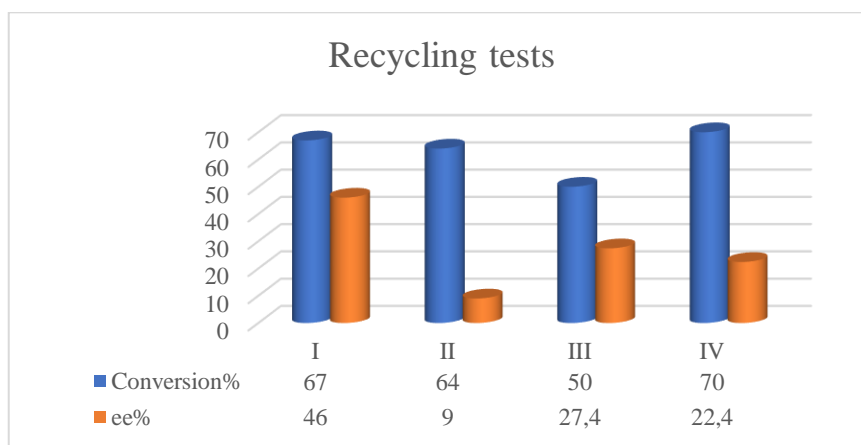


**Figure 2.21.** Recycling tests for the hexakisadduct **3c(R,S)** ( $C_{60}$ -INDABOX<sub>6</sub>).

### 2.3.2.2 Asymmetric Diels-Alder

As stated, Diels-Alder [4+2] cycloaddition occurs between a conjugated diene and an alkene (**Figure 2.8**). Here, asymmetric Diels-Alder tests were conducted on a scale of 0.33 mmol of alkene, 3-acryloyl-2-oxazolidinone (as dienophile), copper triflate and the fullerene-based adduct to drive the stereochemistry of the cycloaddition, using known reaction conditions.<sup>31b,46</sup> The chosen ligand and copper triflate were mixed for 30 minutes in a vial in DCM. After 30 minutes, freshly distilled dienophile and cyclopentadiene were added and allowed to react for 24 hours at room temperature.

Then, the reaction mixture was purified by means of a silica gel pad (hexane/ethyl acetate 3:1) and the crude was analysed by <sup>1</sup>H-NMR in order to determine the conversion and the *endo/exo* ratio (**Figure 2.22**). The enantiomeric excess was determined by chiral HPLC (Chiralcel OD-H, hexane/isopropanol 90:10).

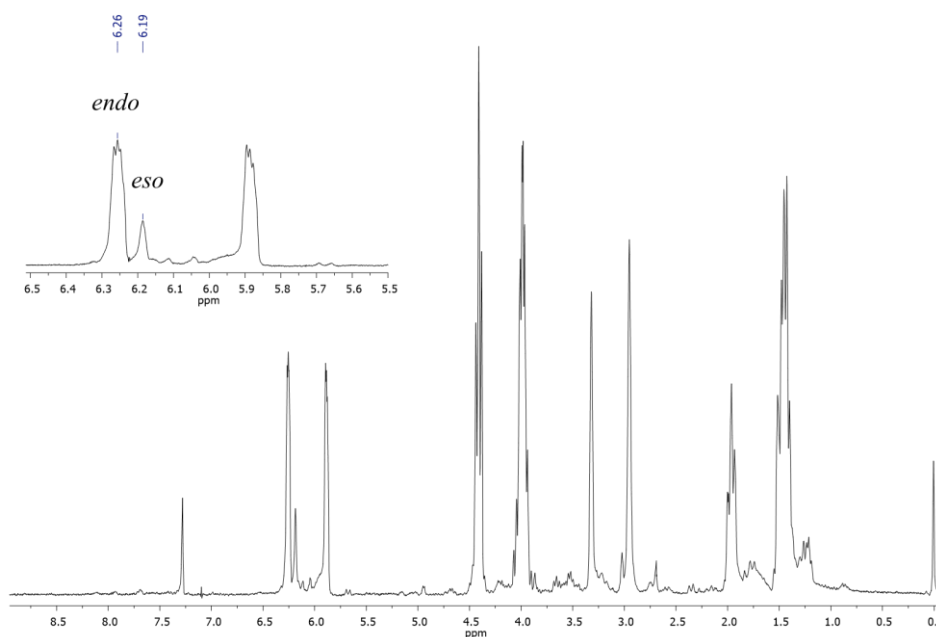


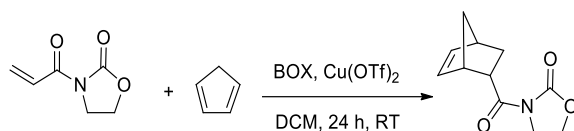
**Figure 2.22.** <sup>1</sup>H-NMR spectrum of Diels-Alder reaction crude. In the inset, the magnification highlighting the signals for the *endo* and *exo* products is reported.

As for the study of the Henry reaction, initially, the unsupported BOXs **1a-1d** were tested under the Diels-Alder conditions in order to have an insight on the performances of the catalytic systems without fullerene (entries 1-3). All the systems gave almost quantitative conversions but the selectivity was rather low,

except in the case of IndaBOX that is known to be the among best catalysts in asymmetric Diels-Alder reaction (entry 3).<sup>25, 47</sup>

Both mono- and hexakis- C<sub>60</sub>-adducts showed very low ee values compared to the unsupported BOXs (entries 4-9), comparable to the values obtained in the presence of Lewis acid (Cu(OTf)<sub>2</sub>) alone (entry 13). Regarding the C<sub>60</sub>-IL<sub>10</sub>-BOX hybrids (entries 10, 11, 12), the different activity of the catalysts in terms of endo/exo ratio can be attributed to the fact that the hybrids were insoluble in the reaction media (DCM) compared to the other two classes of adducts. This led to a lower complexation with the metal, and to a generic and not asymmetric catalysis.

**Table 2.8.** summary table of the data of the asymmetric reaction of Diels-Alder.



	Entry	Catalyst	Conv. <sub>b</sub> (%)	Endo/Exo <sub>b</sub>	ee (%) <sup>c</sup>
BOX	1	<b>PhBOX (1a)</b> 5% mol + Cu(OTf) <sub>2</sub>	92	82 : 18	12
	2	<b>iPrBOX (1b)</b> 5% mol + Cu(OTf) <sub>2</sub>	99	85 : 15	4
	3	<b>IndaBOX (1c(R,S))</b> 5% mol + Cu(OTf) <sub>2</sub>	95	90 : 10	76
C <sub>60</sub> -BOX	4	<b>C<sub>60</sub>-PhBOX (2a)</b> 5% mol + Cu(OTf) <sub>2</sub>	93	78 : 22	0
	5	<b>C<sub>60</sub>-iPrBOX (2b)</b> 5% mol + Cu(OTf) <sub>2</sub>	97	80 : 20	4
	6	<b>C<sub>60</sub>-IndaBOX (2c(R,S))</b> 5% mol + Cu(OTf) <sub>2</sub>	94	80 : 20	20
C <sub>60</sub> -BOX <sub>6</sub>	7	<b>C<sub>60</sub>-PhBOX<sub>6</sub> (3a)</b> 5% mol + Cu(OTf) <sub>2</sub>	95	87 : 13	0
	8	<b>C<sub>60</sub>-iPrBOX<sub>6</sub> (3b)</b> 5% mol + Cu(OTf) <sub>2</sub>	94	86 : 14	4
	9	<b>C<sub>60</sub>-IndaBOX<sub>6</sub> (3c(R,S))</b> 5% mol + Cu(OTf) <sub>2</sub>	90	83 : 17	20
IL-Hybrid	10	<b>C<sub>60</sub>-IL<sub>10</sub>-PhBOX (5a)</b> 2% mol + Cu(OTf) <sub>2</sub>	88	90 : 10	0
	11	<b>C<sub>60</sub>-IL<sub>10</sub>-iPrBOX (5b)</b> 2% mol + Cu(OTf) <sub>2</sub>	93	90 : 10	2
	12	<b>C<sub>60</sub>-IL<sub>10</sub>-IndaBOX (5c(R,S))</b> 2% mol + Cu(OTf) <sub>2</sub>	91	90 : 10	8
	13	5% Cu(OTf) <sub>2</sub>	92	82 : 18	-

The high conversion values and the low ee obtained, in all cases, indicate that the cyclopentadiene, under the conditions examined, is too reactive and follows a general Lewis acid-mediated cycloaddition, ignoring the chiral induction due to the presence of chiral BOX-copper complex. However, the possibility to recycle the catalytic system was investigated for the Diels-Alder reaction. At the end of each

reaction, the C<sub>60</sub>-INDABOX<sub>6</sub> adduct (**3c(R,S)**) was precipitated from ethyl ether and reused in a new cycle adding fresh reagents. The hexakis-adduct has proved to be the most stable system, maintaining almost unchanged both activity and selectivity (**Figure 2.23**).

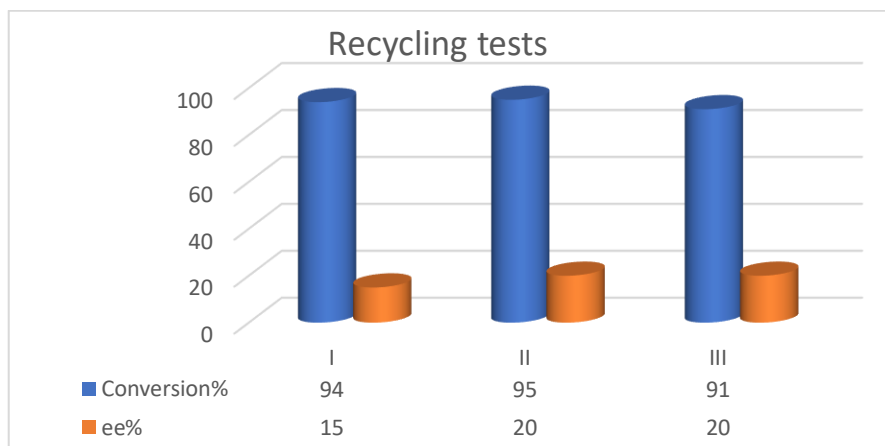
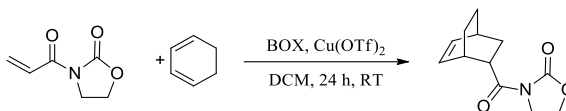


**Figure 2.23.** Recycling tests for the Diels-Alder reaction with hexakisadduct **3c(R,S)**

To verify the catalytic properties of these adducts with respect to the asymmetric Diels-Alder reaction, an attempt was done using the less reactive 1,3-cyclohexadiene, under the same conditions.

Unfortunately, the results were not satisfying (**Table 2.9**). Conversions resulted, as expected, lower than those achieved with pentadiene and, furthermore, for this substrate it was not possible to determine the enantiomeric excess.

**Table 2.9.** Diels-Alder reaction with 1,3-cyclohexadiene.



	Entry	Catalyst	Conv.(%)	Endo/Exo	ee(%)
BOX	1	PhBOX ( <b>1a</b> ) 5% mol + Cu(OTf) <sub>2</sub>	37	48 : 52	-
	2	iPrBOX ( <b>1b</b> ) 5% mol + Cu(OTf) <sub>2</sub>	36	47 : 53	-
	3	IndaBOX ( <b>1c(R,S)</b> ) 5% mol + Cu(OTf) <sub>2</sub>	39	47 : 53	-
C <sub>60</sub> -BOX <sub>6</sub>	4	C <sub>60</sub> -PhBOX <sub>6</sub> ( <b>3a</b> ) 5% mol + Cu(OTf) <sub>2</sub>	40	47 : 53	-
	5	C <sub>60</sub> -iPrBOX <sub>6</sub> ( <b>3b</b> ) 5% mol + Cu(OTf) <sub>2</sub>	39	49 : 51	-
	6	C <sub>60</sub> -IndaBOX <sub>6</sub> ( <b>3c(R,S)</b> ) 5% mol + Cu(OTf) <sub>2</sub>	56	45 : 55	-
	7	5% Cu(OTf) <sub>2</sub>	No reaz.	-	-



## 2.4 Conclusions

A set of chiral bisoxazolines were prepared through simple one-pot reactions, and subsequently they were anchored to C<sub>60</sub> fullerene to form three types of hybrid molecular systems with possible catalytic applications: monoadducts, hexakisadducts and hybrid [5:1] adducts with ionic liquids. The simple steps of separation and purification allowed obtaining comparable or superior (in the case of hexakisadducts) yields to those reported in the literature. The structure and the addition patterns of the products have been confirmed by carbon and proton NMR and IR spectroscopy. These systems were tested, along with copper salts, as asymmetric catalytic systems in the Henry and the Diels-Alder reactions. In both cases the catalysts did not give very high selectivities but, especially for nitroaldol reactions, an increase in conversion and enantiomeric excess was observed compared to the unsupported boxes. This finding, together with the possibility to easily recover and to recycle the catalysts without significant loss of activity, paved the way to further studies on the subject. This work, in fact, represents the first real application of C<sub>60</sub>-bisoxazoline adducts as catalytic systems for asymmetric reactions.

In consideration of the results obtained, it is clear that further optimisations are necessary in order to allow these materials to fulfil their potential and to provide the best performances: both at the level of the catalysts, through better chiral substituents or different bridges between the oxazoline rings, and at the level of the reaction conditions, operating a greater control over the temperature and using different solvents and metal cations.

## 2.5 Experimental section

All the reagents and solvents in this work were used as purchased from the respective companies (Merck, TCI, Fluorochem). The FT-IR spectra of the products obtained have been recorded on an Agilent Tech CARY630 FT-IR spectrometer. <sup>1</sup>H-NMR were performed at the University of Palermo with a Bruker 300 MHz spectrometer, <sup>13</sup>C-NMR were performed at the University of Namur on a Varian

VNMR spectrometer. Enantiomeric excesses were determined with a LC10 AD Shimadzu Liquid Chromatograph HPLC (Chiralcel OD-H).

### **General procedure for the synthesis of PhBOX and iPrBOX**

In a round bottom flask containing 30 ml of 1,2-dichloroethane, 4.33 mmol of diethyl malonimidate dihydrochloride, 2 equivalents of the corresponding amino-alcohol and 2 equivalents of Et<sub>3</sub>N were added. The reaction mixture was stirred 18 hours at 84°C in inert atmosphere. The mixture was poured into 50 ml of distilled water and extracted three times with dichloromethane; organic fractions were collected, dried over MgSO<sub>4</sub>, and the solvent removed under reduced pressure. The product was purified by column chromatography (dichloromethane/methanol 99:1 + 0.2% v/v of Et<sub>3</sub>N).

**PhBOX:** Diethyl malonimidate dihydrochloride (1.00 gr) and L-(+)- $\alpha$ -phenylglycinol (1.25 gr) reacted in accordance with the general procedure. The product was obtained as a viscous yellow liquid, with a yield of 67%.

<sup>1</sup>H NMR (300 MHz, CDCl<sub>3</sub>)  $\delta$  = 7.32 (q,  $J$  = 4.9, 10H), 5.28 (t,  $J$  = 9.0, 2H), 4.72 (dd,  $J$  = 9.6, 9.0, 2H), 4.33 – 4.03 (m, 2H), 3.69 – 3.50 (m, 2H).

<sup>13</sup>C NMR (101 MHz, CDCl<sub>3</sub>)  $\delta$  = 168.27, 166.15, 164.63, 163.03, 141.96, 141.38, 138.76, 128.84, 128.01, 126.79, 77.35, 77.03, 76.71, 75.35, 69.71, 35.01, 28.39.

UV (CH<sub>2</sub>Cl<sub>2</sub>, nm)  $\lambda$  = 270 nm.

**iPrBOX:** Diethyl malonimidate dihydrochloride (1.00 gr) and L-valinol (1.012 mL,  $d=0.926\text{gr/mL}$ ) reacted in accordance with the general procedure. The product was obtained as a viscous yellow liquid, with a yield of 63%.

<sup>1</sup>H NMR (300 MHz, CDCl<sub>3</sub>)  $\delta$  = 7.56 – 7.02 (m, 1H), 4.46 – 4.14 (m, 2H), 4.09 – 3.77 (m, 4H), 3.35 (s, 2H), 1.91 – 1.61 (m, 2H), 1.16 – 0.70 (m, 12H).

<sup>13</sup>C NMR (101 MHz, CDCl<sub>3</sub>)  $\delta$  = 167.12, 163.33, 161.54, 77.34, 77.02, 76.70, 72.11, 70.52, 64.38, 57.83, 34.55, 32.42, 28.32, 18.61, 17.96. UV (CH<sub>2</sub>Cl<sub>2</sub>, nm)  $\lambda$  = 273 nm.

### Synthesis of *tert*-Leucinol

*Tert*-Leucine (16 mmol) was dissolved in 45 mL anhydrous THF with 2.5 equivalent of NaBH<sub>4</sub> in inert atmosphere at 0 °C. A solution of I<sub>2</sub> (19 mmol) in anhydrous THF was added to the *tert*-Leucine solution *via* cannula under stirring maintaining the solution at 0°C in inert atmosphere for 15 minutes and the reaction was refluxed overnight.

Then the reaction is brought at room temperature and methanol is added until the powder at the bottom of the flask was completely dissolved (30 mL) and then the solution was stirred for 30 minutes. Hence, 100 mL KOH solution (20%) is added and the resulting solution is stirred at room temperature for 4 h. Then the organic fractions were, dried over MgSO<sub>4</sub> and, the solvent removed under reduced pressure until obtaining the desired product in 75% of yield.<sup>48</sup>

### Synthesis of *t*BuBOX

Diethyl malonimidate dihydrochloride (1.00 gr) and *tert*-Leucinol (1.06 gr) reacted in accordance with the general procedure. The product was obtained as a viscous yellow liquid, with a yield of 65%.

<sup>1</sup>H NMR (300 MHz, CDCl<sub>3</sub>)  $\delta$  = 4.28 – 4.05 (m, 4H), 3.91 (t, 2H), 3.37 (s, 2H), 0.91 (s, 18H)

### Synthesis of IndaBOX

In a round bottom flask containing 52 ml of DCM, 2.5 mmol of diethyl malonimidate dihydrochloride and 4,7 mmol (*1R,2S*)-*cis*-1-amino-2-indanol were added. The reaction mixture was stirred for 18 hours in argon. The mixture was poured into distilled water and extracted with dichloromethane. The organic fractions were, dried over MgSO<sub>4</sub> and, the solvent removed under reduced pressure. The resulting solid is recrystallized from isopropanol, giving white needle-shaped solid with a yield of 57%.

<sup>1</sup>H NMR (300 MHz, CDCl<sub>3</sub>)  $\delta$  = 7.46 (dt, *J* = 12.9, 6.3, 2H), 7.37 – 7.19 (m, 6H), 5.58 (t, *J* = 6.7, 2H), 5.36 (tt, *J* = 5.5, 2.7, 2H), 3.51 – 3.07 (m, 6H).

<sup>13</sup>C NMR (101 MHz, CDCl<sub>3</sub>)  $\delta$  = 161.96, 141.61, 139.64, 128.50, 127.44, 125.22, 83.57, 77.37, 77.05, 76.73, 76.66, 39.66, 28.71. UV-Vis (CH<sub>2</sub>Cl<sub>2</sub>, nm)  $\lambda$  = 266 nm.

### General procedure for the synthesis of C<sub>60</sub>-BOX

3,5 mmol of the corresponding BOX, 2 equivalents of CBr<sub>4</sub> and 4 equivalents of DBU were added to a C<sub>60</sub> fullerene solution (1,3 equivalents) in 30 mL of o-DCB. The mixture was stirred for 18 hours at room temperature. After removing the reaction solvent under vacuum, the crude was purified by column chromatography (SiO<sub>2</sub>), eluting first with toluene, to eliminate the not reacted C<sub>60</sub>, then with toluene/ethyl acetate 5:1 (+0.2% v/v of triethylamine). The solvent was removed under reduced pressure and the solid was re-dissolved in the minimum amount of chloroform and re-precipitated in hexane.

**C<sub>60</sub>-PhBOX:** brown solid, yield 48%.

<sup>1</sup>H NMR (300 MHz, CDCl<sub>3</sub>) δ = 7.59 – 7.04 (m, 10H), 5.78 – 5.42 (m, 2H), 5.13–4.81 (m, 2H), 4.51 (dt, *J* = 21.0, 8.4, 2H).

<sup>13</sup>C NMR (101 MHz, CDCl<sub>3</sub>) δ = 160.64, 146.41, 146.29, 145.47, 145.30, 145.21, 144.89, 144.68, 143.89, 143.03, 142.96, 142.17, 141.25, 140.89, 138.88, 138.84, 77.32, 77.00, 76.68.

FT-IR (KBr, cm<sup>-1</sup>) ν = 523, 697, 1661. UV-Vis (CH<sub>2</sub>Cl<sub>2</sub>, nm) λ = 253, 320.

**C<sub>60</sub>-<sup>i</sup>PrBOX:** black crystalline solid, yield 39%.

<sup>1</sup>H NMR (300 MHz, CDCl<sub>3</sub>) δ = 7.40 – 7.04 (m, 2H), 4.71 – 3.97 (m, 5H), 1.43 – 0.69 (m, 12H).

<sup>13</sup>C NMR (101 MHz, CDCl<sub>3</sub>) δ = 158.78, 146.78, 146.33, 145.53, 145.28, 145.18, 145.14, 144.79, 144.70, 144.61, 144.52, 143.89, 143.83, 142.96, 142.89, 142.18, 142.13, 142.07, 141.93, 140.84, 140.74, 138.74, 138.66, 77.33, 77.01, 76.69, 73.39, 72.74, 71.46, 33.34, 19.36, 18.49.

FT-IR (KBr, cm<sup>-1</sup>) ν = 527, 1668. UV-Vis (CH<sub>2</sub>Cl<sub>2</sub>, nm) λ = 254, 316.

**C<sub>60</sub>-IndaBOX:** light brown solid, yield 46%.

<sup>1</sup>H NMR (300 MHz, CDCl<sub>3</sub>) δ = 7.67 – 6.84 (m, 8H), 5.96 – 5.77 (m, 1H), 5.73 – 5.46 (m, 1H), 3.69 – 3.13 (m, 2H).

$^{13}\text{C}$  NMR (101 MHz,  $\text{CDCl}_3$ )  $\delta$  = 159.44, 145.99, 145.16, 145.04, 144.55, 144.46, 144.22, 144.15, 143.79, 143.64, 142.83, 142.81, 142.70, 142.64, 142.09, 142.02, 141.88, 141.82, 140.50, 139.20, 139.01, 138.23, 77.34, 77.02, 76.70, 39.86, 21.46. FT-IR (KBr,  $\text{cm}^{-1}$ )  $\nu$  = 523, 738, 1660. UV-Vis ( $\text{CH}_2\text{Cl}_2$ , nm)  $\lambda$  = 256.

#### **General procedure for the synthesis of $\text{C}_{60}\text{-BOX}_6$**

10 equivalents of the corresponding BOX, 100 equivalents of  $\text{CBr}_4$  and 20 equivalents of DBU were added to a solution of  $\text{C}_{60}$  (0,1 mmol) in o-DCB (7 mL). The mixture was stirred for 72 hours at room temperature. The reaction mixture was precipitated in 100 mL of hexane and the crude collected by centrifugation. The crude was dissolved in dichloromethane and washed with water. The organic layers were dried over  $\text{MgSO}_4$  and the solvent eliminated under vacuum. The product was purified by column chromatography ( $\text{SiO}_2$ , toluene/ethyl acetate 9:1 + 0,2% v/v of triethylamine). The solvent was removed under reduced pressure and the solid was re-dissolved in the minimum amount of chloroform and re-precipitated in hexane.

**$\text{C}_{60}\text{-PhBOX}_6$** : crystalline light brown solid, yield 68%.

$^1\text{H}$  NMR (300 MHz,  $\text{CDCl}_3$ )  $\delta$  = 7.71 – 6.89 (m, 60H), 5.82 – 5.15 (m, 11H), 5.10 – 4.59 (m, 10H), 4.56 – 4.17 (m, 10H).

$^{13}\text{C}$  NMR (101 MHz,  $\text{CDCl}_3$ )  $\delta$  = 160.97, 145.86, 145.58, 142.09, 142.03, 141.65, 128.73, 127.01, 35.66 – 34.13.

FT-IR (KBr,  $\text{cm}^{-1}$ )  $\nu$  = 528, 702, 1660.

**$\text{C}_{60}\text{-}^i\text{PrBOX}_6$** : crystalline light orange solid, yield 67%.

$^1\text{H}$  NMR (300 MHz,  $\text{CDCl}_3$ )  $\delta$  = 7.56 – 7.02 (m, 1H), 4.46 – 4.14 (m, 2H), 4.09 – 3.77 (m, 4H), 3.35 (s, 2H), 1.91 – 1.61 (m, 2H), 1.16 – 0.70 (m, 12H).

$^{13}\text{C}$  NMR (400 MHz,  $\text{CDCl}_3$ )  $\delta$  = 165.05, 159.85, 68.55, 62.76, 58.22, 57.74, 36.92, 29.15, 19.56, 18.67, 18.02, 17.56.

FT-IR (KBr,  $\text{cm}^{-1}$ )  $\nu$  = 668, 1390, 1538, 1670,

**$\text{C}_{60}\text{-IndaBOX}_6$** : crystalline light brown solid, yield 65%.

$^1\text{H}$  NMR (300 MHz,  $\text{CDCl}_3$ )  $\delta$  = 7.51 (d,  $J$  = 6.6, 1H), 7.44 – 7.21 (m, 6H), 5.81 – 5.51 (m, 3H), 3.41 (dd,  $J$  = 18.0, 6.9, 2H), 3.22 (dd,  $J$  = 17.7, 9.3, 2H), 1.62 (s, 1H), 1.27 (s, 1H), 0.09 (s, 1H), 0.02 (s, 1H).

$^{13}\text{C}$  NMR (400 MHz,  $\text{CDCl}_3$ )  $\delta$  = 159.39, 144.72, 144.33, 143.43, 141.30, 139.24, 128.43, 127.45, 125.58, 84.17, 45.99, 36.65, 8.62.

FT-IR (KBr,  $\text{cm}^{-1}$ )  $\nu$  = 526, 698, 1666.

### **Synthesis of Dibromopropyl malonate**

To a solution of 3-bromo-1-propanol (1,7 mmol) and pyridine (1 equivalent) in 35 ml of 1,2-dichloroethane at 0°C in inert atmosphere, 1 equivalent of malonyl dichloride is added dropwise. The mixture was stirred 1 hour at 0 °C, then 48 hours at room temperature. The reaction mixture is then washed twice with a 5% HCl solution, then twice with a saturated  $\text{NaHCO}_3$  solution. The organic layers were collected, dried over  $\text{MgSO}_4$  and the solvent removed by reducing pressure. The resulting blue oily liquid is purified on a silica gel column (petroleum ether/ethyl acetate 15:1 and 9:1). The final product is obtained as a colourless liquid with a yield of 52%.

### **General procedure for the synthesis of $\text{C}_{60}$ -dibromopropylmalonate<sub>5</sub>-BOX ([5:1] adducts)**

To a solution of the corresponding  $\text{C}_{60}$ -BOX (0.8 mmol) in 9 ml of *o*-DCB, 10 equivalents of dibromopropyl malonate were added, 50 equivalents of  $\text{CBr}_4$  and 20 equivalents of DBU. The mixture was stirred for 72 hours at room temperature.

After removing the solvent under vacuum, the crude was purified by column chromatography (toluene/ethyl acetate 10:1 +0,2% triethylamine).

**$\text{C}_{60}$ -dibromopropylmalonate<sub>5</sub>-PhBOX:** red solid, yield 31%.

$^1\text{H}$  NMR (300 MHz,  $\text{CDCl}_3$ )  $\delta$  = 7.43 – 6.85 (m, 10H), 5.44 (s, 1H), 4.58 (t,  $J$  = 57.5, 9H), 3.48 (d,  $J$  = 4.6, 11H), 2.62 – 2.00 (m, 12H), 1.59 (s, 4H), 1.27 (s, 1H), 0.09 (s, 1H), 0.01 (d,  $J$  = 5.0, 1H).

$^{13}\text{C}$  NMR (400 MHz,  $\text{CDCl}_3$ )  $\delta$  = 163.56, 163.17, 160.69, 145.75, 141.34, 140.92, 128.68, 127.72, 126.99, 75.76, 70.20, 69.00, 64.69, 53.42, 31.31, 29.03.

FT-IR (KBr,  $\text{cm}^{-1}$ )  $\nu = 541, 703, 1238, 1744$ .

**C<sub>60</sub>-dibromopropylmalonate<sub>5</sub>-<sup>i</sup>PrBOX:** red solid, yield 36%.

<sup>1</sup>H NMR (300 MHz, CDCl<sub>3</sub>)  $\delta = 7.28$  (s, 1H), 5.32 (s, 1H), 4.28 (d,  $J = 107.0$ , 6H), 3.47 (s, 5H), 2.28 (s, 4H), 1.60 (s, 1H), 1.28 – 0.53 (m, 3H).

<sup>13</sup>C NMR (400 MHz, CDCl<sub>3</sub>)  $\delta = 163.54, 163.17, 145.64, 141.15, 140.84, 134.42, 129.67, 128.97, 72.98, 70.91, 68.96, 64.66, 53.42, 31.30, 29.67, 29.05, 19.16, 18.14$ .

FT-IR (KBr,  $\text{cm}^{-1}$ )  $\nu = 529, 712, 1239, 1748$ .

**C<sub>60</sub>-dibromopropylmalonate<sub>5</sub>-IndaBOX:** red solid, yield 38%.

<sup>1</sup>H NMR (300 MHz, CDCl<sub>3</sub>)  $\delta = 7.57 - 6.88$  (m, 8H), 4.47 (dd,  $J = 18.1, 6.2$ , 11H), 3.83 – 3.25 (m, 12H), 2.27 (dd,  $J = 43.7, 38.1$ , 12H), 2.07 – 1.25 (m, 6H), 1.38 – 1.02 (m, 3H).

<sup>13</sup>C NMR (400 MHz, CDCl<sub>3</sub>)  $\delta = 163.64, 163.13, 159.29, 145.54, 142.67, 140.74, 128.48, 125.88, 125.74, 64.64, 54.42, 31.33, 29.67, 29.05$ .

FT-IR (KBr,  $\text{cm}^{-1}$ )  $\nu = 525, 712, 1232, 1744$ .

### General procedure for the synthesis of C<sub>60</sub>-IL<sub>10</sub>-BOX

0,2 mmol of the corresponding **C<sub>60</sub>-dibromopropylmalonate<sub>5</sub>-BOX** were dissolved in 2 mL of chloroform and 100 equivalents of 1,2-dimethylimidazole were added. The reaction mixture was stirred for 72 hours at room temperature. The solvent was removed under vacuum and the residue obtained is dissolved in the minimum amount of methanol, precipitated from ethyl ether and centrifuged.

**C<sub>60</sub>-IL<sub>10</sub>-PhBOX:** black viscous liquid, yield 87%.

<sup>1</sup>H NMR (300 MHz, MeOD)  $\delta = 7.84 - 7.30$  (m, 24H), 4.32 (dd,  $J = 16.0, 7.8$ , 48H), 3.85 (s, 44H), 3.06 – 2.34 (m, 45H), 2.34 – 2.28 (m, 6H).

<sup>13</sup>C NMR (400 MHz, CDCl<sub>3</sub>)  $\delta = 162.84, 144.94, 14.69, 124.96, 124.08, 121.59, 120.83, 119.57, 119.05, 118.82, 118.67, 78.04, 77.79, 76.94, 57.61, 44.87, 34.46, 34.21, 34.06, 31.68, 28.37, 8.96, 8.62, 8.16$ .

FT-IR (KBr,  $\text{cm}^{-1}$ )  $\nu = 538, 668, 1628$ .

**C<sub>60</sub>-IL<sub>10</sub>-<sup>i</sup>PrBOX:** black viscous liquid, yield 97%.

<sup>1</sup>H NMR (300 MHz, MeOD)  $\delta$  = 7.94 – 7.21 (m, 24H), 4.25 (dd,  $J$  = 63.1, 55.4, 34H), 3.85 (s, 40H), 3.04 – 2.34 (m, 50H), 2.34 – 2.30 (m, 4H).

<sup>13</sup>C NMR (400 MHz, CDCl<sub>3</sub>)  $\delta$  = 144.80, 123.46, 123.41, 122.52, 122.47, 121.71, 121.56, 121.35, 120.79, 120.61, 119.89, 64.20, 45.27, 34.41, 34.14, 28.20, 27.31, 8.86, 8.58, 8.49.

FT-IR (KBr, cm<sup>-1</sup>)  $\nu$  = 668, 1635.

**C<sub>60</sub>-IL<sub>10</sub>-IndaBOX:** black viscous liquid, yield 93%.

<sup>1</sup>H NMR (300 MHz, MeOD)  $\delta$  = 7.51 (dd,  $J$  = 67.8, 49.2, 24H), 4.62 (t,  $J$  = 76.9, 48H), 3.85 (s, 17H), 2.70 (s, 19H), 1.94 (d,  $J$  = 242.4, 16H).

<sup>13</sup>C NMR (400 MHz, CDCl<sub>3</sub>)  $\delta$  = 163.44, 159.68, 144.79, 141.62, 140.89, 124.79, 123.33, 122.60, 121.74, 120.14, 63.71, 45.27, 34.38, 28.36, 8.73.

FT-IR (KBr, cm<sup>-1</sup>)  $\nu$  = 668, 1628.

### General procedure for asymmetric Henry's reactions

The fullerene-BOX ligand, the copper(II) salt and the solvent were mixed in a screw cap vial and stirred for 30 minutes at room temperature. Then 0,4 mmol of aldehyde and 10 equivalents of nitromethane were added and the system were allowed to react for the proper time. The progress of the reaction was monitored by TLC (hexane/ethyl acetate 5:1). The mixture was purified by silica gel plug, (hexane/ethyl acetate 5:1 + 0.2% v/v of triethylamine). The conversion was estimated by <sup>1</sup>H-NMR of the crude, while the enantiomeric excess was determined by HPLC with chiral column Chiralcel OD-H (hexane/isopropanol 90:10, 1,2 ml/min, 215 nm).

### Synthesis of 2-Oxazolidinone

Equimolar amounts of urea and 2-aminoethanol (0.12 mol) were reacted in DMF for 6 hours at 160 °C. The mixture was brought to dryness and the remaining solid was recrystallised from butanone. The final product was obtained as a white solid with a yield of 85%.



$^1\text{H}$  NMR (300 MHz,  $\text{CDCl}_3$ )  $\delta$  = 6.54 (s, 1H), 4.44 (dd,  $J$  = 8.7, 7.3, 1H), 3.64 (t,  $J$  = 8.0, 1H).

### **Synthesis of 3-acryloyl-2-oxazolidinone<sup>49</sup>**

To a suspension of NaH (0,025 mol) in anhydrous THF (20 ml), a solution of 2-oxazolidinone (1 equivalent) in 25 ml anhydrous THF was added *via* cannula. The mixture was stirred for 1 hour at room temperature in inert atmosphere. 1 equivalent of acryloyl chloride was then slowly added and the mixture stirred for 3 hours. The reaction mixture was then cooled to 0 °C and quenched with 30 ml of cold distilled water. The mixture was extracted with ethyl ether (3 times) and dichloromethane (3 times), and the organic fractions dried over  $\text{MgSO}_4$  and. The solvent was removed under vacuum and the residual solid was purified by column chromatography ( $\text{SiO}_2$ , hexane/ethyl acetate 1:1). The final product (yield 53%) was collected as a white solid.

$^1\text{H}$  NMR (300 MHz,  $\text{CDCl}_3$ )  $\delta$  = 7.51 (dd,  $J$  = 17.0, 10.5, 1H), 6.57 (dd,  $J$  = 17.0, 1.8, 1H), 5.92 (dd,  $J$  = 10.5, 1.8, 1H), 4.46 (t,  $J$  = 9.7, 6.3, 2H), 4.10 (t,  $J$  = 8.0, 2H).

### **General procedure for asymmetric Diels-Alder reactions**

In a vial with a screw cap containing 1 ml of dichloromethane, the fullerene-BOX and  $\text{Cu}(\text{OTf})_2$  were added and stirred for 30 minutes at room temperature. Then 0,33 mmol of 3-acryloyl-2-oxazolidinone and 4 equivalents of freshly distilled cyclopentadiene were added. After 24 hours the mixture is purified by silica gel plug (ethyl hexane/acetate 3/1 +0.2%  $\text{Et}_3\text{N}$ ). The conversion and diastereomeric ratio were determined by  $^1\text{H}$ -NMR of the crude, while the enantiomeric excess was determined by HPLC (chiral column Chiralcel OD-H, hexane/isopropanol 90/10, 0,7 ml/min, 215 nm).

### **General procedure for catalyst recycling**

At the end of a reaction conducted according to the general procedure, 3 ml of diethyl ether were added in the vial and the precipitated fullerene-BOX system was recovered by centrifugation.

The ether solutions were dried under vacuum and purified by silica gel plug as indicated in the general procedure, and the obtained products were analysed by <sup>1</sup>H-NMR and HPLC. New reagents and solvents were added to the residual solid for a new catalytic cycle.

### 3.6 References

1. (a) Roth, S.; Park, H. J., Nanocarbonic transparent conductive films. *Chem. Soc. Rev.* **2010**, *39* (7), 2477-2483; (b) Su, D. S.; Schlögl, R., Nanostructured Carbon and Carbon Nanocomposites for Electrochemical Energy Storage Applications. *ChemSusChem* **2010**, *3* (2), 136-168; (c) Vilatela, J. J.; Eder, D., Nanocarbon composites and hybrids in sustainability: a review. *ChemSusChem* **2012**, *5* (3), 456-78.
2. Campisciano, V.; Gruttadauria, M.; Giacalone, F., Modified Nanocarbons for Catalysis. *ChemCatChem* **2019**, *11* (1), 90-133.
3. Su, D. S.; Perathoner, S.; Centi, G., Nanocarbons for the development of advanced catalysts. *Chem. Rev.* **2013**, *113* (8), 5782-816.
4. Balch, A. L.; Winkler, K., Two-component polymeric materials of fullerenes and the transition metal complexes: A bridge between metal-organic frameworks and conducting polymers. *Chem. Rev.* **2016**, *116* (6), 3812-3882.
5. Nagashima, H.; Nakaoka, A.; Tajima, S.; Saito, Y.; Itoh, K., Catalytic hydrogenation of olefins and acetylenes over C<sub>60</sub>Pdn. *Chem. Lett.* **1992**, *21* (7), 1361-1364.
6. Fagan, P. J.; Calabrese, J. C.; Malone, B., The Chemical Nature of Buckminsterfullerene (C<sub>60</sub>) and the Characterization of a Platinum Derivative. *Science* **1991**, *252* (5009), 1160-1161.
7. Sulman, E.; Matveeva, V.; Semagina, N.; Yanov, I.; Bashilov, V.; Sokolov, V., Catalytic hydrogenation of acetylenic alcohols using palladium complex of fullerene C<sub>60</sub>. *J. Mol. Catal. Chem.* **1999**, *146* (1), 257-263.
8. Toganoh, M.; Matsuo, Y.; Nakamura, E., Synthesis and catalytic activity of rhodium diene complexes bearing indenyl-type fullerene  $\eta^5$ -ligand. *J. Organomet. Chem.* **2003**, *683* (2), 295-300.
9. Maggini, M.; Scorrano, G.; Prato, M., Addition of azomethine ylides to C<sub>60</sub>: synthesis, characterization, and functionalization of fullerene pyrrolidines. *J. Am. Chem. Soc.* **1993**, *115* (21), 9798-9799.
10. Bingel, C., Cyclopropanierung von Fullerenen. *Chem. Ber.* **1993**, *126* (8), 1957-1959.

11. Beejapur, H. A.; Campisciano, V.; Franchi, P.; Lucarini, M.; Giacalone, F.; Gruttadauria, M., Fullerene as a Platform for Recyclable TEMPO Organocatalysts for the Oxidation of Alcohols. *ChemCatChem* **2014**, *6* (8), 2419-2424.
12. Giacalone, F.; Gruttadauria, M., Covalently Supported Ionic Liquid Phases: An Advanced Class of Recyclable Catalytic Systems. *ChemCatChem* **2016**, *8* (4), 664-684.
13. Beejapur, H. A.; Campisciano, V.; Giacalone, F.; Gruttadauria, M., Catalytic Synergism in a C60IL10TEMPO2 Hybrid in the Efficient Oxidation of Alcohols. *Acc. Chem. Res.* **2015**, *357* (1), 51-58.
14. Campisciano, V.; La Parola, V.; Liotta, L. F.; Giacalone, F.; Gruttadauria, M., Fullerene–Ionic-Liquid Conjugates: A New Class of Hybrid Materials with Unprecedented Properties. *Chem.: Eur. J.* **2015**, *21* (8), 3327-3334.
15. Andrés, J. M.; González, M.; Maestro, A.; Naharro, D.; Pedrosa, R., Recyclable Chiral Bifunctional Thioureas Derived from [60] Fullerene and Their Use as Highly Efficient Organocatalysts for the Asymmetric Nitro-Michael Reaction. *Eur. J. Org. Chem.* **2017**, *2017* (19), 2683-2691.
16. Wynberg, H., Chance, necessity and asymmetric catalysis. *Recl. Trav. Chim. Pays-Bas* **1981**, *100* (11), 393-399.
17. (a) Shaw, S.; White, J. D., Asymmetric Catalysis Using Chiral Salen–Metal Complexes: Recent Advances. *Chem. Rev.* **2019**, *119* (16), 9381-9426; (b) Kadassery, K. J.; MacMillan, S. N.; Lacy, D. C., Resurgence of Organomanganese(I) Chemistry. Bidentate Manganese(I) Phosphine–Phenol(ate) Complexes. *Inorg. Chem.* **2019**, *58* (16), 10527-10535; (c) Durand, D. J.; Fey, N., Computational Ligand Descriptors for Catalyst Design. *Chem. Rev.* **2019**, *119* (11), 6561-6594; (d) Whitesell, J. K., C<sub>2</sub> symmetry and asymmetric induction. *Chem. Rev.* **1989**, *89* (7), 1581-1590.
18. Petri, A.; Seidelmann, O.; Eilitz, U.; Leßmann, F.; Reißmann, S.; Wendisch, V.; Gutnov, A., Pd-catalyzed asymmetric conjugate addition of arylboronic acids to 2-nitroacrylates: a facile route to β<sup>2</sup>-homophenylglycines. *Tetrahedron Lett.* **2014**, *55* (1), 267-270.
19. König, A.; Fischer, C.; Alberico, E.; Selle, C.; Drexler, H.-J.; Baumann, W.; Heller, D., Oxidative Addition of Aryl Halides to Cationic Bis(phosphane)rhodium

Complexes: Application in C–C Bond Formation. *Eur. J. Inorg. Chem.* **2017**, 2017 (13), 2040-2047.

20. Gaálová, J.; Hejda, S.; Stavárek, P.; Sýkora, J.; Fajgar, R.; Kluson, P.; Izák, P., Pervaporation of (R)/(S)-methyl 3-hydroxybutyrate ( $\Sigma$ MHB) from a mixture containing an ionic liquid, methanol and Ru catalyst. *Sep. Purif. Technol.* **2019**, 222, 45-52.

21. Zhou, Y.; Shan, Z., Chiral Diols: A New Class of Additives for Direct Aldol Reaction Catalyzed by l-Proline. *J. Org. Chem.* **2006**, 71 (25), 9510-9512.

22. Fernández González, D.; Brand, J. P.; Mondière, R.; Waser, J., Ethynylbenziodoxolones (EBX) as Reagents for the Ethynylation of Stabilized Enolates. *Acc. Chem. Res.* **2013**, 355 (8), 1631-1639.

23. (a) Das, D.; Mal, R.; Mittal, N.; Zhu, Z.; Emge, T. J.; Seidel, D., Chiral bisoxazoline ligands designed to stabilize bimetallic complexes. *Beilstein J. Org. Chem.* **2018**, 14, 2002-2011; (b) Kitagaki, S.; Murata, S.; Asaoka, K.; Sugisaka, K.; Mukai, C.; Takenaga, N.; Yoshida, K., Planar Chiral [2.2]Paracyclophane-Based Bisoxazoline Ligands: Design, Synthesis, and Use in Cu-Catalyzed Inter- and Intramolecular Asymmetric O–H Insertion Reactions. *Chem. Pharm. Bull.* **2018**, 66 (10), 1006-1014.

24. Evans, D. A.; Woerpel, K. A.; Hinman, M. M.; Faul, M. M., Bis(oxazolines) as chiral ligands in metal-catalyzed asymmetric reactions. Catalytic, asymmetric cyclopropanation of olefins. *J. Am. Chem. Soc.* **1991**, 113 (2), 726-728.

25. Desimoni, G.; Faita, G.; Jørgensen, K. A., C<sub>2</sub>-Symmetric Chiral Bis(Oxazoline) Ligands in Asymmetric Catalysis. *Chem. Rev.* **2006**, 106 (9), 3561-3651.

26. Nishiyama, H.; Sakaguchi, H.; Nakamura, T.; Horihata, M.; Kondo, M.; Itoh, K., Chiral and C<sub>2</sub>-symmetrical bis(oxazoliny)pyridine)rhodium(III) complexes: effective catalysts for asymmetric hydrosilylation of ketones. *Organometallics* **1989**, 8 (3), 846-848.

27. Lowenthal, R. E.; Abiko, A.; Masamune, S., Asymmetric catalytic cyclopropanation of olefins: bis-oxazoline copper complexes. *Tetrahedron Lett.* **1990**, 31 (42), 6005-6008.

28. Corey, E. J.; Imai, N.; Zhang, H. Y., Designed catalyst for enantioselective Diels-Alder addition from a C<sub>2</sub>-symmetric chiral bis(oxazoline)-iron(III) complex. *J. Am. Chem. Soc.* **1991**, *113* (2), 728-729.
29. Maggi, R.; Lanari, D.; Oro, C.; Sartori, G.; Vaccaro, L., Heterogeneous Bisoxazoline/Copper Complex: A Green Catalyst for the Enantioselective Reaction of Nitromethane with Substituted Benzaldehydes. *Eur. J. Org. Chem.* **2011**, *2011* (28), 5551-5554.
30. Corma, A.; García, H.; Moussaif, A.; Sabater, M. J.; Zniber, R.; Redouane, A., Chiral copper(ii) bisoxazoline covalently anchored to silica and mesoporous MCM-41 as a heterogeneous catalyst for the enantioselective Friedel–Crafts hydroxyalkylation. *Chem. Commun.* **2002**, (10), 1058-1059.
31. (a) Jørgensen, K. A.; Johannsen, M.; Yao, S.; Audrain, H.; Thorhauge, J., Catalytic Asymmetric Addition Reactions of Carbonyls. A Common Catalytic Approach. *Acc. Chem. Res.* **1999**, *32* (7), 605-613; (b) Johnson, J. S.; Evans, D. A., Chiral Bis(oxazoline) Copper(II) Complexes: Versatile Catalysts for Enantioselective Cycloaddition, Aldol, Michael, and Carbonyl Ene Reactions. *Acc. Chem. Res.* **2000**, *33* (6), 325-335.
32. Christoffers, J.; Baro, A., Construction of Quaternary Stereocenters: New Perspectives through Enantioselective Michael Reactions. *Angew. Chem.* **2003**, *42* (15), 1688-1690.
33. Lee, A.; Kim, W.; Lee, J.; Hyeon, T.; Kim, B. M., Heterogeneous asymmetric nitro-Mannich reaction using a bis (oxazoline) ligand grafted on mesoporous silica. *Tetrahedron: Asymmetry* **2004**, *15* (17), 2595-2598.
34. Gothelf, K. V.; Jørgensen, K. A., Asymmetric 1,3-Dipolar Cycloaddition Reactions. *Chem. Rev.* **1998**, *98* (2), 863-910.
35. Wisniak, J., Louis Henry: The Henry reaction and other organic syntheses. *Rev. Ciencia Quim.* **2018**, *49*.
36. Gogoi, N.; Boruwa, J.; Barua, N. C., A total synthesis of (–)-bestatin using Shibasaki's asymmetric Henry reaction. *Tetrahedron Lett.* **2005**, *46* (44), 7581-7582.
37. Luzzio, F. A., ChemInform Abstract: The Henry Reaction: Recent Examples. *ChemInform* **2001**, *32* (22).

38. Diels, O.; Alder, K., Synthesen in der hydroaromatischen Reihe. *Liebigs Ann.* **1928**, *460* (1), 98-122.
39. Woodward, R. B.; Sondheimer, F.; Taub, D.; Heusler, K.; McLamore, W. M., The Total Synthesis of Steroids I. *J. Am. Chem. Soc.* **1952**, *74* (17), 4223-4251.
40. Corey, E. J.; Weinshenker, N. M.; Schaaf, T. K.; Huber, W., Stereo-controlled synthesis of dl-prostaglandins F<sub>2</sub>. alpha. and E<sub>2</sub>. *J. Am. Chem. Soc.* **1969**, *91* (20), 5675-5677.
41. (a) Lamparth, I.; Hirsch, A., Water-soluble malonic acid derivatives of C<sub>60</sub> with a defined three-dimensional structure. *J. Chem. Soc., Chem. Commun.* **1994**, (14), 1727-1728; (b) Hirsch, A.; Lamparth, I.; Karfunkel, H. R., Fullerene Chemistry in Three Dimensions: Isolation of Seven Regioisomeric Bisadducts and Chiral Trisadducts of C<sub>60</sub> and Di(ethoxycarbonyl)methylene. *Angew. Chem.* **1994**, *33* (4), 437-438; (c) Djojo, F.; Hirsch, A., Synthesis and Chiroptical Properties of Enantiomerically Pure Bis- and Trisadducts of C<sub>60</sub> with an Inherent Chiral Addition Pattern. *Chemistry - A European Journal* **1998**, *4* (2), 344-356.
42. Seifermann, S. M.; Réthoré, C.; Muller, T.; Bräse, S., Soccer goes BOXing: Synthetic access to novel [6:0] hexakis[(bisoaxazoliny)methano]fullerenes. *Sci. Rep.* **2013**, *3*, 2817.
43. Hirsch, A.; Lamparth, I.; Groesser, T.; Karfunkel, H. R., Regiochemistry of Multiple Additions to the Fullerene Core: Synthesis of a Th-Symmetric Hexakis adduct of C<sub>60</sub> with Bis(ethoxycarbonyl)methylene. *J. Am. Chem. Soc.* **1994**, *116* (20), 9385-9386.
44. Zhou, Z.-M.; Li, Z.-H.; Hao, X.-Y.; Zhang, J.; Dong, X.; Liu, Y.-Q.; Sun, W.-W.; Cao, D.; Wang, J.-L., Catalytic effect and recyclability of imidazolium-tagged bis(oxazoline) based catalysts in asymmetric Henry reactions. *Org. Biomol. Chem.* **2012**, *10* (10), 2113-2118.
45. Evans, D. A.; Seidel, D.; Rueping, M.; Lam, H. W.; Shaw, J. T.; Downey, C. W., A New Copper Acetate-Bis(oxazoline)-Catalyzed, Enantioselective Henry Reaction. *J. Am. Chem. Soc.* **2003**, *125* (42), 12692-12693.
46. (a) Didier, D.; Schulz, E., *A Reusable TNF-Tagged Chiral Bis(oxazoline)-Copper Catalyst for Diels- Alder Transformations*. 2012; Vol. 23, p 1309-1314; (b) Le Maux, P.; Dorcet, V.; Simonneaux, G., Asymmetric copper-catalyzed Diels-

- Alder reaction revisited: control of the structure of bis(oxazoline) ligands. *Tetrahedron* **2013**, *69* (38), 8291-8298; (c) Meracz, I.; Oh, T., Asymmetric Diels–Alder reactions in ionic liquids. *Tetrahedron Lett.* **2003**, *44* (34), 6465-6468.
47. Reymond, S.; Cossy, J., Copper-Catalyzed Diels–Alder Reactions. *Chem. Rev.* **2008**, *108* (12), 5359-5406.
48. McKennon, M. J.; Meyers, A. I.; Drauz, K.; Schwarm, M., A convenient reduction of amino acids and their derivatives. *J. Org. Chem.* **1993**, *58* (13), 3568-3571.
49. Narasaka, K.; Iwasawa, N.; Inoue, M.; Yamada, T.; Nakashima, M.; Sugimori, J., Asymmetric Diels-Alder reaction catalyzed by a chiral titanium reagent. *J. Am. Chem. Soc.* **1989**, *111* (14), 5340-5345.



*Chapter 3*

*Novel nanobuilding blocks for 3D  
emitting materials*

### 3 Introduction

As mentioned previously, the aim of this thesis is the synthesis of novel building blocks based on nanocaged molecular bricks such as  $C_{60}$  and POSS (**Figure 3.1**).

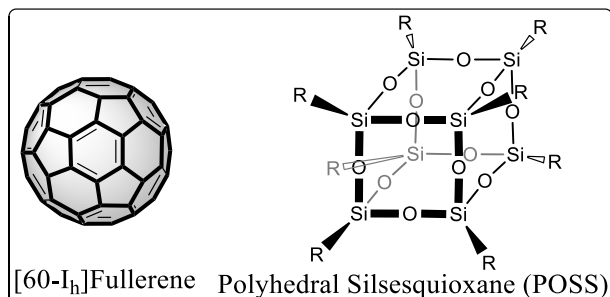


**Figure 3.1.**  $C_{60}$  Fullerene and Polyhedral Oligomeric Silsesquioxane (POSS).

The main goal stands in exploiting the well-defined geometry of these two complementary nanocages (**Figure 3.2**), in order to access to 3D metallo-polymeric network which could find applications in various fields<sup>1</sup>: from catalysis to optoelectronics, from gas storage to water remediation.

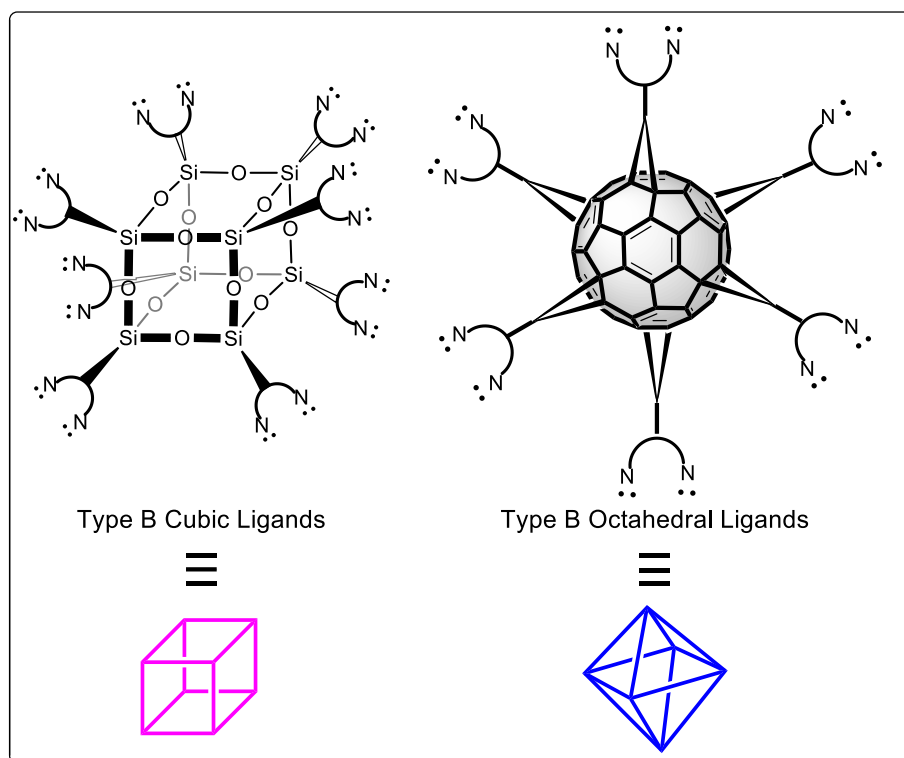


**Figure 3.2.**  $C_{60}$  and POSS 3D geometries.

In the past decade, investigations on 3D materials experienced an exponentially growth. One of the most explored family of this kind of solid materials is represented by those hybrid structures named metal-organic frameworks (MOFs). The establishment of porosity in these polymeric metal-organic structures has been a challenging goal during the development of this field. Such a wide class of materials possess high porosity due to free inner volumes greater than 90% and high surface area that extends over 6000 m<sup>2</sup>/g. These properties, together with the extraordinary degree of variability for both the organic and inorganic components of their structures, make MOFs of interest for potential applications in diverse areas: chemical separations, ion exchange, sensing and catalysis.<sup>2</sup>

Classical MOFs are synthesized by metallic cation (MC) units connected by organic linkers (OL). Choosing suitable metal centres and organic linkers it is possible to tune the materials morphology as well as to modify their macroscopic properties. The MCs can display different geometries in function of the nature of the selected metal (**Figure 3.3**).

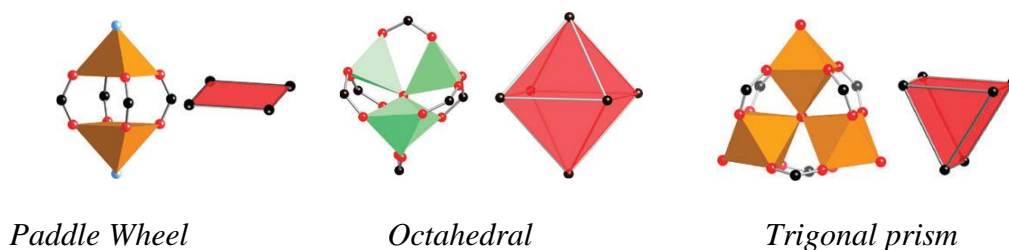


**Figure 3.3.** Metallic cations common geometries.

The final 3D organization of the MOFs is highly influenced by the geometry of the MC as well as by the structure and the coordination properties of the organic linkers. Various OLs, usually constituted by structures with an aromatic core and carboxylic functionalities, have been already described in the literature.<sup>3</sup>

In order to achieve our goal, a set of suitable ligands, able to further coordinate metal centres, were initially thought to functionalize the **C<sub>60</sub>** and **POSS** in an octahedral or cubic fashion, respectively. At this purpose, ligands such as 2,2':6',2''-terpyridine and bisoxazolines (BOX)-like moieties were covalently anchored respectively on the POSS and on the **C<sub>60</sub>** nanostructures. The resulting derivatives were used for complexing different cationic species (e.g. Eu(III), Tb(III)).

The choice of the metal cations was motivated by the specific goals of the research field which are related to the tuning of the emission properties of the final 3D structures. From a more fundamental point of view, the understanding of the coordination properties of the nanocaged building blocks will contribute to extend the general knowledge on the 3D organization obtained via self-assembly of organic nano-entities mediated by metal centres. These new 3D polymeric structures may find application in sensing and nanotechnology (e.g. light emitting diodes).

### 3.1 Photochemistry of Lanthanides

The extraordinary properties of the Lanthanides attracted the attention of the researchers by very far.<sup>4</sup>

The intense line-like emission is one of the most attractive features of luminescent lanthanide compounds, that results in a high colour purity of the emitted light. The coloured emission depends on the nature of the lanthanide ion as well as on the environment (coordination shell and nature of the ligands) of that given ion. The electronic  $[Xe]4f^n$  configurations ( $n = 0-14$ ) indeed generate a rich variety of electronic levels. The trivalent ions of the lanthanide series are characterized by a gradual filling of the 4f orbitals, from  $4f^0$  (for  $La^{3+}$ ) to  $4f^{14}$  (for  $Lu^{3+}$ ).<sup>5</sup> One of the most interesting features of these ions is their photoluminescence. Several lanthanide ions show luminescence in the visible or near-infrared spectral regions upon irradiation with ultraviolet radiation. The colour of the emitted light depends on the ion: for example it goes from the  $Gd^{3+}$  that emits in the ultraviolet, passing through the  $Eu^{3+}$ ,  $Tb^{3+}$ ,  $Sm^{3+}$  and  $Tm^{3+}$  that emit in the visible to  $Yb^{3+}$ ,  $Nd^{3+}$  and  $Er^{3+}$  that are well-known for their near-infrared luminescence covering , in this way, the entire light emission spectrum.<sup>6</sup>

It deserves to be mentioned that in the discussion of lanthanides emission we refer often to “luminescence” rather than “fluorescence” or “phosphorescence”. Considering the mechanism leading to emission: *fluorescence* is singlet-to-singlet emission (i.e., a spin-allowed transition)<sup>7</sup> and *phosphorescence* is triplet-to-singlet emission (i.e., a spin forbidden transition).<sup>8</sup> In the case of lanthanides the energy levels are well defined since their emission comes from transitions in the 4f shell, that are shielded by the  $5s^2$  and  $5p^6$  sub level.

Although photoluminescence of lanthanide ions can be an efficient process, all lanthanide ions suffer from weak light absorption. They have in general small molar absorption coefficients ( $\epsilon$ ) and as a consequence, a very limited amount of radiation absorbed by direct excitation within the 4f levels. The luminescence intensity is not only proportional to the luminescence quantum yield (defined as the number of photons emitted as the number of photons absorbed)<sup>9</sup>, but also to the amount of light absorbed; weak light absorption results in weak luminescence.<sup>5</sup> However, the problem of weak light absorption can be overcome by the so-called antenna effect (or sensitization).

The ligands can sensitize the central lanthanide ions by ligand-to-metal energy transfer, the so-called “antenna effect”.<sup>10</sup> Usually, ternary lanthanide complexes utilizing organic ligands have shown really efficient luminescence properties. Aromatic ligands, can efficiently absorb light and transfer energy to the lanthanide ions.<sup>11</sup> Furthermore, the introduction of ligands with high affinity properties through the metal cations can replace the solvent molecules coordinated with lanthanide ions to reduce the quenching effect thus enhancing the overall emission.<sup>11b, 12</sup>

### **3.2 C<sub>60</sub>-BOX<sub>6</sub>: complexation study of novel Carbon building-blocks**

In the previous chapter C<sub>60</sub> functionalized with bisoxazolines were synthesized and employed as efficient catalysts (Chapter 2). What already discussed in the previous chapter has revealed that metal complexes of hexakis-adducts of fullerene are promising catalytic systems that can be used in the field of asymmetric catalysis.

Herein, these hexakis-adducts properly complexed with a lanthanide (III) ion (**Figure 3.4**), will be used with the aim of obtaining 3D polymeric materials with photoluminescent properties.

Eu(III) and Tb(III) were selected as target metals to achieve this goal were because of their well-known photoluminescent properties.<sup>13</sup> Before investigating the absorption and emission properties of the fullerene-BOX hybrid once complexed with those cations, a preliminary investigation was conducted on the corresponding C<sub>60</sub>-BOX mono-adduct (easier to prepare and to study) which will be used in the further studies as reference compound.

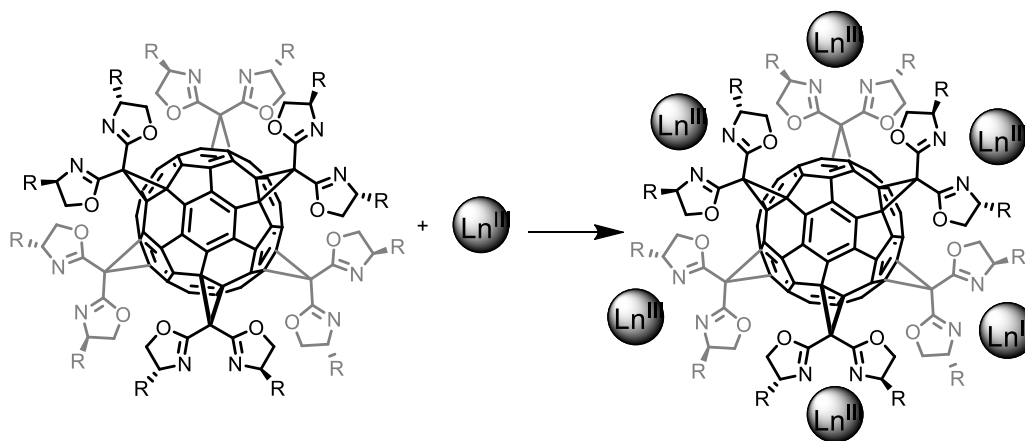


**Figure 3.4.**  $\text{Ln}^{3+}$  complex of  $\text{C}_{60}$ - hexakis-adduct.

The ability of the unsupported BOXs to complex both cations was initially evaluated via UV-Vis absorption titrations experiments.

First of all, titration experiments were performed adding increasing amount of Eu triflate (dissolved in  $\text{CH}_3\text{CN}$ ) to a solution of BOX-based ligand dissolved in DCM. The titration was followed via UV-Vis spectroscopy. From **Figure 3.5** it is possible to note that by adding a metal solution to the ligand solution, the absorption band of the ligand start to increase suggesting that the complexation takes place.

Looking at the plots of the maximum of absorption vs the equivalent of metal added (Abs vs  $[\text{M}]/[\text{L}]$ ) it is possible to note that in the case of the iPrBOX (**Figure 3.5b**) and INDABOX (**Figure 3.5d**) the complex formed has a 2:1 stoichiometry. These experiments indicate that the  $\text{Eu}^{3+}$  is complexed by two ligands. On the other hand, in the case of the PhBOX the plot suggests an initial formation of a complex with 2:1 stoichiometry that, after further addition of metal, gives rise probably to the formation of a complex with 1:1 stoichiometry. Exactly the same behaviour has been obtained using Tb triflate as the metal salt.

Once ensured that both metal ions are able to form complexes with BOX ligands, analogous experiments were performed using the  $\text{C}_{60}$ -BOX mono-adducts.

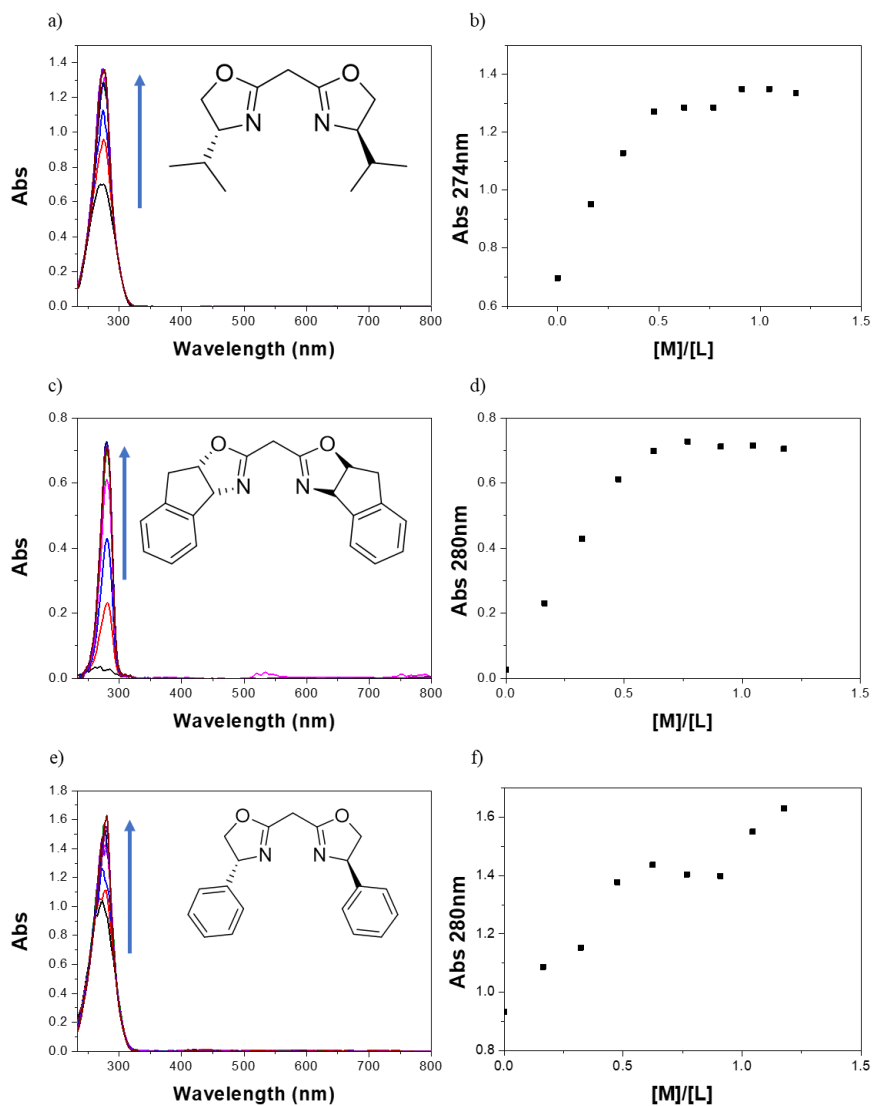


**Figure 3.5** UV-vis absorption spectra of BOXs in  $\text{CH}_2\text{Cl}_2$  ( $1.3 \times 10^{-5}$  M) upon titration with  $\text{Eu}(\text{OTf})_3$  in  $\text{CH}_3\text{CN}$  ( $1.4 \times 10^{-3}$  M). Maximum of absorption vs equivalent of metal added (second row).

Unfortunately, due to the elevate extinction coefficient of the fullerene,<sup>14</sup> , the spectra are dominated by the absorption of the  $\text{C}_{60}$  (**Figure 3.6**), and it is not possible to understand if the complexation take place or not. In order to have some insight on the possible formation of a complex, an attempt to plot the variation of the maximum of abs vs the M/L ratio was performed. However, as it can be clearly observed in the figure, no clear trend emerged.

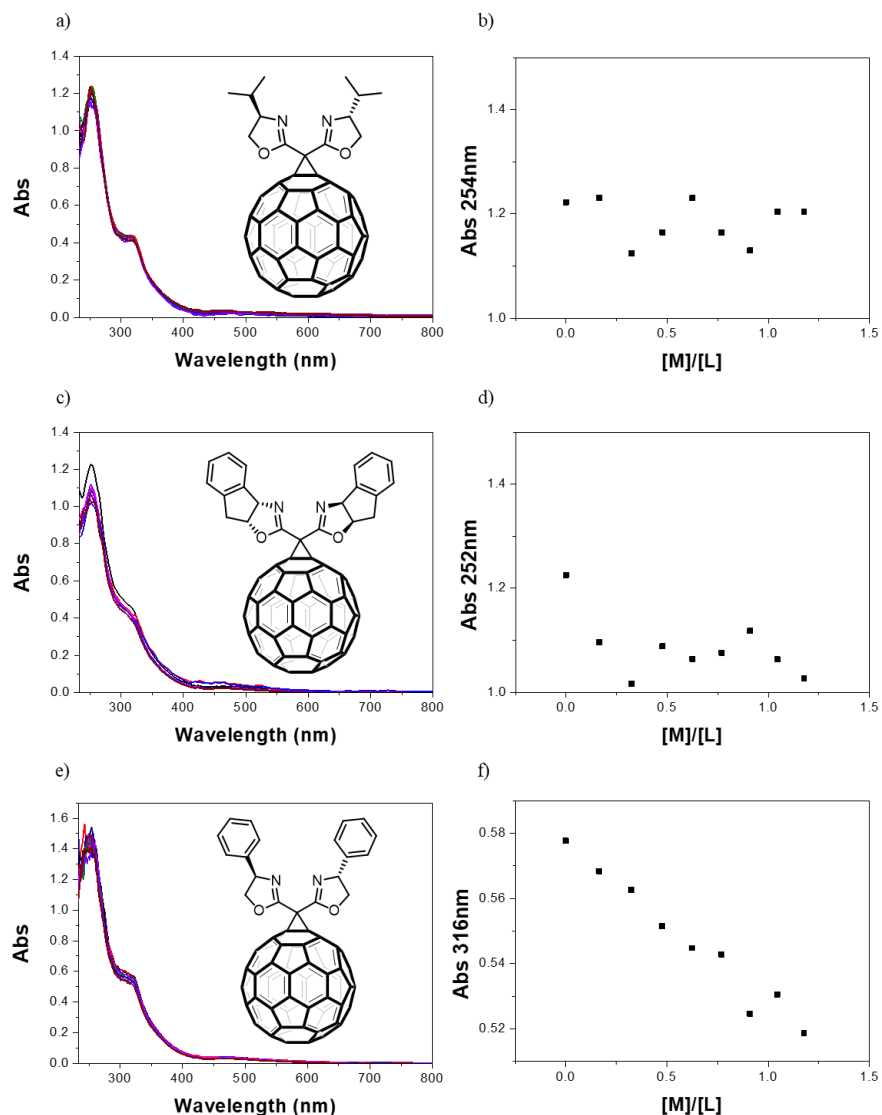


**Figure 3.6.** UV-vis absorption spectra of C<sub>60</sub>-BOX in CH<sub>2</sub>Cl<sub>2</sub> ( $1.3 \times 10^{-5}$  M) upon titration with Eu(OTf)<sub>3</sub> in CH<sub>3</sub>CN ( $1.3 \times 10^{-3}$  M). Europium (first row). Maximum of absorption vs equivalent of metal added (second row).

Although in C<sub>60</sub>-PhBOX (**Figure 3.6 e, f**) spectra seems that a decreasing of the absorption band of the adduct is occurring, a more accurate analysis indicates that such decreasing is not indicative for a complexation; in fact, the decrease is only of 0.05 absorbance units and can be ascribed to a dilution factor. Basically, these titrations do not give any useful information about the complexation of the Europium with the C<sub>60</sub>-BOXs.

Prompted by the fact that titration experiment on the unsupported BOXs showed that is possible to form this kind of complexes, emission experiments were performed to definitely check if these systems are suitable for the formation of



novel 3D carbon-based emitting materials. Emission titration experiments were performed firstly on the unsupported BOXs and then on the fullerene-adducts (**Figure 3.7**).

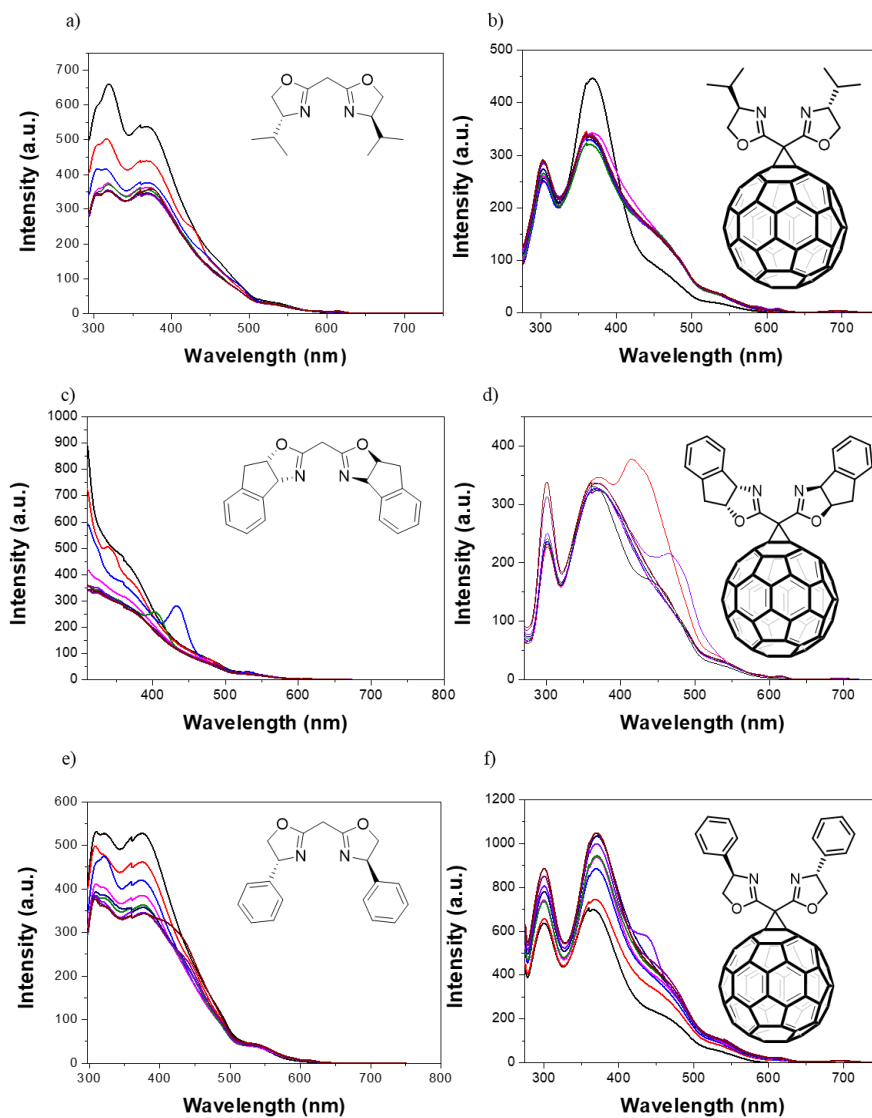


**Figure 3.7.** Emission spectra of both BOXs (a, c, e) and C<sub>60</sub>-BOX monoadducts (b, d f) in CH<sub>2</sub>Cl<sub>2</sub> (1.3 × 10<sup>-5</sup> M) upon titration with Eu(OTf)<sub>3</sub> (1.3 × 10<sup>-3</sup> M): 0 eq. - 1 eq.

By analysing the emission spectra of the BOXs, it is possible to see that under the selected conditions, only minor changes in the emission spectra occurred. No emission band related to the formation of of Eu@BOX complex can be observed. In addition, the characteristic line-like Eu(III) emission bands, in the region between 550-700 nm were not detected.

This can be due to the fact that probably the so-called antenna effect, it is not so efficient to result in a strong emission of the metal centre.

In the case of the C<sub>60</sub> monoadducts (**Figure 3.7 b, d, f**), in addition, there is a reason strictly related to the kind of support used.

In particular, Sariciftci and co-workers, reported that the emission of a polymer, poly[2-methoxy,5-(2'-ethyl-hexyloxy)-*p*-phenylene vinylene] (reported as MEH-PPV), is completely quenched after its grafting onto a C<sub>60</sub> fullerene.<sup>15</sup>

Later on, Nierengarten and co-workers, report the complete quenching of oligo(phenylenevinylene) (OPV) fluorescence when this moiety is covalently anchored onto C<sub>60</sub>.<sup>16</sup> They argued that once the OPV catch the light an energy transfer process from the OPV singlet to the C<sub>60</sub> singlet state occurs. Under such conditions, the intense fluorescence band characteristic of the OPV moiety is not observed, whereas the typical fluorescence band of the fulleropyrrolidine fragment is detected.

In both cases the intense photoluminescence of MEH-PPV in the first example, and of the OPV in the second, is however, almost completely quenched, implying a strong interaction of the two components in the excited state.

Considering the above, the C<sub>60</sub>-BOX systems, although showed good applicability in catalysis, are not suitable for photoluminescent materials and as a consequence hexakis-adducts were not further tested.

Hence, at this point, the nano-scaffold was replaced in order to have an inert support with well-established geometry able to form, when properly functionalized, auto assembled 3D material in presence of metal, with particular emission properties. The use of a proper ligand with high molar absorption coefficient and high affinity toward the complexation of metal and possessing also the ability to behaves as antenna system was envisaged.

### 3.3 Conclusions

Innovative building blocks, based on C<sub>60</sub> with well established geometry were synthesized with the aim of obtaining, in the presence of suitable metals, auto-assembled photoemissive 3D materials. In particular, octahedral C<sub>60</sub> bisoxazoline hexakis-adduct (C<sub>60</sub>-BOX<sub>6</sub>) complexed with Europium and Terbium ions were

obtained and characterized also focusing on their photophysical behaviour. In order to better understand the mechanisms involved in the complexation with the  $\text{Eu}^{3+}$  and  $\text{Tb}^{3+}$  ions, a complete study on the unsupported ligands was performed as well. Subsequently, once anchored on the fullerene, all the resulting materials were exhaustively investigated.

Although the fullerene-based systems proved to be active catalysts (Chapter 2) once complexed with Copper, they did not display a similar promising behaviour when employed for photophysical investigations. The selected ligands exhibit an inefficient ligand to metal energy transfer (LMCT). Furthermore, a more in-depth bibliographic research has revealed that  $\text{C}_{60}$  fullerene is not a good scaffold for the selected purpose since harvests the light absorbed by the ligand preventing the right transferring to the metal. As a consequence, the bisoxazoline- $\text{C}_{60}$  systems were not further considered as possible emitting materials.

In order to preserve the initial objective related to the synthesis of building units for the construction of 3D organization while considering the possibility of photophysical application, the use of silsesquioxanes-based structures was considered. Polyhedral oligomeric silsesquioxanes (POSS) constitutes an inert (from the photophysical point of view) scaffold. Moreover, it presents a series of additional advantages as a thermal and chemical stability as well as the possibility of an easy functionalization. In the next chapter the synthesis of novel POSS-based ligands will be presented.

### 3.4 References

1. (a) Lin, R. B.; Xiang, S.; Xing, H.; Zhou, W.; Chen, B., Exploration of porous metal–organic frameworks for gas separation and purification. *Coord. Chem. Rev.* **2019**, *378*, 87-103; (b) Asatkar, A. K.; Bedi, A.; Zade, S. S., Metallo-organic conjugated systems for organic electronics. *Israel Journal of Chemistry* **2014**, *54* (5-6), 467-495; (c) Lusby, P. J., Supramolecular coordination chemistry. *Annual Reports on the Progress of Chemistry - Section A* **2013**, *109*, 254-276; (d) Burnworth, M.; Knapton, D.; Rowan, S. J.; Weder, C., Metallo-supramolecular polymerization: A route to easy-to-process organic/inorganic hybrid materials. *Journal of Inorganic and Organometallic Polymers and Materials* **2007**, *17* (1), 91-103.
2. James, S. L., Metal-organic frameworks. *Chem. Soc. Rev.* **2003**, *32* (5), 276-288.
3. Ali Akbar Razavi, S.; Morsali, A., Linker functionalized metal-organic frameworks. *Coord. Chem. Rev.* **2019**, *399*, 213023.
4. Vleck, J. H. V., The Puzzle of Rare-earth Spectra in Solids. *J. Phys. Chem.* **1937**, *41* (1), 67-80.
5. Binnemans, K., Lanthanide-based luminescent hybrid materials. *Chem. Rev.* **2009**, *109* (9), 4283-4374.
6. Elbanowski, M.; Mąkowska, B., The lanthanides as luminescent probes in investigations of biochemical systems. *J. Photochem. Photobiol.* **1996**, *99* (2), 85-92.
7. Melhuish, W. H., Nomenclature, symbols, units and their usage in spectrochemical analysis-Part VI: molecular luminescence spectroscopy. In *Pure Appl. Chem.*, 1984; Vol. 56, p 231.
8. Verhoeven, J. W., Glossary of terms used in photochemistry (IUPAC Recommendations 1996). In *Pure Appl. Chem.*, **1996**; Vol. 68, p 2223.
9. Basic Principles of Fluorescence Spectroscopy. In *Handbook of Fluorescence Spectroscopy and Imaging*, pp 1-30.
10. (a) Wu, J.; Ye, Z.; Wang, G.; Jin, D.; Yuan, J.; Guan, Y.; Piper, J., Visible-light-sensitized highly luminescent europium nanoparticles: preparation and application for time-gated luminescence bioimaging. *J. Mater. Chem.* **2009**, *19* (9),

1258-1264; (b) Zhang, D.; Wang, X.; Qiao, Z.-a.; Tang, D.; Liu, Y.; Huo, Q., Synthesis and Characterization of Novel Lanthanide(III) Complexes-Functionalized Mesoporous Silica Nanoparticles as Fluorescent Nanomaterials. *J. Phys. Chem. C* **2010**, *114* (29), 12505-12510.

11. (a) Zhao, Y.-F.; Chu, H.-B.; Bai, F.; Gao, D.-Q.; Zhang, H.-X.; Zhou, Y.-S.; Wei, X.-Y.; Shan, M.-N.; Li, H.-Y.; Zhao, Y.-L., Synthesis, crystal structure, luminescent property and antibacterial activity of lanthanide ternary complexes with 2,4,6-tri(2-pyridyl)-s-triazine. *J. Organomet. Chem.* **2012**, *716*, 167-174; (b) Kong, L.; Kong, K.; Zhao, Y.; Chu, H., Tuning the luminescence properties of lanthanide coordination polymers with Ag@SiO<sub>2</sub> nanoparticles. *Dalton Trans.* **2017**, *46* (19), 6447-6455.

12. Wang, A.-L.; Zhou, D.; Chen, Y.-N.; Li, J.-J.; Zhang, H.-X.; Zhao, Y.-L.; Chu, H.-B., Crystal structure and photoluminescence of europium, terbium and samarium compounds with halogen-benzoate and 2,4,6-tri(2-pyridyl)-s-triazine. *J. Lumin.* **2016**, *177*, 22-30.

13. Wang, X.-J.; Qu, Y.-R.; Zhao, Y.-L.; Chu, H.-B., Effect of the Composition of Lanthanide Complexes on Their Luminescence Enhancement by Ag@SiO<sub>2</sub> Core-Shell Nanoparticles. *Nanomaterials* **2018**, *8* (2), 98.

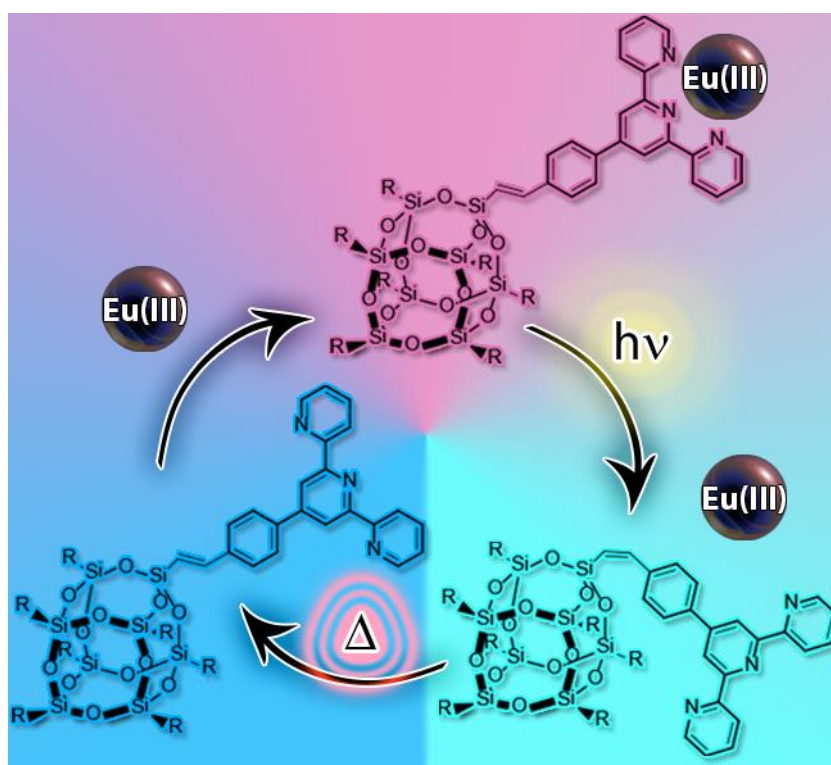
14. Palit, D. K.; Sapre, A. V.; Mittal, J. P.; Rao, C. N. R., Photophysical properties of the fullerenes, C<sub>60</sub> and C<sub>70</sub>. *Chem. Phys. Lett.* **1992**, *195* (1), 1-6.

15. Sariciftci, N. S.; Smilowitz, L.; Heeger, A. J.; Wudl, F., Photoinduced electron transfer from a conducting polymer to buckminsterfullerene. *Science* **1992**, *258* (5087), 1474-1476.

16. Figueira-Duarte, T. M.; Gégout, A.; Nierengarten, J.-F., Molecular and supramolecular C<sub>60</sub>-oligophenylenevinylene conjugates. *Chem. Commun.* **2007**, (2), 109-119.

# Chapter 4

## *Tuneable Emission of Polyhedral Oligomeric Silsesquioxane- Based Nanostructures Self-Assembled in the Presence of Europium(III) Ions: Reversible trans-to-cis Isomerization*



This chapter is based on:

ChemPlusChem, **2019**, Accepted Author Manuscript. doi:10.1002/cplu.201900575

## 4 Introduction

Polyhedral Oligomeric Silsesquioxanes (POSS,  $T_8$ ) with their cubic symmetry represent an ideal building block for the construction of 3D networks. POSS exhibits an inner inorganic nanocage surrounded by eight organic moieties, which can be easily functionalized thus offering a wide range of possibilities for the synthesis of novel hybrid solids.<sup>1</sup> POSS nanostructures have attracted an increasing interest in recent decades. Due to their exceptional features, they found application in several fields from catalysis<sup>2</sup> to polymer sciences.<sup>3</sup> Imidazolium functionalized POSS nanostructures were efficiently employed as catalysts in the conversion of  $CO_2$ <sup>4</sup> or as support for Pd nanoparticles.<sup>5</sup> The exceptional chemical-physical characteristics of the nanocage (rigidity and thermal stability) were also exploited to improve the thermal stability of a number of polymers.<sup>6</sup> POSS functionalized with proper fluorophores successfully acted as nanosensors for the detection of toxic industrial chemicals and chemical warfare agent simulants,<sup>7</sup> whereas when the POSS rigid core is endowed with mesogenic moieties, the resulting hybrids show liquid crystal properties.<sup>8</sup> Recently Carbonell *et al.* proposed the use of POSS-based nanocages functionalized with terpyridine moieties as efficient nanostructure for the formation of luminescent metallopolymers in presence of  $Zn^{2+}$  and  $Fe^{2+}$  cations.<sup>9</sup> Moreover, it was also described by Cheng *et al.* that when POSS units are functionalized with fluorescent dyes, the resulting materials display an efficient emission intensity due to a combination of the improved dispersion of the fluorophore along with the increased thermal stability as a consequence of the inorganic core.<sup>10</sup>

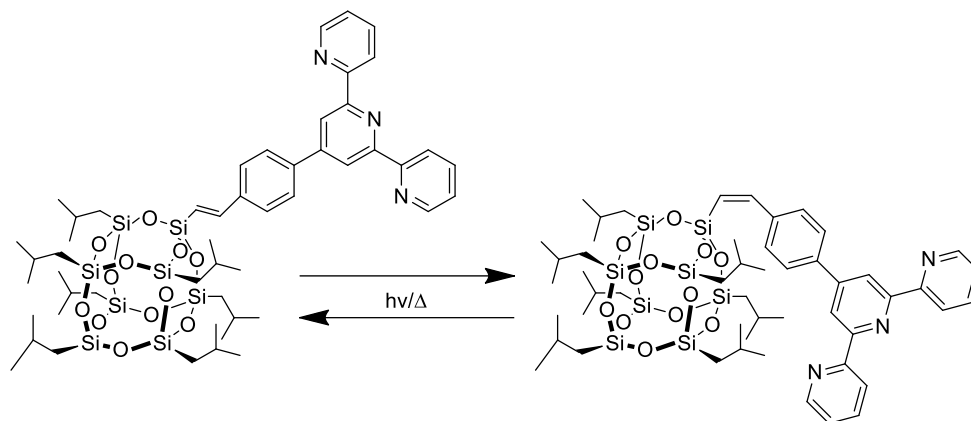
Due to their peculiar luminescent properties, lanthanides trivalent ions (Ln(III)) and in particular Eu, Tb and Yb, have attracted the raising attention of the scientific community for the design of advanced functional materials<sup>11</sup> with possible applications in fields as different as electronics or bio-medicine.<sup>12</sup> The unique properties of Ln(III) include long-lived excited states, sharp line-like emission bands and large Stokes shifts. However, direct excitation of these cations is hardly obtained without laser sources due to the strongly forbidden character of the  $f-f$  transitions. For this reason, a species able to absorb photons at short wavelengths and to transfer the energy to the lanthanides, which emit lights at much longer

wavelength, is normally used in the process usually called “antenna effect”. Terpyridine-based ligands are largely employed for this purpose because of their light-harvesting antenna effect combined with high-affinity metal-bindings.<sup>13</sup> Moreover, it is known, that independently from the ligand used, the local chemical environment has a strong influence on the emission of Ln(III).<sup>14</sup>

On the other side, it would be interesting to have systems in which a controlled and tuneable emission can be obtained only via slightly chemical modification of the structure of the ligand not requiring an *ex-novo* synthesis pathway. For this purpose, the photochemical *cis-trans* isomerization of double bonds (vinyl, stilbene and azo compounds), have been the subject of a large variety of investigations. In some cases configurational changes can be associated with different fluorescence emissions regulated by the photoisomerization process, as well as even on/off fluorescent switching<sup>15</sup> and photostabilization<sup>16</sup> via reversible *cis-trans* isomerization.<sup>17</sup>

To the best of my knowledge, photoisomerization studies in presence of POSS-based hybrid materials have never been carried out. Herein, two novel Eu<sup>3+</sup> complexes are proposed. employing as ligands POSS nanostructures functionalized with one (M-POSS) or eight (O-POSS) terpyridine moieties. The reversible *trans* to *cis* isomerization of the carbon-carbon vinyl moiety connecting the POSS nanocage to the terpyridine ligand is presented (**Scheme 4.1**). The O-POSS architectures display a switchable blue-green emission as consequence of the configurational changes. This switchable behaviour is even more evident in presence of Eu species. In this case a reversible “blue-red-green” emission can be easily achieved making the O-POSS-based Eu(III) complex an extremely promising and innovative material for organic-inorganic hybrid emitting devices.<sup>18</sup>





**Scheme 4.1.** *Trans-cis* isomerization of M-POSS

## 4.1 Results and Discussion

The synthesis of functionalized polyhedral oligomeric silsesquioxane with 4'-phenyl-2,2':6,2''-terpyridine units was achieved via Heck coupling reaction following a procedure previously described in our research group.<sup>9</sup> The M-POSS was achieved reacting for three days at 100°C in dimethylformamide (DMF) the monovinyl-heptaisobutyl POSS (MV) with Br-terpyridine derivative using a species of Pd as catalyst, obtained in situ mixing Pd(OAc)<sub>2</sub> and tris(*o*-tolyl)phosphine. After the reaction, Pd<sup>0</sup> is filtered off and the M-POSS is obtained by precipitation from the cooled reaction solvent as with powder in 80% of yield.

The O-POSS was obtained by reacting octavynyl-POSS with Br-terpyridine derivative with the above mentioned catalyst in DMF for 1 week. After, the Pd<sup>0</sup> was removed by filtration and the crude was precipitated in water. The final product was obtained in 68% of yield after several washing of the crude with methanol, acetonitrile and acetone.

The structures of the corresponding mono- (M-POSS) and octa-functionalized POSS (O-POSS) are presented in **Figure 4.1**.

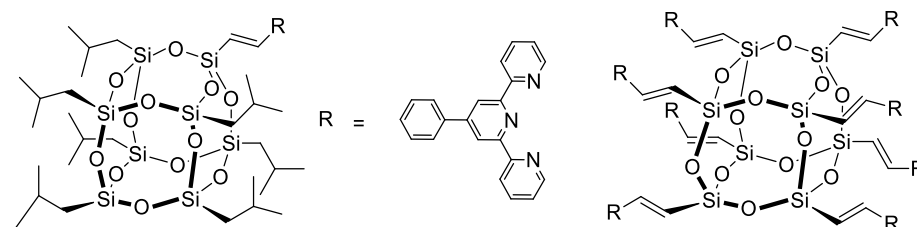


**Figure 4.1.** Functionalized M-POSS and O-POSS.

Both M- and O-POSS were characterized via  $^1\text{H}$ -,  $^{13}\text{C}$ - and  $^{29}\text{Si}$ -NMR. In the case of the M-POSS, proton NMR helped to understand if the functionalisation has taken place. This can be possible by comparison of the spectra of 4'-phenyl-2,2':6',2''-terpyridine and of the monovinyl-heptaisobutyl-POSS with the spectrum of the final material (**Figure 4.2**).

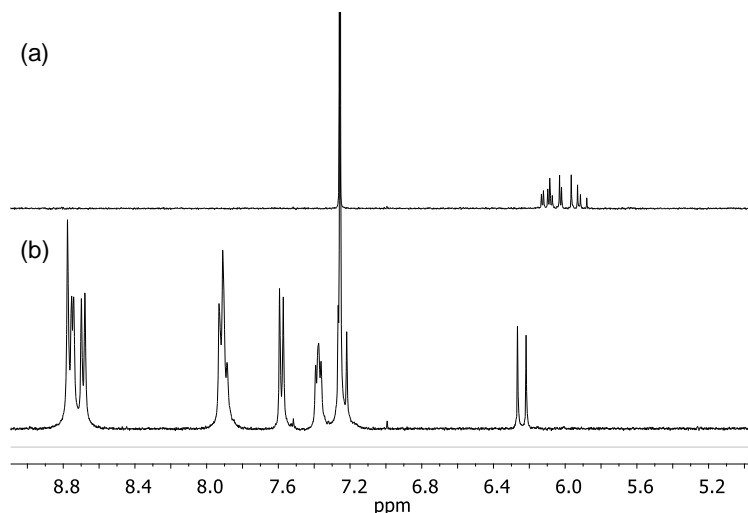


**Figure 4.2.** Selected region of the  $^1\text{H}$ -NMR spectra of the MV (a) and M-POSS (b).

In **Figure 4.2a** it is possible to see the loss of the multiplicity of the proton in the vinyl region of the starting material and in **Figure 4.2b** the typical pattern of the aromatic protons of the terpyridine in the aromatic part of the spectrum, together to the signal of the vinyl proton at 6.3 ppm that suggests the right functionalisation of nanocage.

To confirm this finding, the solid state  $^{13}\text{C}$ -NMR of the starting material and the final product are reported in **Figure 4.3** for comparison.

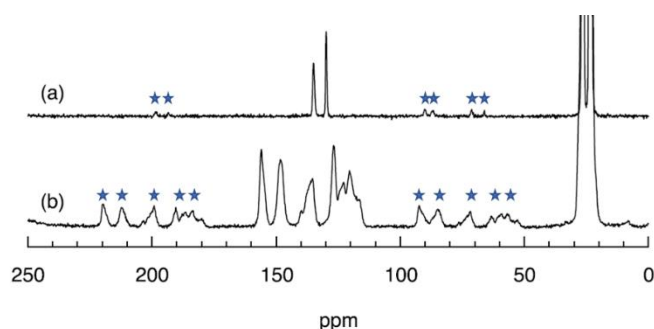


**Figure 4.3.** Solid-state  $^{13}\text{C}$  CP-MAS spectra of MV (a) and M-POSS (b). Stars indicate spinning side bands

The spectrum in **Figure 4.3b** shows the pattern related to the terpyridine carbons, confirming the good outcome of the reaction.

In addition, solid state  $^{29}\text{Si}$ -NMR were registered in order to check the integrity of the hollow nanocage (**Figure 4.4**).

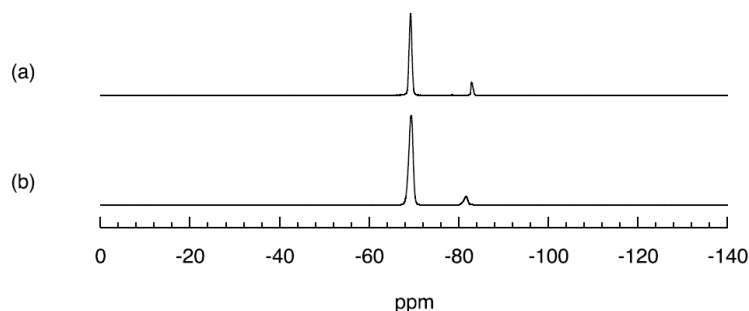


**Figure 4.4.** Solid-state  $^{29}\text{Si}$  MAS NMR spectra of MV (a) and M-POSS (b).

The spectra show that the structure of the skeleton of the POSS, before (**Figure 4.4a**) and after the functionalisation (**Figure 4.4b**), did not change, thus confirming the structural integrity.  $^{29}\text{Si}$  MAS solid state NMR spectra of monovinyl-heptaisobutyl POSS and M-POSS display two signals in the region of the  $\text{T}^3$  units with a relative abundance of 7:1, corresponding to the Si atoms linked to the isobutyl groups and to the vinyl functionality.

Analogous characterizations were performed on the O-POSS. However, in this case the direct comparison with the starting materials via  $^1\text{H}$ -NMR was not possible. O-POSS structures present a combination of two broad bands in  $^1\text{H}$ -NMR. This behaviour was previously observed in literature and it is attributed to the presence of aggregates as consequence of the  $\pi$ - $\pi$  stacking interactions between terpyridine moieties (**Figure 4.5**).

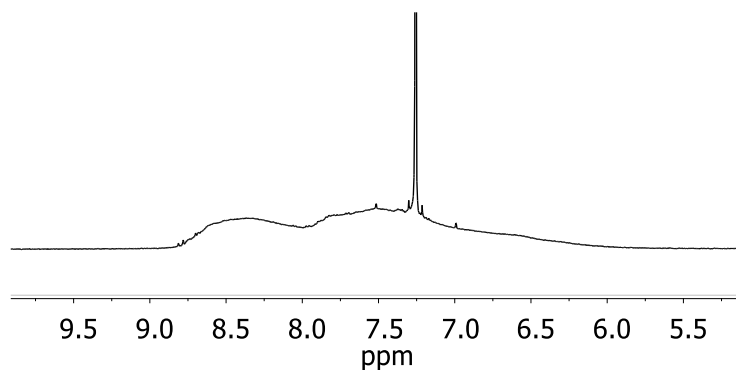


**Figure 4.5.** Selected region of the  $^1\text{H}$ -NMR spectrum of the O-POSS. The broad signal is due to the  $\pi$  -  $\pi$  stacking interaction between the terpyridine.

Due to the difficulties encountered with the solution-state NMR characterization of O-POSS,  $^{13}\text{C}$ - and  $^{29}\text{Si}$ - NMR spectra were recorded in solid state conditions. Solid-state  $^{13}\text{C}$  CP-MAS confirmed the pattern for the carbon of the terpyridine moieties (**Figure 4.6**) whereas the solid-state  $^{29}\text{Si}$  MAS NMR validate the integrity of the structure (**Figure 14**).

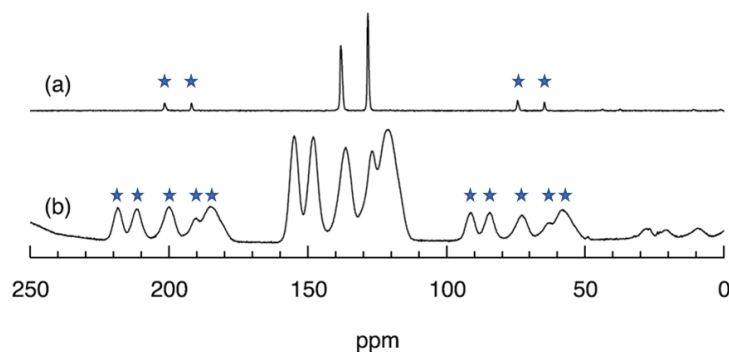


**Figure 4.6.** Solid-state  $^{13}\text{C}$  CP-MAS of the OV (a) and O-POSS (b) Stars indicate spinning side bands

In particular,  $^{29}\text{Si}$ -NMR displays one signal typical of a closed  $\text{T}_8\text{R}_8$  structure corresponding to completely condensed  $\text{T}^3$  silicon units. It is interesting to note that this resonance line is dramatically broadened. It is known that the solid-state  $^{29}\text{Si}$ -NMR spectra are strongly dependent on the T–O–T angle;<sup>19</sup> the broadening of the signals can hence be ascribed to the distribution of conformations with the consequential distortion of the T–O–T angles (**Figure 4.7**).

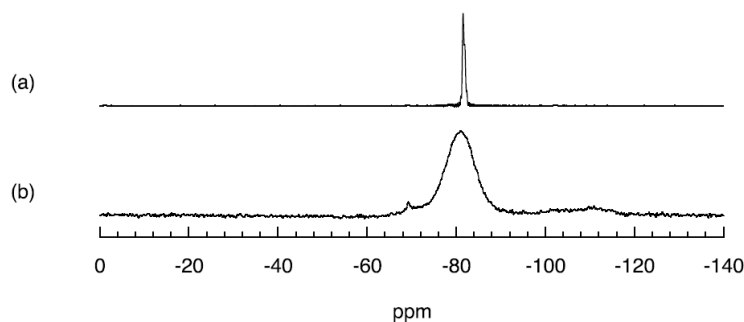


**Figure 4.7.** Solid-state  $^{29}\text{Si}$  MAS NMR spectra of the OV (a) and O-POSS (b)

Due to the notable light-emitting performance of the lanthanides, our attention was focused to this series of cations in order to form binary metal complexes (in presence of M-POSS) or 3D supramolecular assemblies (with O-POSS) generated through coordination of the POSS-based nanostructures with the selected metal. In

particular, Eu trivalent ions were selected as target cations since they exhibit intense emission from *f-f* electronic transitions. Moreover, both POSS structures depicted in **Scheme 4.2** have *trans* carbon-carbon double bonds that can be isomerized to the *cis* form with important implication for both emission and coordinating properties.

Prior to the investigation of the luminescent behaviour as function of the *trans-cis* isomerization, the stoichiometry of the Eu@POSS complexes (both mono- and octa-functionalized) was addressed selecting the M-POSS as initial benchmark. Quantitative information on the stoichiometry of the complex in function of increasing amount of Eu(III) were obtained via  $^1\text{H-NMR}$  titration experiments (**Figure 4.8**).

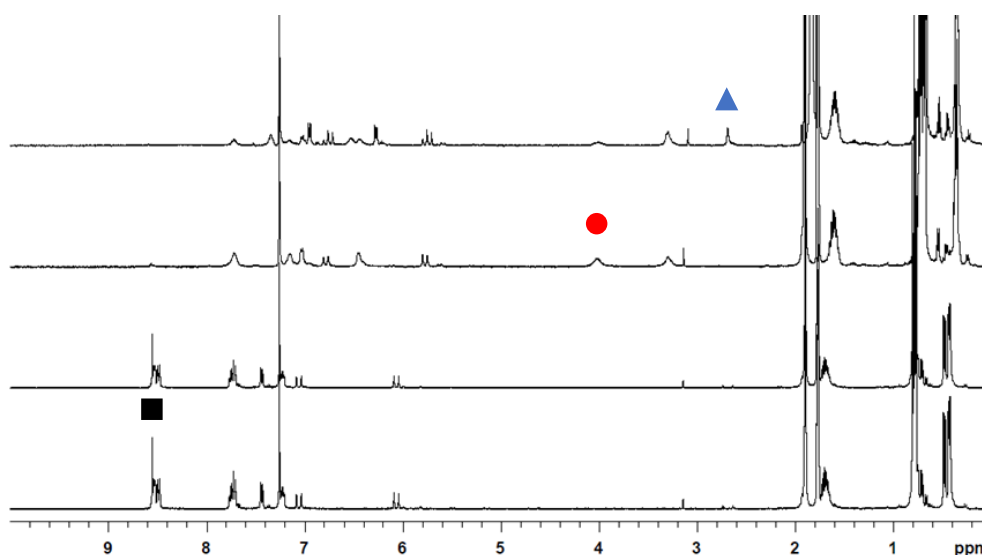


**Figure 4.8.**  $^1\text{H-NMR}$  titration of M-POSS with 0, 0.25, 0.5 and 1 eq of  $\text{Eu}(\text{OTf})_3$ . Black square indicates aromatic proton signals of the terpyridine, red circle indicates one of the signals related to the 2:1 ( $\text{Eu@2-M-POSS}$ ) complex and blue triangle indicates one of the signals related to the 1:1 complex ( $\text{Eu@M-POSS}$ ).

The variations of the normalized integrated areas of selected signals upon addition of increasing amounts of  $\text{Eu}(\text{OTf})_3$  are reported in **Figure 4.9a**. A progressive disappearance of the M-POSS free ligand contribution was observed after addition of increasing amount of Eu(III). The characteristic terpyridine signals (at 8.5 ppm), labelled with a black square, were followed for this investigation.

The complete disappearance of these signals was achieved in correspondence of 0.5 eq of  $\text{Eu}^{3+}$ . This result suggests the formation of a complex characterized by a metal

to ligand stoichiometry of 1:2 (Eu@2-M-POSS). It should be mentioned that a novel pattern of signals corresponding to the formation of the terpyridine-Eu(III) complex (red circles) was evident immediately after the first additions of Eu(III) (see **Figures 4.8** and **4.9a**).

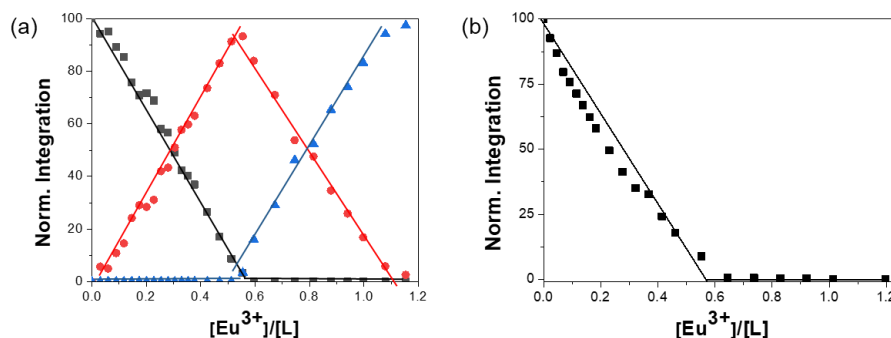


**Figure 4.9.** Changes in normalized integrated areas of selected signals of  $^1\text{H-NMR}$  titration experiments in  $\text{CD}_3\text{Cl}:\text{CD}_3\text{CN}$  (7:3) of (a) M-POSS (b) O-POSS upon addition of 0-1.2 equivalents of  $\text{Eu}(\text{OTf})_3$  (■ = free ligand; ● = 1:2 complex; ◀ = 1:1 complex) Line connecting the point in the plot are guides for the eyes.

Finally, in the presence of an excess of  $\text{Eu}(\text{OTf})_3$ , an additional set of signals appears (blue triangles) which can be reasonably attributed to the formation of the 1:1 complex (Eu@M-POSS) (**Figure 4.10**).

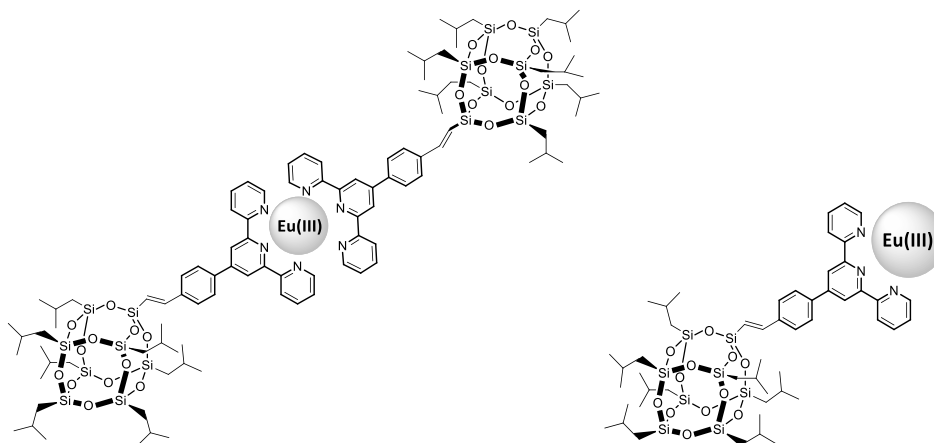


**Figure 4.10.** Schematic representation of the two different type of complexes: to the left the Eu@2M-POSS and to the right the Eu@M-POSS.

Furthermore, in order to assign each proton to the respective  $^1\text{H-NMR}$  signal, a two-dimensional nuclear magnetic resonance spectroscopy (2D-NMR) correlation

spectroscopy experiment (COSY) was performed to a solution of the 2:1 complex (**Figure 4.11**).

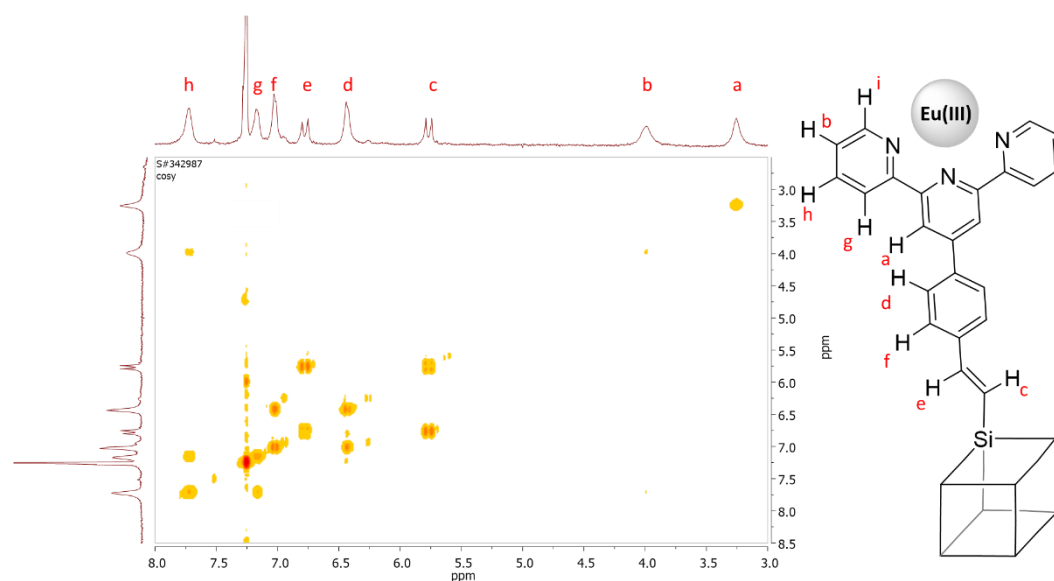


**Figure 4.11.** 2D-NMR COSY of Eu@2M-POSS complex.

COSY spectra are a routine procedure for the structural determination of organic compounds. The homonuclear  $^1\text{H}$  shift correlation obtained with this experiment allows assigning precisely the chemical shift to the different protons (as evidence in the figure). Moreover, in our case the presence of the paramagnetic Eu(III) ion causes a shift to higher or lower frequencies (compared to the non-complexed ligand) of almost all signals.

This shift is mainly due to pseudo-contact (dipolar) contribution, which depends from the structure of the complex. It is related to the distance between the paramagnetic centre and the position of the nucleus under study. The shift is larger for nuclei close to the metal centre and it may have positive or negative sign as a function of the angle between the principal magnetic axis of the system and the vector connecting the paramagnetic centre with the proton.<sup>20</sup>

In addition, the relaxation rate may be significantly increased by the interaction with the metal centre. This phenomenon, called paramagnetic relaxation enhancement (PRE), may be responsible of significant broadening of the signals. This effect strongly depends from the distance between the paramagnetic metal and

the nuclei under investigation ( $1/r^6$ ), and it may broaden the signals under study beyond detection.

Indeed, the signal of the proton labelled “i” is not observed in the spectrum because the large PRE, while all the other expected signals are observed, despite some broadening is observed for the signal closer to the metal centre.

The complexation properties of the O-POSS in presence of Eu(III) species was assessed as well.  $^1\text{H-NMR}$  spectrum of O-POSS shows a very broad band in the aromatic region due to the  $\pi$ - $\pi$  stacking interactions (**Figure 4.5**) between the terpyridine units, as reported previously.<sup>9</sup> Hence, the formation of the Eu(III) complex was indirectly followed by monitoring the disappearance of the  $^1\text{H}$  bands upon addition of  $\text{Eu}(\text{OTf})_3$  (**Figure 4.12**). The complete disappearance of the  $^1\text{H}$  contributions was achieved in correspondence of 0.5 equivalents  $\text{Eu}(\text{OTf})_3$  (**Figure 4.9b**) thus indicating the formation of 1:2 complex ( $\text{Eu}@2\text{O-POSS}$ ), as previously observed when M-POSS was selected as ligand. Considering that lanthanides cations can accommodate up to nine coordinating atoms, the formation of complexes characterized by a metal to ligand stoichiometry of 1:2 could be considered as a consequence of the steric hindrance of the POSS nanostructure and indicates that the coordination shell of Eu(III) is only partially completed by the terpyridine moieties. Interestingly, a more detailed analysis of the aliphatic region in the  $^1\text{H-NMR}$  spectrum of O-POSS evidenced the shift of another signal at 1.9 ppm during the titration experiments (**Figure 4.12**).

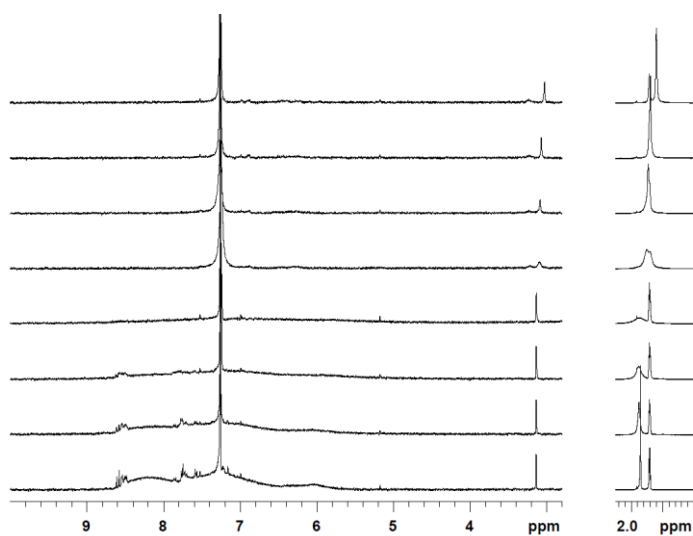


**Figure 4.12.**  $^1\text{H-NMR}$  titration of O-POSS with  $\text{Eu}(\text{OTf})_3$  (left). Part of the aliphatic region of de spectrum (1-2 ppm) highlighting the shift of the signal of water (right).



This signal was attributed to the presence of water molecules completing the first coordination shell of the Eu cations. It deserves to be mentioned that no signals corresponding to free terpyridine moieties were observed after titration. This evidence allows confirming that water plays only the role of co-ligand completing the coordination sphere and it is not able to promote the removal of the terpyridine moieties. The formation of both M-POSS and O-POSS based Eu(III) complexes was also followed by monitoring the changes in the absorption and emission spectra.

Upon addition of  $\text{Eu}(\text{OTf})_3$  to a solution of M-POSS, the absorption band at 290 nm corresponding to the  $\pi\text{-}\pi^*$  transition of the terpyridine decreases remarkably. Concomitantly, the appearance of a novel absorption band above 330 nm was progressively observed (**Figure 4.13a**). These absorption bands can be attributed to the metal/ligand complex. A plateau was reached in correspondence of a M/L ratio equal to 0.5 (**Figure 4.13a**) further confirming the formation of the  $\text{Eu}@2\text{M-POSS}$ .

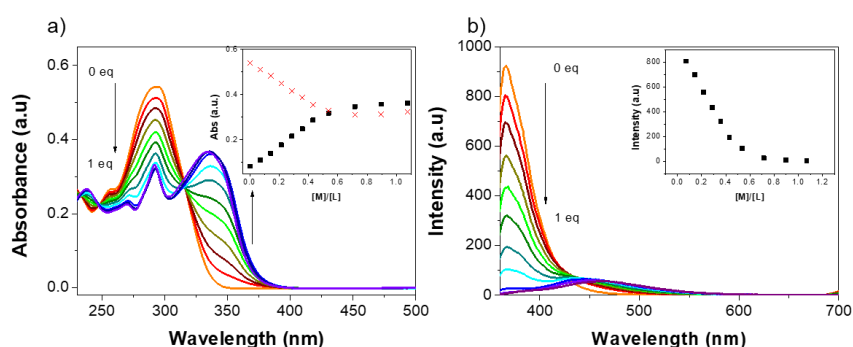


**Figure 4.13.** (a) UV-vis absorption spectra of M-POSS in  $\text{CH}_2\text{Cl}_2$  ( $1.3 \times 10^{-5}$  M) upon titration with  $\text{Eu}(\text{OTf})_3$  in  $\text{CH}_3\text{CN}$  ( $1.4 \times 10^{-3}$  M). Inset shows the normalized absorption changes at 290 nm (red crosses) and 330 nm (black squares). (b) Emission spectra of M-POSS in  $\text{CH}_2\text{Cl}_2$  upon titration with  $\text{Eu}(\text{OTf})_3$ : 0 eq. - 1 eq.  $\lambda_{\text{ex}} = 310$  nm  $\text{OD}_{315\text{ nm}} = 0.27$  slits 2.5-5 and band pass filter (360 – 100 nm). Inset shows the fluorescence intensity at 366nm.

The fluorescence spectra followed a similar trend. As expected, the emission band of the terpyridine in the M-POSS ( $\lambda_{\text{max.}} = 365$  nm) was completely quenched upon addition of 0.5 equivalents of metal cations (see **Figure 4.13b**). As a direct consequence of complex formation, a new emission band at  $\lambda_{\text{max}}$  ca. 455 nm was observed. This broad emission band can be attributed to the ligand-centred transitions. However, under the selected conditions, the characteristic Eu(III)

emission (in the region between 550 – 700 nm) was not detected. This behaviour could be attributed to the incomplete energy transfer from the terpyridine to the europium and/or the influence of the solvent polarity as well as the presence of water molecules. M-POSS possess seven hydrophobic isobutyl groups surrounding the nanocage with consequent generation of a “hydrophobic shell” influencing the self-association process.<sup>21</sup> In order to better understand the reason behind the absence of this emission, a novel set of experiments employing a mixture of solvents of different polarity ((CH<sub>3</sub>CN (97%):CH<sub>2</sub>Cl<sub>2</sub> (3%)) was performed as well.

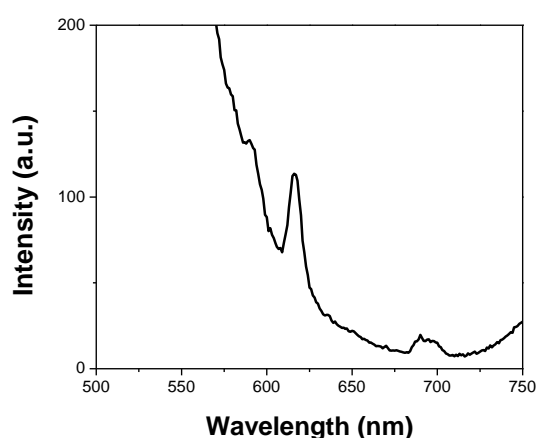


**Figure 4.14.** Typical Europium line like emission centred at 616 nm clearly visible in the presence of Eu@2M-POSS dissolved in the following mixture of solvents: CH<sub>3</sub>CN (97%):CH<sub>2</sub>Cl<sub>2</sub> (3%).

**Figure 4.14** shows a non-resolved emission centered at 617 nm clearly visible in the novel mixture of solvent thus confirming the role played by the solvent on the emission of M-POSS structures.

However, a different behaviour with an improved emission should be expected in presence of O-POSS based ligands in which the isobutyl groups are replaced by terpyridine moieties.

As expected, the addition of Eu(OTf)<sub>3</sub> to a solution of O-POSS, the absorption band at 290 nm corresponding to the  $\pi$ - $\pi^*$  transition of the terpyridine start to decrease. At the same time, the appearance of a new absorption band above 330 nm was progressively observed (**Figure 4.15**).

The plot of the absorption bands in function of the equivalent of metal added confirmed the stoichiometry of the complex. Looking in **Figure 4.15** it is possible to see that, after adding 0.5 equivalent of Eu(III), the plateau was reached

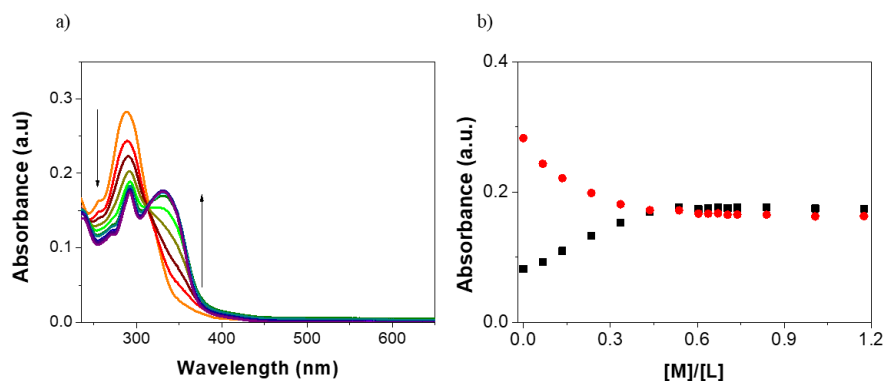


**Figure 4.15.** UV-Vis absorption spectra of O-POSS in  $\text{CH}_2\text{Cl}_2$  ( $1 \times 10^{-5}$  M) upon titration with  $\text{Eu}(\text{OTf})_3$  in  $\text{CH}_3\text{CN}$  ( $1.4 \times 10^{-3}$  M) (a). Normalized absorption changes at 290 nm (red circles) and 330 nm (black squares) (b).

Continuing with the emission titration, as expected, the addition of  $\text{Eu}(\text{OTf})_3$  causes a progressive decrease of the terpyridine emission band ( $\lambda_{\text{max}} = 390$  nm) with a complete disappearance in correspondence of 0.5 equivalents of metal (formation of 1:2 complex, **Figure 4.16a**).

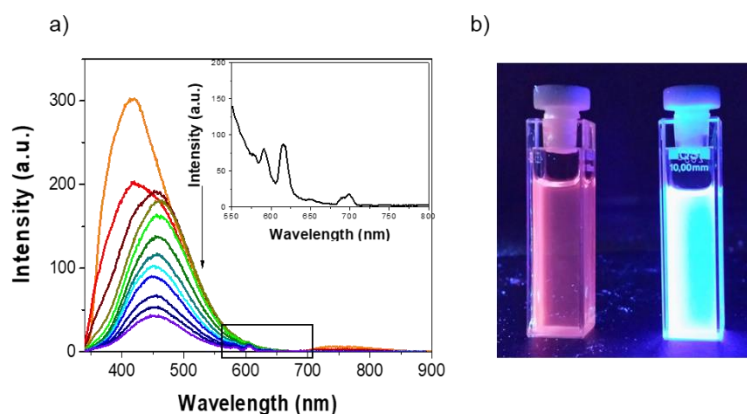


**Figure 4.16.** (a) Emission spectra of O-POSS [ $1 \times 10^{-5}$  M] in  $\text{CH}_2\text{Cl}_2$  upon addition of  $\text{Eu}(\text{OTf})_3$  [ $1.4 \times 10^{-3}$  M] in  $\text{CH}_3\text{CN}$  ( $\lambda_{\text{ex}} = 313$  nm OD= 0.15 slits 5 nm). Inset shows the characteristic Eu(III) line-like emission. (b) Picture of visible emission of O-POSS solutions under UV irradiation at 356 nm. In blue free O-POSS emission and in red  $\text{Eu}@2\text{O-POSS}$  complex emission.

Also in this case, a broad emission ligand centred band was still present. It is noteworthy that once the complex was formed, the characteristic Eu(III) line-like emission was clearly observed. The five sharp emission peaks at 580, 591, 617, 650 and 698 nm (inset **Figure 4.16a**), were assigned to the  $^5D_0 \rightarrow ^7F_J$  ( $J = 0, 1, 2, 3, 4$  and 5) transitions, with the most intense at 617 nm corresponding to the  $^5D_0 \rightarrow ^7F_2$  emission. It is important to underline that, under the highly diluted conditions ( $10^{-7}$  M) employed to monitor the absorption and emission features of the Eu@O-POSS complex, a perfectly homogeneous and transparent solution was always obtained during the titration experiments and this solution was characterized by a red emission evident also to the naked eyes (**Figure 4.16b**).

However, precipitation of the Eu@2O-POSS assembled structure in the solid state was achieved. By mixing a solution of O-POSS in DCM and a solution of Eu triflate, a form of a pale-yellow powder can be easily obtained in more concentrated solution.

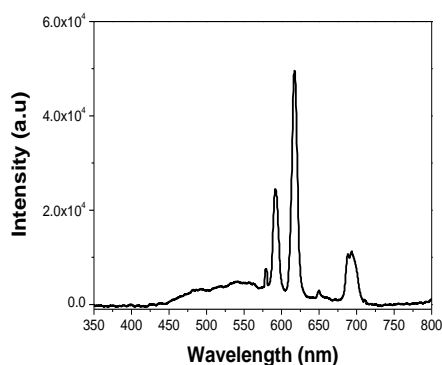


**Figure 4.17.** (a) Solid state emission of Eu@2OPOSS complex.

Hence, solid state emission properties of the Eu@O-POSS complex were evaluated as well. As can be clearly seen in **Figure 4.17**, the emission spectrum of the solid displays excellent features characterized by a strong emission intensity as well as by a narrow half emission width of c.a. 10 nm. Moreover, the decrease of the intensity of the emission band of the complexed ligand suggests that the energy transfer from the terpyridine ligands to the Eu(III) is more efficient in the solid state. The more intense emission of Eu@O-POSS complex, compared to the M-POSS-based structures, can be considered as a consequence of the increased local concentration of the terpyridine surrounding the nanocage. This constitute an

indication of the important role played by the 3D metallopolymeric network protecting Eu(III) against non-radiative deactivation. These differences in the emission arising from the different environments in the assembled coordination complexes could be due to the molecular packing inducing higher emission.<sup>22</sup>

Once proved the emission properties of the Eu@O-POSS, an investigation of the *trans-cis* reversible isomerization was performed. It is well known that UV light irradiation may promote *trans* to *cis* isomerization of the vinyl group. The formation of the *cis*-isomer was monitored via <sup>1</sup>H-NMR spectroscopy selecting the M-POSS as target molecule. The formation of an almost equimolecular mixture of *cis* and *trans* isomers was achieved through irradiation of the *trans*-M-POSS at 356 nm. As can be clearly seen in **Figure 4.18**, the initial <sup>1</sup>H-NMR spectrum displays, in the vinyl region, only one signal at 6.22 ppm (coupling constant  $J = 19.1$  Hz) corresponding to the vinyl group in *trans* configuration. After 1h irradiation, a novel signal at 5.70 ppm (coupling constant  $J = 15.2$  Hz) corresponding to the *cis* form appears together with a series of signals in the aromatic part of the spectrum.

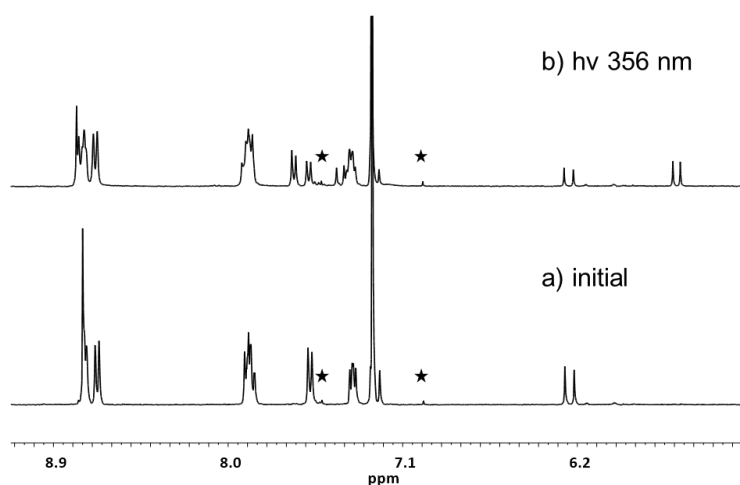


**Figure 4.18.** <sup>1</sup>H-NMR spectrum of M-POSS (a) before and (b) after irradiation at 356 nm. \* in the figure, indicate the <sup>13</sup>C satellites

Once proved the possibility to form the *cis*-M-POSS structure, the *trans*-to-*cis* photoisomerization process was followed at different irradiation times via UV-visible and fluorescence spectroscopies. Upon irradiation, a decrease of the absorbance of the UV-Visible band centred at 290 nm and the concomitant appearance of a shoulder were observed (**Figure 4.19**). A more evident transition

was clearly distinguished in the fluorescent spectra. An almost complete disappearance of the emission band of *trans*-M-POSS at 366 nm together with the appearance of a novel emission band at 460 nm (attributed to the *cis* form) was observed after 60 minutes of irradiation at 356 nm (**Figure 4.19**, green line). Interestingly, under the conditions employed in the fluorescence experiments, a total *trans*-to-*cis* conversion was achieved after 1h irradiation.

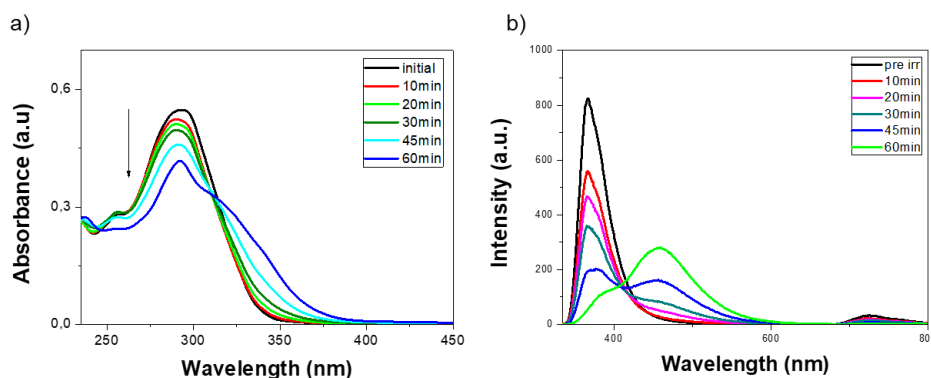


**Figure 4.19.** UV-Vis absorption (left) and emission (right) spectra of M-POSS in CH<sub>2</sub>Cl<sub>2</sub> ( $1.3 \times 10^{-5}$  M) upon different irradiation times at 356nm. ( $\lambda_{\text{irrad}} = 356$  nm);  $\lambda_{\text{ex}} = 314$  nm, slits 2.5, 5 nm (bandpass filter 360 – 1100 nm).

The reversibility of the isomerization process was achieved via thermal treatment, heating the M-POSS solution at 50 °C during 1h (**Figure 4.20a**). Indeed, after thermal treatment at 50 °C the band at 460 nm disappeared while the contribution at 366 nm was completely restored. The process can be repeated multiple times with highly consistent results. Excitation spectra of the M-POSS at the maximum of the respectively emissions (370 nm for the *trans*- form and 460 nm for the *cis*- form) were recorded being practically coincident with the corresponding absorption spectra of *trans*- and *cis*- configurations, respectively (**Figure 4.20**), indicating that the detected emission corresponds to the *trans*- and to the *cis*- forms without observing of the excimers formation in these conditions.

Analogous irradiation experiments were carried out in presence of O-POSS. The photoisomerization process of O-POSS at different irradiation times was followed by UV-Visible and fluorescence spectroscopies.

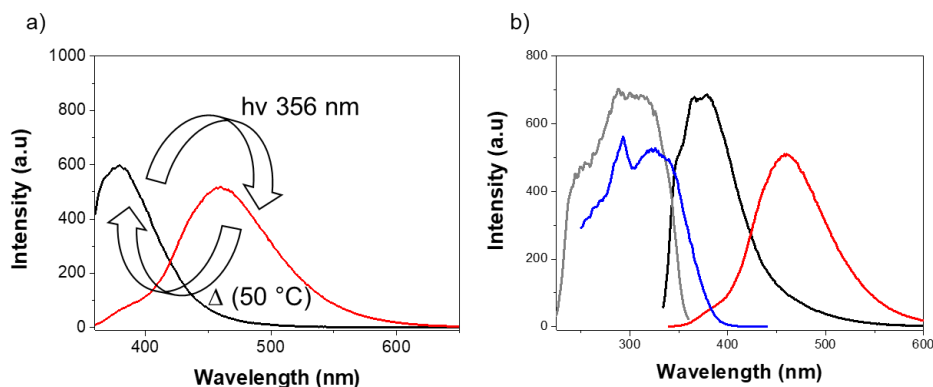


**Figure 4.20.** (a) Reversible Emission spectra of *trans*-M-POSS solution (black line) and *cis*-M-POSS (red line) ( $1.0 \times 10^{-5}$  M) in DCM registered at  $\lambda_{\text{ex}} = 314$  nm slits 2.5, 5 nm (bandpass filter 360 – 1100 nm). (b) Excitation and emission spectra of M-POSS in the *trans*- (grey and black spectrum respectively) and *cis*- (blue and red spectrum) configurations.

*Trans*-to-*cis* photoisomerization occurred under UV light irradiation also in presence of the O-POSS nanostructures. In agreement with the previously described behaviour of M-POSS, a decrease of the absorption band of the ligand (ca. 285 nm) and the appearance of a shoulder was observed (**Figure 4.21**). Moreover, the emission band of the ligand was quenched almost completely and a novel broad emission band, corresponding to the *cis* form, appeared at 510 nm (**Figure 4.21b**).

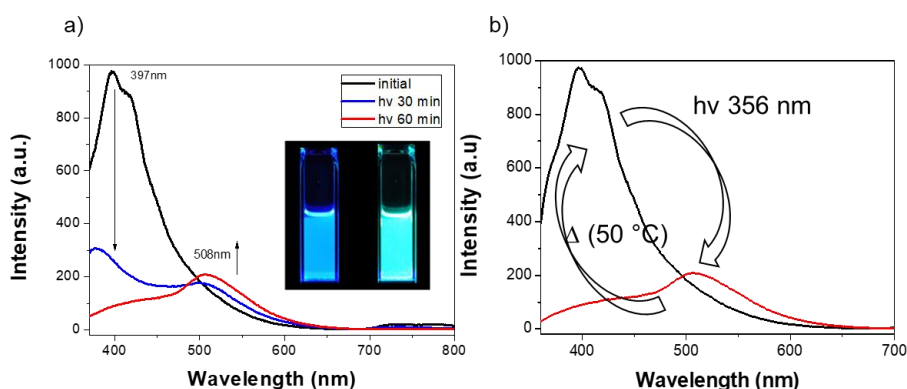


**Figure 4.21.** (a) Emission spectra of O-POSS before and after irradiation at 356 nm at different times. Inset shows the digital photograph of the cuvette at initial and final time taken under UV light at 356 nm. (b) Emission spectra of *trans*- O-POSS solution (black line) and *cis*- O-POSS (red line) in DCM.  $C = 1.2 \times 10^{-5}$  M;  $\lambda_{\text{ex}} = 314$  nm; slits 5, 10.

The broader emission band of the *cis*-O-POSS compared to the *trans*- isomer could be ascribed to the presence of excimers favoured by the *cis*-configuration of the

double bond. Interestingly, in the case of O-POSS nanostructures the *trans* to *cis* isomerization was accompanied by an evident change in colour that passed from blue (*trans*-O-POSS) to green (*cis*-O-POSS). As previously observed for the M-POSS, also the octa-functionalized analogues display a reversible isomerization. Due to the relevant interest that could present a tuneable photochromism of the self-assembled 3D network, the isomerization process of the Eu@O-POSS complex was followed as well via UV-Visible and fluorescence spectroscopies. It is worth highlighting that under UV irradiation the Eu@O-POSS complexes release almost completely the coordinated Eu(III) ions.

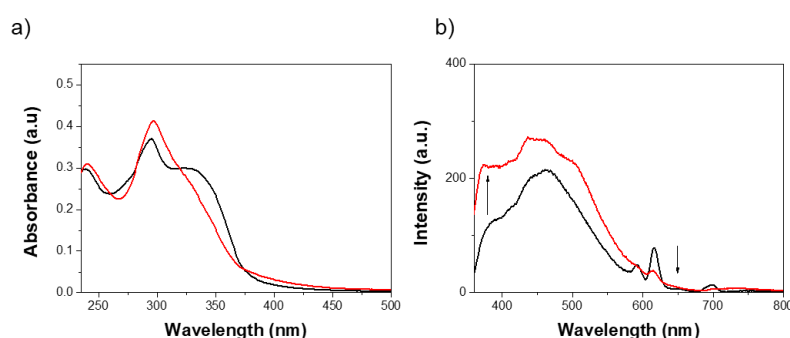
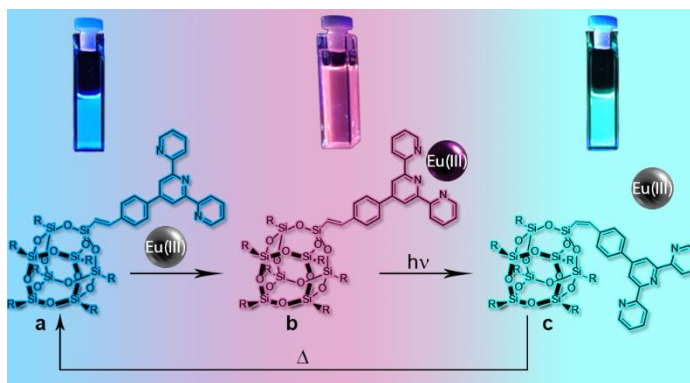


**Figure 4.22.** (a) UV-visible and (b) emission spectra of Eu@O-POSS (1:2) before (black line) and after irradiation (red line) at 356 nm for 60 minutes. [O-POSS] =  $1.3 \times 10^{-5}$  M;  $\lambda_{\text{ex}}$  = 314 nm; slits 5, 10; (bandpass filter 360 – 1100 nm).

As we can observe in the **Figure 4.22**, the characteristic Eu(III) emission bands disappeared after 1h irradiation. This behaviour can be ascribed to elevate steric hindrance of the O-POSS in the *cis* forms hindering the coordination of the metal centre. Changes in fluorescence emission of the Eu@O-POSS under UV light exposure can be detected also at naked eyes (**Scheme 4.3**).

*Trans*-O-POSS (a) displays an evident blue emission, after formation of the Eu@*trans*-O-POSS complex a shift through the red is clearly observed (b), UV-irradiation of the Eu@*trans*-O-POSS causes the release of the Eu(III) ions due to the formation of the *cis*-O-POSS isomer whose free (non-complexed) form emits in the green (c).





**Scheme 4.3.** Schematic representation of the tuneable emission of (a) *trans*-O-POSS in dichloromethane solution; (b) Eu@*trans*-O-POSS; (c) *cis*-O-POSS after irradiation at 356 nm (60 minutes) under UV lamp. (R = phenyl-2,2':6',2''-terpyridine).

After thermal treatment the *cis*-O-POSS can be completely converted in the *trans* isomer and the cycle can be repeated without detrimental effect on O-POSS nanostructure.

Moreover, in presence of small amount of solvent the solid Eu@O-POSS can be easily shaped as a film as illustrated in **Figure 4.23**. This behaviour can pave the way toward the application in materials science.



**Figure 4.23.** Film of the acronym of the University of Namur designed employing the *trans*-O-POSS (first two letters on the right), Eu@*trans*-O-POSS (letters in the middle) and *cis*-O-POSS (last two letters on the right) under UV lamp (356 nm).

## 4.2 Conclusions

The absorption and emission properties of two novel silsesquioxane-based Eu complexes were investigated. The stoichiometry of the complexes (Eu@2M-POSS and Eu@2O-POSS) was evaluated via  $^1\text{H-NMR}$  as well as UV-Vis and fluorescence titration experiments. The solutions of Eu@2O-POSS display a

bright-red luminescence under UV light at room temperature and an even more intense emission can be achieved in solid state. Interestingly both M- and O-POSS nanostructures display a reversible trans to cis isomerization of the carbon-carbon double bond linking the silsesquioxane core to the terpyridine moieties. In the case of O-POSS nanocages this isomerization was monitored also in presence of Eu(III) cations and was accompanied by an evident modification of the colour which passed from blue (*trans*-O-POSS) to red (Eu@*trans*-O-POSS) and finally to green (*cis*-O-POSS) as consequence of the release of the metal cations. After thermal treatment, the *cis*-O-POSS can be completely converted in the *trans* isomer and the cycle can be repeated without detrimental effect on O-POSS nanostructure. This switchable and reversible “blue-red-green” emission together with the easy dispersion, solubility in organic solvents and the possibility of forming films makes the emitting solid promising for applications in materials science and in particular in the preparation of advanced light emitting devices.

### 4.3 References

1. Pescarmona, P. P.; Aprile, C.; Swaminathan, S., Silsesquioxanes and their use as precursors for catalysts and as model compounds. In *New and Future Developments in Catalysis*, Suib, S. L., Ed. Elsevier: 2013.
2. (a) Duchateau, R.; van Meerendonk, W. J.; Huijser, S.; Staal, B. B. P.; van Schilt, M. A.; Gerritsen, G.; Meetsma, A.; Koning, C. E.; Kemmere, M. F.; Keurentjes, J. T. F., Silica-Grafted Diethylzinc and a Silsesquioxane-Based Zinc Alkyl Complex as Catalysts for the Alternating Oxirane–Carbon Dioxide Copolymerization. *Organometallics* **2007**, *26* (17), 4204-4211; (b) Kunthom, R.; Jaroentomeechai, T.; Ervithayasuporn, V., Polyhedral oligomeric silsesquioxane (POSS) containing sulfonic acid groups as a metal-free catalyst to prepare polycaprolactone. *Polymer* **2017**, *108*, 173-178; (c) Wada, K.; Nakashita, M.; Mitsudo, T., Active catalysts prepared using a vanadium-containing oligosilsesquioxane for selective photo-assisted oxidation of methane into methanal. *Chem. Commun.* **1998**, (1), 133-134.
3. (a) Kannan, R. Y.; Salacinski, H. J.; Ghanavi, J.-e.; Narula, A.; Odlyha, M.; Peirovi, H.; Butler, P. E.; Seifalian, A. M., Silsesquioxane Nanocomposites as Tissue Implants. *Plastic and Reconstructive Surgery* **2007**, *119* (6), 1653-1662; (b) Rizvi, S. B.; Yang, S. Y.; Green, M.; Keshtgar, M.; Seifalian, A. M., Novel POSS–PCU Nanocomposite Material as a Biocompatible Coating for Quantum Dots. *Bioconjugate Chem.* **2015**, *26* (12), 2384-2396; (c) Zhang, C.; Babonneau, F.; Bonhomme, C.; Laine, R. M.; Soles, C. L.; Hristov, H. A.; Yee, A. F., Highly Porous Polyhedral Silsesquioxane Polymers. Synthesis and Characterization. *J. Am. Chem. Soc.* **1998**, *120* (33), 8380-8391.
4. Bivona, L. A.; Fichera, O.; Fusaro, L.; Giacalone, F.; Buaki-Sogo, M.; Gruttadauria, M.; Aprile, C., Polyhedral Oligomeric Silsesquioxane Based Catalyst for the Efficient Synthesis of Cyclic Carbonates. *Catal. Sci. Technol.* **2015**, *5*, 5000 - 5007
5. (a) Calabrese, C.; Liotta, L. F.; Giacalone, F.; Gruttadauria, M.; Aprile, C., Supported Polyhedral Oligomeric Silsesquioxane-Based (POSS) Materials as Highly Active Organocatalysts for the Conversion of CO<sub>2</sub>. *ChemCatChem* **2019**,

11 (1), 560-567; (b) Bivona, L. A.; Giacalone, F.; Carbonell, E.; Gruttadauria, M.; Aprile, C., Proximity Effect using a Nanocage Structure: Polyhedral Oligomeric Silsesquioxane-Imidazolium Tetrachloro- palladate Salt as a Precatalyst for the Suzuki–Miyaura Reaction in Water. *ChemCatChem* **2016**, *8* (9), 1685-1691.

6. Tsuchida, A.; Bolln, C.; Sernetz, F. G.; Frey, H.; Mülhaupt, R., Ethene and Propene Copolymers Containing Silsesquioxane Side Groups. *Macromolecules* **1997**, *30* (10), 2818-2824.

7. Hartmann-Thompson, C.; Keeley, D. L.; Pollock, K. M.; Dvornic, P. R.; Keinath, S. E.; Dantus, M.; Gunaratne, T. C.; LeCaptain, D. J., One- and Two-Photon Fluorescent Polyhedral Oligosilsesquioxane (POSS) Nanosensor Arrays for the Remote Detection of Analytes in Clouds, in Solution, and on Surfaces. *Chem. Mater.* **2008**, *20* (8), 2829-2838.

8. Mehl, G. H.; Saez, I. M., Polyhedral liquid crystal silsesquioxanes. *Appl. Organomet. Chem.* **1999**, *13* (4), 261-272.

9. Carbonell, E.; Bivona, L. A.; Fusaro, L.; Aprile, C., Silsesquioxane–Terpyridine Nano Building Blocks for the Design of Three-Dimensional Polymeric Networks. *Inorg. Chem.* **2017**, *56* (11), 6393-6403.

10. Cheng, C.-C.; Chu, Y.-L.; Chu, C.-W.; Lee, D.-J., Highly efficient organic-inorganic electroluminescence materials for solution-processed blue organic light-emitting diodes. *J. Mater. Chem. C* **2016**, *4* (27), 6461-6465.

11. Escribano, P.; Julián-López, B.; Planelles-Aragó, J.; Cordoncillo, E.; Viana, B.; Sanchez, C., Photonic and nanobiophotonic properties of luminescent lanthanide-doped hybrid organic–inorganic materials. *J. Mater. Chem.* **2008**, *18* (1), 23-40.

12. Syamchand, S. S.; Sony, G., Europium enabled luminescent nanoparticles for biomedical applications. *J. Lumin.* **2015**, *165*, 190-215.

13. (a) Schubert, U. S.; Winter, A.; Newkome, G. R., Metallo-Supramolecular Architectures Based on Terpyridine Complexes. In *Terpyridine-Based Materials*, Wiley-VCH Verlag GmbH & Co. KGaA: 2011; pp 129-197; (b) Kotova, O.; Comby, S.; Lincheneau, C.; Gunnlaugsson, T., White-light emission from discrete

heterometallic lanthanide-directed self-assembled complexes in solution. *Chem. Sci.* **2017**, *8* (5), 3419-3426.

14. Bekiari, V.; Lianos, P., Multicolor emission from terpyridine–lanthanide ion complexes encapsulated in nanocomposite silica/poly(ethylene glycol) sol–gel matrices. *J. Lumin.* **2003**, *101* (1), 135-140.

15. (a) Chung, J. W.; Yoon, S.-J.; An, B.-K.; Park, S. Y., High-Contrast On/Off Fluorescence Switching via Reversible E–Z Isomerization of Diphenylstilbene Containing the  $\alpha$ -Cyanostilbenic Moiety. *J. Phys. Chem. C* **2013**, *117* (21), 11285-11291; (b) Dugave, C.; Demange, L., Cis–Trans Isomerization of Organic Molecules and Biomolecules: Implications and Applications. *Chem. Rev.* **2003**, *103* (7), 2475-2532.

16. Lima, P. P.; Nolasco, M. M.; Paz, F. A. A.; Ferreira, R. A. S.; Longo, R. L.; Malta, O. L.; Carlos, L. D., Photo–Click Chemistry to Design Highly Efficient Lanthanide  $\beta$ -Diketonate Complexes Stable under UV Irradiation. *Chem. Mater.* **2013**, *25* (4), 586-598.

17. Lin, L.-R.; Tang, H.-H.; Wang, Y.-G.; Wang, X.; Fang, X.-M.; Ma, L.-H., Functionalized Lanthanide(III) Complexes Constructed from Azobenzene Derivative and  $\beta$ -Diketone Ligands: Luminescent, Magnetic, and Reversible Trans-to-Cis Photoisomerization Properties. *Inorg. Chem.* **2017**, *56* (7), 3889-3900.

18. (a) Bian, M.; Wang, Y.; Guo, X.; Lv, F.; Chen, Z.; Duan, L.; Bian, Z.; Liu, Z.; Geng, H.; Xiao, L., Positional isomerism effect of spirobifluorene and terpyridine moieties of “(A)<sub>n</sub>–D–(A)<sub>n</sub>” type electron transport materials for long-lived and highly efficient TADF-PhOLEDs. *J. Mater. Chem. C* **2018**, *6* (38), 10276-10283; (b) Zych, D.; Slodek, A.; Matussek, M.; Filapek, M.; Szafraniec-Gorol, G.; Krompiec, S.; Kotowicz, S.; Siwy, M.; Schab-Balcerzak, E.; Bednarczyk, K.; Libera, M.; Smolarek, K.; Maćkowski, S.; Danikiewicz, W., Highly Luminescent 4'-(4-ethynylphenyl)-2,2':6',2''-Terpyridine Derivatives as Materials for Potential Applications in Organic Light Emitting Diodes. *ChemistrySelect* **2017**, *2* (27), 8221-8233.

19. Cordes, D. B.; Lickiss, P. D., Preparation and Characterization of Polyhedral Oligosilsesquioxanes. In *Applications of Polyhedral Oligomeric Silsesquioxanes*,

Hartmann-Thompson, C., Ed. Springer Science and Business Media: London, **2011**; pp 47-133.

20. Peters, J.; Huskens, J.; Raber, D., Lanthanide induced shifts and relaxation rate enhancements. *Progress in Nuclear Magnetic Resonance Spectroscopy* **1996**, *28* (3-4), 283-350.

21. Au-Yeung, H.-L.; Leung, S. Y.-L.; Tam, A. Y.-Y.; Yam, V. W.-W., Transformable Nanostructures of Platinum-Containing Organosilane Hybrids: Non-covalent Self-Assembly of Polyhedral Oligomeric Silsesquioxanes Assisted by Pt···Pt and  $\pi$ - $\pi$  Stacking Interactions of Alkynylplatinum(II) Terpyridine Moieties. *J. Am. Chem. Soc.* **2014**, *136*, 17910–17913

22. (a) Andres, J.; Chauvin, A.-S., Europium Complexes of Tris(dipicolinato) Derivatives Coupled to Methylumbelliferone: A Double Sensitization. *Eur. J. Inorg. Chem.* **2010**, *2010* (18), 2700-2713; (b) Divya, V.; Freire, R. O.; Reddy, M. L. P., Tuning of the excitation wavelength from UV to visible region in Eu<sup>3+</sup>- $\beta$ -diketonate complexes: Comparison of theoretical and experimental photophysical properties. *Dalton Trans.* **2011**, *40* (13), 3257-3268; (c) Zhang, Z.-M.; Han, F.-F.; Zhang, R.; Li, N.; Ni, Z.-H., Design, syntheses and aggregation-induced emission properties of two new enlarged tetraarylethene-based luminogens. *Tetrahedron Lett.* **2016**, *57* (17), 1917-1920.

*Chapter 5*

*Photoluminescence*

*Lanthanide@POSS-based materials*

## 5 Photoluminescence Lanthanide@POSS-based materials

As already reported in literature (and mentioned in the previous chapter),  $\text{Eu}^{3+}$  ions should be able to accommodate up to nine coordinating atoms/molecules.<sup>1</sup> However, in the case of the systems described in paragraph 4.1, the steric hindrance of the POSS-based structures hinders the formation of complexes in which the metal cation can accommodate 3 silsesquioxanes-based ligands. As commented previously (see part 4.1) the coordination shell of the metal is hence completed by solvent molecules, most probably water (**Figure 4.11**).

Since it is well known that water can negatively affect fluorescence emission,<sup>2</sup> an attempt was done to remove these water molecules from the Eu@POSS complexes adding less hindered and highly coordinating ligands to the reaction mixture. In order to achieve this goal, two strong co-ligands able to absorb photon and promote an energy transfer to europium were selected: 2,2'-oxydiacetic acid (ODA), and 2,2':6',2''-terpyridine (Tpy). In the next paragraph we will report the results of these studies.

Due to the poor solubility of the ODA in the mixture of solvent employed in the previous experiments ( $\text{CDCl}_3:\text{CD}_3\text{CN}$  or  $\text{CH}_2\text{Cl}_2:\text{CH}_3\text{CN}$ ), a series of titration experiments (followed via  $^1\text{H-NMR}$  as well as via UV-Vis and emission spectroscopies) were conducted to study the behaviour of the POSS-Eu systems in a different media. The novel mixture of solvents employed in this study was constituted by  $\text{CH}_2\text{Cl}_2:\text{MeOH}$ .

Since the nature of the solvent could strongly influence the coordination properties of the selected ligand, titration experiments similar to the ones reported in the previous chapter were performed in presence of  $\text{CH}_2\text{Cl}_2:\text{MeOH}$ .

The UV-Vis spectra of both M-POSS (**Figure 5.1a**) and O-POSS (**Figure 5.1b**) show that the free terpyridine absorption band centred at 290 nm decreases during the titration and a new band, assigned to the formation of the Eu@POSS complex, appears at 330 nm. A plateau was reached after addition of 0.5 eq of  $\text{Eu}(\text{OTf})_3$  solution (inset) suggesting an Eu(III) to ligand stoichiometry equal to 2:1. These results are in agreement with the ones obtained in presence of  $\text{CH}_2\text{Cl}_2:\text{CH}_3\text{CN}$ .



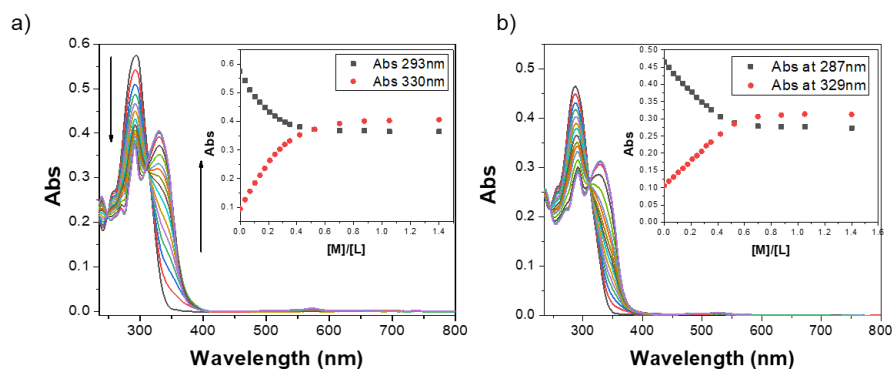


**Figure 5.1.** UV-Vis absorption spectra of M-POSS and O-POSS in  $\text{CH}_2\text{Cl}_2$  ( $1.3 \times 10^{-5}$  M) upon titration with  $\text{Eu}(\text{OTf})_3$  in MeOH ( $1.3 \times 10^{-3}$  M)

Emission spectra (**Figure 5.2**) confirmed further this behaviour. Both experiments allow excluding a major role of methanol as co-ligand under the conditions employed for the absorption and emission studies.

Concerning the M-POSS (**Figure 5.2a**), the emission band of the terpyridine at 365 nm was completely quenched upon addition of 0.5 equivalents  $\text{Eu}^{3+}$  and a new emission band at 455 nm was observed. This second emission band can be attributed to the ligand-centred transitions.

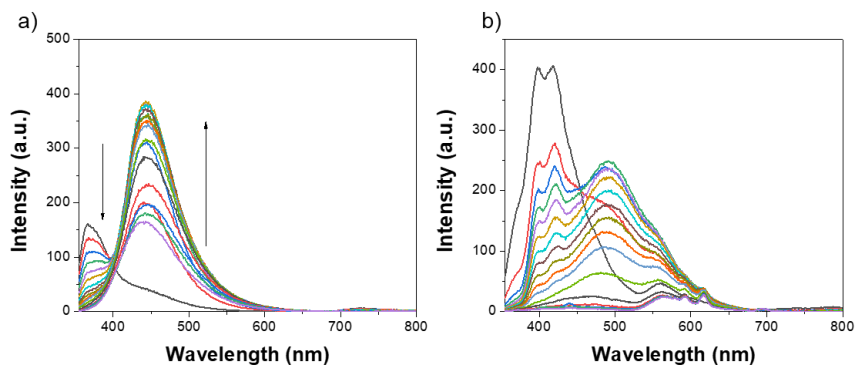


**Figure 5.2.** Emission spectra of (a) M-POSS and (b) O-POSS in  $\text{CH}_2\text{Cl}_2$  upon addition of  $\text{Eu}(\text{OTf})_3$  in MeOH. Solution of M-POSS and O-POSS in DCM at  $C = 1.3 \times 10^{-5}$  M were titred with  $\text{Eu}(\text{OTf})_3$  in MeOH  $C = 1.3 \times 10^{-3}$  M. (M-POSS:  $\lambda_{\text{ex}} = 335$  nm slits = 2.5-5 nm bandpass filter 360 – 1100 nm; O-POSS:  $\lambda_{\text{ex}} = 335$  nm slits = 5-5 nm bandpass filter 360 – 1100 nm).

A similar behaviour was observed in the case of O-POSS (**Figure 5.2b**). In this case, the quenching of the free terpyridine emission band (400 nm) and the simultaneous increases of the ligand centred transition emission band (490 nm) was detected. This last band disappears slowly during the titration and, as consequence

of the energy transfer from the terpyridine to the Eu, the typical Eu line like bands in the region between 580 and 698 nm (assigned to the  $^5D_0 \rightarrow ^7F_j$  transitions) appear.

Titration experiments were also performed following the evolution of the typical signals of the terpyridine via  $^1H$ -NMR. However, a slightly different behaviour was observed in presence of the novel mixture of solvents [ $CDCl_3$ :MeOD] when the titration experiment was followed via  $^1H$ -NMR. This different behaviour could be attributed to the higher concentrations employed in the NMR experiments.

In the previous  $^1H$ -NMR experiments performed in chloroform:acetonitrile we observed: (1) the formation of the Eu@2M-POSS (2:1 complex) (2) the complete disappearance of the free terpyridine after adding 0.5 eq of  $Eu^{3+}$  and (3) the formation of Eu@M-POSS (1:1 complex) after adding an excess of metal (**Figure 4.8** and **4.9a**). On the other hand, when methanol (instead of acetonitrile) is added to the reaction mixture, different species form in solution (**figure 5.3**).

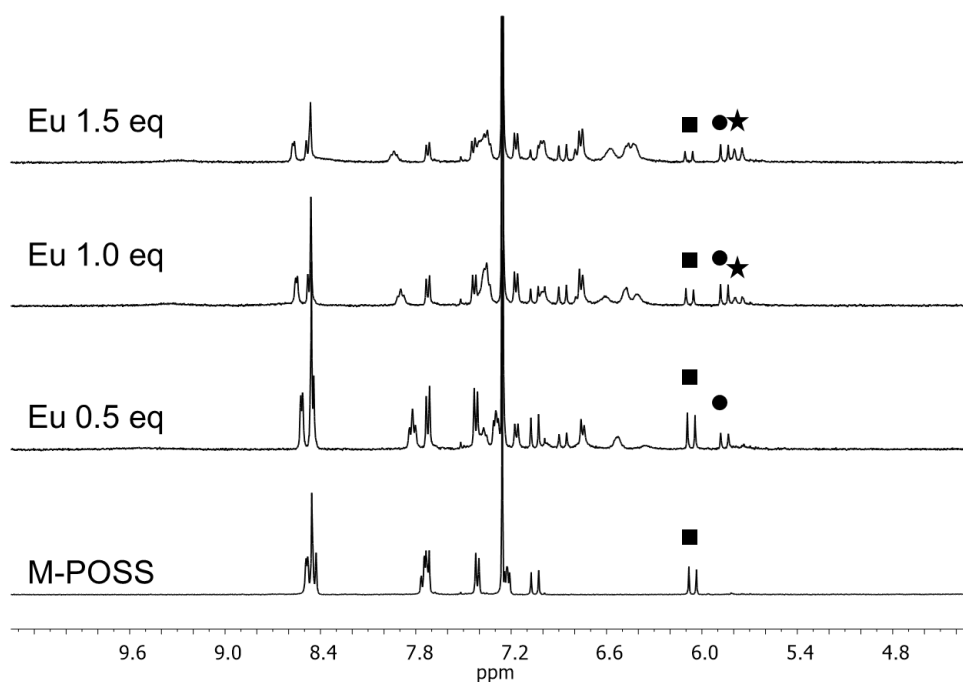


**Figure 5.3.**  $^1H$ -NMR titration of M-POSS solution in  $CDCl_3$ :MeOD 3:1 with  $Eu(OTf)_3$ .

It is important to underline that the formation of a M-POSS/Eu complex was always observed. This is evident by looking to the shift of different signals in the aromatic region of the spectra (protons related to the aromatic rings of the terpyridine) and by observing the region between 5.6 ppm and 6.2 ppm which corresponds to the C-

C double bond. In this last region it is possible to note the disappearance of the signals attributed to the vinyl group of the free terpyridine (when titration is performed with  $\text{CDCl}_3:\text{CD}_3\text{CN}$  solvent mixture). However, by changing solvent mixture (using  $\text{CDCl}_3:\text{MeOD}$  as solvent) two major differences can be immediately detected. First of all, the completely disappearance of the signals corresponding to the free terpyridine (black squares) was never observed even when a large excess of metal was added to the mixture. Moreover, an equilibrium between three different species: the free ligand, the 2:1 complex (Eu@2M-POSS black circles) and the 1:1 complex (Eu@M-POSS black stars) was observed.

## 5.1 $^{139}\text{La}$ -NMR characterisation

So far, the formation of complexes was studied only by  $^1\text{H}$ -NMR titration experiments. Besides, it was interesting to confirm previous results directly by recording NMR spectra of the metal centre of interest. However, since  $\text{Eu}^{+3}$  is paramagnetic and cannot be easily studied by NMR, it was preferred to choose a diamagnetic metal of the lanthanide series, as the lanthanum. Replacing  $\text{Eu}^{+3}$  with  $\text{La}^{+3}$  is supposed to not significantly affect the formation of coordination complexes, as the elements of lanthanide series are chemically similar. La has two quadrupolar NMR active nuclei:  $^{138}\text{La}$  and  $^{139}\text{La}$ . The latter was chosen because is characterised by sharper resonance lines and higher natural abundance (99.9%).  $^{139}\text{La}$  ( $I=7/2$ ) yields broad signals because of the efficient quadrupolar relaxation mechanism. Its signal become even broader when La is found in complexes (because reduced molecular tumbling) or in asymmetric environments.

Two different experiments were performed to verify the formation of MPOSS-La complexes in equilibrium with the free ligand (**Figure 5.4**). The  $^{139}\text{La}$ -NMR spectra reported in **Figure 5.4a** show the NMR spectrum of the La triflate. Its signal (labelled with black square) is observed at -30 ppm (with respect to  $\text{LaCl}_3$  in water at 0 ppm) and is characterised by a linewidth at half height (LW) of 2.3 kHz. Upon addition of M-POSS was observed a significant decrease of its integrated area and, at the end of the titration experiment, the presence of a new, broad signal (LW = 6.7 kHz), at around 90 ppm (labelled with black star) which is assigned to the bound  $\text{La}^{+3}$  in slow exchange on the chemical shift time scale.

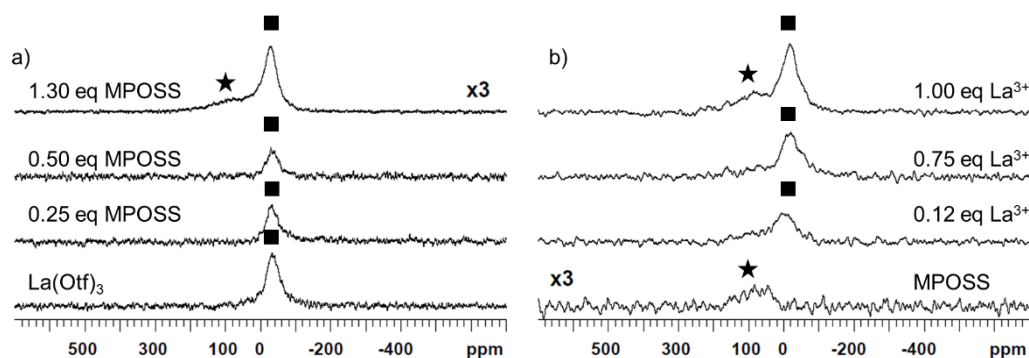


**Figure 5.4.** a)  $^{139}\text{La}$ -NMR titration of  $\text{La}(\text{OTf})_3$  in  $\text{CDCl}_3:\text{MeOD}$  3:1 with M-POSS and b)  $^{139}\text{La}$ -NMR titration of M-POSS in  $\text{CDCl}_3:\text{MeOD}$  3:1 with  $\text{La}(\text{OTf})_3$ . In Figure stars point out complexed metal while squares free metal.

This result is in agreement with data reported in the literature.<sup>3</sup> Indeed, both the LW and the chemical shift are generally increased when the water molecules in the first coordination shell are replaced by nitrogen or oxygen donor sites.

A counter-experiment was performed starting from M-POSS and adding  $\text{La}(\text{OTf})_3$ . Upon addition of a small amount of  $\text{La}^{3+}$ , the appearance of a signal at 90 ppm (labelled with black star) was observed, confirming the formation of MPOSS-La complexes and the assignment of the resonance line. Immediately after a second addition of metal, a second signal (labelled with black square) at -30 ppm appears, confirming the equilibrium between the free metal and the complexed one.

The formation of M-POSS- $\text{La}^{3+}$  complexes was studied by  $^1\text{H-NMR}$ , by adding  $\text{La}(\text{OTf})_3$  to a solution of M-POSS (**Figure 5.5**). Upon addition of only 0.12 eq. of  $\text{La}^{3+}$  a new series of signals was observed (black stars in **Figure 5.5**). After the addition of 0.5 eq of  $\text{La}^{3+}$ , a series of signal was observed (stars in **figure 5.5**). The intensity of all these resonance lines increase at increasing amounts of  $\text{La}^{3+}$ . All these new signals remain in their positions till the end of the titration confirming the results obtained following the  $^{139}\text{La}$ . Hence, the formation of M-POSS-La complexes in equilibrium with the free ligand.

These findings have been confirmed by means of a counter titration carried out by adding M-POSS to a  $\text{La}(\text{OTf})_3$  solution.

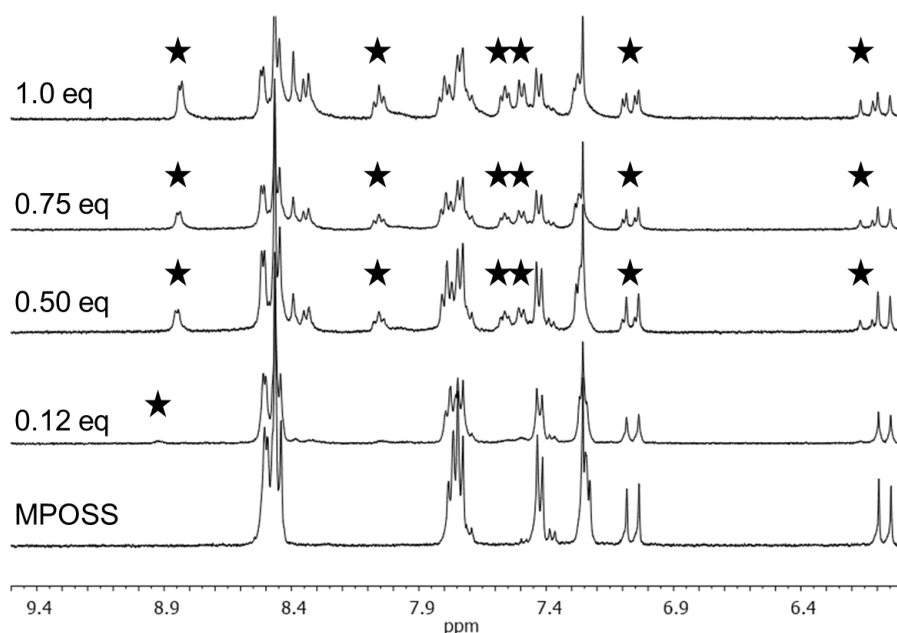


**Figure 5.5.**  $^1\text{H-NMR}$  titration of M-POSS solution in  $\text{CDCl}_3:\text{MeOD}$  3:1 with  $\text{La}(\text{OTf})_3$  In Figure stars point out signals related to the complex.

The NMR data confirm that methanol can act as co-ligand competing with water molecules to complete the coordination shell of the metal centre. Otherwise, when CH<sub>3</sub>CN was present in the mixture the coordination shell was completed by the residual water molecules.

This represent a good indication that water molecules can be replaced if another co-ligand is present in the mixture. The next step was hence the use of active ligands able to replace water (and methanol) in the metal coordination shell and at the same time enhancing the emission of the final complex.

## 5.2 Replacing water molecules

The first attempt to replace water molecules from the coordination sphere of Eu(III) in the Eu@POSS complexes has been carried out on the Eu@2M-POSS by adding ODA molecules (**Figure 5.6**).

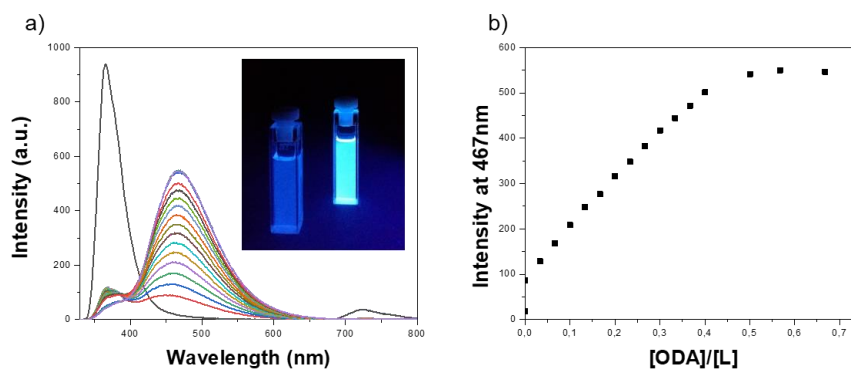


**Figure 5.6.** (a) Emission spectra of Eu@2M-POSS in  $\text{CH}_2\text{Cl}_2$  ( $1.3 \times 10^{-5}$  M) upon titration with ODA in MeOH ( $1.3 \times 10^{-3}$  M) (b) Emission intensity at 422 nm versus ligand concentration (intensity vs  $[\text{ODA}]/[\text{M-POSS}]$ ). ( $\lambda_{\text{ex}} = 335\text{nm}$  slits = 2.5-5nm bandpass filter 360 – 1100 nm).

The emission band of M-POSS (black line) centred at 368 nm was almost completely quenched after the addition of 0.5 eq. of metal (**Figure 5.6a**). Consequently, a new emission band centred at 422 nm (red line) appeared. This weak emission is attributed to the formation of the Eu@2M-POSS complex. Interestingly, upon addition of increasing amount of ODA a significant (above 5-fold) increase of the emission intensity was observed. This change in intensity is also clear to the naked eye. Eu@2M-POSS-ODA displays higher emission intensity as shown in the inset (**Figure 5.6a**). Analogous experiments were performed adding terpyridine as co-ligand (**Figure 5.7**). The first step was the formation of the Eu@2M-POSS complex. Then a Tpy solution in DCM was added until 0.5 equivalents of co-ligand were reached.

In this second experiment the trend was similar of the first one. It is possible observe the initial quenching of the emission band of the M-POSS, centred at 366 nm, due to the complexation with  $\text{Eu}^{3+}$  ions followed by the formation of a new band at 439 nm attributed to the ligand-centred transitions.

After addition of Tpy the band centred at 429 nm start to increase, reaching a maximum after 0.4 eq (see the inset in **Figure 5.7a**), and then start to decrease. Hence, a new band start to grow at 369 nm due to the formation of the complex Eu@Tpy.

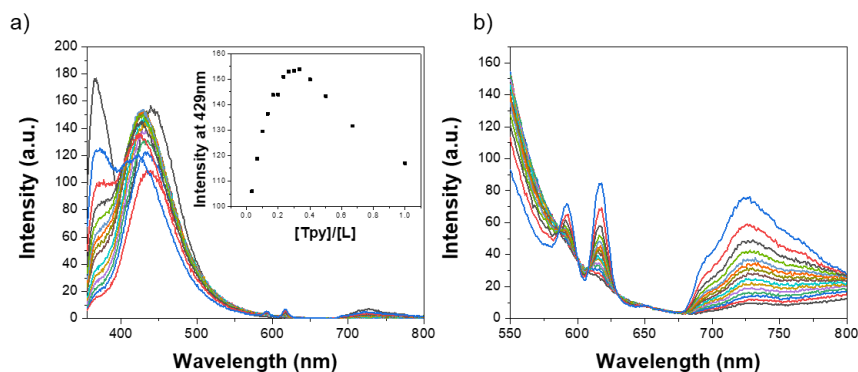


**Figure 5.7** (a) Emission spectra of Eu@2M-POSS solution titrated with Tpy solution. ( $\lambda_{\text{ex}} = 335\text{nm}$ ; slits = 2.5-5nm; bandpass filter 360 – 1100 nm). (b) Magnification of the region between 550nm and 800 nm showing the typical line like bands of the Europium. ( $\lambda_{\text{ex}} = 335\text{nm}$ ; slits = 5-10nm; bandpass filter 360 – 1100 nm).

It is noteworthy that, with the help of the Tpy as co-ligand (which most probably replace the water molecules from the metal coordination shell), the energy transfer to the metal centre was more effective and the typical line-like band of the europium appears in the region between 580 and 698 nm (assigned to the  $^5D_0 \rightarrow ^7F_J$  transitions).

To be sure that both M-POSS and co-ligand (ODA or Tpy) complex together the metal and that no competitive coordination take place (e.g. ODA or Tpy molecules replacing the main POSS-based ligands),  $^1\text{H-NMR}$  experiments were performed as well.

Since ODA is often used in the deprotonated form, while in our case it was employed at protonated ligand, preliminary experiments were performed to verify that ODA (in its protonated form) can complexes  $\text{Eu}^{3+}$  ions.

The titration experiments were performed adding increasing amounts of  $\text{Eu}(\text{OTf})_3$  to a solution of ODA in deuterated methanol. Immediately after the first addition of metal to the ODA solution (**Figure 5.8**), the signal of the ODA (labelled with black square) disappears, and the growth of three signals (black circles) due to the formation of Eu@ODA complexes was visible.



Upon addition of increasing amount of  $\text{Eu}(\text{OTf})_3$  a progressive shift of these signals was also observed indicating that ODA is complexing the metal.

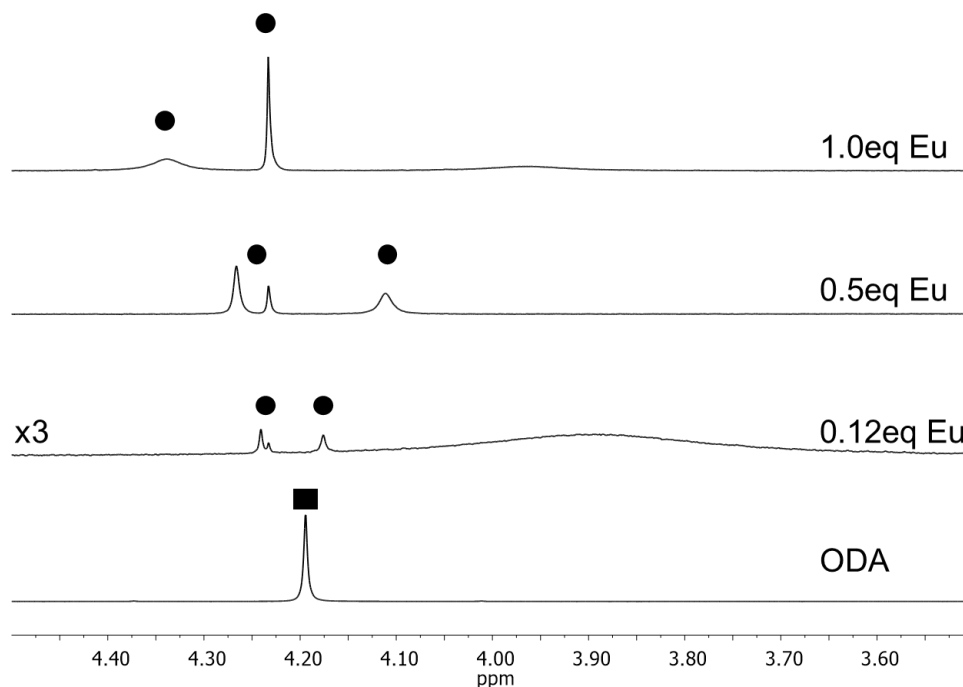


**Figure 5.8.**  $^1\text{H}$ -NMR titration of ODA solution in MeOD with  $\text{Eu}(\text{OTf})_3$ .

Then, a series of titration experiments was performed by mixing together M-POSS and ODA in order to verify that the simultaneous complexation of the metal occurs. In particular, for this investigation three different ratios between the M-POSS and the ODA (2:1, 1:1, 1:2 M-POSS:ODA) were selected. The titration performed using a solution of M-POSS:ODA in 1:1 ration is reported in **Figure 5.9**. As can be clearly seen in the figure a shift of the typical signals corresponding to the M-POSS based ligand (mainly in the aromatic region) together with a relevant modification of the pattern corresponding to the ODA is present.

It is possible to see that the signal of the ODA (black square) decreases until disappearance and at the same time, signals related to the M-POSS (black circles) shift in a new position. This experiment proves that both silsesquioxane-based ligand and ODA co-ligand are playing an active role in the complexation of europium and, more importantly, ODA is not competing with the M-POSS replacing it from the metal coordination shell. In **Figure 5.10** the shift of the vinyl proton in function of the equivalent of metal added is reported, confirming that the stoichiometry of the final complex is  $\text{Eu}@2\text{M-POSS-ODA}$ .

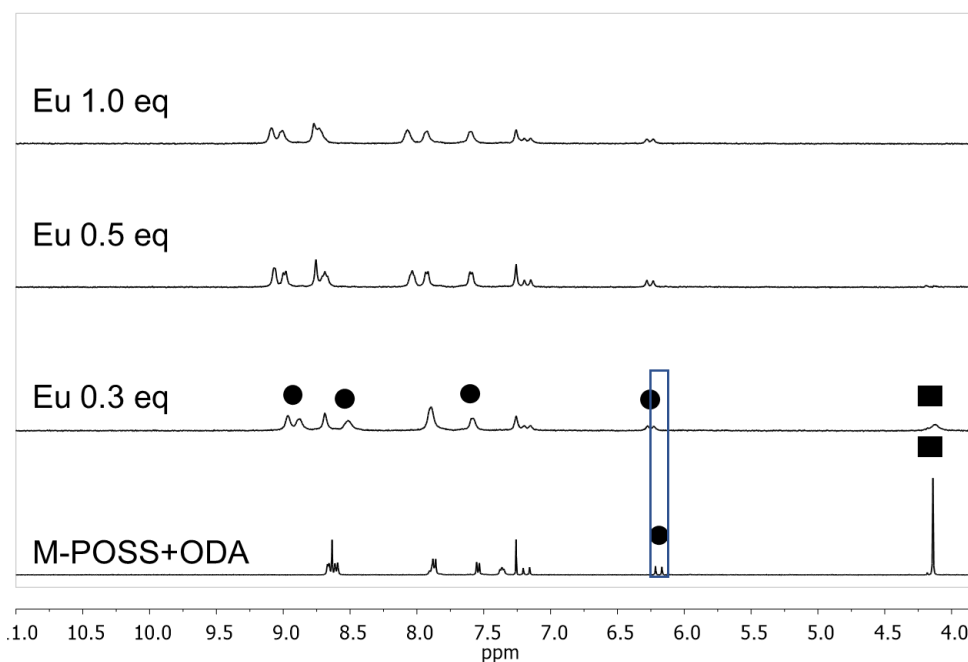


**Figure 5.9.**  $^1\text{H-NMR}$  titration of M-POSS:ODA 1:1 solution in  $\text{CDCl}_3\text{:MeOD}$  3:1 with  $\text{Eu}(\text{OTf})_3$ .

From **Figure 5.10a** emerged that if the modification of the chemical shifts (of some selected signals) is plotted in function of the Europium/total ligand ratio (M/L where L indicates the concentration of M-POSS ligand + ODA co-ligand) a plateau is reached in correspondence of a M/L value of c.a. 0.3 indicating that the complex is formed by 3 ligands per each metal centre.

On **Figure 5.10b** is represented a similar plot in function of a Europium/POSS-based ligand (M/L-POSS) ratio. In the last case a plateau is reached in correspondence of M/L-POSS ratio of c.a. 0.5 indicating that 2 M-POSS based ligand are present per each metal centre. This investigation suggests the presence of a complex in which 2 silsesquioxane-based ligands are coordinating the metal centre while the coordination shell of europium is completed by one molecule of ODA, hence supporting the hypothesis of the formation of a  $\text{Eu@2-M-POSS-1-ODA}$ .

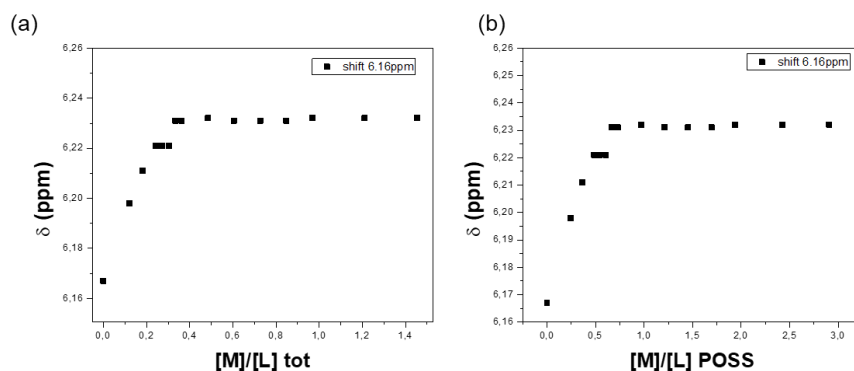


**Figure 5.10.** Plot of the shift of the signal at 6.16 ppm in function of the equivalents of Europium added in relation of the total amount of ligand (a) and in function of the equivalents of Europium added in relation of the M-POSS (b).

Analogous experiments were conducted on Tpy, firstly monitoring the evolution of the Tpy signals in complexing the metal in  $^1\text{H-NMR}$  titration. After adding 0.3 equivalents of europium, two new signals appears in the region between 5.5 ppm and 7.0 ppm (black circles in **Figure 5.11**). Suggesting the formation of the  $\text{Eu@2Tpy}$  complex. Once 0.5 equivalents of  $\text{Eu}^{3+}$  were added, a new set of signals at 9.5 ppm, 6.8 ppm and 5.1 ppm start to grow (black stars) suggesting now the formation of  $\text{Eu@Tpy}$  complex. Also in this case, the different species that are formed in solution are in equilibrium. This behaviour is particularly evident in the last spectrum in which in presence of 1 equivalent of metal an equilibrium between three different species is present in solution.

Hence, in agreement with the previous observation in the case of the M-POSS, at the end of the titration three different species are in equilibrium: free Tpy,  $\text{Eu@2Tpy}$  and  $\text{Eu@Tpy}$ .

As for the M-POSS:ODA system, in order to verify the simultaneous complexation of the metal by the two ligands, a series of titrations were performed by mixing together M-POSS and Tpy.

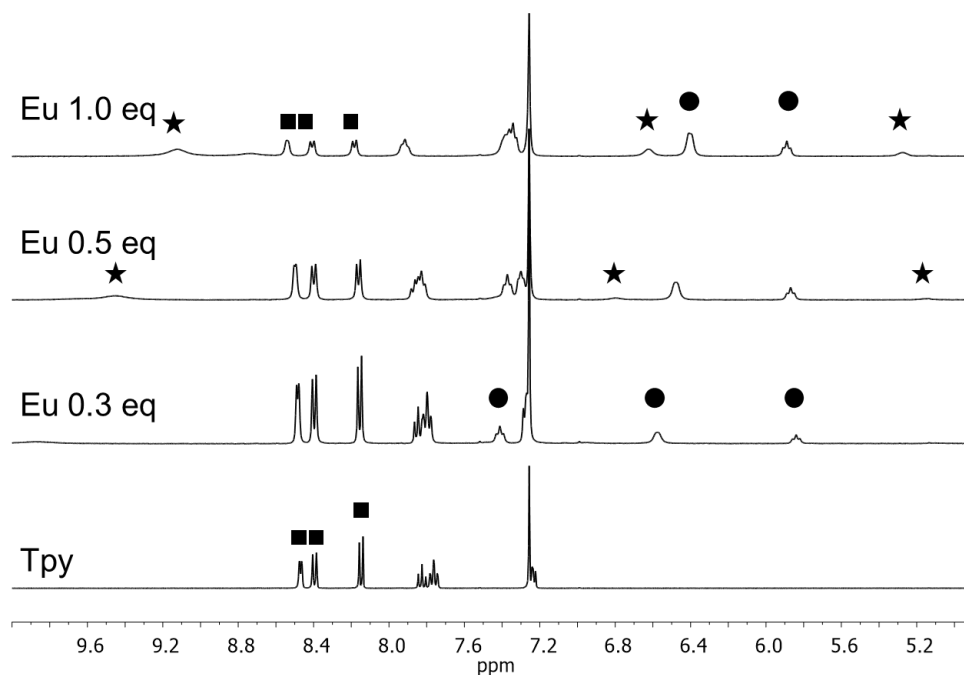


**Figure 5.11.**  $^1\text{H-NMR}$  titration of Tpy solution in  $\text{CDCl}_3:\text{MeOD}$  3:1 with  $\text{Eu}(\text{OTf})_3$ .

In particular, three different ratios between the M-POSS and Tpy were chosen: 2:1, 1:1, 1:2. In **Figure 5.12** the titration performed with a 1:1 M-POSS:Tpy ratio is reported. In this case, however, the signals of the phenyl-terpyridine in M-POSS as well as the protons of the free-terpyridine, are overlapped in the aromatic region of the spectrum making difficult both the discrimination of each single contribution and the evolution of the complexes in solution. Focusing the attention to the region between 5.2 ppm and 7.0 ppm, can be argued that both ligands take part to the complexation since it is possible to recognize the typical of pattern (black stars) corresponding to the formation of europium complexes with M-POSS or with the Tpy (see **Figure 5.12**).

Similar  $^1\text{H-NMR}$  experiments in presence of O-POSS were not performed, due to the fact that signals in O-POSS are very broad and it is not possible to diversify and assign the different contributions to each species. Hence, emission investigations aimed to verify the possibility to improve the emission properties in the  $\text{Eu}@\text{O-POSS}$  complexes were performed.

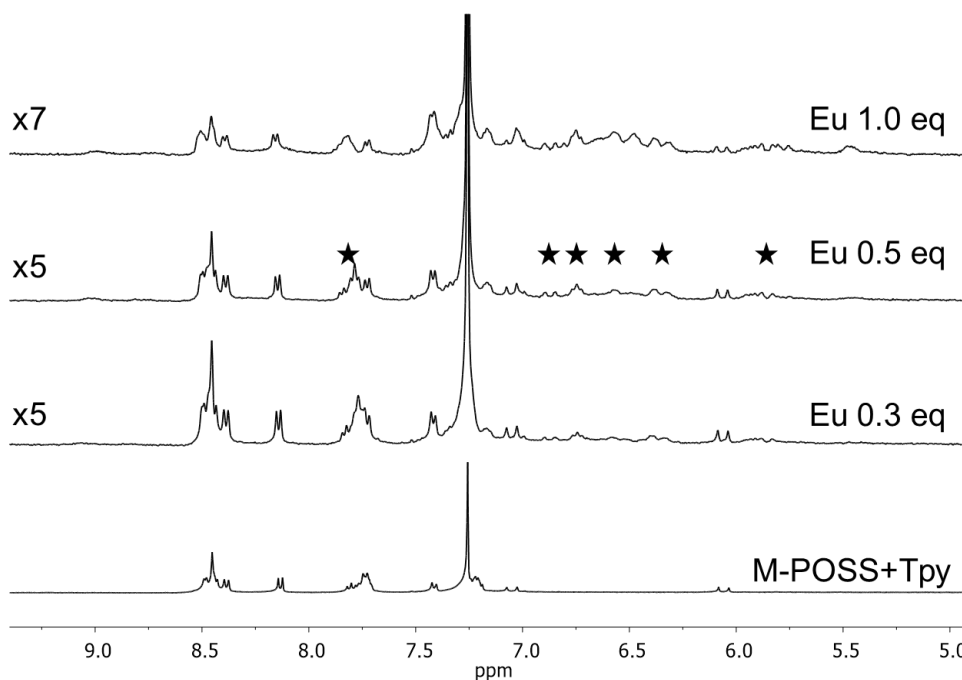


**Figure 5.12.**  $^1\text{H-NMR}$  titration of M-POSS:Tpy 1:1 solution in  $\text{CDCl}_3$ :MeOD 3:1 with  $\text{Eu}(\text{OTf})_3$ .

### 5.3 “Rainbow” full emission spectrum

As seen in section 4.1 emission titration experiments revealed that the emission band of O-POSS (black line) centred at 410 nm is completely quenched after adding 0.5 eq. of metal as consequence of the complexation with the Europium (**Figure 4.15a**). Furthermore, the energy transfer from the terpyridine to the metal, allow transition in the f-f shell of the metal and the typical line like band of the Europium resulted clearly visible (**Figure 4.15a** inset).

Interestingly, after addition of ODA as co-ligand, an increase of the europium emission (at 590 nm and 620 nm) as well as an increase of the emission band at 490 nm corresponding to the ligand centred emission band were observed (**Figure 5.13**). As we can see in the inset (**Figure 5.13b**), different emission properties were observed for Eu@2-POSS complexes in the absence (right) or in presence of ODA as a co-ligand (left).

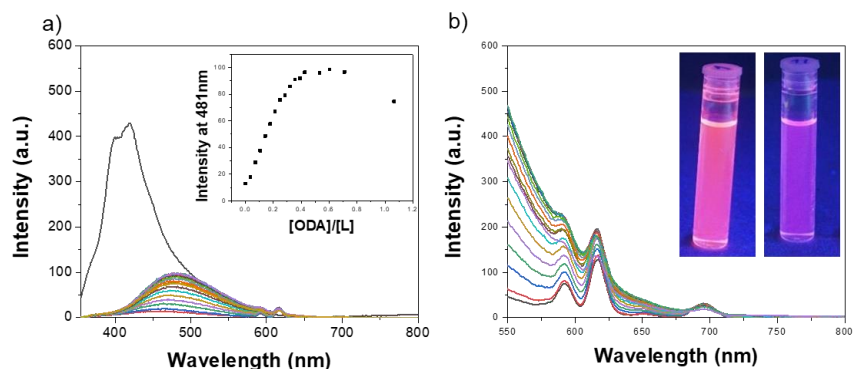


**Figure 5.13.** (a) Emission spectra of Eu@2O-POSS solution titrated with ODA solution ( $\lambda_{\text{ex}} = 335\text{nm}$ ; slits = 5-5nm; bandpass filter 360 – 1100 nm); in the inset plot of the intensity at 481 nm vs equivalent of ODA added. (b) Magnification of the region between 550 nm and 800 nm showing the typical line like bands emission of the europium ( $\lambda_{\text{ex}} = 335\text{ nm}$ ; slits = 10-10 nm; bandpass filter 360 – 1100 nm).

Emission titration experiments were performed for the Eu@O-POSS in the presence of Tpy as a co-ligand. (**Figure 5.14**).

The intensity of the line like band of the europium, in the region between 580 and 698 nm (assigned to the  $^5\text{D}_0 \rightarrow ^7\text{F}_j$  transitions) increases and a shift of the metal ligand band is observed (**Figure 5.14b**).

It is observed a red-shift in the presence of ODA and a blue-shift in the presence of Tpy. The shift on the band indicates that the co-ligand added (in our case ODA or Tpy) is also coordinating the metal centre. However, this coordination may result in a different symmetry.

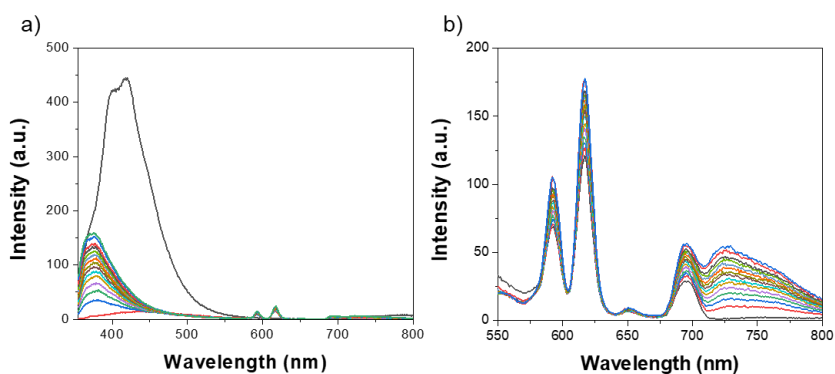


**Figure 5.14.** (a) Emission spectra of Eu@2O-POSS solution titrated with Tpy solution ( $\lambda_{\text{ex}} = 335\text{nm}$ ; slits = 5-5nm; bandpass filter 360 – 1100 nm). (b) Magnification of the region between 550 nm and 800 nm showing the typical line like bands of the europium ( $\lambda_{\text{ex}} = 335\text{nm}$ ; slits = 10-10nm bandpass filter 360 – 1100 nm).

In the previous chapter the tuning of the emission properties of the Eu@O-POSS complexes was achieved via *cis-trans* isomerization of the double bond (blue-green emission).

In the present investigation the role played by the use of co-ligands as ODA (purple emission) or Tpy was also proved. In order to challenge even more our system an additional investigation was performed. The objective was to achieve a fine modulation of the emission properties of the Eu/O-POSS systems combining the different possibilities (*cis-trans* isomerization and use of co-ligands) with the use of other metal centres. On this topic, it was recently published an article in which the Europium is combined with terbium to obtain compounds with different emitting properties.<sup>4</sup> For this reason the Terbium was selected as target metal for our investigation. Moreover, it possesses characteristic bands at 490 nm, 544 nm, 585 nm and 622 nm that fall in the region of interest.

So we prepared different complexes with different ratio of metals (Eu:Tb 2:1 and Eu:Tb 1:1. the

In the case of  $\text{Eu}_{0.66}\text{Tb}_{0.33}\text{@O-POSS}$  solution (ratio Eu/Tb = 2) was observed a combination of the typical emission bands of the Terbium (544nm, 585nm) and the Europium, see **Figure 5.15a**. With this complex an orange emission was observed. Other O-POSS complexes were prepared with another metal ratio.

Particular relevant was the  $\text{Eu}_{0.5}\text{Tb}_{0.5}\text{@O-POSS-Tpy}$  (ratio Eu/Tb = 1 in the presence of Tpy as co-ligand). The last complex allows obtaining a yellow emission.

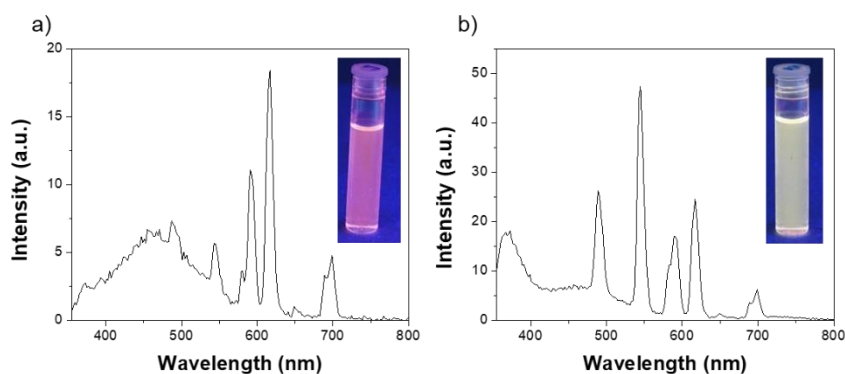


**Figure 5.15.** (a) Emission spectra of  $\text{Eu}_{0.66}\text{Tb}_{0.33}\text{@O-POSS}$ .(b) Emission spectra of  $\text{Eu}_{0.5}\text{Tb}_{0.5}\text{@O-POSS-Tpy}$ . ( $\lambda_{\text{ex}} = 335$  nm; slits = 10-10 nm; bandpass filter 360 – 1100 nm).

Finally, combining the last experiments with the possibility of the *trans/cis* isomerisation of the C-C double bond, a series of “emitting” complexes displaying different colours was obtained. **Figure 5.16** shows the picture of the metal complexes based on O-POSS in solution, 1 = *trans*-O-POSS, 2 = *cis*-O-POSS, 3 = Eu<sub>0.5</sub>Tb<sub>0.5</sub>@O-POSS-Tpy, 4 = Eu@2O-POSS-ODA, 5 = Eu<sub>0.66</sub>Tb<sub>0.33</sub>@O-POSS, 6 = Eu@O-POSS under UV light. The emission colours cover the region from red to blue simulating a rainbow effect.

It is worth highlighting the versatility of the O-POSS complexes. With the proposed systems a controlled and tuneable emission can be obtained only via slightly chemical modification of the metal environment not requiring an *ex-novo* synthesis pathway of the ligands.

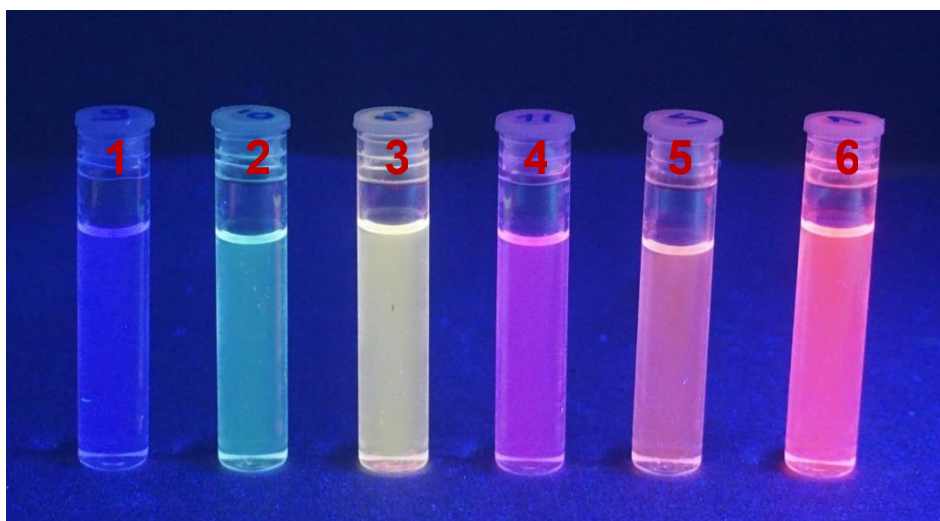


**Figure 5.16.** Complete pattern of colour obtained with O-POSS with Eu, Tb and ODA or Tpy as co-ligands.

## 5.4 Conclusions

Innovative building blocks based on POSS, complexed with Eu(III) cations proved to be excellent photoemissive 3D materials.

The terpyridine-silsesquioxane based Eu complexes showed switchable and reversible “blue-red-green”.

In the first series of complexes the coordination shell of the metal was completed by some molecules of water. The presence of water had no strong detrimental effect on the emission of the material, however still results in a decrease in fluorescence emission hence, in the second part of the work the light-emitting properties of the



selected systems were further enhanced replacing the molecules of water with selected ligands. The use of ODA and terpyridine helped to replace water molecule from the coordination sphere of the metal during the complexation improving the emission of both Eu@M-POSS and Eu@O-POSS complexes. Moreover, fine tuning of these two co-ligands, together with the use of terbium ions, led to the development of a series of luminescent materials with interesting emission properties and able to cover the complete visible spectrum of colours, from the blue to the red passing by the green, the yellow, the purple and the orange. What makes the last part of the work extremely promising is the fact that the entire range of colours was obtained only employing a single material, two metals and two co-ligands and that no ex-novo synthesis was needed.

## 5.5 Experimental Section

**Materials and method:** Monovinyl-isobutyl substituted POSS (MV), octavinyl POSS (OV), DMF anhydrous, Et<sub>3</sub>N (99.5%), Eu(III) and Tb(III) triflate (99.999%) were purchased from Sigma Aldrich. 4'-(4-Bromophenyl)-2,2':6',2''-terpyridine, Palladium acetate, tris(2-methylphenyl)phosphine were purchased from TCI chemicals. Acetonitrile (CH<sub>3</sub>CN) and dichloromethane (DCM) used for the spectrofluorometric measurements were of spectroscopic grade and these were purchased from Carl Roth. Quantitative <sup>1</sup>H-NMR experiments were performed at 25 °C on a Varian VNMRS spectrometer. UV-visible measurements were performed on Cary 5000 Spectrophotometer (Varian) and fluorescence measurements were performed on Cary Eclipse (Agilent technologies). The measurements were carried out using 10 mm suprasil quartz cuvettes from Hellma Analytics. Irradiation test were performed with an ASASHI SPECTRA Xenon Light Source 300W MAX-303.

**Synthesis of M-POSS:** To an oven-dried, double neck 50 mL flask under flowing N<sub>2</sub>, 400 mg of MV (0.42 mmol), 10.8 mg of palladium acetate, 29.2 mg of tris(2-methylphenyl)phosphine (0.096 mmol), 280 mg of 4'-(4-bromophenyl)-2, 2':6', 2''-terpyridine (0.72 mmol), 14 mL of anhydrous DMF and 4 mL of Et<sub>3</sub>N were added. The reaction mixture was heated at 100 °C for 3 days under N<sub>2</sub> atmosphere. After that, the mixture was cooled at room temperature and filtered to remove the palladium metal. The filtrate was cooled down precipitating the M-POSS.

M-POSS, white powder. **Yield: 80 %.** <sup>1</sup>H-NMR (400 MHz, CDCl<sub>3</sub>) δ (ppm) = 0.69-0.62 (m, 14H), 0.95-1.00 (m, 42H), 1.81-1.95 (m, 7H), 6.27-6.22 (d, 1H), 7.27-7.22 (d, 1H), 7.37-7.34 (t, 2H), 7.59-7.57 (d, 1H), 7.92-7.86 (m, 4H), 8.69-8.67 (d, 2H), 8.74-8.73 (d, 2H), 8.75 (s, 2H). <sup>13</sup>C-NMR (100 MHz, CDCl<sub>3</sub>) δ (ppm) = 22.60, 23.96, 25.82, 118.77, 119.81, 121.47, 123.96, 127.43, 127.61, 136.99, 138.39, 138.65, 147.38, 149.24, 149.77, 156.06, 156.30. MAS <sup>29</sup>Si-NMR (99.3 MHz) δ (ppm) = -68.27, -80.17. Elemental analysis (%) for C<sub>51</sub>H<sub>79</sub>N<sub>3</sub>O<sub>12</sub>Si<sub>8</sub>; calculated: C = 53.23, H = 6.92, N = 3.65; found: C = 52.45, H = 6.79, N = 3.22.

**Synthesis of O-POSS:** To an oven-dried, double neck 50 mL flask under flowing N<sub>2</sub>, 135 mg of OV (0.21 mmol), 20.8 mg of palladium acetate (0.09 mmol), 58 mg of tris(2-methylphenyl)phosphine (0.018 mmol), 1 g of 4'-(4-bromophenyl)-2, 2':6', 2''-terpyridine (2.57 mmol), 14 mL of anhydrous DMF and 4 mL of Et<sub>3</sub>N were added. The reaction mixture was heated at 100 °C for 7 days under N<sub>2</sub> atmosphere. After that, the mixture was cooled and filtered to remove the Pd<sup>0</sup> and then precipitated in 50 mL of deionized water. The precipitate was, for first, washed with water (2 x 25 ml) sonicating in a bath and centrifuging 10 minutes at 4500 rpm. The same procedure was repeated washing the solid with acetonitrile (5 x 25 ml), then with methanol (5 x 25 ml) and finally with acetone (2 x 25mL). O-POSS was obtained as a pale brown powder. Yield: 68 %. MAS <sup>29</sup>Si-NMR (99.3 MHz) δ (ppm) = -80.29. Elemental analysis (%) for C<sub>51</sub>H<sub>79</sub>N<sub>3</sub>O<sub>12</sub>Si<sub>8</sub>; calculated: C = 71.48, H = 4.17, N = 10.87; found: C = 67.04, H = 3.99, N = 9.78.

**Synthesis of Eu@2O-POSS:** In a single-neck 50 mL flask 50 mg of O-POSS (0.016 mmol), 39 mg of Eu (III) triflate (0.065 mmol) and 20 mL of a mixture of DCM and CH<sub>3</sub>CN (65%:35%) were added. The mixture was cooled at 50°C for 24h. After this time, the volume of the mixture was reduced by evaporation under reduced pressure and a pale yellow precipitate was collected under vacuum. The solid was washed on the filter with DCM and CH<sub>3</sub>CN and dried under vacuum.

**Irradiation procedure:** Irradiation tests for <sup>1</sup>H-NMR were performed in “5 mm Thin Wall Natural Quartz NMR Sample Tubes” from NORELL. Absorption and emission experiments were performed in 10 mm suprasil quartz cuvettes from Hellma Analytics. All the irradiation tests were carried out by placing the samples at a distance of 21 cm from the UV source.

## 5.6 References

1. (a) Gangan, T. V. U.; Sreenadh, S.; Reddy, M. L. P., Visible-light excitable highly luminescent molecular plastic materials derived from Eu<sup>3+</sup>-biphenyl based  $\beta$ -diketonate ternary complex and poly(methylmethacrylate). *J. Photochem. Photobiol.* **2016**, *328*, 171-181; (b) Maynard, B. A.; Smith, P. A.; Ladner, L.; Jaleel, A.; Beedoe, N.; Crawford, C.; Assefa, Z.; Sykora, R. E., Emission enhancement through dual donor sensitization: modulation of structural and spectroscopic properties in a series of europium tetracyanoplatinates. *Inorg. Chem.* **2009**, *48* (14), 6425-6435; (c) Foster, D. R.; Richardson, F., Magnetic circularly polarized luminescence of 9-coordinate europium (III) complexes in aqueous solution. *Inorg. Chem.* **1983**, *22* (26), 3996-4002.
2. Dobretsov, G. E.; Syrejschikova, T. I.; Smolina, N. V., On mechanisms of fluorescence quenching by water. *Biophysics* **2014**, *59* (2), 183-188.
3. Peters, J.; Huskens, J.; Raber, D., Lanthanide induced shifts and relaxation rate enhancements. *Progress in Nuclear Magnetic Resonance Spectroscopy* **1996**, *28* (3-4), 283-350.
4. Zhou, Y.; Zhang, H.-Y.; Zhang, Z.-Y.; Liu, Y., Tunable Luminescent Lanthanide Supramolecular Assembly Based on Photoreaction of Anthracene. *J. Am. Chem. Soc.* **2017**, *139* (21), 7168-7171.

***Chapter 6***  
***General conclusions***

## 6 General conclusions

The aim of the present Thesis was exploring the properties of carbon and silica nanoform derivatives.

In particular C<sub>60</sub> fullerene and polyhedral oligomeric silsesquioxane (POSS) were chosen, as representative of each class, for their peculiar geometry. They were thought as suitable starting materials for the synthesis of innovative molecular building blocks to be employed, once complexed with metals, in the creation of auto assembled three dimensional structures to be applied in the fields of catalysis and as photoluminescence materials.

About the C<sub>60</sub>, even if already combined with BOX ligands, it has never been employed as possible asymmetric catalyst. Herein, fullerene was successfully functionalised with different chiral BOXs obtaining 12 catalytic systems to test as possible chiral inducer in the asymmetric Henry and Diels-Alder reactions. The idea was to prepare different materials with different solubility profiles in order to evaluate different aspects in the reaction conditions as well as the possibility of recycling and reusing a homogeneous catalyst, which normally is not reusable. In fact, even if BOXs were widely used in asymmetric catalysis, never were recycled and reused due to their low stability and ease of degradation. Tests performed with all the materials showed that, once anchored on the fullerene, BOXs gain robustness and stability, allowing recovery and reuse without loss in terms of activity.

C<sub>60</sub> adducts, and in particular the hexakis adducts with their tetrahedral symmetry, seemed to be suitable for the construction of 3D photoluminescence material. To this purpose C<sub>60</sub>-BOXs were then tested, once complexed with Europium and Terbium ions, as possible emissive materials. Unfortunately, due to the fullerene peculiar photophysical properties along with the weak ability of the BOXs to transfer the harvested light energy, these systems have been dismissed as possible emitting materials.

On the other hand, maintaining the goal of building 3D photoluminescence auto assembled materials, the POSS showed really interesting results. The POSS with its really high thermal and mechanical stability and with its peculiar inert nature, together with the terpyridine, that showed good ability in the so called antenna

effect, proved to be ideal nanobuilding block for the construction of unprecedented 3D emissive organic-inorganic hybrid materials.

In particular, POSS-terpyridine alkenyl bridged showed exceptional tuneable blue-red-green emission in presence of Europium ions. In fact, under irradiation, *trans*-OPOSS shows blue light emission, once complexed with the Europium, Eu@OPOSS, shows bright red luminescence and *cis*-OPOSS emits green light. Furthermore, once the materials are dissolved in the right medium, they can be shaped as film resulting in thin luminescent materials.

Moreover, from an in depth study of the these metal@POSS materials merged out that, since the luminescence is affected by the presence of water molecules in the coordination shell of the metal, under the right conditions it is possible to play with proper co-ligands to remove and replace these water molecules obtaining different materials able to emit in different way under UV irradiation.

In fact, OPOSS, complexed with Eu or Tb or a mix of both and in presence of ODA or Tpy as co-ligand, is able to provide fascinating luminescent solutions that cover the complete visible spectrum of colours, from the blue to the red.

What emerged from the study of these nanoforms is fascinating and inspiring. On one hand, certainly, with regard to the chemistry of fullerene, this study allows for a possible transfer of knowledge, acquired on the C<sub>60</sub>, to other carbon nanoforms. Regarding the POSS, on the other hand, new steps were already done towards the preparation of novel 3D materials. In fact, even if the POSS-terpyridine materials showed really fascinating results, an attempt to improve the results can be done trying to synthesise more ordered MOF-like materials in order to obtain crystalline emitting devices.

This can be achieved by changing the bridge between the POSS hallow cage and the organic terpyridine moieties. The idea is to change the non-directional alkenyl group with a more rigid spacer able to direct in the right way the organic part toward the formation of more rigid and stable structure.

***Chapter 7***  
***Outlooks***



## 7 Outlooks

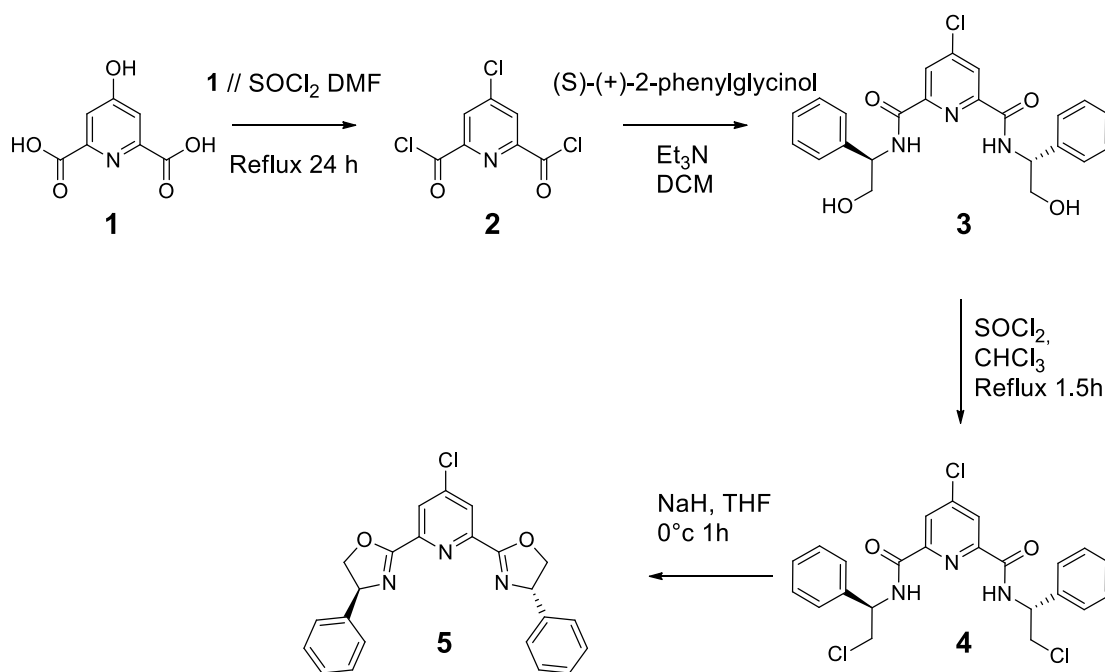
Unprecedented novel 3D nanobuilding blocks have been synthesized with carbon and silica nanoforms. In particular, C<sub>60</sub> and POSS derivatives properly functionalized to form innovative materials with well established geometries (octahedral and cubic respectively), have been successfully achieved. Each type of structures found application in different fields. The fullerene-adducts in the field of catalysis and the terpyridine-POSS in the field of emitting materials. Even if the results are promising and exciting, there is always room for improving the performances.

### 7.1 C<sub>60</sub>-PyBOX asymmetric catalysts

The catalytic systems based on the C<sub>60</sub>-BOX showed good applicability in the asymmetric Henry and Diels-Alder reactions and, as additional value, showed easy recoverability and reusability. Although in terms of conversions and enantiomeric excess they showed good results, if compared with the parent unsupported catalysts, these are too far from the acceptable values for big scale processes. Since C<sub>60</sub> adducts showed good robustness, a natural consequence could be to change the type of bisoxazoline using those displaying better performances in asymmetric catalysis. As already mentioned, bisoxazoline can differ each other, apart from the substituent on the oxazoline moiety, in the bridge that connect the two rings. In this work were used boxes with methylene bridge, but an interesting improvement can be done by using pyridine bridged bisoxazoline (PyBOX). PyBOX were the first type bisoxazoline used in catalysis in 1989<sup>1</sup> and since then they were extensively used as catalysts in different asymmetric processes<sup>2</sup> such as additions to C=O and C=N double bonds,<sup>3</sup> three-membered ring formation from C=C and C=X double bonds,<sup>4</sup> allylic oxidations,<sup>5</sup> Diels-Alder<sup>6</sup> and hetero-Diels-Alder,<sup>7</sup> 1,3-dipolar cycloadditions,<sup>8</sup> and polymerisation and oligomerisation of alkenes and alkynes.<sup>9</sup>

With the aim to improve efficiency and selectivity of asymmetric reactions the idea is to change the catalyst and the first step towards the realization of a new catalytic system based on C<sub>60</sub> is the synthesis of the new bisoxazolines. Although the ideas in this chapter are presented as “possible outlooks”, several synthetic pathways were already examined and a first PyBOX has been already obtained. The challenge here is to design PyBOX

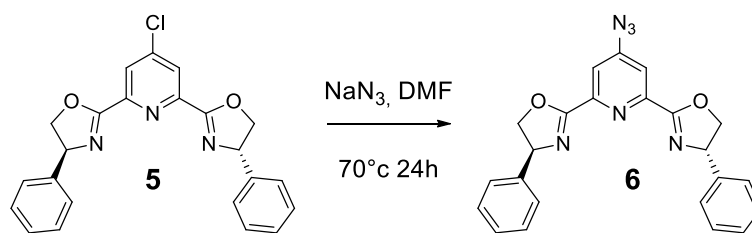
properly functionalized in order to react with fullerene. The solution to these problems comes from an in-depth literature research: in fact, for comparison of different reported synthetic procedures was possible to tune a route towards the achievement of the desired PyBOX properly functionalized with right substituent that allow anchoring on fullerene cage. Below it is reported the synthesis of a Phenyl-PyBOX already obtained and ready for the functionalization on the C<sub>60</sub> (**Scheme 7.1**).



**Scheme 7.1.** Synthetic pathway for the Ph-PyBOX achievement.

Even if the synthesis is reported in literature was not trivial obtain the product **5**. In fact, it was not possible follow only one procedure, but was necessary acting like in the construction of a puzzle picking up by different reported procedures.<sup>10</sup>

Once obtained the phenyl derivative **5**, it is necessary a suitable group to the functionalization on the C<sub>60</sub>. One appropriate can be the azide.



**Scheme 7.2.** Azide derivative of Ph-PyBOX synthesis.

The desired product was obtained by substitution of the chlorinated moiety, and finally, the right PyBOX is ready for the functionalization on the fullerene to obtain novel supported asymmetric catalysts C<sub>60</sub>-based.

## 7.2 POSS terpyridine evolution

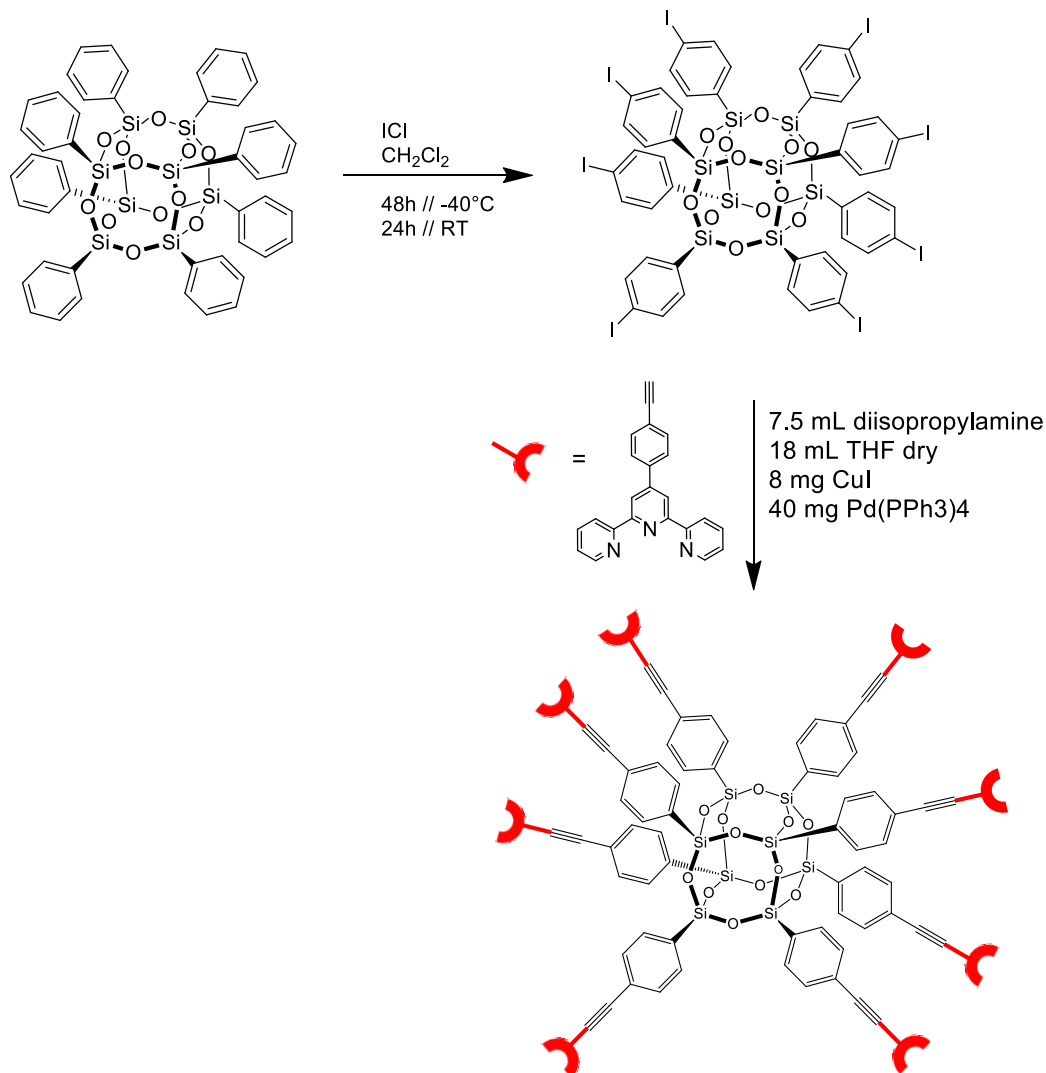
Also talking about the chemistry of the Ln@POSS systems seen in the previous chapter, it could be possible to improve the already exciting results. In fact, since the materials obtained showed good results and promising applicability in the field of emitting materials, the final goal to obtain ordered 3D structure was not achieved. Indeed, materials obtained don't showed any crystallinity behaviour, but they appear amorphous. A possibility could be to change type of connection between the cage and the organic moiety using a more rigid, longer and directional spacer in respect to the vinyl group that is not linear (**Figure 7.1**).



**Figure 7.1.** Octa-vinyl POSS and Octa-phenyl POSS

The use of this new type of spacer can help in the packaging of more ordered 3D structure and, furthermore, contribute to improve, with a supplementary  $\pi$  system able to catch and transfer light harvested acting so as a better “antenna”.

In this case too, first two steps were already done (**Scheme 7.3**).



**Scheme 7.3.** Scheme for the synthesis of the new POSS-based structure.

For first electrophilic aromatic substitution on the octa-phenyl POSS was performed to have a suitable organic moiety able to react with an alkyne.<sup>11</sup> Then, ethynylphenyl-terpyridine was allowed to react in the Sonogashira coupling reaction conditions, to obtain eight rigid arms POSS. The so obtained structure is already under investigation for the realization of self-assembled, in presence of metal, 3D crystalline structure.

### 7.3 References

1. Nishiyama, H.; Sakaguchi, H.; Nakamura, T.; Horihata, M.; Kondo, M.; Itoh, K., Chiral and C<sub>2</sub>-symmetrical bis (oxazolinyropyridine) rhodium (III) complexes: effective catalysts for asymmetric hydrosilylation of ketones. *Organometallics* **1989**, *8* (3), 846-848.
2. Babu, S. A.; Krishnan, K. K.; Ujwaldev, S. M.; Anilkumar, G., Applications of Pybox Complexes in Asymmetric Catalysis. *Asian J. Org. Chem.* **2018**, *7* (6), 1033-1053.
3. (a) Evans, D. A.; Kozlowski, M. C.; Murry, J. A.; Burgey, C. S.; Campos, K. R.; Connell, B. T.; Staples, R. J., C<sub>2</sub>-Symmetric Copper(II) Complexes as Chiral Lewis Acids. Scope and Mechanism of Catalytic Enantioselective Aldol Additions of Enolsilanes to (Benzyloxy)acetaldehyde. *J. Am. Chem. Soc.* **1999**, *121* (4), 669-685; (b) Evans, D. A.; Sweeney, Z. K.; Rovis, T.; Tedrow, J. S., Highly Enantioselective Syntheses of Homopropargylic Alcohols and Dihydrofurans Catalyzed by a Bis (oxazoliny) pyridine– Scandium Triflate Complex. *J. Am. Chem. Soc.* **2001**, *123* (48), 12095-12096; (c) Iwama, T.; TSUJIYAMA, S.-i.; Kinoshita, H.; Kanematsu, K.; Tsurukami, Y.; Iwamura, T.; WATANABE, S.-i.; Kataoka, T., A New Entry to Enantioselective Synthesis of  $\alpha$ -Nethylene- $\beta$ -hydroxy Ketones by the Chalcogeno-Baylis-Hillman Reaction. *Chem. Pharm. Bull.* **1999**, *47* (7), 956-961.
4. (a) Doyle, M. P.; Protopopova, M. N., New aspects of catalytic asymmetric cyclopropanation. *Tetrahedron* **1998**, *54* (28), 7919-7946; (b) Doyle, M. P.; Forbes, D. C., Recent advances in asymmetric catalytic metal carbene transformations. *Chem. Rev.* **1998**, *98* (2), 911-936; (c) Augier, C.; Malara, L.; Lazzeri, V.; Waegell, B., Competition between catalytic epoxidation and oxidative cleavage of trans-stilbene by ruthenium complexes associated with bidentate ligands. *Tetrahedron Lett.* **1995**, *36* (48), 8775-8778.
5. (a) Andrus, M. B.; Lashley, J. C., Copper catalyzed allylic oxidation with peresters. *Tetrahedron* **2002**, *58* (5), 845-866; (b) Schulz, M.; Kluge, R.; Gelalcha, F. G., Asymmetric peroxidation of prochiral allylic and benzylic compounds with tert-butyl hydroperoxide and chiral bisoxazoline–copper complexes. *Tetrahedron: Asymmetry* **1998**, *9* (24), 4341-4360.

6. (a) Evans, D. A.; Kozłowski, M. C.; Tedrow, J. S., Cationic bis (oxazoline) and pyridyl-bis (oxazoline) Cu (II) and Zn (II) Lewis acid catalysts. A comparative study in catalysis of Diels-Alder and aldol reactions. *Tetrahedron Lett.* **1996**, *37* (42), 7481-7484; (b) Desimoni, G.; Faita, G.; Guala, M.; Pratelli, C., An efficient catalyst for highly enantioselective exo-Diels–Alder reaction between alkenoyl-1, 3-oxazolidin-2-ones and cyclopentadiene. *Tetrahedron* **2002**, *58* (15), 2929-2935.
7. Yao, S.; Johannsen, M.; Audrain, H.; Hazell, R. G.; Jørgensen, K. A., Catalytic Asymmetric Hetero-Diels–Alder Reactions of Ketones: Chemzymatic Reactions. *J. Am. Chem. Soc.* **1998**, *120* (34), 8599-8605.
8. Sanchez-Blanco, A. I.; Gothelf, K. V.; Jørgensen, K. A., Lanthanide-catalyzed endo-and enantioselective 1, 3-dipolar cycloaddition reactions of nitrones with alkenes. *Tetrahedron Lett.* **1997**, *38* (45), 7923-7926.
9. (a) Nomura, K.; Warit, S.; Imanishi, Y., Olefin Polymerization by the (Pybox) RuX<sub>2</sub> (ethylene)–MAO Catalyst System. *Macromolecules* **1999**, *32* (14), 4732-4734; (b) Nomura, K.; Sidokmai, W.; Imanishi, Y., Ethylene polymerization catalyzed by ruthenium and iron complexes containing 2, 6-bis (2-oxazolin-2-yl) pyridine (Pybox) ligand-cocatalyst system. *Bull. Chem. Soc. Jpn.* **2000**, *73* (3), 599-605.
10. (a) Nesper, R.; Pregosin, P.; Püntener, K.; Wörle, M.; Albinati, A., Palladium (II) complexes of chiral tridentate nitrogen pybox ligands. *J. Organomet. Chem.* **1996**, *507* (1-2), 85-101; (b) Guo, J.; Wang, B.; Bi, J.; Zhang, C.; Zhang, H.; Bai, C.; Hu, Y.; Zhang, X., Synthesis, characterization and 1,3-butadiene polymerization studies of cobalt dichloride complexes bearing pyridine bisoxazoline ligands. *Polymer* **2015**, *59*, 124-132; (c) Lundgren, S.; Lutsenko, S.; Jönsson, C.; Moberg, C., Polymer-Supported Pyridine–Bis(oxazoline). Application to Ytterbium-Catalyzed Silylcyanation of Benzaldehyde. *Org. Lett.* **2003**, *5* (20), 3663-3665.
11. Shanmugan, S.; Cani, D.; Pescarmona, P. P., The design and synthesis of an innovative octacarboxy-silsesquioxane building block. *Chem. Commun.* **2014**, *50* (75), 11008-11011.

## *List of abbreviations*

% v/v	=	volume/volume/ percentage
<sup>1</sup> H-NMR	=	proton nuclear magnetic resonance
<sup>13</sup> C-NMR	=	carbon nuclear magnetic resonance
0D	=	zero dimension
1D	=	one-dimensional
2D	=	two-dimensional
3D	=	three-dimensional
a. u.	=	arbitrary units
Abs	=	absorbance
BOX	=	bisoxazoline
BTCBA	=	benzylthiophene-C <sub>60</sub> bisadduct
CDCl <sub>3</sub>	=	deuterated chloroform
CH <sub>2</sub> Cl <sub>2</sub>	=	dichloromethane
CH <sub>3</sub> CN	=	acetonitrile
CNF	=	carbon nanoforn
CNT <sub>s</sub>	=	carbon nanotubes
CP-MAS	=	cross coupling-magic angle spin
dba	=	dibenzylideneacetone
DBU	=	1,5-diazabicyclo(5.4.0)undec-7-ene
DCM	=	dichloromethane
DMF	=	dimethylformamide
ED	=	odd-parity electric dipole
EL	=	electroluminescence
EQ	=	electric quadrupole
eq	=	equivalent
Et <sub>3</sub> N	=	triethylamine
FMFN	=	functionalized magnetic fullerene nanocomposite
FT-IR	=	Fourier transform infrared spectroscopy
HOMO	=	highest occupied molecular orbital
HPLC	=	high-performance liquid chromatography

I <sub>h</sub>	=	truncated icosahedron
IL	=	ionic liquid
IUPAC	=	International Union of Pure and Applied Chemistry
K	=	kelvin
L	=	ligand
LC	=	liquid crystal
LED	=	light emitting diode
LUMO	=	lowest unoccupied molecular orbital
M	=	metal
MBTCBA	=	2-(4-methoxybenzyl)thiophene-C <sub>60</sub> bis-adduct
MC	=	metallic cation
MCM	=	Mobil Crystalline Materials or Mobil Composition of Matter
MD	=	even-parity magnetic dipole
MEH-PPV	=	poly[2-methoxy,5-(2'-ethyl-hexyloxy)-p-phenylene vinylene]
MeOH	=	methanol
MLS	=	MOF like structure
MOF	=	metal-organic frameworks
MOSFET	=	metal-oxide-semiconductor field-effect transistor
M-POSS	=	mono terpyridine polyhedral oligomeric silsesquioxanes
MS	=	mesoporous silica
MV	=	monovinyl-heptaisobutyl polyhedral oligomeric silsesquioxanes
MWNT	=	multiwalled carbon nanotube
ODA	=	oxydiacetic acid
o-DCB	=	1,2-dichlorobenzene or orthodichlorobenzene
OL	=	organic linkers
OLED	=	organic light emitting diode
O-POSS	=	octa terpyridine polyhedral oligomeric silsesquioxanes
OPV	=	oligo(phenylenevinylene)
OTf	=	triflate
OV	=	octavinyl polyhedral oligomeric silsesquioxanes
P	=	pressure
PCBM	=	[6,6]-phenyl-C <sub>61</sub> -butyric acid methyl ester



PCU	=	poly(carbonate-urea)urethane
PET	=	polyethylene terephthalate
PFO	=	polydioctylfluorene
Ph-PyBOX	=	phenyl pyridine bridged bisoxazoline
PL	=	photo luminescence
POSS	=	polyhedral oligomeric silsesquioxanes
PSC	=	polymer solar cells
PyBOX	=	pyridine bridged bisoxazoline
RT	=	room temperature
SBA	=	Santa Barbara Amorphous type material
SILP	=	supported ionic liquid phase
SiNWs	=	silicon nanowires
SiODs	=	Si quantum dots
SWNT	=	single wall carbon nanotube
TEMPO	=	2,2,6,6-tetramethylpiperidine-1-oxyl
THF	=	tetrahydrofuran
TICs	=	toxic industrial chemicals
TME	=	tumour microenvironment
Tpy	=	2,2':6',2''-terpyridine
UV-Vis	=	ultraviolet visible
VDW	=	stronger van der Waals
VLS	=	vapor liquid solid
$\lambda$	=	wavelength
$\lambda_{ex}$	=	excitation wavelength

# *Curriculum Vitae*

## **Personal Information**

Surname / First name CINÀ Valerio

Home address via Trabucco, 125 - 90146 Palermo, Italy

Telephones (+39) 349 89 24 006

E-mail valerio.cina@unipa.it

Nationality Italian

Place and date of birth Palermo (Italy), 25 November 1986

Gender Male

## **Education and Training**

### **2016 – Present**

**PhD position** at Department of Biological, Chemical and Pharmaceutical Sciences and Technologies, University of Palermo (UNIPA), Italy in partnership with Unit of Nanomaterial Chemistry (CNano), University of Namur (UNamur), Belgium  
Research project: “*Synthesis and applications of novel fullerenes and silsesquioxanes based structures*”; tutor: Prof. F. Giacalone and Prof. C. Aprile

### **2016**

**Master’s degree in Chemistry** curriculum Chemistry of Molecular Systems with mark of 110/110 cum laude. Università Degli Studi di Palermo, Palermo  
Thesis title "Characterization and sequestering skills of co-polymers Calixarene-Cyclodextrin pre- and post-modified"

### **2013**

**Bachelor’s degree in Chemistry**, with mark 92/110. Università Degli Studi Di Palermo, Palermo

Thesis title: "Synthesis and characterization of chiral Calix[4]resorcarenes".

### **Pre-University studies**

Secondary school diploma: Classical certificate School-leaving examination taken in (year): 2005

Italian secondary school diploma.

### **Stages**

2-month visiting period at ITQ-UPV Valencia, Spain under supervision of Prof H. Garcia from 31 May 2018 to 31 July 2018

Stage at University of Namur Unité de Chimie des Nanomatériaux in September 2016

Stage at University of Palermo to STEBICEF (Department of Biological, Chemical and Pharmaceutical Sciences and Technologies) Department, from March to October 2013.

## **Skills and Techniques**

### **Scientific Instrument and Techniques:**

- Advanced laboratory skills in chemistry
- Solution state NMR Spectroscopy ( $^1\text{H}$ ,  $^{29}\text{Si}$ ,  $^{13}\text{C}$ )
- Transmission Electron Microscopy
- Scanning Electron Microscopy and EDX analysis
- $\text{N}_2$  physisorption analysis
- X-ray powder diffraction (XRD)
- UV-DRS (diffuse reflectance)
- UV-Vis
- Fluorescence
- FT-IR
- HPLC

### **Language:**

Italian	Spoken, native	Written, native
English	Spoken, intermediate	Written, intermediate
French	Spoken, beginner	Written, beginner

### **Computer skills:**

Operating systems: Windows,

Usual programs: Office, OpenOffice.

Scientific programs: Origin (plots of numerical data),  
MestreNova, ChemDraw.

### **Mentoring:**

Supervision of Bachelor students during their thesis

**03/2019 – 07/2019** Michael Tumin.

Supervision of Master students during their thesis

**2018/2019** Mariano Guagliardo, Title: “*Bisoxazoline-Fullerene systems in asymmetric catalysis*”.

## **Publications List**

### **Tuneable Emission of Polyhedral Oligomeric Silsesquioxane- Based Nanostructures Self-Assembled in the Presence of Europium(III) Ions: Reversible *trans-to-cis* Isomerization**

Valerio Cinà, Esther Carbonell, Hermenegildo Garcia, Luca Fusaro, Michelangelo Gruttadauria, Francesco Giacalone, Carmela Aprile.

In: ChemPlusChem Accepted Author Manuscript. doi:[10.1002/cplu.201900575](https://doi.org/10.1002/cplu.201900575)

### **Pre- and post-modification of mixed cyclodextrin-calixarene co-polymers: A route towards tunability.**

Cinà, V., Russo, M., Lazzara, G., Chillura Martino, D., Lo Meo, P.

In: Carbohydrate Polymers 157, pp. 1393-1403

### **Chemical and pharmaceutical evaluation of the relationship between triazole linkers and pore size on cyclodextrin-calixarene nanosponges used as carriers for natural drugs.**

Massaro, M., Cinà, V., Labbozzetta, M., Lazzara, G., Lo Meo, P., Poma, P., Riela, S., Noto, R.

In: RSC Advances 6(56), pp. 50858-50866

## **Conferences active participation**

09/2018 Annual NISM Meeting. Poster contribution:

Light-induced trans-cis isomerization of terpyridine functionalized POSS nanostructures self-assembled in presence of Eu<sup>3+</sup> ions.

12/2018 17th YBMRS 2018. Poster contribution:

Light-induced trans-cis isomerization of terpyridine functionalized POSS nanostructures self-assembled in presence of Eu<sup>3+</sup> ions.

03/2019 Congresso congiunto delle Sezioni Sicilia e Calabria SCI 2019 Oral Contribution:

Tuneable Emission of POSS-based nanostructures self-assembled in presence of Eu<sup>3+</sup> ions: reversible trans-to-cis isomerization

04/2019 IV China-Italy Bilateral Symposium on Organic Chemistry. Oral contribution:

Bisoxazoline-Fullerene Hybrid Systems for Asymmetric Catalysis.

08/2019 Europacat 2019. Oral Contribution:

Fullerene-bisoxazoline systems in asymmetric catalysis.

09/2019 XXXIX Convegno Nazionale della Divisione di Chimica Organica CDICO2019. Oral Contribution:

Fullerene-bisoxazoline systems in asymmetric catalysis.

## Seminars and courses attended

- “Chaire Francqui 2016/2017 – Prof. R. Lazzaroni: STM, AFM”
- “Le recrutement des chercheurs”
- French course (6 months)
- “Making Public displays Interactive: From Application Design to Long-Term Deployment”
- “When I’m sixty-four...la sicurezza sociale dei giovani ricercatori: diritti e doveri degli studenti del dottorato di ricerca e situazione previdenziale”
- “Inside the review process”
- “Pulmonary Drug Administration”
- “Médecine légale, vaste science méconnue mais omniprésente et haute en couleur”
- “What do you know about colors?”
- “Simple rules to explain the complex beauty of fractals”
- “Publishing in a Nature Research Journal”+ practical workshop”
- “Les céramiques”
- “From Prehistory to Magritte: the artist’s touch through scientific analysis”
- “Easy way from science to the web”
- “Beautiful information: How to use colours in data visualisation”
- “Supramolecular Colorlands”
- “Les couleurs du vivant. Origine, fonctions et applications bio-inspirées”
- “Vision humaine et colorimétrie”
- “Interferential colour and fluorescence in nature”
- “Formation and initiation to documentary research”
- “Utilisation de logiciels de gestion bibliographique (ENDNOTE | MENDELEY| ZOTERO)”
- Green Chemistry course (3 months)
- "Programma Horizon 2020 - le azioni rivolte alla ricerca d'eccellenza - 11 luglio 2019".